THE FORMATION OF ACOUSTICAL FIELDS IN OCEANIC WAVEGUIDES

RECONSTRUCTION OF INHOMOGENEITIES IN SHALLOW WATER

In two volumes

Volume 2

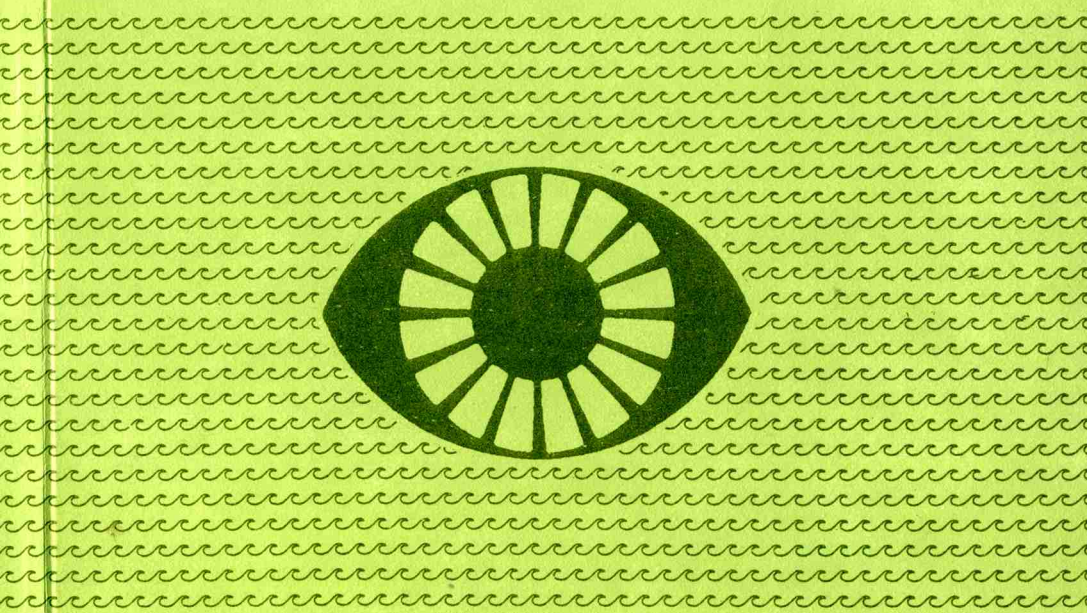

Nizhny Novgorod • 1998

Published on the decision of the Editorial-Board of IAP RAS

The Formation of Acoustical Fields in Oceanic Waveguides. Reconstruction of Inhomogeneities in Shallow Water. Nihzny Novgorod: IAP RAS, 1998. In two volumes. V. 2. 172 p.

The state-of-the-art investigations in field of acoustical probing of different types (including of spatially-localized) oceanic inhomogeneities in shallow water waveguides are presented in this book. The problems associated with reconstruction of parameters of inhomogeneities (bodies or randomly distributed perturbations) in refractive oceanic waveguides in presence of additive noise reverberation are studied. The optimal tomographical algorithms are discussed for observation of inhomogeneities in shallow water region. Most of investigations are based on analysis of the experimental data. The book can be interesting for researchers and students associated with hydroacoustics and acoustics of ocean.

Reviewers

Yu.V. Petukhov,
A. I. Saichev

Editor

V. A. Zverev

Co-editor

A. I. Khil'ko

Editorial Group

N. N. Kralina (secretary),
V. G. Burdukovskaia

ISBN 5-201-09313-2

CONTENTS

Volume 1

Preface 5

E. Yu. Gorodetskaya, A. I. Malekhanov, A. G. Sazontov, N. K. Vdovicheva. Acoustic coherence effects on signal processing in shallow water channels 7

A. V. Lebedev, B. M. Salin. The investigation of acoustic fluctuations in a lake environment 59

V. P. Antonov, V. V. Borodin, G. N. Kuznetsov, A. A. Kuz'menko, V. P. Tebyakin. Parameter estimation for upper layers of multi-layered bottom in shallow sea 69

S. N. Gurbatov, B. Kerman, N. V. Pronchatov-Rubtsov, O. V. Lebedev. Acoustic methods for determining bubble concentrations in subsurface layers 77

G. M. Glebova, G. N. Kuznetsov. Estimating parameters of signal sources and characteristics of noise field by asing spatially separated vector-scalar modules 109

I. P. Smirnov, J. W. Caruthers, A. I. Khil'ko, P. A. Elmore. Emission tomography reconstruction of bubble plumes entrained by breaking wind waves 138

Volume 2

I. P. Smirnov, J. W. Caruthers, and A. I. Khil'ko. Tomographic reconstruction of bubble clouds in random inhomogeneous oceanic environment 189

A. L. Matveyev, A. G. Sazontov, and N. K. Vdovicheva. Acoustic transmission fluctuations from the Barents sea: observation and numerical modeling 221

B. V. Kerzhakov, V. V. Kulinich, M. A. Raevskii, A. A. Stromkov. Experimental checking of the mode theory of acoustic scattering in an ocean waveguide with rough surface 239

V. V. Borodin and M. Yu. Galaktionov. Fundamentals of the high-frequency forward-scattering sonar 259

TOMOGRAPHIC RECONSTRUCTION OF BUBBLE CLOUDS IN RANDOM INHOMOGENEOUS OCEANIC ENVIRONMENT

I.P. Smirnov, J.W. Caruthers, and A.I. Khil'ko

Introduction

Various types of spatially-localized inhomogeneities practically always exist in real oceanic environment. The examples of such a kind of inhomogeneities are the bubble plumes, entrained by breaking wind waves [1], fish shoals [2], icebergs, ships etc. The observations of such inhomogeneities make it possible to solve some practical problems.

The location and sizes of such inhomogeneities can be reconstructed by the acoustical tomography methods [3]. Another reconstruction method is associated with the distant measuring of the noise emitted by the observed inhomogeneities [16, 22]. This method can be not effective for long distances due to losses of acoustical signals in oceanic environment. In this case, the tomographic reconstruction can be based on the diffraction of probing acoustical waves by the observed inhomogeneities [3, 4, 6]. But besides the additive noise background, in diffraction tomography method there is reverberation noise. An a priori information about the observed object and the oceanic environment is needed for the effective procedure of useful signals filtration. Otherwise the solution can be unstable and not uniquely defined.

The peculiarity of the discussing problem is the random nature of the observed objects (bubble plumes, fish shoals etc.). The traditional problem of oceanic tomography [3] is directed to reconstruction of the regular perturbation of the sound speed profile. Tomographic reconstruction of random perturbations of oceanic environment must be formulated as the statistical problem. The measurements of the scattered field statistical moments (for example, the moments of the random time delays) can be used for solution of this problem.

As it was shown [5, 6, 16], the space/frequency/time structures of statistical moments, in particular, the coherence structure, are inhomogeneous and have different scales of changeability. Such phenomena can be associated with the layered structure of ocean environment.

The random spatially-localized bubble plume image construction was investigated in this work for refractive randomly-inhomogeneous layered oceanic waveguides. The models of an observed random cloud of bubbles

and uniformly distributed in space random perturbations of oceanic environment were introduced. The influence of the noise level and other parameters of the problem on the result of the tomographic image construction was analyzed numerically.

1 Reconstruction of image in inhomogeneous environment

1.1 Analysis of integral equations

Generally, the problem of bubbles cloud image reconstruction in the refractive oceanic waveguide with the sound speed profile $c_0(\mathbf{r})$ can be formulated as follows. Let we assume, that the cloud of bubbles has not sharp boundaries, the concentration of bubbles n is not great, so it is possible to neglect by the collect oscillations of bubbles. Thus, we consider, that there are many bubbles on the scale of wave length of an illuminating field λ, and the incident field of frequency f_0 does not initiate of the nonlinear effects. In such conditions, the acoustic field in the environment with bubbles is possible to describe by the wave equation with effective sound velocity $c_{ef} = c_0\left(1+\beta c_v^2\right)^{-1/2}$, where $\beta = 4\pi an\left(\omega_0^2-\omega^2\right)^{-1}$, $\omega_0 = 2\pi f_0 = \left(3\rho_v c_v^2/\rho a^2\right)^{1/2}$, ρ_v, c_v are the density and the sound velocity in bubble gas, respectively.

Let us introduce

$$\varepsilon(\mathbf{r}) = \omega^2\left(\frac{1}{c_0^2(\mathbf{r})} - \frac{1}{c_{ef}^2(\mathbf{r})}\right),$$

where c_0 is the local sound velocity in the unperturbed environment. The equation for complex amplitude of sound pressure of scattered by local inhomogeneity acoustic wave can be presented [3] in the following form:

$$p(\mathbf{r}) = p_0(\mathbf{r}) + \int_\sigma G_0(\mathbf{r},\mathbf{r}')\,\varepsilon(\mathbf{r}')\,p(\mathbf{r}')\,d\mathbf{r}', \qquad (1)$$

where $p_0(\mathbf{r}) = \int\limits_S G_0(\mathbf{s},\mathbf{r})\,f(\mathbf{s})\,d\mathbf{s}$ is the field of the illuminating source $f(\mathbf{s})$, $G_0(\mathbf{r}_1,\mathbf{r}_2)$ is the Green function of unperturbed environment with $c(\mathbf{r}) \equiv c_0(\mathbf{r})$.

The scattered field $p_s = p - p_0$ is random due to randomness of the bubbles parameters. The p_0 is also random due to the waveguide environment fluctuations.

The equation (1) is the basis for the classical tomographic problem formulation. If we consider the magnitude $\varepsilon(\mathbf{r})$ as the unknown value, and the scattered field in the left part of (1) as the measured data, we obtain an integral Lipman-Shvinger equation [8] in respect to the unknown environment perturbation $\varepsilon(\mathbf{r})$. This equation is nonlinear.

The important stage of the solution of such equation is the solution in the Born approximation, where the value $p(\mathbf{r})$ in integral is replaced by $p_0(\mathbf{r})$. Under this approach, the discussed equation becomes the linear first kind Fredholm type integral equation for unknown function $\varepsilon(\mathbf{r})$.

Where the measurements are carried out on rather large distances from the observed object, the kernel of an integral equation can be reduced to the Fourier or Fresnel integral equation, which can be conversed analytically [3] :

$$\widetilde{\varepsilon}(\mathbf{r}') = \frac{1}{\|N\|} \iiint A(\mathbf{r}) [p(\mathbf{r}) - p_0(\mathbf{r}) + n(\mathbf{r})] \Phi(\mathbf{r}', \mathbf{r}) \, d\mathbf{r}, \qquad (2)$$

where $\|N\|$ is a normalizing term, $A(\mathbf{r})$ is aperture of measurements, $\Phi(\mathbf{r}', \mathbf{r})$ is the kernel of the inverse transformation, $n(\mathbf{r})$ is an additive noise. In (2) the distribution $\widetilde{\varepsilon}(\mathbf{r}')$ is the image of the original distribution $\varepsilon(\mathbf{r})$. The image differs from the original because of the aperture distortions $A(\mathbf{r})$ influence of noise and other factors [3].

The Green function $G_0(\mathbf{r}_1, \mathbf{r}_2)$ has the more complex form in an inhomogeneous environment. The model of environment structure is necessary to use for correct reconstruction [3].

For overcoming of difficulties associated with an discussed ill-posed problem it is possible to use the regularization algorithms, and also to realize of the reconstruction using different point of viewing and different frequencies [12, 13]. In the case of an inhomogeneous environment, the random object tomographic reconstruction problem has some features [3]. According to first of them, it is necessary to assume, that the time of observations t_{obs} essentially exceeds the coherence time of fluctuations, $T < t_{obs}$, so there is the possibility for the average values measurements. We also assume, that during the observation the object can be consider as the stationary one.

The equation for the image reconstruction can be reduced from the equation for propagation of the coherence functions [10]. It can be also formally obtained by averaging (1). Assuming the statistical independence of the fields, we receive for tomographic image from (1) the following expression:

$$\psi(\mathbf{r}_1, \mathbf{r}_2) = \psi^{(0)}(\mathbf{r}_1, \mathbf{r}_2) + \\ + \int \cdots \int \left(G_0(\mathbf{r}_1, \mathbf{r}_1') \, G_0^*(\mathbf{r}_2, \mathbf{r}_2')\right) \psi(\mathbf{r}_1', \mathbf{r}_2') \, E(\mathbf{r}_1', \mathbf{r}_2') \, d\mathbf{r}_2' d\mathbf{r}_1', \qquad (3)$$

where

$$\psi(\mathbf{r}_1, \mathbf{r}_2) = \langle p(\mathbf{r}_1) p^*(\mathbf{r}_2) \rangle$$
$$\psi^{(0)}(\mathbf{r}_1, \mathbf{r}_2) = \langle p_0(\mathbf{r}_1) p_0^*(\mathbf{r}_2) \rangle$$

are the coherence functions of the fields, $E(\mathbf{r}_1', \mathbf{r}_2') = \langle \varepsilon(\mathbf{r}_1') \varepsilon^*(\mathbf{r}_2') \rangle$ is the correlation function of spatially-localized random inhomogeneity. The averaging of Green functions is associated with the presence of the randomly-distributed sound speed volume and ocean surface fluctuations.

As for the regular model of ocean, the equation (3) can be reduced to more simple integral equation if restrict the considerations by only Born scattering. From the equation (3) we receive in this case

$$\psi(\mathbf{r}_1, \mathbf{r}_2) = \psi^{(0)}(\mathbf{r}_1, \mathbf{r}_2) + \\ + \int \cdots \int \Phi_0(\mathbf{r}_1, \mathbf{r}_2, \mathbf{r}_1', \mathbf{r}_2') \psi^{(0)}(\mathbf{r}_1', \mathbf{r}_2') E(\mathbf{r}_1', \mathbf{r}_2') \, d\mathbf{r}_1' d\mathbf{r}_2', \tag{4}$$

where the kernel Φ_0 defines of the Fourie or Fresnel transformations. The solutions of such equations can be found with

$$\int \cdots \int A(\mathbf{r}_1) A^*(\mathbf{r}_2) (\psi(\mathbf{r}_1, \mathbf{r}_2) + \sigma(\mathbf{r}_1, \mathbf{r}_2)) \times \\ \times \Phi_0^{-1}(\mathbf{r}_1, \mathbf{r}_2, \mathbf{r}_1', \mathbf{r}_2') \, d\mathbf{r}_1 d\mathbf{r}_2 = \widetilde{\Sigma}_0(\mathbf{r}_1', \mathbf{r}_2') + \widetilde{E}(\mathbf{r}_1', \mathbf{r}_2'), \tag{5}$$

where Φ_0^{-1} is the inverse transformation, $\widetilde{\Sigma}_0$ is the illumination source image, $\widetilde{E}$ is the image of the inhomogeneities. One can see from (5), that the image of the inhomogeneity is formed as the convolution of the measured data with pulse characteristic [10], that defines of the image as the distorted original distribution of the observation object. These distortions are caused by measurement limits. The reconstruction can be complete if we assume, that the measurements are carried out in an infinite plane and that the noise is absent. Such transformation can be seen as the ideal one [10]. All kinds of distortions can be formally included into the aperture function $A(\mathbf{r})$. The specified separation of operations underlies the radio-optical approach for understanding of the image construction [10].

For future analysis it can be useful to define the concept of an image [10, 11]. Namely, by the *image* we consider the distribution of intensity, constructed by the imaging system. We also assume, that the image is approximately characterized by the mutual-univalent correspondence with original distribution of the field in near region of the observed object surface. The image is characterized by a field of vision and a spatial resolution. In general case, the spatial resolution depends from the location in the field of vision [10]. Besides, the field of vision can be essentially inhomogeneous with the complex form and nonuniformity in respect to the space resolution.

It is necessary also to consider these values as the statistical because of the influence of the background of additive noise and reverberation.

Usually the objects of observation have the complex three-dimensional structure. If the observation is carried out through the systems with the limited input aperture, the reconstructed image can be build only like the planar (or shadow) image. For example, for the Fourie or the Fresnel images the longitudinal spatial resolution (along direction, perpendicular to measuring aperture) is practically absent or on an order less (respectivęly) in comparison with an appropriate space resolution in the image of cross plane distribution of observation object. It can be use a tomographic principle for elimination of the specified distortions. Such approach consists of the joining of the information about separate partial planar (shadow) images (tomographical projections), which are obtained, under different point of viewing in a summarized image [12]. In layered oceanic waveguides the concept of tomographic projections can be more complex, because the each of partial waveguide waves can be considered as the additive tomographic projection.

In conclusion of this section we would like to mark the rather important circumstance. The tomographic image reconstruction requires of an a priori information about the observation object, the refractive environment, random inhomogeneities of an ocean and the construction of the observation system. All these models are multiparametric. Due to this the hypothesizes about the location and form of the object can be complex problem. The searching of a global extrema associated with solution (reconstructed parameters of observed inhomogeneity) can be difficult [9]. Thus there is a problem of the hypotheses searching optimization. The optimal trajectory in the parameters space can be found by the use an a priori information about of all features of concrete problem. Such information can be detected from the natural and numerical experiments. It is possible to test the global structure of solutions by a preliminary investigation. It allows to realize the rough review of a field of vision as the first stage of reconstruction. The detail analysis of the problem solution with needed quality can be realized during the second stage [16]. The specified algorithms can be built only by rendering concrete physical and mathematical models of observations.

2 Development of the models

2.1 Model of oceanic environment

Consider the oceanic volume as the layered refractive waveguide with a given profile of the refractile index $n(\mathbf{r}) = n(z)$. If the frequency of the probing waves is sufficiently high, the approach of geometric acoustics can be used (see [15]).

Pulse signals distribution in refractive waveguides has a series of features, which are important from the point of view of the tomographic reconstruction problem. First of them, is the "depth - time delay" structure of pulses. In fact, that the pulse signals, coming on separate rays, draw in the plane "time delay-depth" the structure, similar like the saw tooth pulses with a varying phase (see Fig. 1).

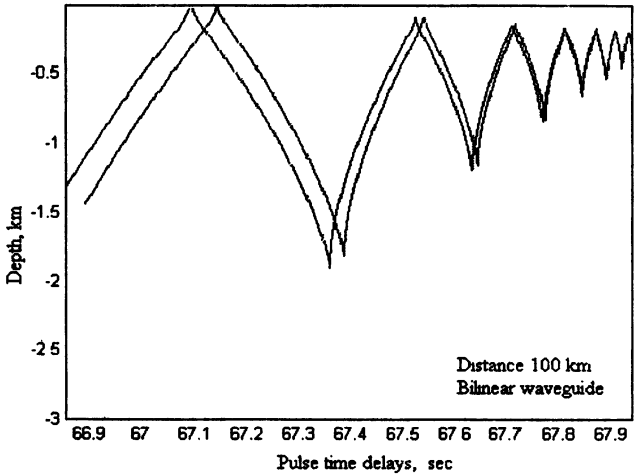

Fig.1. The depth-time delay dependace for pulse calculated for the bilinear oceanic waveguide [5].

The group of pulses, associated with signals propagating in region near the waveguide axes are not resolved in time and, interfering, form the certain summarized "bunch". Each of one-half oscillations cycles of summarized pulse in $\{\tau, z\}$ plane can be corresponded to an "inhomogeneous wave" (Fig. 2) [5, 6]. Besides, it is known [18, 16],

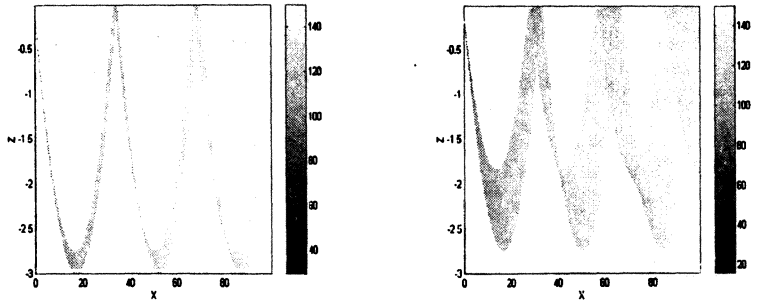

The first wave

The second wave

Fig.2. The intensity of the refracted waves
(logarithmic scale)

that the presence of smooth local extrema in dependencies of ray cycles of exit ray angles leads to the creation of the weekly divergent bundles of rays. They form an interference peaks (or pulses)

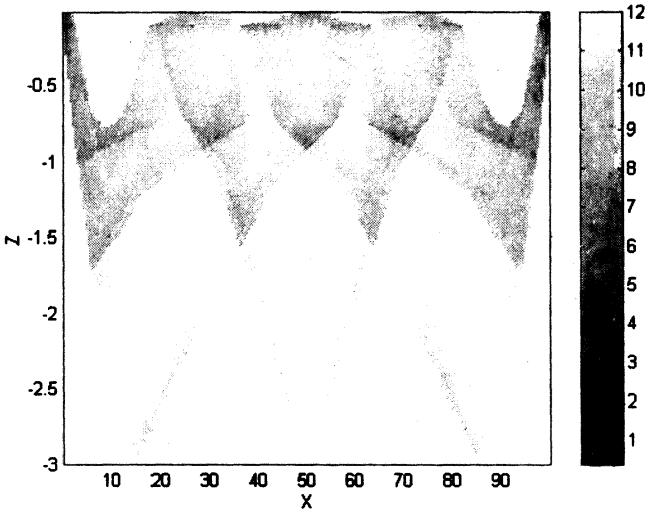

Fig. 3. The distribution of CPC in the oceanic volume

in the plane $\{\tau, z\}$, having rather large intensity and coherence.

The local inhomogeneities reconstruction is possible only in regions, where the intensity of the probing waves are large. Analogously, because of the symmetrical situation, the receiver does not "feel" the inhomogeneity, if it is situated in a region associated with the week sensitiveness of the receiving system. Such effects in summary can be described by translational characteristics of the waveguide [17]. The distribution of one of the translational characteristics - *coefficient of the power coupling (CPC),* - calculated for bilinear oceanic waveguide is shown in the Fig.3.

The regions, where CPC is large (dark in the Fig. 3), are sensible in respect of the local inhomogeneities existence. In fact, that the CPC distributions, generally, define of the inhomogeneity of the field of vision for observation system. The use of CPC in integral equation as regulating factors permits to reject of the regions, where the reconstruction is practically impossible.

2.2 The local inhomogeneity model

Let we consider the localized in space bubble cloud as the observation object. The plume can be represented as the local perturbation of the refractive index where the bubble sizes are small in comparison with the wave length.

We describe the stationary local perturbation $\varepsilon(\mathbf{r})$ of the refractive index in the neigborhood of point $\mathbf{r}^*$ by the moment functions

$$\begin{gathered} \Xi(\mathbf{r}) = \langle \varepsilon(\mathbf{r}) \rangle = \varepsilon_0 \vartheta(\mathbf{r} - \mathbf{r}^*), \\ \Phi(\mathbf{r}_1, \mathbf{r}_2) = \langle (\varepsilon(\mathbf{r}_1) - \Xi(\mathbf{r}_1))(\varepsilon(\mathbf{r}_2) - \Xi(\mathbf{r}_2)) \rangle = \\ = \varepsilon_1^2 \varphi\left(\tfrac{\mathbf{r}_1+\mathbf{r}_2}{2} - \mathbf{r}^*, \mathbf{r}_1 - \mathbf{r}_2\right), \end{gathered} \tag{6}$$

where values $\varepsilon_0, \varepsilon_1^2$ are the quantitative, and $\vartheta(\mathbf{R}), \varphi(R_2)$ are the functions, describing the spacial distribution of the local inhomogeneity. The local character of such description is reflected in the following properties of the functions:

$$\vartheta(\mathbf{0}) = \varphi(\mathbf{0}, \mathbf{0}) = 1,$$
$$\vartheta(\mathbf{R}) \underset{\|\mathbf{R}\| \to \infty}{\to} 0, \ \varphi(\mathbf{R}_1, \mathbf{R}_2) \underset{\|\mathbf{R}_1\| + \|\mathbf{R}_2\| \to \infty}{\to} 0.$$

Integral parameters

$$\begin{gathered} \sigma_x = \tfrac{1}{\sqrt{2\pi}} \int_{-\infty}^{+\infty} \vartheta(x, 0)\, dx, \sigma_z = \tfrac{1}{\sqrt{2\pi}} \int_{-\infty}^{+\infty} \vartheta(0, z)\, dz; \\ \sigma = \sqrt{\tfrac{1}{2\pi} \iint_{-\infty}^{\infty} \vartheta(\mathbf{R})\, d\mathbf{R}} \end{gathered} \tag{7}$$

- the generalized scales of the inhomogeneity - describe its spatial sizes.

The Gaussian functions can be used for this purpose:

$$\begin{aligned} \vartheta(\mathbf{R}) &= \exp\left(-\tfrac{\|\mathbf{R}\|^2}{2\sigma^2}\right), \\ \varphi(\mathbf{R}_1,\mathbf{R}_2) &= \exp\left(-\tfrac{\|\mathbf{R}_1\|^2+\|\mathbf{R}_2\|^2}{2\sigma^2}\right). \end{aligned} \tag{8}$$

Asymmetric local inhomogeneities of scales σ_x, σ_z can be described by the Gaussian functions:

$$\begin{aligned} \vartheta(\mathbf{R}) &= \exp\left(-\tfrac{|\mathbf{R}_x|^2}{2\sigma_x^2} - \tfrac{|\mathbf{R}_z|^2}{2\sigma_z^2}\right), \\ \varphi(\mathbf{R}_1,\mathbf{R}_2) &= \exp\left(-\tfrac{|\mathbf{R}_{1x}|^2+|\mathbf{R}_{2x}|^2}{2\sigma_x^2} - \tfrac{|\mathbf{R}_{1z}|^2+|\mathbf{R}_{2z}|^2}{2\sigma_z^2}\right). \end{aligned}$$

By this way we constructed the parametric model of the local inhomogeneity with parameters $\left\{\varepsilon_0, \varepsilon_1^2, \sigma_x^2, \sigma_z^2, r^*\right\}$.

Generally, the set of the diffracted waves appears due to scattering by the local inhomogeneity. In Born approach, where the inhomogeneities are relatively weak, these diffraction waves are small in comparison with the incident wave. The Born approach corresponds to the complementary time delay τ^ε [14] for the same ray trajectories in terms of geometric acoustic. The mean value $\langle\tau^\varepsilon\rangle$ and dispersion $T^2/2$ may be found using the moment of functions of the refractive index

$$\begin{aligned} \langle\tau^\varepsilon\rangle &= \int_C \Xi(\mathbf{r})\, dl = \varepsilon_0 \int_C \vartheta(\mathbf{r}-\mathbf{r}^*)\, dl = \varepsilon_0 \int_0^l \vartheta(\mathbf{r}(l)-\mathbf{r}^*)\, dl, \\ T^2/2 &= \int_0^l \int_0^l \Phi(\mathbf{r}(l_1),\mathbf{r}(l_2))\, dl_1 dl_2. \end{aligned} \tag{9}$$

Finally for the Gaussian models (8), it is possible to obtain the following approximate formulas

$$\begin{aligned} \langle\tau^\varepsilon\rangle &= \varepsilon_0 \int_C \exp\left(-\tfrac{\|\mathbf{r}-\mathbf{r}^*\|^2}{2\sigma^2}\right) dl, \\ T^2/2 &\simeq \sqrt{2\pi}\sigma\varepsilon_1^2 \int_C \exp\left(-\tfrac{\|\mathbf{r}-\mathbf{r}^*\|^2}{2\sigma^2}\right) dl \end{aligned} \tag{10}$$

2.3 The reverberation model

The random inhomogeneities of the oceanic waveguide can be classified as the three types: volume inhomogeneities (turbulent pulsations, internal waves etc.), surface inhomogeneities, generated by the wind and bottom

inhomogeneities. For the simplicity, we focus on the deep sea model neglecting by the bottom inhomogeneities influence. For the first two kinds of inhomogeneities we use the following models.

Volume inhomogeneities Let we consider the distributed in the volume space fluctuations of the refractive index $n(\mathbf{r})$ as the homogeneous in space fluctuations with stationary Gaussian statistic [1, 19] and the coherence function

$$\Phi(\mathbf{r}_1, \mathbf{r}_2) = \langle \tilde{n}(\mathbf{r}_1), \tilde{n}(\mathbf{r}_2) \rangle = \\ = \epsilon_0^2 \exp\left(-\frac{1}{2}\left[\frac{(x_1-x_2)^2}{\varrho_x^2} + \frac{(z_1-x_2)^2}{\varrho_z^2}\right]\right),$$

where ϵ_0^2 is the dispersion of fluctuations, $\varrho_{z,x}$ are scales of coherence.

As it was demonstrated in [16], for the pulse signal with the coherence function

$$\Psi_\xi(\tau) = \int_{-\infty}^{\infty} \exp(i\omega\tau)\, d\mathbf{S}_\xi(\omega)$$

the coherence function of received signals under the geometric acoustics approach has the form

$$k_\eta(\mathbf{r}_1, \mathbf{r}_2; \tau) = \sum_{j \in J_1} \sum_{j' \in J_2} \left\langle A_j^{(1)} A_{j'}^{(2)} \right\rangle \exp(i\Psi_{jj'})\, k_{jj'}(\tau + \tau_{jj'}), \\ k_{jj'}(\tau) \equiv \int_{-\infty}^{+\infty} \exp\left(i\omega\tau - \left(\frac{T_{jj'}\omega}{2}\right)^2\right) d\mathbf{S}_\xi(\omega). \tag{11}$$

Here the translation function $T_{jj'}$ is the *statistical difference of times* (SDT) between the rays - the geometric characteristic of the waveguide, describing the correlation of waves, brought by different rays. SDT properties are studied in [16]. In particular, for small horizontal scale ϱ_x of fluctuations

$$T_{jj'}^2 \simeq 4\sqrt{2\pi}\frac{\epsilon_0^2}{c_0^2}\varrho_x \left(\frac{l_j + l_{j'}}{2} - \varrho_x \sum_l \frac{\nu_l}{\sin\left|\theta_l^j - \theta_l^{j'}\right|}\right), \tag{12}$$

where l_j are the lengths and θ_l^j are the slide angles of the rays, respectively.

For example, if the correlation function of the signal is

$$k_\xi(\tau) = k_\xi(0) \exp\left(-\frac{\tau^2}{\tau_\xi^2} - i\omega_0\tau\right),$$

where τ_ξ is the pulse duration, ω_0 is the central frequency, then

$$k_{jj'}(\tau) = k_{jj'}(0) \exp\left(-\frac{\tau^2}{\tau_0^2 + T_{jj'}^2}\right) \exp\left(-\frac{i\omega_0\tau}{1 + (T_{jj'}/\tau_0)^2}\right).$$

In nonperturbed by the local inhomogeneities environment the time delay of the pulse is a random value with statistic, which depends on the statistic of the stationary refractive index fluctuations.

The surface scattered field It is well known, that the spectrum of the surface wind waves can be described by the empiric Pierson-Moskovitz spectrum [20]. The spectrum of scattering signal in this case can be expressed by the following formula:

$$W_\zeta(K) = \frac{\beta_0}{K^4} \exp\left[-\frac{0.74g^2}{v^4K^2}\right],$$

where $|K| = |K_p| = |K_s \cos\alpha - K_r \cos\beta|$ is the wave vector, corresponding to resonance Bregg component, K_s is the horizontal projection of incidents under the angle α ray, K_r and β are the same parameters for the scattered wave, v is the wind velocity, g is the gravitational constant, $\beta_0 = 6.4 \cdot 10^{-4}$, $K_0 = \frac{\Omega_s^2}{g}$, Ω_s is the characteristic frequency of the Pierson-Moskovitz spectrum. Taking into account of the wind waves movement and also the large-scale surface waves movement, we can represent the normalized frequency spectrum of scattering signals in the form

$$W_\zeta(\Omega) = \frac{0.74g^2}{v^4K_p^2} \frac{(\Omega \pm \Omega_s)^{-5}}{2\pi} \exp\left[-\frac{0.74g^2}{v^4K_p^2} \frac{(\Omega \pm \Omega_s)^{-4}}{2\pi}\right].$$

Every element area of the scattering surface gives the contribution into the result signal. It can be described by the coefficient of the surface scattering for fixed Doppler frequency Ω:

$$m_{dA} = 4K_s^2K_r^2W_\zeta(\Omega)\sin^2(\Theta_s + \alpha^*)\sin^2(\Theta_r + \alpha^*) \times \\ \times \frac{|\cos\gamma^{dA}|^N}{\int_{-\pi/2}^{\pi/2} |\cos\gamma^{dA}|^N d\gamma^{dA}},$$

where $N = 21.75 \cdot \exp\left(-0.74v/\sqrt{\frac{2K_p}{g}}\right)$, dA is the scattering element, $\Theta_{s,r}$ are vertical incident and scattering angles of rays, respectively, α^* is the

mean square slope of the sea surface, that can be taken from the Cox-Munk spectrum

$$\alpha^* = 10^{-3} \cdot \sqrt{1.5 + 2.54 \cdot v\left(\frac{m}{s}\right)},$$
$$N = 16.095 \frac{v}{\sqrt{2Kg}},$$

γ^{dA} is the angle between vectors $\mathbf{k}$ and $\mathbf{v}$, N is the coefficient of the spectrum anisotropy.

For the result intensity of the scattered wave with the frequency ω we have

$$p_{rev}(\omega) = \sqrt{I_0} \iint b_s(r_s, r_a) \frac{\sqrt{m_{dA}}}{r_s r_r} b_r(r_a, r_r)\, dA, \tag{13}$$

where $b_{s,r}$ are the transmission losses from the source to the element area of scattering dA and from it to the receiver, respectively, I_0 is the intensity of the wave near the source.

2.4 Model of probing signals

As it is well known [15], the acoustical signals in the refractive waveguides are formed as the interference of the partial waves and have the complex structure. The success of the tomographic reconstruction depends especially from the possibilities for separation of different wave components.

As the probing signals, the short pulse signals with complex modulation are necessary to use for better separation of partial wave pulses (rays pulses in our case). In our future discussion we will use the signals with linear frequency modulation (LFM-signal):

$$\xi_0(t) = \left(\frac{8}{\pi T_\xi^2}\right)^{1/4} \exp\left(-\frac{t^2}{T_\xi^2}\right) \cos\left(\omega_0 t + \alpha t^2/2\right), \tag{14}$$

where $(\alpha T_\xi \ll \omega_0)$ and the coherence function

$$\Psi(\tau) \simeq \exp\left(-\frac{\tau^2}{\tau_\xi^2}\right) \cos\omega_0 \tau,$$
$$\tau_\xi^2 = 2T_\xi^2 / \left(1 + \alpha^2 T_\xi^4/4\right). \tag{15}$$

2.5 The signal filtration

Let we consider the source S, radiating the periodic sequence of pulse signals (14)

$$\xi(t) = \sum_{k=0}^{\infty} \xi_0(t - kT_0).$$

We put the receiver with the uniform diagram in point R. The received signal consists of the pulses, refracted in the oceanic volume or reflected from the waveguide boundaries.

Accordingly to our approach,we divide the boundaries of the waveguide into *regular* (the bottom) and *irregular* (the ocean surface). The surface parameters have the random time fluctuations (due to influence of the wind waves). In this association, we call of the received pulses as the *regular pulses*, if they arrive to the receiver after refraction from the bottom. The another kind of pulses, are the *irregular* pulses which reflected from the surface of ocean.

In unperturbed environment l-th regular pulse arrives to the point R with the time delay τ_l^0. If there are the random fluctuations ε of the refractive index n in ocean volume, the time delay of regular pulse becomes random and has the form

$$\begin{aligned} \tau_l &= \tau_l^0 + \tilde{\tau}_l^{\varepsilon} \equiv \\ &\equiv \int\limits_{C_l} n\,ds + \int\limits_{C_l} \varepsilon\,ds, \end{aligned}$$

where C_l is the trajectory (ray) of the l-th pulse. According to our approach, we neglect by the random fluctuations of the amplitudes A_l and trajectories of the regular pulses.

Irregular pulses arrive to the receiving point after reflection from the random surface. Their number M, amplitudes α_m and time delays $\mathcal{T}_m$ are random and mostly defined by the irregular boundary fluctuations statistic.

The interval of observation $[0,T]$ is assumed to be sufficiently large in comparison with the period T_0 of the probing pulses, so the number of pulses is large: $[T/T_0] \gg 1$. Also we assume that the period T_0 exceeds significantly the pulse duration T_ξ and the time of coherence of the random fluctuations of the waveguide parameters, so the realizations of this values for different pulses can be regarded as independent from the each other. Assume, however, that the statistics of all parameters of the waveguide are the same in the observation interval.

The receiving scattered pulse signal can be written in the form

$$\begin{aligned} \eta(t) = \sum_{k=0}^{\infty} \Bigg(\sum_l A_l \xi_0 \left(t - kT_0 - \tau_l^{(k)} \right) + \\ + \sum_{m_i=1}^{M_k} \alpha_m^{(k)} \xi_0 \left(t - kT_0 - \mathcal{T}_m^{(k)} \right) \Bigg) + \tilde{n}(t), \end{aligned}$$

where the parameters are as follows:

1. $\tau_l^{(k)}$ is the time delay of the pulse number k for the ray number l; the mean value $\left\langle \tau_l^{(k)} \right\rangle = \bar{\tau}_l = \tau_l^0 + \tau_l^e$ and dispersion $\sigma_l^2 = \left\langle \left(\tau_l^{(k)} - \bar{\tau}_l \right)^2 \right\rangle$ depends on the ray and doesn't depend on the pulse number k;

2. M_k is the random number of irregular pulses, which are generated by the pulse k; the mean value $\langle M_k \rangle = \bar{M}$ doesn't depend on k;

3. $\alpha_m^{(k)}$, $m = \overline{1, M_k}$, is the random amplitude of the irregular pulse number m; the mean value of the amplitude is determined by the irregular boundary and doesn't depend on the pulse number: $\left\langle \alpha_m^{(k)} \right\rangle = \bar{\alpha}$;

4. $\mathcal{T}_m^{(k)}$, $m = \overline{1, M_k}$ is the random delay of this pulse; the mean value $\left\langle \mathcal{T}_m^{(k)} \right\rangle = \mathcal{T}_0$.

Finally, the mutual coherence function of the received signals and the replica is defined for the periodic pulse sequence by the formula

$$K(\tau) = \lim_{T\to\infty} \frac{1}{T} \int_0^T \xi_0(t)\, \eta(t+\tau)\, dt =$$

$$= \lim_{T\to\infty} \frac{1}{T} \int_0^T \sum_{n=0}^{\infty} \xi_0(t - nT_0) \left(\sum_{k=0}^{\infty} \left(\sum_l A_l \xi_0 \left(t + \tau - \tau_l^{(k)} - kT_0 \right) + \right. \right. \tag{16}$$

$$\left. \left. + \sum_{m=1}^{M_k} \alpha_m^{(k)} \xi_0 \left(t + \tau - kT_0 - \mathcal{T}_m^{(k)} \right) \right) + \tilde{n}(t+\tau) \right) dt.$$

The contribution of additive noise Let we consider

$$\frac{1}{T} \int_0^T \sum_{n=0}^{\infty} \xi_0(t - nT_0)\, \tilde{n}(t+\tau)\, dt \cong$$

$$= \frac{1}{T_0} \frac{1}{[T/T_0]} \sum_{n=0}^{[T/T_0]} \underbrace{\int_{nT_0}^{nT_0+T_\xi} \xi_0(t - nT_0)\, \tilde{n}(t+\tau)\, dt}_{\zeta_n}.$$

For big number of pulses $[T/T_0] \gg 1$ and small time of correlation of the additive noise $T_{\tilde{n}} \ll T_0$ the terms ζ_n in the last sum are statistically independent from the each other and have zero mean values. So, by Bernoulli law with high probability

$$\frac{1}{T_0} \frac{1}{[T/T_0]} \sum_{n=0}^{[T/T_0]} \zeta_n \cong \frac{1}{T_0} \langle \zeta_n \rangle = 0.$$

According to more real model [19], the influence of additive noise is associated with finite noise coherence in the pulse and time of observation scales.

The contribution of irregular pulses Supposing that the following conditions are hold

$$T \gg T_0 \gg T_\xi,\ T_0 \gg \tau - \mathcal{T}_0,$$

consider the expression

$$\begin{gathered}\frac{1}{T}\int\limits_0^T \sum_{n=0}^{\infty} \xi_0\left(t - nT_0\right) \sum_{k=0}^{\infty} \sum_{m=1}^{M_k} \alpha_m^{(k)} \xi_0\left(t + \tau - kT_0 - \mathcal{T}_m^{(k)}\right) dt \cong \\ \cong \frac{1}{T} \sum_{k=0}^{[T/T_0]} \sum_{m=1}^{M_k} \alpha_m^{(k)} \Psi\left(\tau - \mathcal{T}_m^{(k)}\right).\end{gathered} \tag{17}$$

Let we transform the sum for a fixed k:

$$\begin{gathered}\sigma_k(\tau) \equiv \sum_{m=1}^{M_k} \alpha_m^{(k)} \Psi\left(\tau - \mathcal{T}_m^{(k)}\right) = \\ = M_k \frac{1}{M_k} \sum_{m=1}^{M_k} \alpha_m^{(k)} \Psi\left(\tau - \mathcal{T}_m^{(k)}\right).\end{gathered}$$

If we assume that the numbers of irregular pulses M_k are large for all k, and also statistics of random values M_k, $\alpha_m^{(k)}, \mathcal{T}_m^{(k)}$ are independent from the each other and don't depend of n, k (i.e. are the same in the interval of integration), then accordingly to Bernoulli law we have

$$\begin{gathered}\sigma_k(\tau) \simeq \langle M_k \rangle \left\langle \alpha_m^{(k)} \right\rangle \left\langle \Psi\left(\tau - \mathcal{T}_m^{(k)}\right) \right\rangle = \\ = \bar{M}\bar{\alpha} \left\langle \Psi\left(\tau - \mathcal{T}\right) \right\rangle,\end{gathered}$$

where $\bar{M}, \bar{\alpha}$ are the corresponding mean values.

Finally, for the sum (17), describing irregular pulses contribution to the coherence function (reverberation), we obtain the following approximate expression

$$\begin{gathered}\frac{1}{T} \sum_{n=0}^{[T/T_0]} \sum_{k=0}^{[T/T_0]} \sum_{m=1}^{M_k} \alpha_m^{(k)} \Psi\left(\tau - \mathcal{T}_m^{(k)} - (k-n)T_0\right) \cong \\ \cong \frac{\bar{M}\bar{\alpha}}{T_0} \left\langle \Psi\left(\tau - \mathcal{T}\right) \right\rangle \equiv K_1(\tau)\end{gathered} \tag{18}$$

Note, that the mean values $\bar{M}, \bar{\alpha}, \mathcal{T}_0, \sigma_{\mathcal{T}}^2$ are (for fixed locations of the source and the receiver) defined only by the random surface perturbations. They can be calculated for given parameters of the random boundary.

The contribution of regular pulses Let we consider the first term in the sum (16), which is responded for the regular pulses correlation. Assuming that for all rays

$$T \gg T_0 \gg T_\xi,\ T_0 \gg \tau - \bar{\tau}_l,$$

we receive

$$\frac{1}{T}\int_0^T \sum_{n=0}^{\infty} \xi_0(t-nT_0) \sum_{k=0}^{\infty}\sum_l A_l \xi_0\left(t+\tau-\tau_l^{(k)}-kT_0\right)\,dt \cong$$
$$\cong \sum_l A_l \frac{1}{T_0}\frac{1}{[T/T_0]} \sum_{k=0}^{[T/T_0]} \Psi\left(\tau-\tau_l^{(k)}\right).$$

According to the Bernoulli law (as values $\tau_l^{(k)}$ are independent for different k), we have

$$\frac{1}{[T/T_0]} \sum_{k=0}^{[T/T_0]} \Psi\left(\tau-\tau_l^{(k)}\right) \cong \langle \Psi(\tau-\tau_l)\rangle,$$

so

$$\frac{1}{T}\int_0^T \sum_{n=0}^{\infty} \xi_0(t-nT_0) \sum_{k=0}^{\infty}\sum_l A_l \xi_0\left(t+\tau-\tau_l^{(k)}-kT_0\right)\,dt \cong$$
$$\cong \frac{1}{T_0}\sum_l A_l \langle \Psi(\tau-\tau_l)\rangle \equiv K_2(\tau). \tag{19}$$

For given statistic of the refractive index ε of the fluctuations we can find the statistic of time delay τ_l fluctuations, and then (for given coherence function of the pulse) the function $K_2(\tau)$, containing the information about the fluctuations can be calculated. Similarly, we can get the function $K_1(\tau)$ using of the statistic of the irregular boundary fluctuations.

Finally, we receive the following representation for the mutual coherence function of the receiving signals and replica

$$K(\tau) = \lim_{T\to\infty} \frac{1}{T}\int_0^T \xi(t)\,\eta(t+\tau)\,dt \cong$$
$$\cong K_1(\tau) + K_2(\tau) \cong \tag{20}$$
$$\cong \frac{1}{T_0}\left[\bar{M}\bar{\alpha}\langle \Psi(\tau-\mathcal{T})\rangle + \sum_l A_l \langle \Psi(\tau-\tau_l)\rangle\right].$$

This formula shows that formally the irregular boundary can be interpreted as the complementary ray, through which the pulse signal passes with random time delay $\mathcal{T}$ and the amplitude $\bar{M}\bar{\alpha}$. It differs from the regular pulses the essentially large dispersion of the time delay and small energy.

Gaussian model of fluctuations Let the time delay of irregular pulse $\mathcal{T}$ has the Gaussian statistic with parameters $\left(\mathcal{T}_0, T_{nr}^2/2\right)$.

For the normal distribution of the refractive index fluctuations ε, the time delays of the regular pulses τ_l will be also normal with the parameters $\left(\bar{\tau}_l, T_l^2/2\right)$, where the mean delays $\bar{\tau}_l$ and their dispersions $T_l^2/2$ could be calculated (see sections 2.2, 2.3), using the statistic of $\varepsilon(\mathbf{r})$.

For the functions $K_{1,2}(\tau)$ we receive in this case

$$K_1(\tau) = \tfrac{1}{T_0}\bar{M}\bar{\alpha}\left\langle\Psi(\tau-\mathcal{T})\right\rangle =$$
$$= \tfrac{1}{T_0}\tfrac{\bar{M}\bar{\alpha}}{\sqrt{\pi T_{nr}^2}}\int\limits_{-\infty}^{+\infty}\Psi(\tau-\mathcal{T}_0-x)\exp\left(-\tfrac{x^2}{T_0^2}\right)dx,$$

$$K_2(\tau) = \tfrac{1}{T_0}\sum_l A_l\left\langle\Psi(\tau-\tau_l)\right\rangle =$$
$$= \tfrac{1}{T_0}\sum_l \tfrac{A_l}{\sqrt{\pi T_l^2}}\int\limits_{-\infty}^{+\infty}\Psi(\tau-\bar{\tau}_l-x)\exp\left(-\tfrac{x^2}{T_l^2}\right)dx.$$

In particular, for LFM-pulse (14), using of Poisson integral we obtain

$$\int\limits_{-\infty}^{+\infty}\exp\left(-\tfrac{(\Delta\tau+x)^2}{\tau_\xi^2}\right)\cos\omega_0(\Delta\tau+x)\exp\left(-\tfrac{x^2}{T^2}\right)dx =$$
$$= \sqrt{\tfrac{\pi\tau_\xi^2}{1+(\tau_\xi/T)^2}}\exp\left(-\tfrac{(\Delta\tau_\iota/T)^2+(\omega_0\tau_\xi/2)^2}{1+(\tau_\xi/T)^2}\right)\cos\omega_0\Delta\tau\tfrac{(\tau_\xi/T)^2}{1+(\tau_\xi/T)^2}.$$

So, for the pulse with the coherence function (15)

$$K_1(\tau) = \tfrac{1}{T_0}\bar{M}\bar{\alpha}\sqrt{\beta_{nr}}\exp\left(-\beta_{nr}\left(\left(\tfrac{\tau-\mathcal{T}_0}{\tau_\xi}\right)^2+\left(\tfrac{\omega_0 T_{nr}}{2}\right)^2\right)\right)\times$$
$$\times\cos\omega_0\beta_{nr}(\tau-\mathcal{T}_0),$$
$$K_2(\tau) = \tfrac{1}{T_0}\sum_l A_l\sqrt{\beta_l}\exp\left(-\beta_l\left(\left(\tfrac{\tau-\bar{\tau}_l}{\tau_\xi}\right)^2+\left(\tfrac{\omega_0 T_l}{2}\right)^2\right)\right)\times \qquad (21)$$
$$\times\cos\omega_0\beta_l(\tau-\bar{\tau}_l),$$
$$\beta_{nr}\equiv\tfrac{\tau_\xi^2}{\tau_\xi^2+T_{nr}^2},\ \beta_l\equiv\tfrac{\tau_\xi^2}{\tau_\xi^2+T_l^2}.$$

From this formulas it can be seen, that the maximal value of the correlative moment $K_2(\tau)$ for one pulse is achieved where $\tau=\bar{\tau}$. If the differences in pulses time delays are greater then the time of pulse correlation τ_ξ, then the function $K(\tau)$ has the sequence of local extrema at points $\bar{\tau}_l$:

$$K(\bar{\tau}_l)\cong\tfrac{\langle A_l\rangle}{T_0}\sqrt{\beta_l}\exp\left(-\beta_j\left(\tfrac{\omega_0 T_l}{2}\right)^2\right).$$

The only exception of it is the range of delays, that are closed to the mean time delay of irregular pulses $\tau \cong \mathcal{T}_0$, when these pulses contribution into the correlative function is compared with the regular pulses contribution.

So, we can get the information about time delay fluctuations of pulses with different time delays by the searching of this function local extrema (that are disposed in different pulse volumes). The similar way to extract of the information about the local inhomogeneities, situated in these volumes.

3 Tomographic schemes

Let we assume that the vertically-distributed receiving array with n hydrophones. Suppose that we know of the time delays $\boldsymbol{\mathcal{T}} = \left\{ \tau_{ki}^{(0)},\ i = \overline{1, i_k} \right\}_{k=1}^{n}$ for all pulses arriving to every hydrophone. Random perturbations of the refractive index lead to small random variations of these delays $\boldsymbol{\mathcal{T}}^{\varepsilon} = \left\{ \tau_{ki}^{(\varepsilon)},\ i = \overline{1, i_k} \right\}_{k=1}^{n}$. Because of small sizes of the observed local inhomogeneities the variations will be received only by finite number of hydrophones (which are situated on the rays passing of the inhomogeneities). Due to this, it is possibilities to reconstruct of the local inhomogeneities.

The process of reconstruction can be presented as the procedure with the following steps:

- the determination of the number of local inhomogeneities;
- the localization of the probable regions of their concentration;
- the estimation of the parameters of each inhomogeneity.

3.1 Discussion of the equations

According to the mathematical formulation of the problem, for the statistical moments $\Xi(\mathbf{r}), \Phi(\mathbf{r}_1, \mathbf{r}_2)$ of the time delay random fluctuations we have from (9) the following systems of the integral-functional equations

$$\langle \tau_{ki}^{\varepsilon} \rangle = \int_0^{l_{ki}} \Xi(\mathbf{r}_{ki}(l))\, dl,$$

$$T_{ki}^2/2 = \int_0^{l_{ki}} \int_0^{l_{ki}} \Phi(\mathbf{r}_{ki}(l_1), \mathbf{r}_{ki}(l_2))\, dl_1 dl_2 \quad \left(k = \overline{1, n},\ i = \overline{1, i_k}\right)$$

(index k relates to hydrophone, i - to the ray, connecting it with the source $\left\{\mathbf{r} = \mathbf{r}_{ki}(l), l = \overline{1, l_{ki}}\right\}$).

Consider the first of the systems. In more general case the appropriate mathematical problem can be formulated as follows: *let* $\left\{\mathbf{r}_i(l) : [0, l_i] \to R^3, \quad i \in I\right\}$ *be a given set of continuous functions,* $\left\{\beta_i, l_i > 0, \ i \in I\right\}$ *- given set of real numbers (I - finite or infinite index set); it is necessary to find the continuous function* $\Xi(\mathbf{r}) : R^3 \to R^1$, *for which*

$$\int_0^{l_i} \Xi(\mathbf{r}_i(l))\, dl = \beta_i, \ i \in I.$$

The formulated system of the equations are of integral-functional type. In the above general formulation the solution of the problem is unknown. But if we restrict the set of all possible solutions to only set of analytical functions, then the problem can be reduced to the classical problems of the functional analysis.

Consider the case $\mathbf{r} \in R^2$ for the simplicity. After parametrization of the ray by the longitudinal coordinate x

$$\mathbf{r}_i(x) = (x, z_i(x)), \ x \in [0, X]$$

the equations (27) can be rewritten as

$$\int_0^X \Xi(x, z_i(x))\ \alpha_i(x)\, dx = \beta_i, \ i \in I,$$

$$\alpha_i(x) \equiv \sqrt{1 + z_i'^2}.$$

By expanding of unknown function $\Xi(x, z)$ into a power series

$$\Xi(x, z) = \sum_{k,l=0}^{\infty} t_{kl} x^k z^l \tag{22}$$

we can reduce system (27) to the linear system with infinite number of unknowns $\{t_{kl}\}$ and the set of equations, numbered by index $i \in I$:

$$\begin{aligned} &\sum_{k,l=0}^{\infty} t_{kl} p_{kl}^{(i)} = \beta_i, \ i \in I, \\ &p_{kl}^{(i)} \equiv \int_0^X x^k z_i^l(x)\ \alpha_i(x)\ dx. \end{aligned} \tag{23}$$

This problem is well known in functional analysis [21, p. 264] as the "moments problem": *to find a linear functional (vector)* $\mathbf{t} \equiv \{t_{kl}\} \in l_2$, *taking given values* β_i, $i \in I$ *on the given set of vectors* $\mathrm{P} = \left\{\mathbf{p}^{(i)} \equiv \left\{p_{kl}^{(i)}\right\} \in l_2\right\}$:

$$\left\langle \mathbf{t}, \mathbf{p}^{(i)} \right\rangle = \beta_i, \; i \in I. \tag{24}$$

Dividing if it is necessary each of equations (24) by the norm vector $\mathbf{p}^{(i)}$ and making the corresponding change β_i to $\beta_i / \left\|\mathbf{p}^{(i)}\right\|$, we can always consider the set of these vectors as normalized one: $\left\|\mathbf{p}^{(i)}\right\|^2 = \sum\limits_{k,l=1}^{\infty} \left(p_{kl}^{(i)}\right)^2 = 1$, $i \in I$. Next, applying if necessary, the orthogonalizing process, we can always consider this set as the orthogonal one P.

The geometrical meaning of the system (24) is in searching of vector $\mathbf{t} \in l_2$, having the given projections on the given directions $\mathbf{p}^{(i)}$. As we can easily see for orthonormal set P of the solution it has the form

$$\mathbf{t} = \sum_{i \in I} \beta_i \mathbf{p}^{(i)} + \mathbf{t}_{\perp}, \tag{25}$$

where $\mathbf{t}_{\perp}$ is an arbitrary orthogonal to the set P vector. So, if the closure of the linear span of this set doesn't coincide with the hole space, the problem solution is unique. Otherwise, where the set P is full in l_2, the only solution of the problem has the form

$$\mathbf{t} = \sum_{i \in I} \beta_i \mathbf{p}^{(i)}. \tag{26}$$

From theoretical point of view it gives the complete solution of the problem (23). The unknown vector is represented by the formula (22), where the coefficients t_{kl} form the vector $\mathbf{t}$, which can be found from (25). The vector set P must be preliminary normalized and orthogonalized. The problem solution is unique, if this set is full in l_2. Particularly, it must be infinite.

As for the initial problem (27), for the determination of function $\Xi(x, z)$, we need to have an infinite number of rays for the time delays measuring. As it is impossible in practice, one must refuse to solve the problem in general form (27) and focus to more special formulations, using the information about the problem solution.

Let, for example, we consider the local inhomogeneity model (6). The equation system (27) in this case can be reduced to

$$\varepsilon_0 \int_0^X \vartheta\left(\mathbf{r}_i(x) - \mathbf{r}^*\right) \alpha_i(x)\, dx = \beta_i, \; i \in I. \tag{27}$$

Unknown parameter ε_0 can be easily excluded from the system after dividing of the equations by one of them, the first, for example,

$$\int_0^X \left(\beta_i \vartheta\left(\mathbf{r}_1(x) - \mathbf{r}^*\right) \alpha_1(x) - \beta_1 \vartheta\left(\mathbf{r}_i(x) - \mathbf{r}^*\right) \alpha_i(x)\right) dx = 0, \quad i \in I. \tag{28}$$

The unknown in this system is the function $\vartheta(\mathbf{r})$, describing the inhomogeneity spacial distribution in respect of its central point $\mathbf{r}^* \equiv (x^*, z^*)$ (which is also unknown). Taking into account the local nature of the inhomogeneity, we can easily approximate this function in the neighborhood of zero by the function with small number of free parameters. The simplest case of such approximation is Gaussian one (8) with only one parameter σ - the spherical inhomogeneity size:

$$\vartheta(\mathbf{r}) = \exp\left(-\frac{\|\mathbf{r}\|^2}{2\sigma^2}\right).$$

For this approximation the functional system (27) converts to nonlinear algebraic system for σ and $\mathbf{r}^*$

$$\begin{gathered} \beta_i \Phi_1(\sigma, \mathbf{r}^*) = \beta_1 \Phi_i(\sigma, \mathbf{r}^*), \; i \in I, i \neq 1 \\ \Phi_i(\sigma, \mathbf{r}^*) \equiv \int_0^X \exp\left(-\frac{\|\mathbf{r}_i(x) - \mathbf{r}^*\|^2}{2\sigma^2}\right) \alpha_i(x)\, dx. \end{gathered} \tag{29}$$

The solvability of the last system depends from the number of equations. If it less than three, the solution is not unique. If it greater than three, the system becomes overdetermined and (as β_i are known only approximately) does not have solution in general case. So one can find only the generalized solution of the system. It can be constructed by means of different schemes. For example, one can find parameters, for which the residual function

$$f(\sigma, \mathbf{r}^*) = \sum_{i \in I} \left(\beta_i \Phi_1(\sigma, \mathbf{r}^*) - \beta_1 \Phi_i(\sigma, \mathbf{r}^*)\right)^2$$

is minimal.

Also one can chose from the set of all equations (29) only three equation, which are corresponding to maximal values of the right parts β_i, for example. The solution of the resulting system can be obtained with the

following transformations. If neglect with the ray horizon variations on the inhomogeneity scale, then after calculating of integrals in (29),

$$\beta_i \alpha_1 (x^*) \exp\left(-\frac{(z_1(x^*)-z^*)^2}{2\sigma^2}\right) = \beta_1 \alpha_n (x^*) \exp\left(-\frac{(z_i(x^*)-z^*)^2}{2\sigma^2}\right),$$
$$i = 2,3,4.$$

Taking the logarithm of both sides and excluding σ^2 one can receive the equation

$$\gamma_{41} z_{34}^{(-)} z_{24}^{(-)} z_{23}^{(-)} + \gamma_{42} z_{14}^{(-)} z_{34}^{(-)} z_{31}^{(\dot{-})} + \gamma_{43} z_{14}^{(-)} z_{24}^{(-)} z_{12}^{(-)} = 0,$$
$$z_{ij}^{(-)}(x^*) \equiv z_i(x^*) - z_j(x^*),$$
$$\gamma_{ji}(x^*) \equiv \ln \beta_j \alpha_i (x^*) - \ln \beta_i \alpha_j (x^*)$$

for the coordinate x^*. After numerical solution of this equation one can find other unknowns by formulas

$$z^* = \frac{\gamma_{41} z_{34}^{(-)} z_{34}^{(+)} - \gamma_{43} z_{14}^{(-)} z_{14}^{(+)}}{\gamma_{41} z_{34}^{(-)} - \gamma_{43} z_{14}^{(-)}}, \quad \sigma^2 = \frac{z_{14}^{(-)} \left(z_{14}^{(+)} - z^*\right)}{\gamma_{41}},$$
$$\varepsilon_0 = \beta_1 / \Phi_1 (\sigma, x^*, z^*).$$

3.2 Local inhomogeneities parameters estimation

Presented in the previous section methods assume the full reconstruction of the moment function $\vartheta(\mathbf{r})$. But in practice the considerations can be restricted only by more special questions. They are, for example, the number the location of the inhomogeneities and their sizes. Some of the results in this direction are represented in next sections.

Geometrical method of localization The problem of the local inhomogeneities number determination is, really, of pure geometrical type. Initially, the ray trajectories in nonperturbed volume can be calculated in advance. Neglecting of its variances in perturbed volume, one can find the regions, associated with intersection of the rays, which bring the pulses with perturbed time delays of pulses. These regions are suspected for containing of the local inhomogeneities.

This problem is of not trivial kind in multiray situation, where the number of inhomogeneities is also unknown. Further obstruction is the random mistakes in time delays. Consequently, this problem solution can be obtained only in probabilistic form. For example, one can choose the probability density (the localization function $F_{loc}(\mathbf{r})$) of the inhomogeneities presence

in the region. Modes (i.e. the local extrema) of this function can be accepted as possible regions of inhomogeneities localization. Accordingly, the modes number gives the estimation of the local inhomogeneities number.

Consider the following estimation procedure of the described above parameters. For every hydrophone of the receiving array (on the horizon z) and every arriving to this hydrophone pulse let $p_l(z)$ be the probability of the time delay variation (in consequence of the volume perturbation by local inhomogeneities). This probability depends from the local inhomogeneities size, its location with respect the pulse trajectory, the intensity of pulse, the antenna systems etc. Methods of this probability estimation may be different and do not affect on the described procedure. The matrix of probabilities $\|p_l(z)\|$ is the base on which the localization function $F_{loc}(\mathbf{r})$ will be calculated.

The calculation of this function is performed as follows. Let we separate the observation region on the set of small elements Ω_{ij}. For central point $\mathbf{r}^*$ of the element Ω^* let calculate all energetic rays passing through it and find its horizons z_l in the receiving array cross-section. Then we can determine the number of rays, for which the corresponding probabilities $p_l(z)$ are larger than some fixed level (0.5, for example) and subtract from it the number of the rays, for which the probabilities are less than this level: $B_1(\mathbf{r}^*) = \Sigma_l(-1)^{i_l}$. After normalizing of the received function $B_1(\mathbf{r})$, we can obtain the function

$$F_{loc}(\mathbf{r}) = \frac{\max(B(\mathbf{r}), 0)}{\iint \max(B(\mathbf{r}), 0)\, d\mathbf{r}}.$$

At points of local inhomogeneities location this function would have the local extrema. Really, for all rays passing such points the probabilities $p_l(z)$ would be high, so with high probability the function $B_1(\mathbf{r})$ in these points would be equal to numbers of passing rays.

There can be the local extrema of this function, which is not associated with the local inhomogeneity. For all points of inhomogeneity, which are intersecting by the ray, the value $p_l(z)$ is the same. So, for all such points the localization function will have the local extrema. But the probability, that other rays, passing these points, intersect of local inhomogeneities are not big. Hence, the corresponding extrema would not be the same large, because these other rays will give a negative contribution to the sum B_1.

As the false local extrema are situated on the rays, connecting the source and the receiver, then after summation of the localization functions for the different sources the main extremum (wich are the same for all functions) would increase, while the other extrema (because they are different) would

decrease. The other possible criterium is associated with the local extremum movement while the source of probing waves location changed.

Estimation of the generalized sizes Let the ray connecting the source with a fixed hydrophone, propagates through the central point $\mathbf{r}^*$ of local inhomogeneity of the space scales σ_x, σ_z. For the hydrophone on the vertical distance h from this central point we have from (6,7) the time delay shift

$$\begin{aligned}
\tau^\varepsilon(h) &= \varepsilon_0 \int_0^X \vartheta\left(\mathbf{r}_h(x) - \mathbf{r}^*\right) \sqrt{1 + \left(z_h'(x)\right)^2}\, dx = \\
&= \varepsilon_0 \int_0^X \vartheta\left(x - x^*, z_h(x) - z^*\right) \sqrt{1 + \left(z_h'(x)\right)^2}\, dx \cong \\
&\cong \varepsilon_0 \sqrt{1 + \left(z_0'(x^*)\right)^2} \int_0^X \vartheta\left(x - x^*, z_h(x^*) - z^*\right)\, dx \cong \\
&\cong \varepsilon_0 \sqrt{1 + \left(z_0'(x^*)\right)^2} \int_0^X \vartheta\left(x - x^*, q(x^*)\, h\right)\, dx \cong \\
&\cong \varepsilon_0 \sqrt{1 + \left(z_0'(x^*)\right)^2} \int_{-\infty}^{+\infty} \vartheta\left(x - x^*, q(x^*)\, h\right)\, dx,
\end{aligned} \tag{30}$$

where the vector-function $\mathbf{r}_h(x)$ describes the trajectory C_h of the ray, connecting the source and the hydrophone at point h, X is the distance between the source and the receiving array system, $q(x^*) = \frac{d}{dh} z_h(z^*)$. In particular,

$$\begin{aligned}
\tau^\varepsilon(0) &\cong \varepsilon_0 \sqrt{1 + \left(z_0'(x^*)\right)^2} \int_{-\infty}^{+\infty} \vartheta\left(x - x^*, 0\right)\, dx = \\
&= \varepsilon_0 \sqrt{1 + \left(z_0'(x^*)\right)^2} \sqrt{2\pi}\sigma_x
\end{aligned}$$

By integration of the function

$$\delta\tau(h) \equiv \frac{\tau^\varepsilon(h)}{\tau^\varepsilon(0)} \cong \frac{1}{\sqrt{2\pi}\sigma_x} \int_{-\infty}^{+\infty} \vartheta\left(x - x^*, q(x^*)\, h\right)\, dx$$

in the neigborhood of $h = 0$, we obtain

$$\langle \delta\tau(h) \rangle \equiv \int_{-\infty}^{+\infty} \delta\tau(h)\, dh \cong \frac{1}{\sqrt{2\pi}\sigma_x} \int_{-\infty}^{+\infty}\int_{-\infty}^{+\infty} \vartheta(x - x^*, q(x^*)\, h)\, dx dh =$$

$$= \frac{1}{\sqrt{2\pi}\sigma_x q(x^*)} \iint_{-\infty}^{\infty} \vartheta(\mathbf{R})\, d\mathbf{R} = \frac{\bar{\sigma}}{q(x^*)},$$

$$\bar{\sigma} \equiv \sqrt{2\pi}\frac{\sigma^2}{\sigma_x}.$$

The value $q(x^*)$, depending only on the central ray, one can express with the focusing factors of the beam F and F^* at distances X and x^*, respectively. Really, for small h

$$|h| \cong \frac{c_S}{c_R}\frac{X}{F}|\Delta\theta|,$$

where $|\Delta\theta|$ is the difference of ray angles at the source, $c_{S,R}$ are the sound speeds at the corresponding points. Similar,

$$|z_h(x^*) - z^*| \cong \frac{c_S}{c^*}\frac{x^*}{F^*}|\Delta\theta|,$$

so

$$|z_h(x^*) - z^*| \cong \frac{c_S}{c^*}\frac{x^*}{F^*}\frac{c_R}{c_S}\frac{F}{X}|h| = \frac{c_R}{c^*}\frac{F}{F^*}\frac{x^*}{X}|h|,$$

and

$$|q(x^*)| \cong \frac{c_R}{c^*}\frac{F}{F^*}\frac{x^*}{X}$$

$$= \frac{c_R F}{X} : \frac{c^* F^*}{x^*} \equiv \nu(X) : \nu(x^*),$$

where

$$\nu(x) \equiv \frac{c(z(x))\, F(z(x))}{x}$$

is the function of the current point of the ray.

For homogeneous environment $c(z(x))\, F(z(x)) = \text{Const}$, so $|q(x^*)| = x^*/X$.

If the coordinate x^* is known (it can be estimated by the geometrical analyzing – see the previous section), then it is possible to estimate the generalized size of the local inhomogeneities by formula

$$\bar{\sigma} = |q(x^*)\, \langle \delta\tau(h) \rangle|.$$

The similar formula can be used also for the local inhomogeneity coordinates determination. For example, measuring of this integral values

for two, passing trough the local inhomogeneity $\langle \delta\tau(h) \rangle_{1,2} = \sigma / q_{1,2}(x^*)$ different rays, it is possible to exclude the unknown scale $\bar{\sigma}$:

$$\frac{\langle \delta\tau(h) \rangle_2}{\langle \delta\tau(h) \rangle_1} = \frac{q_1}{q_2}(x^*) = \pm \frac{F_2}{F_1}(x^*).$$

If we know the ratio of focusing factors as the function of x, we can find from this equation the unknown coordinate x^*.

If the local inhomogeneities is unique, then after integration of function $\delta\tau(h)$ over the vertical cross-section of receiving array system we obtain the integral value

$$\langle \delta\tau(h) \rangle = \frac{\bar{\sigma}}{\sum\limits_l q_l(x^*)} = \frac{\bar{\sigma}}{\bar{q}(x^*, z^*)},$$

where

$$\bar{q}(x^*, z^*) \equiv \sum_l q_l(x^*) = \\ = \frac{x^*}{Xc(z^*)} \sum_l \frac{c(z_l(X))F_l(X)}{F_l(x^*)}$$

is the summary value for all rays l, passed trough central point $(x^*, z_l(x^*) \equiv \equiv z^*)$ of the local inhomogeneity. For the given source, the function $q(x^*, z^*)$ can be calculated previously as the waveguide parameter. For excluding of the unknown parameter σ non depending from it ratio

$$\frac{\langle \delta\tau(h) \rangle_1}{\langle \delta\tau(h) \rangle_2} = \frac{q_1(x^*, z^*)}{q_2(x^*, z^*)}, \tag{31}$$

two different receiving array systems can be used. The right part of the next equality

$$q_{12}(x^*, z^*) \equiv \frac{X_2}{X_1}$$

also depends only from the source and can be calculated a priori. So, (31) can be used for the rough estimation of the coordinates (x^*, z^*) of the local inhomogeneity.

4 Computer simulation

Numerical experiment, realizing the described above procedure of inhomogeneities localizing, were made for bilinear waveguide with the sound profile[1]

[1]Here and below all linea values are presented in kilometers, the time - in seconds.

z	c(z)
0	1.50
-0.2	1.47
-3	1.55

After splitting of the waveguide into elementary cells the calculation of rays, passing trough center points of the cell, was made. The matrix of probabilities $||p||$ of the local inhomogeneities were defined for rays detected in the receiving array cross-section. The probability p for the concrete ray was defined by formula

$$p = \exp\left(-d^2\right), \qquad d^2 = \min_{\mathbf{r}=(x,z)\in C} \left(\left(\frac{x-x_n}{\sigma_x}\right)^2 + \left(\frac{z-z_n}{\sigma_z}\right)^2 \right), \tag{32}$$

where d is the distance of the ray C to the central point (x_n, z_n) of the inhomogeneity, σ_x, σ_z are the sizes of the inhomogeneity in the axes directions. If there are many inhomogeneities, then maximal of values (32) was taken as probability p.

Then the matrix elements p_{ij} were disturbed by random values for the following rule: $\tilde{p}_{ij} = \Phi\left(p_{ij} + \sigma_\xi \xi_{ij}\right)$, where ξ_{ij} are independent realizations of the random uniformly distributed in interval $(-1, 1)$ value, σ_ξ is the noise amplitude

$$\Phi(x) \equiv \begin{cases} 1, & x > 1 \\ x, & 0 \le x \le 1 \\ 0, & x < 0. \end{cases}$$

Finally, the calculation of the localization function $F_{loc}(\mathbf{r})$ was made. Its local extrema were compared with the disposition of the local inhomogeneities.

Some results of the numerical simulations are shown in the figures 4 – 6.

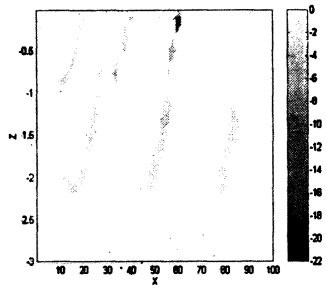

$\sigma_\xi = 0.0$

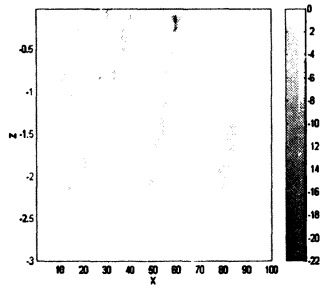

$\sigma_\xi = 1.0$

Fig. 4. One inhomogeneity localization by the system with one source for different noise levels σ_ξ

At the first one, the local inhomogeneity with the central points $(60, -0.1)$, the horizontal 2 and vertical 0.4 sizes was reconstructed. The first series of pictures (see Fig 4) corresponds to graphs of the localization function for one source which was situated in the horizon $z_i = -0.1$.

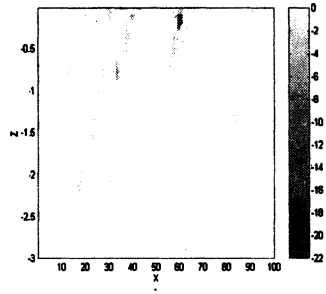

$z_i = \{-0.1; -2.6\}$

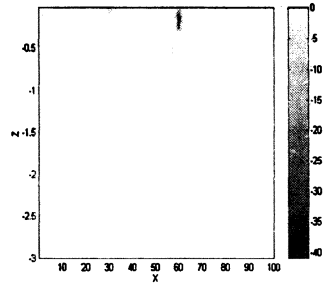

$z_i = \{-0.1; -1; -1.5; -2.6\}$

Fig. 5. Localization of one inhomogeneity by the systems with several sources

As it should be expected, it is possible to improve the quantity of reconstruction (saving other parameters) increasing of the number of source. This result illustrated by the second series of reconstructed images (Fig. 5), where the observation systems are taken with different numbers of sources, but the noise level is fixed $\sigma_\xi = 0.5$.

The similar result of reconstruction was received in the case with the several local inhomogeneities. At the third series of reconstructed images (Fig. 6) where the reconstruction of two inhomogeneities with centers $(35, -0.1), (60, -0.1)$ and sizes $(3, 0.4), (2, 0.4)$, respectively, is represented for the systems with different numbers of sources and zero level of noise.

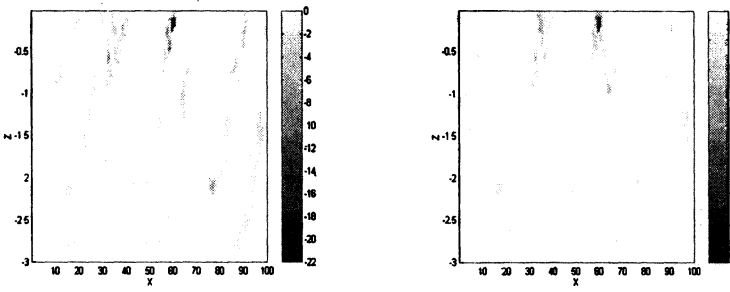

$z_i = \{-0.1\}$ $z_i = \{-0.1; -1.7; -2.5\}$

Fig. 6. Localization of two inhomogeneities by the systems with several sources

5 Conclusions

The possibilities for random spatially-localized inhomogeneities (such as the cloud of bubbles or the fish shoals) were investigated in this work for random inhomogeneous oceanic environment. It was assumed that the surface of ocean was perturbed by the wind waves and the volume of ocean is characterized by the uniformly distributed random fluctuations of sound speed. As the probing signals, the LFM-pulses were used. The receiving system was constructed as the vertically distributed array of hydrophones.

The result of investigations can be formulated as the following: Tomographic reconstruction of spatially-localized random

inhomogeneity parameters can be reduced to solution of the system of the integral-functional equations. The solution of such equations can be effective only by using of a priori information concerns of the problem in form of the models for: the observed object, the oceanic environment as well as the observation system. In our investigation the appropriate physical model of observation object was developed as the three dimension cloud of

random perturbation of oceanic environment refractive index with statistical characteristics differ from the similar characteristics associated with the uniformly distributed fluctuations of oceanic volume.

It is shown that the presence of localized inhomogeneities leads to the appearance of the additive random shifts of the time delays of received pulses. The measurement of the statistical moments of the random time delay shifts gives of the possibilities for tomographic reconstruction.

It was demonstrated that, in fact, the reconstruction is impossible if the inhomogeneities are located in the region with small values of translation function. Translation functions, the small parameters models of problem and the additive tomographical projections arising due to movements of probing signals source were used for solution of the problems associated with optimal searching of solution.

6 Acknowledgments

This work was supported by Russian Foundation of Fundamental Investigations, Grant N 97-02-17536. It was also supported, in part, by the Ocean Acoustics Program (Code 321) and the European Office of the US Office of Naval Research.

References

[1] Farmer D. and Ding L. *Coherent Acoustical Radiation from Breaking Waves.* // JASA. July 1992. 92(2). PP. 397-402

[2] Kerman B.R. *Underwater Sound Generation by Breaking Wind Waves* // JASA. January 1984.V.75(10). PP. 149-165.

[3] Goncharov V.V., Zaicev V.Yu., Kurtepov V.M. at all. *Acoustic Tomography of Ocean.* 1997. Nizhny Novgorod: IAP RAS. 254 p.

[4] Gregg R.F. D. Wurmser. *Low-Frequency Scattering From Intermediate Bubble Plume: Theory and Computerized Parameter Study* // JASA. July 1993. V.94(1). PP. 319-329.

[5] Caruthers J., Khil'ko A.I., Smirnov I.P. *Tomographic Reconstruction of Ocean Inhomogeneities.* Part 1: *Forming Partially Coherent Acoustic Wave Structures in the Ocean with Spatially Localized Noise Sources* / October. 1995. Proc. OCEANS'95. San Diego. PP. 1569-1573.

[6] Abrosimov D.I., Caruthers J., Khil'ko A.I. *Tomographic Reconstruction of Ocean Inhomogeneities.* Part 2: *Applications of Partially Coherent Acoustic Wave Structures to Fresnel Diffraction and Differential Tomography* / October. 1995. Proc. OCEANS'95. San Diego. PP. 1574-1578.

[7] Isakovich M.A. *General Acoustics.* Moscow: Nauka. 1973.

[8] Gorunov A.A. and Saskovetz A.V. *Inverse Scattering Problem in Acoustics.* Moscow. Moscow University. 1989. 151 p.

[9] Tihonov A.N., Arsenin V.Ja., Timonov A.A. *Mathematical Problems of Computerized Tomography.* Moscow. 1987.

[10] Zverev V.A. *Radiooptics.* Moscow: Sovetskoe radio.1975.

[11] Zverev V.A. *Physical Fundaments of Images Construction by Wave Fields.* Nizhni Novgorod. IAP RAS. 1998. 250 p.

[12] Borodina E.L., Khil'ko A.I., Zverev V.A. at all. *Formation of Multiview Images in Oceanic Waveguides by the Dark-Field Method.* In book "*Forming of Acoustical Fields in Ocean Waveguides. Reconstruction of Inhomogeneities*". 1994.Nizhny Novgorod: IAP RAS. PP. 169-202.

[13] Smirnov I.P., Zorin A.Yu., Khil'ko A.I. *About the Choice of Parameters for System of Acoustic Imaging.* In book "*Forming of Acoustical Fields in Ocean Waveguides. Reconstruction of Inhomogeneities*". 1994.Nizhny Novgorod. IAP RAS. PP. 214-247.

[14] Kravtsov Yu.A., Orlov Yu.I. *Geometrical Optics of Inhomogeneous Media.* Moscow: Nauka. 1980.

[15] Brekhovskikh L.M. and Lysanov Yu.P. *Theoretical Fundamentals of Oceanic Acoustics.* Moscow: Gidrometeoizdat. 1982. 264 p.

[16] Smirnov I.P., Caruthers J.W. and Khil'ko A.I. *Multiscale Coherence of the Acoustic Field of a Noise Source in Randomly Inhomogeneous Ocean.* In book: *The Formation of Acoustical Fields in Oceanic Waveguides. Coherence Phenomena.* Ed. by Zverev V.A. 1997. Nizhny Novgorod: IAP RAS. PP. 71-113.

[17] Zorin A.Yu., Smirnov I.P. and Khil'ko A.I. *The Characteristics of Energetic Coupling of the Inhomogeneous Environment Points* // Izv.VUZov - Radiofizika. 1993. V. 36. No 8. PP. 767-770.

[18] Goncharov V.V. and Kurtepov V.M. *Formation and Propagation of Weakly Diverging Bundles of Rays in a Horizontally Inhomogeneous Ocean* // JASA. 1994. V. 40. N 5. PP. 773-781.

[19] Ritov S.M., Kravtsov Yu.A. and Tatarsky V.I. *Introduction to Statistical Radiophysics.* Part II "*Random Fields*". Moscow. Nauka. 1978. 464 p.

[20] Pierson W.J., Moskovitz L. *A Proposed Spectral form for Fully-Developed Wind Seas Based on the Similarity Theory of S.A. Kitaygorodsky* // J. Geophys. Res. 1964. V.69. N 24. PP. 5180-5190.

[21] Kantorovich L.V., Akilov G.P. *The Functional Analysis.* Moscow. Nauka. 1977. 742 p.

[22] Smirnov I.P., Caruthers J.W., Khil'ko A.I. and Elmore P.A. *Emission Tomography Reconstruction of the Bubble Plumes Entrained by Breaking Wind Waves* In book*: The Formation of Acoustical Fields in Oceanic Waveguides. Reconstruction of Inhomogeneities in Shallow Water.* Ed. by Zverev V.A. 1998. Nizhny Novgorod: IAP RAS.

ACOUSTIC TRANSMISSION FLUCTUATIONS FROM THE BARENTS SEA: OBSERVATION AND NUMERICAL MODELING

A. L. Matveyev, A. G. Sazontov, and N. K. Vdovicheva

Introduction

During the recent two decades extensive theoretical attention has been focused on the problem of acoustic coherence in deep water environments Analytical predictions have been compared with relative success to a number of experimental results. The state-of-the-art in this field of knowledge was summarized in the review article by Gorodetskaya *et al.* [1].

The shallow water acoustic propagation is known to face the difficulties that are not encountered in deep–water waveguides [2, 3]. The most striking feature here are the bottom interactions. These interactions cause significant mode stripping: after sufficiently long range higher modes have been attenuated by a loss bottom and only the first mode propagates. Therefore, the behavior of the acoustic mutual coherence function (MCF) in shallow water may be fundamentally different from the corresponding MCF behavior for a deep–water situation. Since bottom effects radically modify the acoustic transmission, any realistic propagation theory in shallow water environments should include them. It is worth commenting that there are a few papers [3–5], which give predictions only for modal intensity fluctuations in such a situation. Moreover, no detailed comparisons between measured and predicted shallow water acoustic coherence has been reported.

A considerable progress in modeling acoustic propagation in a shallow water channel where bottom interactions are important has recently been achieved in Ref. [6]. Here, a general computer program based on the radiation transport equation technique has been developed to implement the theory for describing the fluctuation phenomena caused by fully developed wind seas. In this context, experimental data are of a great interest for validation of the theoretical estimations presented in Ref. [6].

In this paper we report on the fluctuations observed in the Barents Sea and compare the measured vertical coherence with theoretical predictions. The body of this paper is organized as follows. In Sec. 1 we give a short description of the experiment conducted in the Barents Sea, including measured environmental information. Next, in Sec. 2 we report some experimental results of CW measurements of acoustic transmission fluctuations in the region of the experiment. In Sec. 3, using a modal formulation we present

a basic numerical model that allows for estimation of the MCF of vertical separation. Here, the observed spatial coherence of the received signal is compared with the theoretical predictions based on wind seas scattering. Finally, in Sec. 4 we summarize the key results.

1. Description of the experiment

The experiment was performed in the Barents Sea in October of 1990 during the 7-th expedition of the scientific research vessel "Academician Sergey Vavilov" and the 4-th expedition of the scientific research vessel "Academician Ioffe". One of the objectives of this experiment was to measure and determine the nature of acoustic transmission fluctuations in realistic shallow water environments in the 100 – 250 Hz frequency range.

The experiment was conducted in the area characterized by a flat bottom covered with sand–clay sediments. The propagation conditions were downward refracting conditions. A typical season sound speed profile in the region of the experiment is shown in Fig. 1.

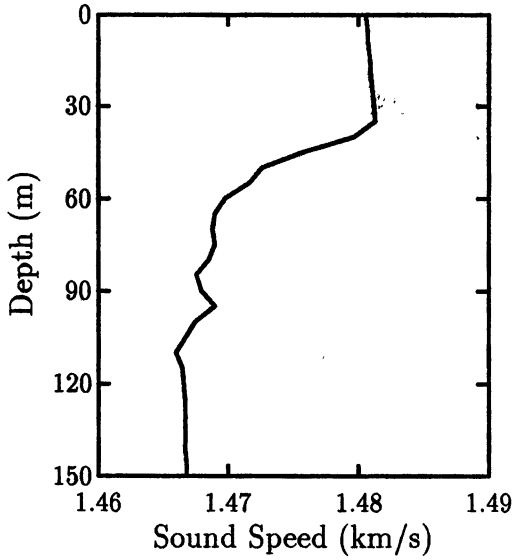

Fig. 1. Sound speed profile from the Barents Sea in the region of the experiment

As seen in Fig. 1, the water sound–speed profile is a summer profile,

almost isovelocity down to 40 m with a subsequent strong thermocline extending to about 60 m.

The acoustic interactions with the bottom caused significant sound attenuation. The measured bottom attenuation coefficient in the region considered was about 0.4 dB/λ. The wave roughness (wind speed) during the experiment was about 10 ± 2 m/s.

The geometry of the experiment is shown in Fig. 2.

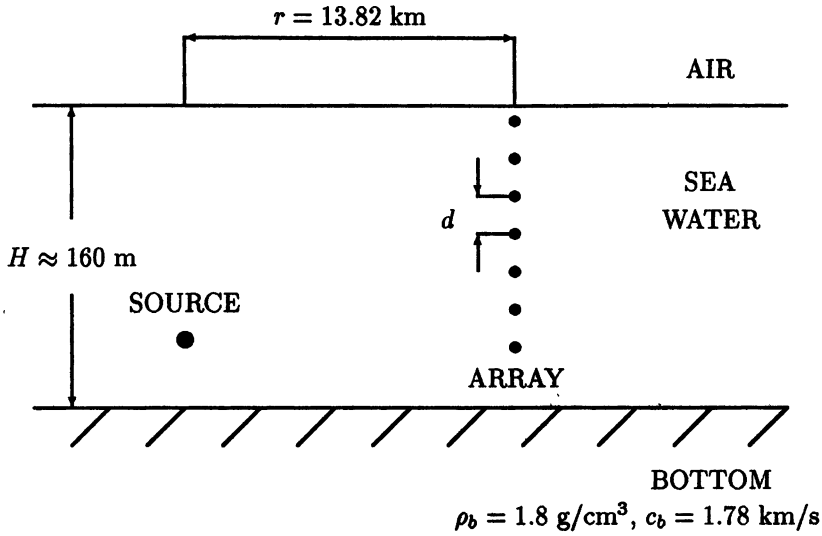

Fig. 2. Experimental geometry (not shown to scale)

Signals of 107 Hz and 240 Hz in the form of continuous waves (CW) from a fixed sound source (located at the depth about 148 m) were employed. The transducers provided the output level referenced to 1 m approximately of 200 dB (1 kW). The signals were received at two vertical arrays separated by approximately 90 m in line perpendicular to the direction of acoustic propagation. The distance between the source and the arrays was 13.82 km. The water depth was measured to be approximately 170 m at the array site. The bathymetry at the source location was measured to be 150 m.

One array (array 1 in what follows) was suspended from board (fixed by anchored barrels). The second one (array 2) was bottom mounted, stretched vertically by an underwater buoy, and covered the channel only partially. Array 1 covered the channel almost completely. However, some of its elements were switched off for some technical reasons. The interelement dis-

tance d was 8.5 m for array 1 and 7.3 m for array 2. The bottom hydrophones for the array considered were at the depths of 155 m and 148.5 m, respectively. For additional details on experimental setup, see Ref. [7, 8].

2. Signal processing and data analysis

For experimental study of the received-signal fluctuations, a characteristic 30 min interval was singled out from the record available. The received CW signals were amplified, filtered with a bandwidth of ± 0.5 Hz, and recorded in the quadrature form.

The sensor signal set at each carrier frequency may be represented by a complex valued array signal vector

$$\mathbf{x}(t_l) = [x_1(t_l), x_2(t_l), \cdots, x_N(t_l)]^T, \qquad \text{for} \quad 1 \leqslant l \leqslant L,$$

where $x_k(t_l)$ designates the value of the k-th sensor signal at the sampling time instant t_l, L corresponds to the number of the time samples, and the superscript "T" denotes the operation of vector transposition. The sample rate was 1 Hz and there were $L = 2056$ sample points. In the analysis to follow, it is assumed that the second–order statistics of the sensor signals do not change significantly in the measurement time interval.

Figure 3 depicts portions of the original graphic recordings of the 107-Hz and 240-Hz CW signals, respectively, showing acoustic pressure (in arbitrary units) versus time. Each portion includes 30 minutes of data for 4 channels of array 1. Figure 4 represents similar graphs for array 2. Analyzing these curves, we can see that in a number of cases there exists a slow, pronounced (in magnitude) variation at the signal level over the time interval selected, which illustrates the nonstationary nature of the propagation conditions. Moreover, the increase of the signal level at one hydrophone can be accompanied by the decrease of the signal level at the neighboring hydrophone of the same array. Note that the temporal reception stability at the higher frequency is somewhat worse.

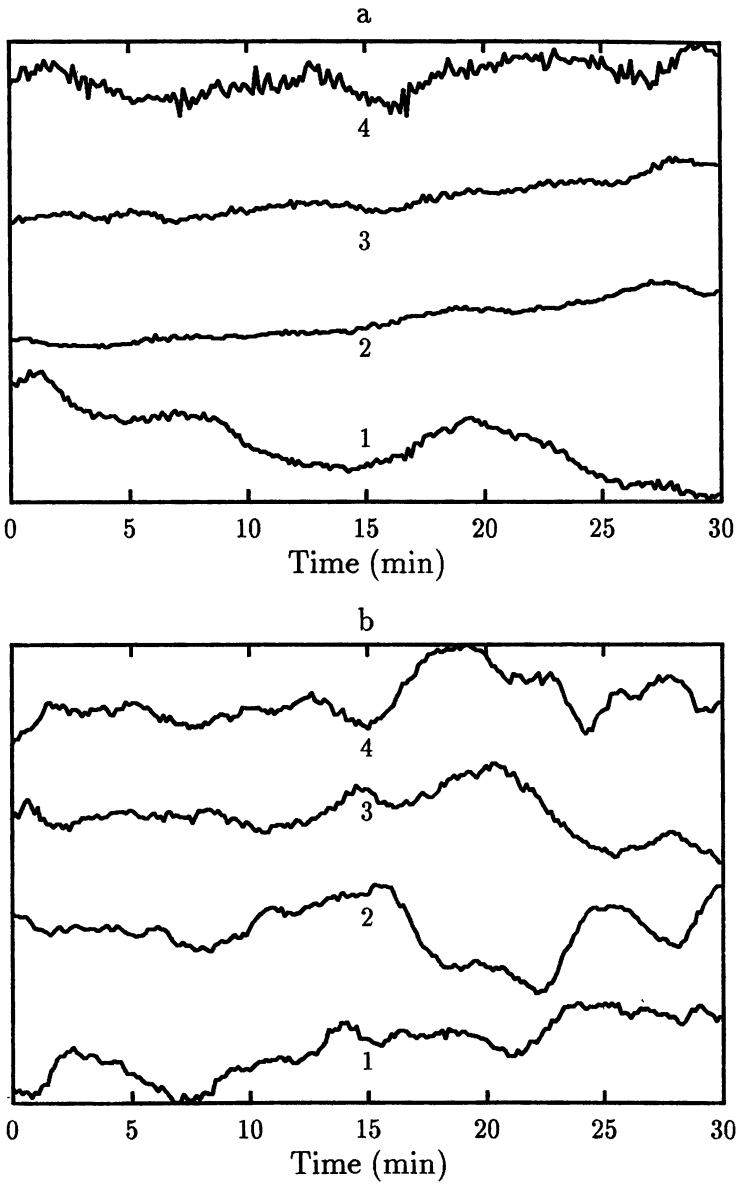

Fig. 3. Time series of the CW amplitudes for 4 channels of array 1 in the 30 min intervals at two selected carrier frequencies: (a) $f_0 = 107$ Hz, (b) $f_0 = 240$ Hz

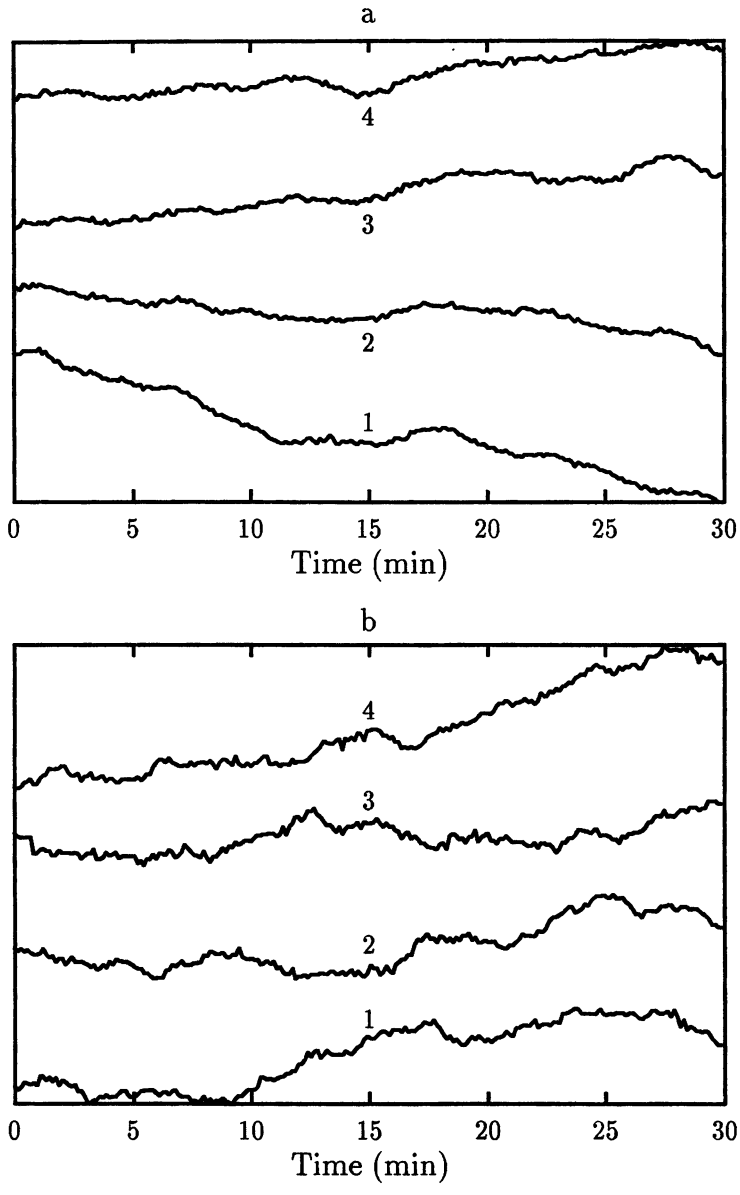

Fig. 4. Time series of the CW amplitudes for 4 channels of array 2 in the 30 min intervals at two selected carrier frequencies: (a) $f_0 = 107$ Hz, (b) $f_0 = 240$ Hz

An intensity time series is formed by

$$I_k(t_l) = |x_k(t_l)|^2 .$$

The graphs shown in Figs. 5, 6 illustrate the behavior of the normalized mean wavefield intensity

$$i_k = \frac{< I_k >}{\frac{1}{N}\sum_{k=1}^{N} < I_k >}, \quad < I_k >= \frac{1}{L}\sum_{l=1}^{L} |x_k(t_l)|^2$$

versus sensor depth for the array considered. (The angular brackets $< \cdots >$ indicate time averaging).

A quantity of some importance is the fluctuation index η. The definition for η is

$$\eta_k = \frac{\sqrt{< I_k^2 > - < I_k >^2}}{< I_k >}. \tag{1}$$

Parameter η is zero in the absence of fluctuations and is equal to 1 in the case of Gaussian statistics of the intensity. The experimental fluctuation indices η_k, Eq. (1), computed as a function of depth sensors are listed in Tables 1 and 2.

In Fig. 7 we plot the power spectra, $S_k(f)$, of the fluctuations observed for the carrier frequency $f_0 = 240$ Hz and two selected array sensor depths. The corresponding quantity is defined as

$$S_k(f) = |FFT\{x_k(t)\}|^2 ,$$

where "FFT" stands for the discrete Fast Fourier Transform. A Hamming filter was used to smooth the spectrum. It is seen from this figure that the frequency spectrum consists of a central peak (at the carrier frequency) corresponding to the coherent component of the registered signal and two lateral peaks corresponding to the scattering component. The spectral density is expressed in dB with respect to the coherent component. The shape of the frequency spectrum is typical of a shallow water environment where rough scattering effects are important.

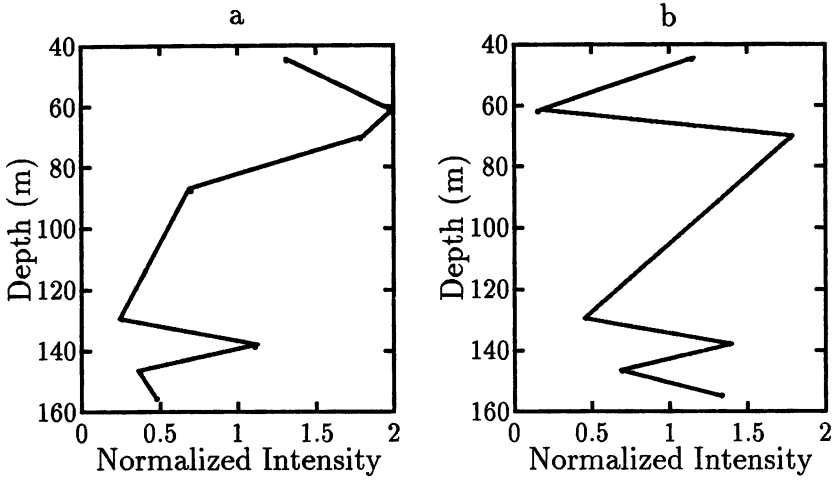

Fig. 5. Magnitude squared of the pressure versus depth along array 1 at (a) $f_0 = 107$ Hz, (b) $f_0 = 240$ Hz

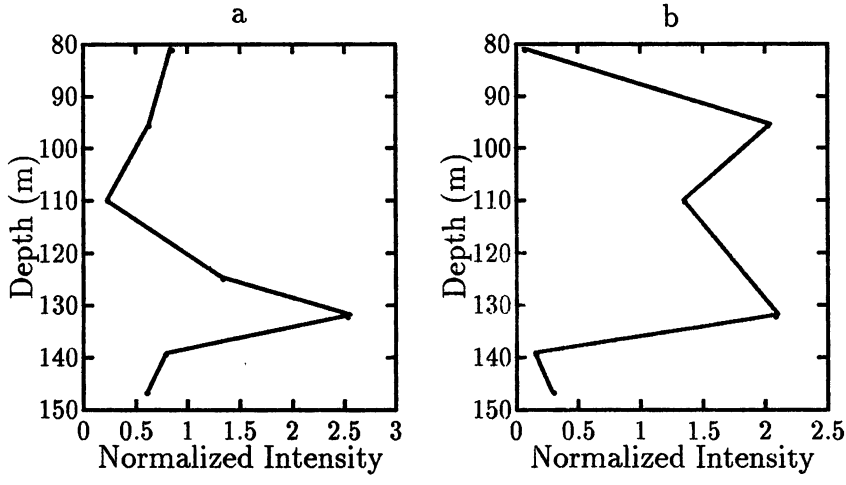

Fig. 6. Magnitude squared of the pressure versus depth along array 2 at (a) $f_0 = 107$ Hz, (b) $f_0 = 240$ Hz

Table 1. Fluctuation index η versus receiver depth for array 1

Receiver depth (m)	Experimental η	
	$f_0 = 107$ Hz	$f_0 = 240$ Hz
44.5	0.22	0.29
61.5	0.11	0.64
70	0.16	0.21
87	0.23	–
129.5	0.36	0.57
138	0.18	0.30
146.5	0.36	0.45
155	0.50	0.36

Table 2. Fluctuation index η versus receiver depth for array 2

Receiver depth (m)	Experimental η	
	$f_0 = 107$ Hz	$f_0 = 240$ Hz
80.8	0.13	0.77
95.4	0.10	0.22
110	0.39	0.67
124.6	0.16	–
131.9	0.13	0.18
139.2	0.16	1.1
146.5	0.53	0.85

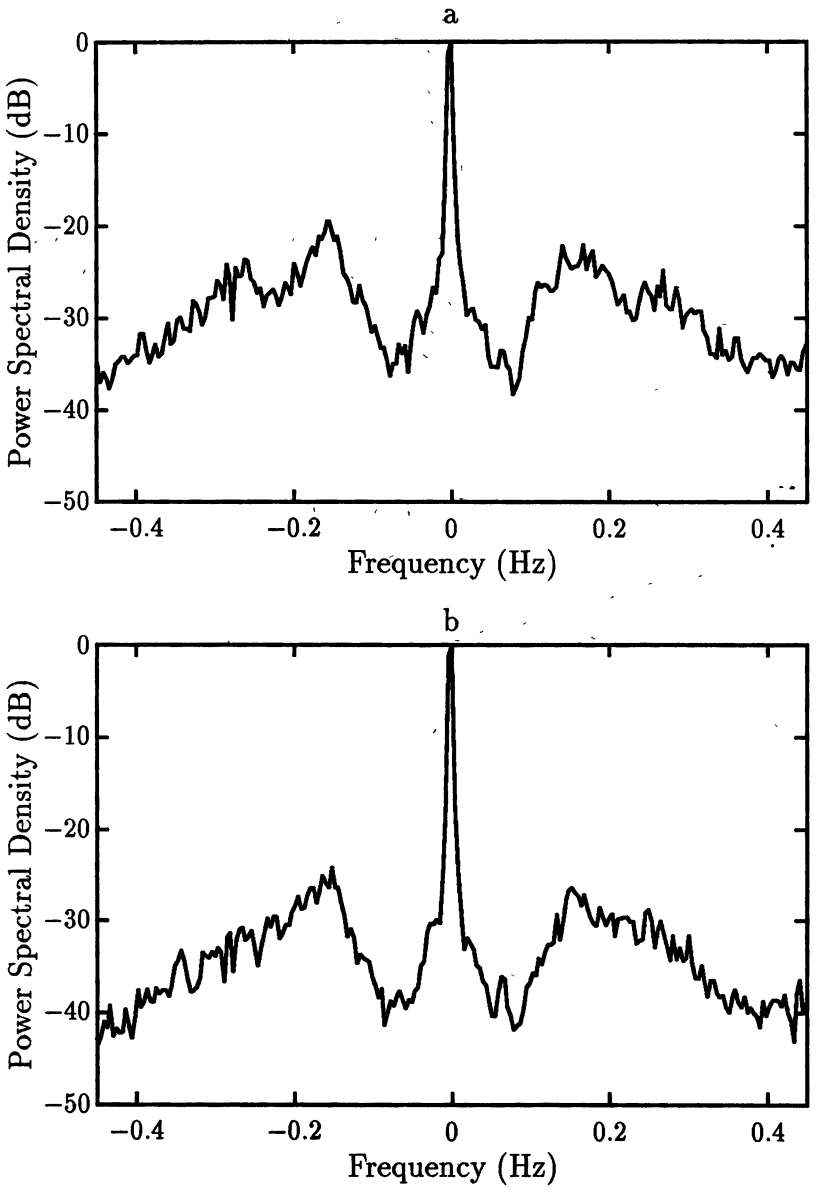

Fig. 7. Spectral density of sound pressure level in dB for two selected receiver depths: (a) $z = 80.8$ m, (b) $z = 139.2$ m

The spatial correlation properties of the received field in the vertical plane are fully determined by the complex coefficient of the correlation between the signal fluctuations at the k-th and j-th hydrophones in the corresponding array. The quantity of interest is defined according to

$$C_{kj} = \frac{\sum_{l=1}^{L} x_k(t_l) \cdot x_j^*(t_l)}{\sqrt{\sum_{l=1}^{L} |(x_k(t_l)|^2 \sum_{l=1}^{L} |(x_j(t_l)|^2}}, \tag{2}$$

where the asterisk denotes complex conjugate. If the data are second–order ergodic, this estimate provides an asymptotically unbiased estimate of the $N \times N$ array correlation matrix. The magnitudes of C_{kj}, Eq. (2), computed between all pairs of sensors are listed in Tables 3 and 4.

Table 3. Absolute values of the correlation coefficient for array 1

$f_0 = 107$ Hz

Depth (m)	155	146.5	138	129.5	87	70	61.5	44.5
155	1.000							
146.5	0.892	1.000						
138	0.877	0.958	1.000					
129.5	0.831	0.896	0.956	1.000				
87	0.906	0.893	0.966	0.933	1.000			
70	0.898	0.934	0.981	0.934	0.986	1.000		
61.5	0.852	0.915	0.974	0.934	0.980	0.985	1.000	
44.5	0.883	0.877	0.946	0.909	0.984	0.975	0.982	1.000

$f_0 = 240$ Hz

Depth (m)	155	146.5	138	129.5	70	61.5	44.5
155	1.000						
146.5	0.934	1.000					
138	0.918	0.914	1.000				
129.5	0.758	0.728	0.831	1.000			
70	0.783	0.838	0.861	0.661	1.000		
61.5	0.545	0.438	0.486	0.202	0.535	1.000	
44.5	0.687	0.588	0.646	0.434	0.730	0.830	1.000

Table 4. Absolute values of the correlation coefficient for array 2

$f_0 = 107$ Hz

Depth (m)	146.5	139.2	131.9	124.6	110	95.4	80.8
146.5	1.000						
139.2	0.965	1.000					
131.9	0.931	0.975	1.000				
124.6	0.925	0.969	0.998	1.000			
110	0.970	0.941	0.948	0.940	1.000		
95.4	0.927	0.976	0.981	0.982	0.917	1.000	
80.8	0.950	0.976	0.986	0.985	0.955	0.988	1.000

$f_0 = 240$ Hz

Depth (m)	146.5	139.2	131.9	110	95.4	80.8
146.5	1.000					
139.2	0.833	1.000				
131.9	0.765	0.614	1.000			
110	0.822	0.761	0.933	1.000		
95.4	0.752	0.641	0.964	0.940	1.000	
80.8	0.224	0.271	0.582	0.517	0.602	1.000

Several conclusions may be drawn from the results presented. First, the vertical coherence depends essentially on the depth location of the sensors because the signal field in shallow water is not constant in the channel and depends on the receiver depth. It is clear that, as the frequency increases, the rate of the coherence loss increases too. This fact, of course, indicates that high frequency scattering occurs at a more rapid rate.

3. Numerical modeling of vertical coherence

In this section, to interpret the measured vertical coherence of acoustic field, a modeling effort is undertaken using a radiation transport equation for multimodal propagation. In this calculations we assume that the random field of wind seas is the dominant source of transmission fluctuations. We suppose the rough surface spectral distribution to be presented by the Pierson–Moskowitz spectrum [9]:

$$F_\eta(æ, \Omega) = \frac{8.1 \times 10^{-3}}{4\pi} æ^{-4} \exp\left(-0.74 \frac{g^2}{æ^2 v^4}\right) \delta\left(\Omega - \sqrt{gæ}\right), \qquad (3)$$

where g is the acceleration of gravity, and v is the wind speed over the ocean surface.

In Ref. [3] the range-independent geoacoustical model was constructed for the experiment considered using only the receiver bathymetry and the sound–speed profile shown in Fig. 1. The environments selected consist of a layer of water $\approx$ 160 m deep overlying a semi–infinite bottom with a constant sound speed of 1780 m/s, density of 1.8 g/cm^3, and attenuation coefficient of 0.4 dB/λ. Below, we present for the given model transport results for a typical wind speed of 10 m/s.

A modal solution for an acoustic pressure field $P(\mathbf{r}, z, t)$ in the random oceanic channel far enough from the source can be formally represented by

$$P(\mathbf{r}, z, t) = \sum_{n=1}^{M} \frac{1}{\sqrt{\kappa_n}} p_n(\mathbf{r}, t)\, \varphi_n(z). \tag{4}$$

Here, $\mathbf{r} = (x, y)$ is the horizontal two–dimensional position vector, z is the vertical coordinate, t is the time, $\varphi_n(z)$ denotes the n-th vertical eigenfunction of the deterministic background medium, and M is the number of propagation modes. Each normal mode is modulated by a random amplitude $p_n(\mathbf{r}, t)$ indicating the effect of the surface on acoustic propagation. The normal mode depth functions $\varphi_n(z)$ satisfy the eigenvalue problem

$$\frac{d^2}{dz^2}\varphi_n(z) + \left[k^2 n_0^2(z) - \kappa_n^2\right]\varphi_n(z) = 0, \quad n = 1, 2, \ldots M, \tag{5}$$

together with an orthonormality relation and appropriate boundary conditions. Here, $n_0(z)$ is the refractive index and k is the reference wavenumber.

In what follows we will be interested only in the behavior of the MCF of vertical separation. The corresponding quantity is defined as

$$\Gamma(\mathbf{r}, z_1, z_2) = < P(\mathbf{r}, z_1, t)\, P^*(\mathbf{r}, z_2, t) > . \tag{6}$$

The angular brackets $< \cdots >$ denote ensemble averaging. Substituting Eq. (4) into Eq. (6), one finds that

$$\Gamma(\mathbf{r}, z_1, z_2) = \sum_{n,m} \frac{1}{\sqrt{\kappa_n \kappa_m}} \Gamma_{nm}(\mathbf{r}) \varphi_n(z_1) \varphi_m(z_2); \tag{7}$$

$$\Gamma_{nm}(\mathbf{r}) = < p_n(\mathbf{r})\, p_m^*(\mathbf{r}) > .$$

In a multimodal channel, where the rough surface scattering is important, for $\Gamma_{nm}(\mathbf{r})$ we can employ the results presented in Refs. [10–12]:[1]

$$\Gamma_{nm}(\mathbf{r}) = < p_n(\mathbf{r}) >< p_m^*(\mathbf{r}) > + [\Gamma_{nn}(\mathbf{r}) - < p_n(\mathbf{r}) >< p_n^*(\mathbf{r}) >]\, \delta_{nm}. \tag{8}$$

[1] For more details see the paper by Gorodetskaya *et al.* [6] in this issue.

Here, $<p_(\mathbf{r})>$ is the coherent field of the n–th mode

$$<\mathrm{p}_n(\mathbf{r},\omega,t)>=\frac{-i\varphi_n(z_0)}{\sqrt{8\pi r}}\exp\left[\left(i\kappa_n-\frac{1}{2}\sigma_n\right)|\mathbf{r}|-i\frac{\pi}{4}\right], \qquad (9)$$

where σ_n is the total modal attenuating parameter and $\Gamma_{nn}(\mathbf{r})$ is the self-modal MCF. It is not difficult to show for the case of cylindrical symmetry, that equation governing the change of $\Gamma_{nn}(\mathbf{r})$ as a result of random surface scattering may be written in the form:

$$\left(\frac{d}{dr}+\frac{1}{r}+\sigma_n^a\right)\Gamma_{nn}(r)=\sum_m a_{nm}\left[\Gamma_{mm}(r)-\Gamma_{nn}(r)\right], \qquad (10)$$

with the following initial conditions:

$$\Gamma_{nn}(r)|_{r=0}=\frac{1}{8\pi}\varphi_n^2(z_0).$$

We introduce in the right-hand side of Eq. (10) an additional loss term σ_n^a resulting from sediment absorption. An explicit expression for σ_n^a can be found in Ref. [3]. The coupling matrix a_{nm} is given by the expression

$$a_{nm}=\frac{\pi}{2}\frac{[\varphi_n'(0)\varphi_m'(0)]^2}{\kappa_n\kappa_m}\int\int_{-\infty}^{\infty}d\Omega\,d\text{æ}_y\,F_\eta(\kappa_n-\kappa_m,\text{æ}_y,\Omega).$$

Equation (10) is commonly known as the *coupled master equation* (see, e. g. [13, 14]) describing the range dependence of the energy transfer between the modes as a result of random scattering.

For the Pierson–Moskowitz distribution, Eq. (3), the calculation of the matrix a_{nm} is given in [13]. The result is:

$$a_{nm}=\frac{8.1\times10^{-3}\sqrt{2}\pi\,[\varphi_n'(0)\varphi_m'(0)]^2}{8\kappa_n\kappa_m k_0^3}f(x_{nm}).$$

Here, $k_0^2=0.74g^2/v^4$, $x_{nm}=0.5\,k_0^2/\left(\kappa_n-\kappa_m\right)^2$, and

$$f(x)=x^{3/2}e^{-x}\left[I_0(x)-I_1(x)\right],$$

where I_0 and I_1 are the modified Bessel functions of order zero and unity, respectively.

The exact solution of Eq. (10) can be written in terms of eigenvectors and eigenvalues of the matrix

$$h_{nm}=\delta_{nm}\left(\sigma_n^a+\sum_{m=1}^{\mathrm{M}}a_{nm}\right)-a_{nm}$$

in the form

$$\Gamma_{nn}(r) = \frac{1}{8\pi r} \sum_{m=1}^{M} g_{nm}(r)\, \varphi_m^2(z_0), \tag{11}$$

with

$$g_{nm}(r) = \sum_{l=1}^{M} U_{nl} \exp(-d_l\, r)\, U_{lm},$$

where U_{nl} is the matrix whose columns contain the eigenvectors of $||h_{nm}||$ with eigenvalues d_l.

Note that the total modal attenuating parameter σ_n entering Eq. (9) is a combination of absorption and scattering losses:

$$\sigma_n = \sigma_n^a + \sigma_n^s,$$

where

$$\sigma_n^s = \sum_{m=1}^{M} a_{nm}.$$

All quantities in Eq. (7) are now calculable: $\Gamma_{nn}(r)$ are found from the solution (11) of the master equation and the normal mode depth functions $\varphi_n(z)$ are found from solutions of Eq. (5).

The plots of correlation versus sensor separation are given in Figs. 8 and 9 for the two arrays considered. (The origin along the x-axis is the depth of the first element in the corresponding array). The vertical coherence function predicted from the wind seas model is in qualitative agreement with presented measurements.

4. Summary and conclusions

In this paper we presented the experimental study of acoustic transmission fluctuations through the Barents Sea. The theoretical calculations of the vertical coherence based on wind seas scattering are compared with the observed spatial coherence of the signals received by vertical arrays operating in realistic shallow water environments. It has been established that the vertical coherence function predicted from the wind seas model is in a good qualitative agreement with the presented measurements. It is clear, however, that a more general consideration based on the range-dependent model is required to test our predictions in detail.

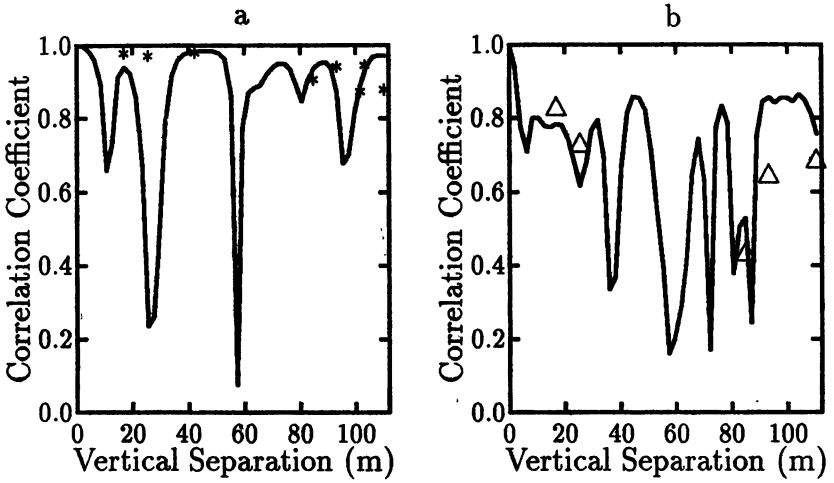

Fig. 8. Computed coherence function of vertical separation along array 1 as compared with observed correlation versus sensor separation: (a) $f_0 = 107$ Hz, (b) $f_0 = 240$ Hz

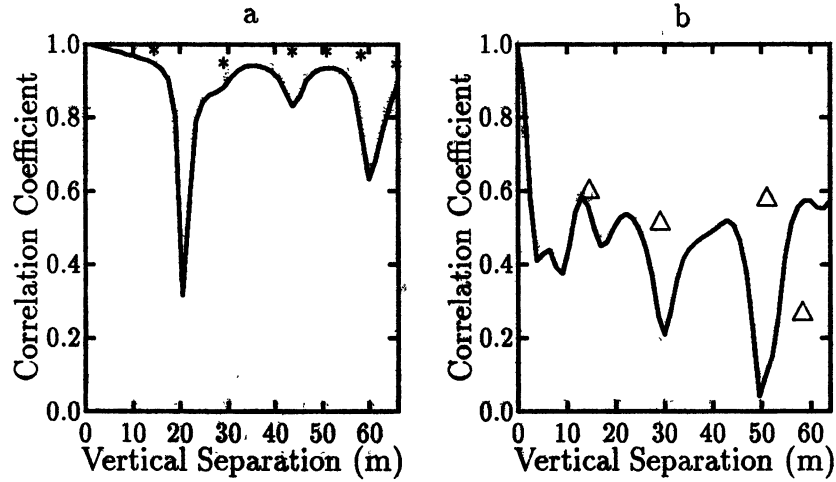

Fig. 9. Computed coherence function of vertical separation along array 2 as compared with observed correlation versus sensor separation: (a) $f_0 = 107$ Hz, (b) $f_0 = 240$ Hz

ACKNOWLEDGMENTS

This work was supported in part by the Russian Foundation for Basic Research under Grants No 96-02-19462, No 96-02-19460, No 97-02-17536, No 97-02-17555 and GEC-Marconi Ltd. (United Kindom) under Contract No B 012621/DB.

References

1. *E. Yu. Gorodetskaya et al.* Acoustic coherence in a deep water: effects on array signal processing // In: Formation of Acoustical Fields in Oceanic Waveguides, edited by V. A. Zverev (Institute of Applied Physics RAS, Nizhny Novgorod, 1997), pp. 5–47.
2. Bottom-Interacting Ocean Acoustics, edited by W. Kuperman and Finn B. Jensen (Plenum Press, New York, 1980).
3. *B. G. Katsnelson and V. G. Petnikov.* Shallow Water Acoustics (Nauka, Moscow, 1997) [in Russian].
4. *D. B. Creamer and B. J. Orchard.* Acoustic wave propagation in a random, shallow-water waveguide // J. Acoust. Soc. Amer., 1994, vol. 95(5), pp. 2927.
5. *D. B. Creamer.* Scintillating shallow-water waveguides // J. Acoust. Soc. Amer., 1996, vol. 99(5), pp. 2825–2838.
6. *E. Yu. Gorodetskaya et al.* Acoustic coherence effects on signal processing in shallow water // In: Formation of Acoustical Fields in Oceanic Waveguides: Reconstruction of inhomogeneities in shallow water, edited by V. A. Zverev (Institute of Applied Physics RAS, Nizhny Novgorod, 1998), Vol. 1, pp. 7–58.
7. *A. L. Matveyev and V. V. Mityugov.* Report on 7-th expedition of SRS "Ac. Sergey Vavilov", Part 7. Moscow, Inst. of Oceanology, AS USSR, 1990 [in Russian].
8. *B. G. Katsnelson et al.* Influence of hydrodynamic variability on the vertical interference structure of sound field in a waveguide // Acoust. Phys., 1992, vol. 38(2), pp. 308–316.
9. *W. J. Pierson and L. Moskowitz.* A proposed spectral form for fully developed wind seas based on the similarity theory of S. A. Kitaigorodskii // J. Geophys. Res., 1964, vol. 69(24), pp. 5181–5190.

10. *B. M. Kudryashov.* On the evaluation of acoustic fields in waveguides with statistically rough surface // In: Mathematical Problems of Geophysics (Nauka, Novosibirsk, 1973), Vol. 4, pp. 256–272 [in Russian].

11. *A. G. Nechaev.* Decay of the interference structure of the sound field in an ocean with random inhomogeneities // Sov. Phys. Acoust., 1987, vol. 33(3), pp. 312–314.

12. *A. G. Sazontov and V. A. Farfel'.* Calculation of the coherence degree and form of a pulse sound signal in an oceanic waveguide with a rough surface // Acoust. Phys., 1995, vol. 41(1), pp. 109–113.

13. *A. Beilis and F. D. Tappert.* Coupled mode analysis of multiply rough surface scattering // J. Acoust. Soc. Amer., 1979, vol. 66(3), pp. 811–826.

14. *M. J. Beran and S. Frankenthal.* Combined volume and surface scattering in a channel using a modal formulation // J. Acoust. Soc. Amer., 1996, vol. 100(3), pp. 1463–1472.

EXPERIMENTAL CHECKING OF THE MODE THEORY OF ACOUSTIC SCATTERING IN AN OCEAN WAVEGUIDE WITH ROUGH SURFACE

B. V. Kerzhakov, V. V. Kulinich, M. A. Raevskii, A. A. Stromkov

INTRODUCTION

Along with the methods of acoustic diagnostics of regular oceanic processes (ocean temperature variations, streams, eddies, etc.), the methods of remote sensing of fluctuations of the ocean medium are also of interest. In this case, we use mathematical models of the scattering theory, which relate the frequency-angular spectra of the acoustic fields to the oceanic fluctuation processes (surface waves, volume fluctuations, and random bottom irregularities). In addition to the ray methods of the scattering theory, an alternative approach, which is based on the transfer equations for the coherence functions of the amplitudes of normal modes, has been proposed recently. In this case we have presented a uniform description of scattering by the volume fluctuations and an irregular boundary of the ocean waveguide. Within the framework of the mode formalism, a number of algorithms for remote diagnostics of surface waves and volume fluctuations were proposed. However, the proposed methods of diagnostics as well as the initial relations of the scattering theory should be checked experimentally. In this paper we discuss the results of approbation of the mode theory of acoustic scattering by surface waves for the stationary acoustic path Sakhalin—Iturup (a Kuril island) with a length of 345 km. The source was located in the Sakhalin coastal shelf at a depth of 100 m. The receiving hydrophone was located in the shelf region of an Iturup island at a depth of 250 m. Radiation frequency was f=387 Hz. Below, the theoretical model of the signal in the ocean waveguide with rough surface and the results of its experimental checking are discussed.

1. THEORETICAL MODEL OF THE TONE SIGNAL IN A SUBSURFACE WAVEGUIDE

In the case of signal propagation along a stationary path with acoustic channel, which is open (fully or partially) toward the surface, we must allow for the influence of both volume and surface phenomena. Theoretical models describing the influence of the volume processes (internal waves, tides, streams, and eddies) on the sound propagation in the ocean were discussed many times and compared with experimental results (see, for example [1]). Experiments were carried out on the stationary paths with acoustic channels whose axes were at a depth of from 500 to 1000 m where the effects of surface waves are negligibly small. If the channel axis is located near the surface, or at a small depth (100—200 m), the channel becomes totally or partially open toward the surface under any seasonal conditions. In this case, in addition to the action of volume nonstationary processes, acoustic are subjected to the scattering by surface waves (and by the ice cover boundaries in a number of cases). Experiments on such a stationary path provide material for constructing a signal model, which can simultaneously allow for the scattering from volume and surface nonstationary inhomogeneities, whereas the existing theoretical models consider these phenomena separately. Therefore, the problem of selection of the above phenomena when analyzing experimental data is timely. Such a separation can be very demonstrative for tone signals if we use the difference in the characteristic time scales of volume fluctuations and surface waves. The characteristic frequencies of surface waves vary from 10^{-2} to 1 Hz, whereas the internal-wave spectrum in the ocean ranges from 10^{-3} to 10^{-5} Hz, not to mention slower volume processes. Therefore, it is natural to assume that fluctuations of the tone signal in the frequency spectrum 10^{-2} Hz $\leq \Delta f \leq 1$ Hz are due to the scattering from surface waves, while the slower fluctuations in the range $\Delta f < 10^{-2}$ Hz are mainly caused by internal waves and other nonstationary volume processes. Accordingly, it is natural to present the fluctuating signal as a set of the high-frequency component (HFC) with characteristic fluctuation frequencies in the range 10^{-2} Hz $\leq \Delta f \leq 1$ Hz, which is due to the scattering from surface waves, and the low-frequency component

(LFC), which is related to the low-frequency factors of the type of internal waves and corresponds to the spectrum range $\Delta f \leq 10^{-2}$ Hz. In this case, surface waves do not influence the shape of the spectrum of the low-frequency component, but influence directly its integral energy. The corresponding phenomenon is described in the theory as decay of the coherent component of the signal in the case of scattering from an irregular boundary of the waveguide. Some effects of the surface-wave influence are discussed below.

2. A MODEL OF THE HIGH-FREQUENCY COMPONENT OF THE SIGNAL

There exist several approaches to describing the scattering of acoustic waves in a refraction waveguide that is open fully or partially toward the surface. Some of the above approaches are based on the ray representation of acoustic field. In this case, the scattering indicatrix of the quasiplane wave propagating along the ray trajectory is calculated depending on the Rayleigh parameter value or using either the method of small perturbations or the method of tangential plane (Kirchhoff's approximation [2]). The concept of the latter approach is close to the method that is based on the simplified presentation of an irregular boundary as a set of local horizontal planes, which are shifted randomly along the vertical [3]. It is obvious from the theory that scattering is resonant for small (compared with unity) values of the Rayleigh parameter, i.e., the frequency-angular spectrum of the reflected wave is determined by the conditions of resonant scattering and the type of the frequency-angular spectrum of vertical shifts of the boundary. For large values of the Rayleigh parameter, the scattered field is formed by the mirror points of reflection from a smoothly irregular surface. The advantage of the ray approach is its obviousness. Unfortunately, in this case it is rather difficult to describe the phenomena of multiple scattering.

For small values of the Rayleigh parameter it is also possible to describe the scattering phenomena within the framework of the mode representation of acoustic field. In this case, the energy distribution of the scattered component of acoustic waves over the frequency and mode

numbers is described by the transfer equation, which allows us to analyze uniformly the phenomena of both single and multiple scattering. Since numerical simulation of the frequency spectrum of the HFC will be performed within the framework of the mode approach, we offer a preliminary description of the basic relations. It is assumed that the waveguide with profile $C(z)$ has an upper boundary $z=\xi(r,t)$. The pressure field of the quasimonochromatic wave with central frequency ω_0 is expanded in terms of orthogonal eigenfunctions of the waveguide with plane boundary $z=0$, i.e,

$$P = \sum_n \int b_{n\omega} \exp(i\omega t)\, d\omega \cdot \varphi_n(z) H_0^{(1)}(k_n r) \qquad (1)$$

Here the eigenfunctions φ_n and the wave numbers k_n correspond to the radiation frequency ω_0.

We can show that for multiple scattering the coherent component of the amplitudes of normal modes $<b_{n\omega}>$ corresponding to the frequency ω_0, (<..> denotes averaging over an ensemble of random shifts $\xi(r,t)$) decays exponentially, i.e.,

$$< b_{n\omega_0} >= b_{n\omega_0}(0) \exp(-\gamma_n r)$$

In the case of a waveguide with smooth profile $C(z)$, for the decay decrement, we obtained a comparatively simple expression [4]

$$\gamma_n = \frac{1}{k_n}\left(\frac{d\varphi_n}{dz}\right)^2 \cdot \int_0^{k_0} d\eta \int_{-\infty}^{\infty} dk_y \frac{\eta\sqrt{k_0^2-\eta^2}}{|h_\eta|} B(k_0 - h_\eta, k_y) \qquad (2)$$

where $d\varphi_n/dz$ is the value of derivative on an unperturbed ($\xi=0$) surface, $k_0=\omega/c(0)$, $h_\eta=(\eta^2-|k_y|^2)^{1/2}$, and $B(k_x,k_y)$ is the spectrum of vertical shifts of the boundary ξ. Let us introduce the spectral density of the mode energy $N_{n\omega}$ in accordance with

$$< b_{n\omega} b^{*}_{n\omega'} >= N_{n\omega}\delta(\omega - \omega').$$

On the basis of the transfer equation for the frequency-angular spectrum of normal modes [4], we obtain the closed transfer equations for $N_{n\omega}$ in the form

$$\frac{dN_{n\omega}}{dr} = \sum_{n'} \int d\omega' W^{n'\omega'}_{n\omega} N_{n'\omega'} - 2\gamma_n N_{n\omega} \ , \qquad (3)$$

where $W^{n'\omega'}_{n\omega}$ is the transition probability, which characterizes the energy exchange between the modes as a result of scattering from an irregular boundary. We take into account that the space—time spectrum of waves has the form

$$B(\vec{k}, \Omega) = B(\vec{k})\delta(\Omega \pm g\sqrt[4]{k_x^2 + k_y^2}).$$

Then for the transition probability $W^{n'\omega'}_{n\omega}$ we obtain [5,6]

$$W^{n'\omega'}_{n\omega=} = \frac{\pi}{2k_n k_{n'}} \left(\frac{d\varphi_n}{dz}\right)^2 \left(\frac{d\varphi_{n'}}{dz}\right)^2 \times$$
$$\times \frac{B(|\omega - \omega'|, \beta) + B(|\omega - \omega'|, -\beta)}{\sqrt{\{\omega - \omega'\}^4 / g^2 - (k_n - k_{n'})^2}}, \qquad (4)$$
$$\beta = \arccos\left(\frac{(k_n - k_{n'})g}{(\omega - \omega')^2} sign(\omega - \omega')\right).$$

In this case, we must fulfill the conditions $(\omega\text{-}\omega')^2 > g|k_n\text{-}k_n|$; otherwise we have

$$W^{n'\omega'}_{n\omega} = 0.$$

In the above expression $B(|\Omega|,\varphi)$ is the frequency-angular spectrum of waves that is normalized according to

$$\int_0^\infty d\Omega \int_0^{2\pi} B(|\Omega|,\varphi)d\varphi = <\xi^2>.$$

Along with the direct numerical integration of transfer equation (3), it can be solved approximately using different methods.

The expansion in terms of multiplicity powers of scattering is the most demonstrative

$$N_{n\omega}(r) = N_n(0)\delta(\omega-\omega_0) + r\sum_{n'} W_{n\omega}^{n'\omega'} N_{n'}(0) + \\ + r^2/2 \sum_{n'n''} \int d\omega' W_{n\omega}^{n''\omega'} W_{n''\omega'}^{n'\omega_0} N_{n'}(0) + \dots \quad , \tag{5}$$

where the monochromatic signal with frequency ω_0 and distribution over modes $N_n(0)$ is assumed to be initial.

To obtain explicitly the frequency spectrum of the scattered component, we write an approximate expression for the first terms of this series in the case where the frequency-angular spectrum of waves is concentrated near α_0, such that the angular width of the spectrum Δ and the frequency of maximum Ω_* satisfy the condition

$$\Delta \left| \frac{dP}{dk_p} \right| \sin\alpha_0 \left| \Omega_*^2 / g << P_*, \right.$$

where P_* is the characteristic scale of variation with respect to the mode number of the quantities $\frac{d\varphi_P}{dz}$, $N_P(0)$.

In this case, for the singly scattered field component, the approximate summation in Eq. (5) yields

$$N^{(1)}_{n,\omega_0+\Omega} = \frac{\pi r}{4k_n k_{n'}}\left(\frac{d\varphi_n}{dz}\right)^2\left(\frac{d\varphi_{n'}}{dz}\right)^2 \left|\frac{dn'}{dk_{n'}}\right| N_{n'}(0)B(\Omega), \qquad (6)$$

$$B(\Omega) = \int_0^{2\pi} B(|\Omega|,\varphi)d\varphi$$

The value of n' is obtained from the equation

$$k_{n'} = k_n - \Omega^2 g^{-1}\cos\alpha_0 \, sign\Omega .$$

In a similar manner, for the doubly scattered component we have

$$N^{(2)}_{n,\omega_0+\Omega} = \frac{\pi^2 r^2}{32k_n^2 k_{n''}k_{n'}}\left(\frac{d\varphi_n}{dz}\right)^4\left(\frac{d\varphi_{n'}}{dz}\right)^2\left(\frac{d\varphi_{n''}}{dz}\right)^2 \times$$

$$\times\left|\frac{dn'}{dk_{n'}}\frac{dn''}{dk_{n''}}\right| \int B(\omega'-\Omega)B(\omega')d\omega' \quad . \qquad (7)$$

Here n' and n'' are related by the equations

$$k_{n'} = k_n + (\Omega-\omega')^2\cos(\alpha_0)g^{-1}sign(\omega'-\Omega),$$

$$k_{n''} = k_{n'} - \omega'^2\cos(\alpha_0)g^{-1}sign(\omega').$$

From the above expressions it follows that the shape of the spectrum of the singly scattered component of acoustic field for waves with relatively narrow frequency-angular spectrum is close to the frequency spectrum of waves. In this case, the signal spectrum is generally asymmetric, i.e., the amplitudes of the side maxima of the spectrum are different in the regions $\Omega>0$ and $\Omega<0$.

The presence of maxima near the zero frequency $\Omega\approx 0$ and the doubled central frequency of the wave spectrum $|\Omega|\approx 2\Omega_*$ is typical of

the spectrum of the doubly scattered component, however, again, the spectrum is asymmetric, i.e.,

$$N_n^{(2)}(\Omega) \neq N_n^{(2)}(-\Omega).$$

The complete symmetry of the spectrum of acoustic signal (under the condition of symmetry of the angular spectrum of waves with respect to α_0) appears only for $\alpha_0=\pi/2$. In this case, as is obvious from Eqs. (6) to (7), the spectrum of the singly scattered component repeats the wave spectrum, while the spectrum of the doubly scattered component is a convolution of the wave spectra.

3. NUMERICAL SIMULATION OF THE SPECTRUM OF THE HIGH-FREQUENCY COMPONENT OF THE SIGNAL

The use of the mode formalism for description of the scattering phenomena on the stationary path requires the presence of a waveguide whose characteristics are uniform along the path. In principle, it is possible to generalize the above results to the waveguide with regular variations of the sound velocity and bottom depth with distance, but their numerical realization is rather difficult. However, it is obvious that an efficient transformation of the energy of normal modes occurs in the region of continental shelf near the transmitter and receiving hydrophones, where the bottom slopes of the order of 0.1 rad are observed. As a result, the coefficients of mode excitation in the shelf differ significantly from the coefficients of excitation by a point source in a waveguide with plane bottom. This phenomenon must be allowed for in numerical simulation. At the same time, on the basic part of the path the bottom is assumed to be plane with the depth H=3200 m. In the modeling, the sound-velocity profile $C(z)$ for the channel with winter hydrology measured near Iturup island and close to the linear one was assumed to be constant along the path (due to the absence of other data). The channel profile $C(z)$ for the fall hydrology (except for the Iturup near-shore region, where the channel axis depth was $z_0\approx$400 m) shows no significant variation along the path and has the axis depth z_0=100 to 140 m. Therefore, we assume that the profile $C(z)$ is constant

on the main section of the path and corresponds to the profile measured at the distance r=320 km. On the path section $0 \le r \le 50$ km, the profile $C(z)$ is also assumed to be constant and corresponding to the measurements for r=40 km. To simulate the field of the point source in the coastal shelf, we use a set of mode programs KRAKEN. In this case, the shelf is presented as a set of a large number (of order of 100) of homogeneous waveguides. In each waveguide, the field is calculated within the framework of the mode program, while when crossing the interface between adjacent waveguides the elements of the matrix of mode transformation are calculated. As a result, at the shelf output we obtain the acoustic-field distribution $P(z)$ for the fall and winter hydrology. In the case of winter hydrology, directly from the above distribution, we obtain the mode excitation coefficients in the shelf

$$\alpha_n^S = \int P_S(z)\varphi_n(z)dz \ . \qquad (8)$$

Correspondingly, $N_n^s = |\alpha_n^s|^2$ are the initial conditions in solving the transfer equations on the uniform section of the path. In the case of fall hydrology, we have a similar situation but it is taken into account that the profile $C(z)$ varies at the distance $r \approx 50$ km (the exact value is unknown). Therefore, the field distribution $P(z)$ in Eq. (8) was calculated for different distances $45 \le r \le 55$ km, and the obtained values of $N_n^s = |\alpha_n^s|^2$ were averaged over the corresponding interval Δr=10 km. In the similar manner (using the reciprocity theorem), we calculated the coefficients of mode transformation in the shelf near the receiving (deep) hydrophone C_n^r and the corresponding values of $N_n^r = |C_n^r|^2$. It was assumed (on the basis of the data available) that main type of soil in the shelf was sand with density ρ = 1.6, longitudinal sound velocity C_l=1600 m/s, and damping coefficient β = 0.1 dB/mHz. The calculated normalized values of N_n^r and N_n^s for the fall and winter hydrology are shown in Fig.1.

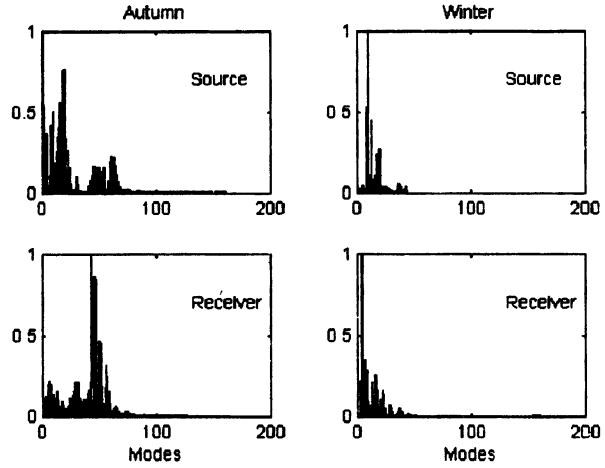

Fig. 1. Normalized coefficients of mode transformation in the shelf regions near the transmitter and receiver.

Strictly speaking, when modeling the spectrum of the high-frequency component of the signal, we must use the data on the frequency-angular spectrum of surface waves obtained synchronously with the measurements of signal fluctuation. Since we did not perform such measurements, in the modeling we used the averaged spectra of surface waves, which generalized the results of multiple full-scale experiments. Therefore, the surface waves were usually a superposition of wind waves due to wind in this water space (with scales of orders $\Delta r \approx 100$ km) and ocean swell arriving from remote stormy regions and thus weakly correlating with local wind parameters. The frequency spectrum of wind waves $B(\Omega)$ is studied most perfectly. For this spectrum we shall use the generally accepted model JONSWAP [7] corresponding to the developed wind waves:

$$B_W(\Omega) = 8.1 \cdot 10^{-3} g^2 \omega^{-5} \exp\left[-1.25(\omega_* / \omega)^4 \right] \times \times \gamma^{\exp\left[-(\Omega-\omega_*)^2 / (2\sigma^2 \omega_*^2) \right]} \quad (9)$$

Here $\omega_*=0.84$ g/v is the frequency of the spectrum maximum, v is the wind velocity, $g=9.8$ m/s^2, γ characterizes the degree of the wave development, and the following values are used for σ:

$$\sigma = \begin{cases} 0.07 & \text{for } \Omega \le \omega_* \\ 0.09 & \text{for } \Omega > \omega_* \end{cases}$$

The following relation is traditionally used for the frequency-angular spectrum of waves:

$$B_W(\Omega,\alpha) = B_W(\Omega)\cos^{2n}(\alpha - \alpha_W)Q(n) \ . \qquad (10)$$

Here the normalizing coefficient $Q(n)$ has the form

$$Q(n) = \pi^{-1}2^{2n-1}\Gamma^2(n+1)/\Gamma(2n+1),$$

where $\Gamma(x)$ is the gamma function. The index n depends on the wind velocity and frequency but since the known approximations of these dependences differ significantly, fixed values of n are often used. It is assumed that $n=4$ and is independent of the frequency Ω in the range of wind velocities under consideration. We use $\gamma=2$, which corresponds to the average degree of wave development.

The ocean swell spectrum is studied to a lesser extent. It is known [7] that when propagating from stormy regions, the frequency-angular spectrum of swell becomes much narrower than that of developed waves, however, there are no generally accepted model spectra of swell. In accordance with [8], in the modeling it is assumed that the frequency-angular spectrum of swell is similar to the spectrum JONSWAP, where we use the ω_s-frequency of the maximum of the swell spectrum and $\gamma=10$, which corresponds to the narrow frequency spectrum of swell. For anisotropy index of the angular spectrum of swell n_s we use the maximum observed $n_s=6$. As a result, the frequency-angular spectrum of swell has the form

$$B_S(\Omega,\alpha) = Q(n_S)B_S(\Omega)\cos^{2n_S}(\alpha-\alpha_S),$$

$$B_S(\Omega) = 1.8 < \varsigma_S^2 > \omega_S^4\omega^{-5}\exp\left[-1.25(\omega_S/\omega)^4\right]\times \times\gamma^{\exp\left[-(\Omega-\omega_S)^2/(2\sigma_S^2\omega_S^2)\right]}. \quad (11)$$

Here $< \varsigma_s^2 >$ is the variance of the surface shift, $\omega_S=2\pi/T_s$, and T_s is the swell period

$$\sigma_S = \begin{cases} 0.07 & \text{for } \Omega \le \omega_S \\ 0.09 & \text{for } \Omega > \omega_S \end{cases}$$

As a rule, in the ocean we observe superposition of wind waves and ocean swell. In this case, when calculating the scattering phenomena as the function $B(\Omega,\alpha)$, we should use a sum of the model spectra of swell and wind waves. Now let us discuss directly the results of numerical simulation of the HFC spectrum on the stationary path. From the current spectra of the signal, which are averaged over six-hour realizations, it is obvious that the singly scattered component that is concentrated near f_{max} of the order of 0.1Hz (below we speak of the frequency value with respect to radiation frequency) is dominating over the doubly scattered component.

For definiteness, it is assumed that the spectrum region $0.5f_{max}\le|f|\le1.5f_{max}$ corresponds to the singly scattered component, while the regions $f\le0.5f_{max}$ and $1.5f_{max} \le |f| \le 0.4$ Hz correspond to the doubly scattered component. Since the signal spectrum is mainly formed by the singly scattered component, numerical simulation is performed in the single approximation of the scattering theory. As the main characteristics of the model spectrum $S(f)$, we consider the asymmetry coefficient of the spectrum (except for its qualitative form) determined by the relation of maxima corresponding to the positive and negative frequencies and the integral energy of the singly scattered spectrum

component. In this case, for the quantitative estimate of the scattering intensity it is convenient to introduce the ratio of the energy of the singly scattered component to the energy of the coherent component. With allowance for the above discussed phenomena of mode transformation in the shelf region near the transmitter and receiver, for this q we have

$$q = \frac{\Sigma_p N_p^{(1)} N_p^r}{\Sigma_p N_p^s N_p^r}. \qquad (12)$$

Let us consider the calculated results for winter hydrology (the second stage). In Fig. 2 we show the normalized spectra of the HFC for the scattering from swell with parameters A_s =1m and T_s=10 s and different propagation angles α_s. Here and below we have

$$A_S = < \varsigma_S^2 >^{1/2}.$$

Obviously, the spectrum is narrow and repeats the shape of the frequency spectrum of swell. For $\alpha=\pi/2$, the spectrum is symmetric, and for $\alpha=0$ and $\alpha=\pi$ we have K= 4 and K=0.25 for the asymmetry coefficient K. Since, theoretically, for $\alpha=0,\pi$ the spectrum asymmetry is maximal, the coefficient K has intermediate value for other values of the angle α. Similar results for the wind waves are given in Fig. 2 for the wind velocity V=12 m/s.

In this case, we have K=2 for $\alpha=0$, K=0.5 for $\alpha=\pi$, and K=1 for $\alpha=\pi/2$. On the basis of these results (and similar results obtained for other parameter values), we conclude that under the conditions of winter hydrology the typical asymmetry of the spectrum is small and does not exceed several dB, which agrees with experimental data. The calculated results for swell with parameters A_s=1 m, T_s=10 s, and $\alpha_s=\pi/4$ are shown in Fig. 3 to represent the type of the spectrum and HFC energy for the case of simultaneous scattering of sound from swell and wind waves. The following values for wind velocity are used: V =10 m/s and V=15 m/s for $\alpha_w=\pi/4$.

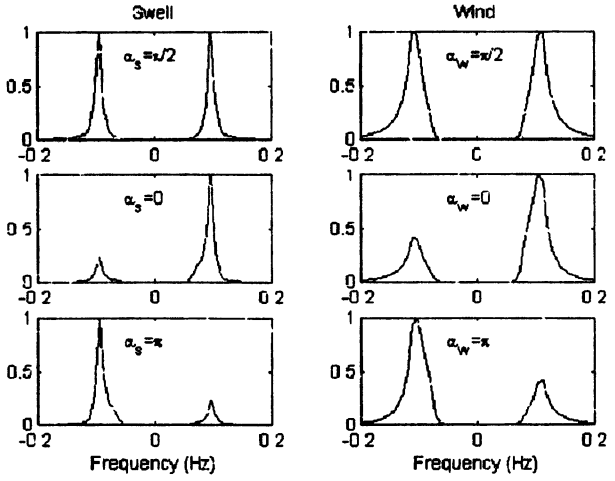

Fig. 2. Angular dependences of the signal frequency spectrum for the winter hydrology.

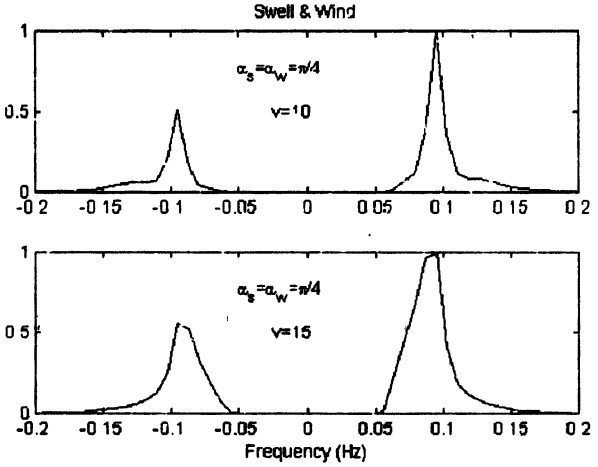

Fig. 3. Signal spectrum for the co-scattering of sound from swell and wind waves (winter hydrology).

For these cases, we calculate q=0.3 for V=10 m/s and q=0.8 for V=15 m/s. For comparison, in Fig. 4 we show experimental values of q.

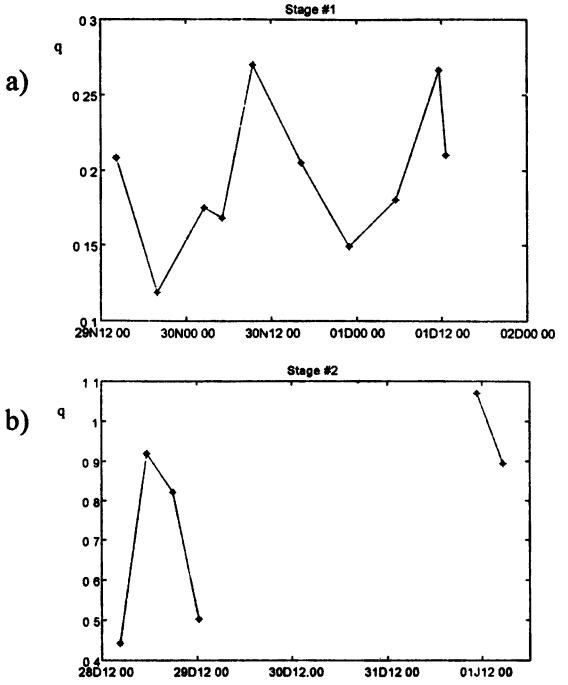

Fig. 4. Experimental values of q for a fall hydrology (a) and for a winter hydrology (b).

It is obvious that typical experimental values of q are in the range from 0.4 to 1, i.e., the modeling results agree with experimental data. Unfortunately, a more specific comparison with experiment can be performed only for the observation interval in which the data on swell (December 28) are available. In this case, with allowance for a certain spread of the meteorological data along the path, in the modeling we used the following swell and wind parameters: A_s=1 m, T_s=10 s, α_s=70°, V=10 m/s, and α_w= 270°. It should be noted that in the meteorological data we have the swell amplitude H_s, which is measured from the wave trough to the wave crest (in our case we have H_s=3 m). For the

quasisinusoidal waves we have $A_s=H_s/2^{3/2}$. In addition, we should take into account that in the meteorological data the angles are read from the direction to the north, and the path is oriented to the north at an angle of 290°. (from source to receiver). In Fig. 5 we show the results of calculation of the HFC spectrum and a typical experimental spectrum of the signal as of December 28.

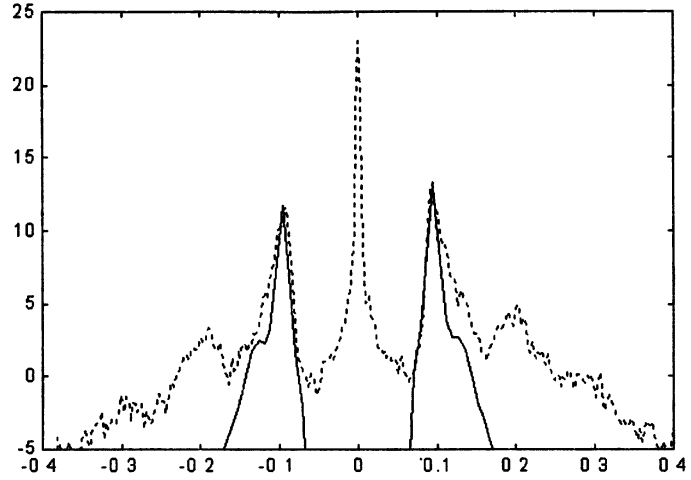

Fig. 5. Typical frequency spectrum of the signal at the second stage: theoretical results are presented by the solid curve and experimental results are given by the dashed curve.

In this case, to compare the spectral levels in the theory and experiment, the experimental spectrum was normalized to the LFC energy. It is obvious from the comparison that the shape, asymmetry character, and the level of the spectrum obtained from the modeling (in the frequency range that corresponds to the singly scattered component) is in good agreement with experiment. The value of q=0.5, which was obtained from model calculations, was also close to experimental data as of December 28, $0.4 \leq q \leq 0.9$. Let us discuss the results of modeling for the first stage (fall hydrology). In Fig.6 we show the results of the spectrum calculation for the scattering from swell with parameters A_s =1 m, T_s=10 s, and propagation angles $\alpha_{s=}=0,\pi$.

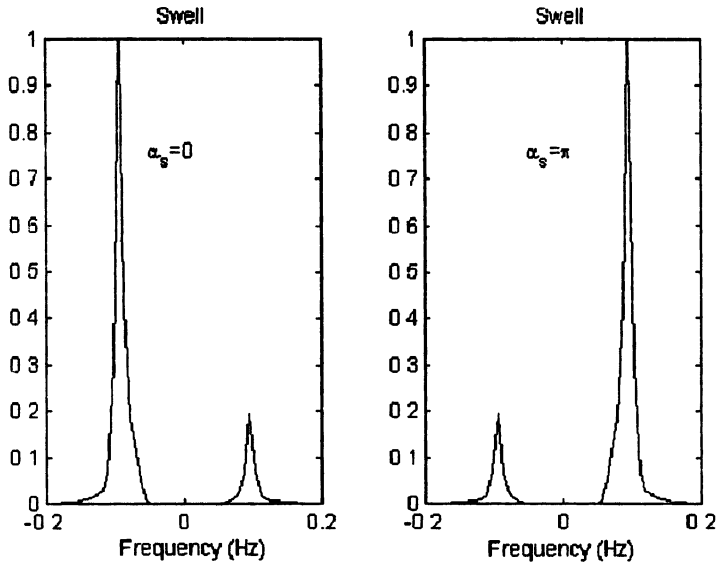

Fig. 6. Frequency spectrum of the signal for the scattering from swell (fall hydrology).

The asymmetry coefficients corresponding to these spectra are $K=1$, $K=0.2$, and $K=5$. Therefore, in this case, the spectrum asymmetry for intermediate values of angles is also several dB. It is of interest that for acute angles of swell propagation ($|\alpha_s|<\pi/2$) the side maximum of the spectrum corresponding to $f>0$ dominates for the winter hydrology, whereas the side maximum with $f<0$ is dominant for the fall hydrology. In the case of scattering from wind waves, the spectrum asymmetry character is similar. Since in the first stage of experiment we have no data on the parameters of swell (which, mainly, determines the type of the HFC spectrum), we use the results of modeling for different values of swell parameters and the wind velocity range observed in the first stage. Since the west wind was observed in the course of the first stage (with changes to the north—west wind), it is assumed that wind and swell propagated at the same angle of 110°, which corresponds to $\alpha_s=\alpha_w=\pi$. The typical values of $V=10$ m/s and $V=15$ m/s were used for the wind velocity (according to the meteorological data). Since the data

for the swell amplitude H_s are absent, it was assumed that H_s =2 m and H_s =3 m. The swell period was T_s=10 s.

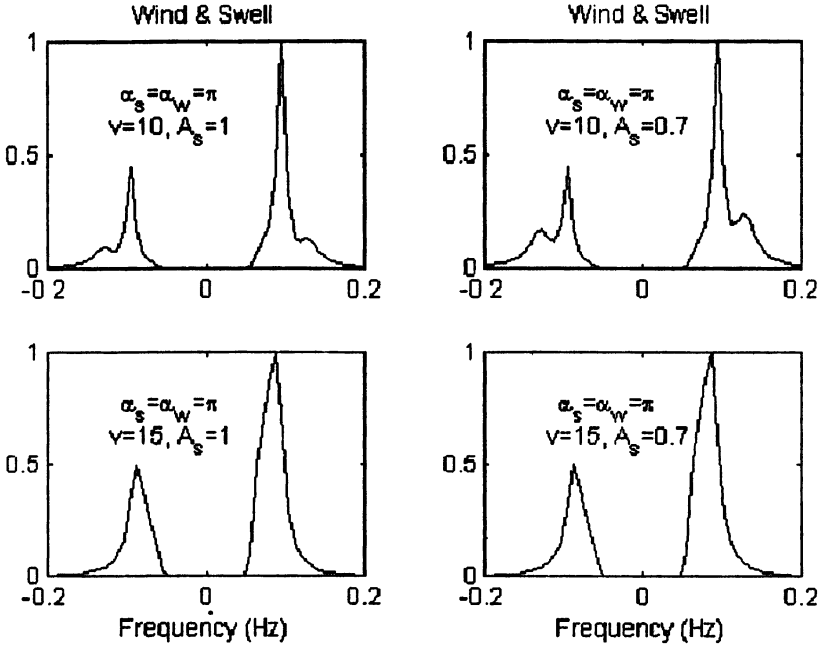

Fig. 7. Frequency spectrum of the signal in the case of co-scattering from wind waves and swell (fall hydrology).

The calculated spectra are given in Fig. 7. The following values were obtained:

q	V(m/s)	$H_s(m)$
0.05	10	2
0.45	15	2
0.1	10	3
0.5	15	3

On the whole, these values are in fair agreement with experimental data (see Fig. 4, where the time dependence of q is given for the first stage).

The model spectrum of the HFC for V= 12 m/s, H_s=0.7 m, and T_s=8 s are compared with a typical experimental spectrum in Fig. 3. In the calculations it was assumed that wind and swell propagation were from the west, i.e., $\alpha_s=\alpha_w=160°$.

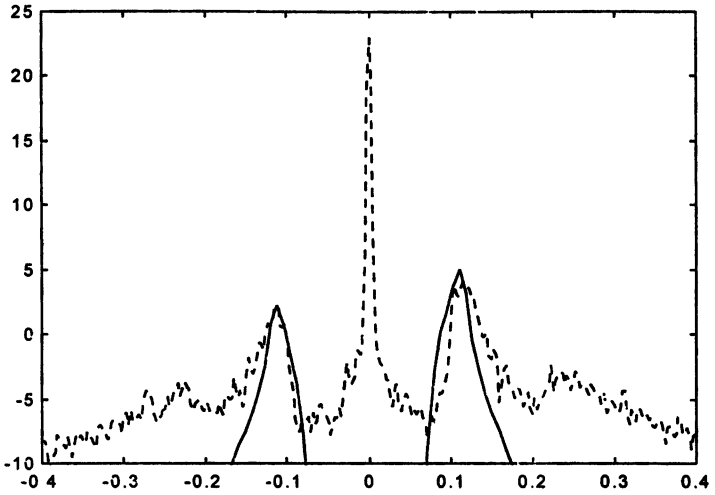

Fig. 8. Typical frequency spectrum of the signal in the fir st stage: theory is shown by the solid curve while the dashed curve represents experimental data.

It is obvious that not only the type but also the level of the HFC spectrum are in fair agreement with experiment. The value of q=0.14, which was obtained from the modeling, is also close to the experimental q=0.17. Therefore, the preliminary results of numerical modeling are in good agreement with the observed acoustic data. Under these conditions it is of interest to perform further improvement of the theoretical model using synchronous measurements of the frequency-angular spectrum of surface waves and the frequency spectra of the signal on the stationary path. In this case, we hope to check not only the theory of single sound

scattering from surface anisotropic waves but also the theory of multiple scattering.

REFERENCES

1. *S.M.Flatte, R.Dashen, W.Munk, K.M.Watson, F.Zachariasen.* Sound transmission through a fluctuating ocean //Cambridge University Press, Cambridge, 1979.
2. *L.M.Brekhovskikh, Yu.Lysanov.*Fundamentals of Ocean Acoustics //Springer-Verlag, Berlin,Germany, 1991.
3. *Rogers L.F. and S.Magruder.* The Dashen-Spofford approach to modeling spectra of forward scattered CW waves // Johns Hopkins University Applied Physics Lab technical memorandum STL-92-135, Dec. 21,1992.
4. *N.S. Gorskaya and M.A.Rayevskii.* On the multiple scattering of low-frequency acoustic waves from surface waves // Akust. Zhur., 1986, vol. 32, No.2, pp.165-171 (in Russian).
5. *N.S. Gorskaya and M.A.Rayevskii.* The spectrum of LF acoustic waves in the case of remote sensing of anisotropic wind waves // Akust. Zhur., 1989, vol. 35, No.3, pp.439-445.
6. *N.S. Gorskaya and M.A.Rayevskii.* On the relation between statistical characteristics of sensing acoustic waves and the wind wave parameters// Akust. Zhur., 1987, vol.33, No.3, pp.463-468.
7. *Hasselmann K and others.* Measurements of wind-wave growth and swell decay during the Joint North Sea Wave Project (JONSWAP)// Dt. Hydrogr. Z.Reihe, A(8),12,95 pp.
8. *Bruning C., Alpers W and Hasselmann K.*Monte-Karlo simulation stadies of the nonlinear imaging of a two dimensional surface wave field by a synthetic aperture radar// Int. J. Remote Sensing. 1990, v.11, n.10, pp.1695-1727.
9. *V.V. Artel'nyiy, N.S. Gorskaya and M.A.Rayevskii.* Statistical characteristics of normal waves in randomly inhomogeneous oceanic waveguides// Preprint No 148, Institute Applied Physics RAS, Nizhny Novgorod, 1986.

FUNDAMENTALS OF THE HIGH-FREQUENCY FORWARD-SCATTERING SONAR

V.V. Borodin and M.Yu. Galaktionov

1. INTRODUCTION TO THE FORWARD-SCATTERING ACTIVE BISTATIC SONAR

In the eighties the idea to use forward-scattering (FS) acoustical methods to detect underwater objects was proposed independently by several authors. In fact, this approach is a particular case of the general active bistatic sonar (ABS) approach. For the FS-ABS scheme objects to be detected and localized are placed in the vicinity of the vertical plane containing the acoustical path from the emitting to the receiving arrays. A hypothesis is that the object strength (TS) should increase considerably in this case (in comparison with the common ABS scheme). This should improve essentiai characteristics of ABS systems – range and probability of detection – when they are working in the FS mode.

1.1. General presentation of the forward-scattering method for ABS

The principle difference between the FS and the classic ABS methods consists of the fact that for the FS scheme the useful signal scattered by the object propagates practically in the same vertical plane where the probing signal from the emitting array does. So, they both come to the receiving array very close to each other in the time and space. In particular, some of them come by the same ray paths. Therefore, for the FS scheme it should be assumed that there is no the possibility to do time selection of scattered signals from probing signals by the same way as it's done for the classic ABS scheme. Thus, there is the problem to distinguish the scattered signal not only on the noise background but also on the background of the strong probing field radiated by the sonar source.

To formalize the FS-ABS approach let consider some realistic random sea environment where fluctuations of signals are due to relatively "slow" fluctuations of the medium being effects of various hydrodynamic wave processes. In this case, the Green's function (GF) of the waveguide, which depends on propagation time delay τ, is also slowly depending on current time t since the environment is depending on it. Thus, it's possible to consider the "instant" spectrum $G_0(\mathbf{r},\mathbf{r}';\omega,t)$. Under the common supposition that the correlation time interval of the interference (sea ambient noise and reverberation) is rather smaller that the stability period of the environ-

ment, the interference may be considered as quasi-stationary. It means that its spectral density depends "slowly" on current time: $K_N(\mathbf{r}_1,\mathbf{r}_2;\omega,t)$. When a localized inhomogeneity is introduced in the environment due to the presence of some object, GF $G_1(\mathbf{r},\mathbf{r}';\omega,t)$ differs from that of the initial environment, but it rests "slowly" depending on time t. The interference may change also because of the effect of this inhomogeneity, but it's usually possible to neglect this effect since the sources of interference (the waveguide's boundaries and volume) are much more homogeneous in time and space that the sonar source. On this way, it's possible to consider the functions G_0 and G_1 as realizations of two random processes having different stochastic properties. So, one can design signal processing algorithms that will use this difference to detect and localize the object.

So far as the FS-ABS is a particular case of ABS systems, one can formulate the underwater detection and localization (UDL) problem in this particular case by using the classical (for ABS) term of echo-signal. In this case the object is considered as secondary source of scattered signals. One has to detect the signals on an interference background, to determine their characteristics and then to answer the question about the type and location of the secondary source. By this way the three main problems – detection, localization and classification – composing the underwater object survey (UOS) problem will be resolved.

In the general case, characteristics of echo-signals depend on:

1) parameters of signals having been radiated by the sonar,
2) location of the object with respect to sonar's emitting and receiving arrays.
3) propagation conditions and corresponding propagation loses,
4) scattering properties of the object; which can be characterized by TS.

TS is determined by the sound scattering (diffraction) on the object's body as well as on medium perturbations that are created by its motion and activity (for example, by the scattering on air baubles in the object's wake). In principle, the object may be also considered as particular case of such a perturbation. Increasing of the TS when using the FS scheme is based on the fact that scattering lobes of bodies and hydrodynamic inhomogeneities are very narrow in the horizontal plane and are focused to the incident direction.

The classic ABS scheme is as follows. Incident field radiated by the emitting array at the location $\mathbf{r}_S$ (the source) is captured by the receiving array at the location $\mathbf{r}_R$ (the receiver). Hereafter arrays are considered as point objects having some patterns. There is a scattering object located at point $\mathbf{r}_T$ (the object) with which the incident field interacts and creates a scattered field. The scattered signals are also captured by the receiving array. For the classic ABS scheme it's possible to do window separation of the scattered and probing signals in time since there is the difference of propagation times for the paths "from source - to receiver" (S-R) and "from source –

to object – to receiver" (S-T-R). The difference is due essentially to the non-zero horizontal angle between the directions S-R and S-T-R (so, the echo-signal arrives always after the source signals). The figure 1.1a presents schematically the time structure of signals at reception when using the classic ABS scheme. The task of the signal processing system at reception consists of detecting the echo-signal on the interference background due to ambient sea noise, reverberation, system noises and signals coming from point noisy sources.

The figure 1.1b shows schematically the time structure of received signal in the FS-ABS case. In despite of possible appearances of new ray paths or normal modes due to scattering by the object's body or accompanying hydrodynamic inhomogeneities, their arrival times will be in the same time window where are the arrival times of the source field. So, the easy time selection as that of the classic ABS case is not more possible for the FS-ABS case.

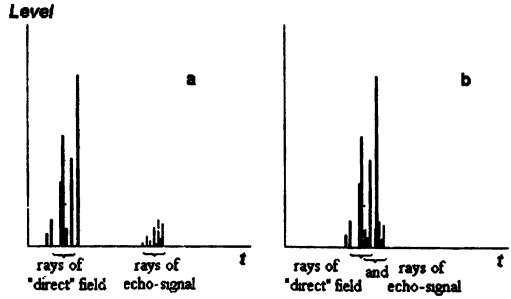

Figure 1.1. Time structure of signals in classic ABS mode (a) and in FS-ABS mode (b).

1.2. Rough estimation of echo-signal level for the FS-ABS

Different authors proposed and considered various principles of functioning of UOS systems when using the FS-ABS approach. Some principles and methods to solving the detection problem were based on the supposition that the spectral density of the process G_1 is greater (in some frequency interval) than that of the process G_0. In this case one may talk about a supplement "modulation" of source fields that arises in this frequency domain and therefore about detecting this modulation. It may be interpreted as result of interference between the source and the scattered field on the receiving array. For this approach, the problem consists of distinguishing the "useful" modulation on the background of "noise" modulations being effect of natural environmental fluctuations.

To see an interest to use FS-ABS systems to solve the UOL problem at least for object detection under the approach based on the detection of SLF modulations of probing signals, one can make a rough quantitative estimating of modulation levels that can be principally reached.

In the case of a free homogeneous medium the complex amplitude of the source field at reception is

$$P_S = B_S(\mathbf{e}_{SR} - \mathbf{e}_S^0; \omega) e^{ikR_{SR}} R_{SR}^{-1}, \; R_{SR} = |\mathbf{r}_R - \mathbf{r}_S|, \; \mathbf{e}_{SR} = \frac{\mathbf{r}_R - \mathbf{r}_S}{R_{SR}}, \tag{1.1}$$

where $B_S(...)$ is the emitting array's lobe, $\mathbf{e}_S^0$ is its compensation vector. Values having double subscripts are determined by two things: the fist subscript corresponds to the first thing and the second subscript corresponds to the second thing. For example, R_{SR} is the range from source to receiver and $\mathbf{e}_{SR}$ is the direction from source to receiver.

The field scattered by some object is a directed spherical wave in the "far field" zone. Its directivity is determined by the scattering amplitude of the object $f_T(\mathbf{e}_{TR}, \mathbf{e}_{ST})$ (the dependence on ω will be usually omitted). Thus, the complex amplitude of the scattered field is

$$P_T = f_T(\mathbf{e}_{TR}, \mathbf{e}_{ST}) e^{ikR_{TR}} R_{TR}^{-1} \cdot B_S(\mathbf{e}_{ST} - \mathbf{e}_S^0) e^{ikR_{ST}} R_{ST}^{-1}. \tag{1.2}$$

The arising modulations of signal envelope and of signal carrier are characterized by coefficients:

$$K_I = \frac{|P_S + P_T|^2 - |P_S|^2}{|P_S|^2} \cdot 100\% = \left(\left| 1 + \frac{P_T}{P_S} \right|^2 - 1 \right) \cdot 100\%, \tag{1.3}$$

$$K_P = \left| \frac{P_T}{P_S} \right| \cdot 100\% = \left| \frac{f_T(\mathbf{e}_{TR}, \mathbf{e}_{ST}) B_S(\mathbf{e}_{ST} - \mathbf{e}_S^0)}{B_S(\mathbf{e}_{SR} - \mathbf{e}_S^0)} \right| \frac{R_{SR}}{R_{TR} R_{ST}} \cdot 100\%. \tag{1.4}$$

If $|P_T / P_S| << 1$ then

$$K_I \approx 2 \operatorname{Re} \frac{P_T}{P_S} \cdot 100\% = 2 \operatorname{Re} \left(\frac{f_T(\mathbf{e}_{TR}, \mathbf{e}_{ST}) B_S(\mathbf{e}_{ST} - \mathbf{e}_S^0)}{B_S(\mathbf{e}_{SR} - \mathbf{e}_S^0)} e^{ik(R_{ST} + R_{TR} - R_{SR})} \right) \times$$
$$\times \frac{R_{SR}}{R_{TR} R_{ST}} \cdot 100\% \le 2K_P. \tag{1.5}$$

It follows from (1.4) that the modulation level of signal envelope is determined by three factors:

1) by the difference between emitting array's lobe for S-R and S-T directions,
2) by the target strength (TS) being determined by the scattering amplitude,
3) by relative positions of the object and of the emitting and receiving arrays.

The minimum modulation level is reached when the object is on the same range from the source and the receiver: $R_{ST} = R_{TR} = \dfrac{R_{SR}}{2\cos\mathrm{ang}(\mathbf{e}_{ST}, \mathbf{e}_{SR})} \approx \dfrac{R_{SR}}{2}$. In this case

$$K_P \geq 4\left|f_T(\mathbf{e}_{TR}, \mathbf{e}_{ST})\right| \left|\frac{B_S(\mathbf{e}_{ST} - \mathbf{e}_S^0)}{B_S(\mathbf{e}_{SR} - \mathbf{e}_S^0)}\right| R_{SR}^{-1} \cdot 100\% \,. \tag{1.6}$$

Thus, the minimum modulation level will be proportional to the total length R_{SR} of the FS-ABS system. Note that the modulation coefficient of the signal envelope depends also on the difference of ranges $R_{ST} + R_{TR} - R_{SR}$.

If the source has no pattern ($B_S = (4\pi)^{-1}$), then

$$K_P \geq 4\left|f_T(\mathbf{e}_{TR}, \mathbf{e}_{ST})\right| R_{SR}^{-1} \cdot 100\% \,. \tag{1.7}$$

It is common to characterize the scattering strength of objects by using the term of equivalent radius (ER) R_T. By definition it is equal to the radius of a perfectly reflecting sphere creating in its "far field" zone a reflected signal of the same level that the object. For the high frequency limit ER is related to the scattering amplitude f_T by the ratio $|f_T| = R_T/2$ [1]. For some objects whose ER for the classic ABS is equal to several meters and for the range $R_{SR} = 100$ km $= 10^5$ m the estimate of the modulation coefficient is

$$K_P \propto 10^{-2}\% \,, \tag{1.8}$$

that is too small value for using the effect to solve UOS problems being of practical interest.

Nevertheless, a waveguide environment offers supplementary opportunities. In this case, one may express the source and echo-signal fields as follows

$$P_S = \sum_{\mu} B_S(\mathbf{e}_{SR}^{\mu} - \mathbf{e}_S^0)\sqrt{F_{SR}^{\mu}}\, e^{ik\Phi_{SR}^{\mu}} R_{SR}^{-1} \,, \tag{1.9}$$

$$P_T = \sum_{\vartheta,\nu} f_T(\mathbf{e}_{TR}^{\nu}, \mathbf{e}_{ST}^{\vartheta})\sqrt{F_{TR}^{\nu}}\, e^{ik\Phi_{TR}^{\nu}} \cdot B_S(\mathbf{e}_{ST}^{\vartheta} - \mathbf{e}_S^0)\sqrt{F_{ST}^{\vartheta}}\, e^{ik\Phi_{ST}^{\vartheta}} R_{TR}^{-1} R_{ST}^{-1} \,, \tag{1.10}$$

where one makes summation over all possible ray paths lying three points. R_C is some range where the sound propagation comes from the spherical law to the cylindrical one. For shallow water environments it may be estimated as 1 km. Values F with different indexes are products of focusing factors of corresponding rays with amplitude coefficients that take account of coherent field weakening due to sound absorption in the water and to scattering from boundaries or volume perturbations.

For every three paths such estimate of the modulation coefficient follows:

$$K_P^{\mu\nu\vartheta} \geq 4\left|f_T(\mathbf{e}_{TR}^{\vartheta}, \mathbf{e}_{ST}^{\nu})\right| \left|\frac{B_S(\mathbf{e}_{ST}^{\nu} - \mathbf{e}_S^0)}{B_S(\mathbf{e}_{SR}^{\mu} - \mathbf{e}_S^0)}\right| \sqrt{F_{ST}^{\nu} F_{TR}^{\vartheta} F_{SR}^{\mu\,-1}} R_{SR}^{-1} \cdot 100\% \,. \qquad (1.11)$$

It's known that the focusing factor in the ocean can reach the value 100. Assuming that the propagation conditions are those where many caustics of field are formed (the shallow water conditions are of this type) and assuming that there is small probability that the receiving array is placed simultaneously near caustics of two between three ray paths in (1.11), the following estimate derives:

$$K_P^{\mu\nu\vartheta} \propto 10^{-1}\% \,. \qquad (1.12)$$

Another opportunity to increase the modulation coefficient is to elaborate such a sonar scheme where the TS grows considerably. Such an opportunity is offered by the fact that for frequencies exceeding several hundreds of Hz, scattering amplitudes of common underwater objects and of accompanying medium perturbations are very narrow and focused on the direction of propagation of the incident field. An ABS system operating in the FS mode is realizing this opportunity. To estimate the modulation coefficient in this case one may use the fact that the integral TS of an object in the high frequency limit of geometrical acoustics is equal to the area $S \sim LD$ of projection of the object on the incident wave front. For common underwater objects it may be assumed that $S \sim 10^3$ m^2. As to accompanying inhomogeneities, the integral TS can practically reach values about 10^4 m^2. Since the angle width of the main lobe of the scattering amplitude may be estimated as $\sim \lambda/2L$ for the horizontal plane and $\sim \lambda/2D$ for the vertical one, then while considering secondary lobes to be small, one can approach the main lobe by the gaussian function $\sqrt{LD}\, \frac{e^{-\frac{(\varphi-\varphi_0)^2}{4(\lambda/2L)^2} - \frac{(\theta-\theta_0)^2}{4(\lambda/2D)^2}}}{\sqrt{2\pi}(\lambda/2\sqrt{LD})}$ and to estimate $R_T \sim 2S/\lambda$. Therefore there is (in principle) an opportunity to design a FS-ABS system so that the modulation coefficient would be about tens of percents:

$$K_P \propto 10\% \,. \qquad (1.13)$$

Spectral density of such a modulation may be compatible in some frequency interval with the background modulations which are due to the sound scattering from natural fluctuations of the environment (e.g. from free internal waves or ocean turbulence). Such modulation levels were observed in sea experiments and were also obtained in computer simulations of the effect by one of the authors.

2. SIGNAL AND INTERFERENCE MODELS FOR ABS

As for the determinist sea environment (DSE) model, as well for the stochastic (SSE) model, the signal model for some ABS system is as following. Electric signals at exits of N_R receivers of the receiving array are proportional to acoustical pressure at points $\mathbf{r}_s$ where the receivers are located. If the hypothesis H_ε is true ($\varepsilon = 1$ if there is a object and $\varepsilon = 0$ if there no object) one may express the signal as a sum:

$$p(\mathbf{r}_s,t) = p_S(\mathbf{r}_s,t) + \varepsilon\, p_T(\mathbf{r}_s,t) + p_N(\mathbf{r}_s,t),\ s = 1,...,N_R,\ t \in (0,T)\ , \quad (2.1)$$

where

$p_S(\mathbf{r}_S,t)$ is the pressure of the incident signal, which is coherent with the signal emitted by the sonar's source array.

$p_T(\mathbf{r}_S,t)$ is the pressure of the echo-signal which is also coherent with the signal emitted by the sonar's source array.

$p_N(\mathbf{r}_S,t)$ is the pressure of the multi-component incoherent interference, which is a mixture of 1) system noise, 2) sea ambient noise, 3) noise of local sources and 4) reverberation noise.

2.1. Model of source field

Let model a sonar's source as omnidirectional point source radiating narrow band signals ($\Delta\omega/\omega << 1$) with normalized spectrum $S_0(\omega)$. When dealing with linear problems, the general Green's function method may be used to calculate spectrum of the field created by the source:

$$p_S(\mathbf{r},\omega) = G(\mathbf{r},\mathbf{r}';\omega) S_0(\omega) \sqrt{W \rho_{Wat} c \gamma / 4\pi}\ , \quad (2.2)$$

where G(.) is the waveguide's frequency GF, W, γ, $\rho_{Wat}c$ are respectively the radiated acoustic power, concentration coefficient of the source array (pattern factor) and wave resistance of the medium.

Modeling of GF depends on what kind of waveguide is used to model sea environments. In some cases the environmental modeling by a determinist waveguide where space-time distributions of all physical fields are perfectly known can be applied. In this case sound field values can be predicted for any time-space point by using some mathematical model. One of such models, the mostly often used for applications, where high-frequency sound fields are used, is the ray model and is presented below. Nevertheless, modeling of sea environments by a deterministic waveguide is not acceptable in most cases. Ocean surface is practically always rough, and its shape

can not be controlled exactly. There are also hydrodynamic motions in the water layer: internal waves, large-scale turbulence, and inhomogeneities of fine structure, which can not be controlled in most cases too. Also, the boundary of the water-ground interface is generally rough and there are inhomogeneities in the bottom as well as in the water. Usually, nothing is known about all these roughness (boundary and volume) from the deterministic point of view. All these reasons lead to the necessity to use a statistical description of ocean parameters effecting the sound propagation. Those parameters are shapes of surface and bottom boundaries described by functions $\zeta_{Surf}(\mathbf{x},t)$, $\zeta_{Bot}(\mathbf{x})$, fluctuations $\mu(\mathbf{x},z,t) = c(\mathbf{x},z,t)/c_0(z)$ of sound speed (SS) field in the water column ($c_0(\mathbf{r})$ is reference sound velocity field), and fluctuations $\mu_L(\mathbf{x},z)$, $\mu_T(\mathbf{x},z)$ of longitudinal and transversal wave velocities in the bottom. It's supposed in this section that the full statistical description of all acoustic and hydrodynamic properties of some ocean area is known, which is needed for developing a sound field model.

In the case where there are random volume fluctuations of the effective sound speed in the waveguide or where the boundaries of the waveguide (surface and bottom) are rough and can be described only statistically, GF is also random and the statistical description shall be applied to it. The most interesting for applications are the two first moments of GF: the mean ("coherent") field $\overline{G}(\mathbf{r},\mathbf{r}';\omega) = E[G(\mathbf{r},\mathbf{r}';\omega)]$ (the averaging $E[.]$ of GF of current waveguide realizations is done over the fluctuation ensemble) and the second moment ("coherence function") $\Gamma(\mathbf{r}_1,\mathbf{r}_2,\mathbf{r}';\omega_1,\omega_2) = E[G(\mathbf{r}_1,\mathbf{r}';\omega_1)G^*(\mathbf{r}_2,\mathbf{r}';\omega_2)]$, or the local angle spectrum $N(\mathbf{e},\omega;\mathbf{R})$ related to the second moment of locally homogeneous fields:

$$\Gamma(\mathbf{r}_1,\mathbf{r}_2,\mathbf{r}';\omega,\omega) = \overline{G}(\mathbf{r}_1,\mathbf{r}';\omega)\overline{G}^*(\mathbf{r}_2,\mathbf{r}';\omega) + K(\mathbf{r}_1,\mathbf{r}_2,\mathbf{r}';\omega),$$
$$K(\mathbf{r}_1,\mathbf{r}_2,\mathbf{r}';\omega) = \oint_{\Sigma|\mathbf{e}|=1} N(\mathbf{e},\omega;\frac{\mathbf{r}_1+\mathbf{r}_2}{2}) e^{j\frac{\omega}{c}\mathbf{e}(\mathbf{r}_1-\mathbf{r}_2)} d\Omega(\mathbf{e}). \qquad (2.3)$$

In the most cases fluctuations μ are effect of hydrodynamic motions in the water layer and of thin vertical fluctuations in the water stratification. Some spectral models of such fluctuations are well-known [2].

Effect of various random factors on sound fields depends on the ratio of the roughness space scale to the field's Fresnel radius and also on the ratio of the roughness time scale to the signal processing period of a sonar on which the real averaging of signal data is done. The scattering from roughness whose scale is smaller or similar to the Fresnel radius gives birth to scattered fields, which are incoherent with the emitted signal. Those fields form the incoherent reverberation interference. Its statistical model based on the ray theory is described below in the section 2.4.4. For common long-range underwater acoustics problems where sound fields of several kHz or

lower are considered the sea free surface may be treated as small-scale roughness from this point of view. Some different situation is for the bottom case. Real bottom surface may contain roughness of various scales. As for the free surface, there is roughness, which creates the incoherent reverberation, but there is also large-scale roughness. The scattering from large-scale bottom and volume roughness creates sound fields which are coherent with the emitted signal but whose parameters (travel times and arrival angles) are random and should be described statistically.

Mostly general and frequency invariant mathematical model for the two first moments of GF is described in [3]. The model is developed for regular stratified (mean-layered) environments with taking into account the multi-time scattering from rough boundaries and large-scale volume inhomogeneities. In the frame of this model, the single-frequency second-order moment that determines the field's space correlation and in particular its angular spectrum, satisfies to some integral Fredholm equation of the second kind. The kernel and free term of the equation are describing the wave scattering from volume and boundaries' inhomogeneities. However, the numerical implementation of this comprehensive mathematical model is rather difficult. Simpler mathematical and numerical models can be built if roughness having different space-time scales and nature (boundary, volume) can be considered separately and do not effect each other. Hereafter, such a model for the two first moments of the SSE GF is presented. The model is based on geometric (ray) approximation that is applicable in the case of high frequency sound fields. For volume roughness the ray model takes into account the multi-time scattering from large-scale volume SS inhomogeneities. This model provides the two first moments of GF when it is averaged on large time-space intervals. It may be applied to predict statistical characteristics of ray structures in SSE. For boundary roughness the ray approach provides two models. The first one shall be applied for large-scale bottom roughness and predicts statistical characteristics of ray structures in waveguides having such roughness. The second model shall be applied for small-scale boundary roughness (bottom as well as free surface) and provides the two first moments of GF when it is averaged on small time-space intervals. It may be applied to predict statistical characteristics of incoherent reverberation.

2.1.1. GF model for deterministic sea environments

Let use the common ray approach to sound propagation modeling in sea environments [4]. In despite of its well-known defects it rests one of the most powerful mathematical and numerical methods allowing to solve the most part of sound propagation problems as in layered as well as in irregular 2D or 3D OWG for frequency range hundreds of Hz - several kHz. Under the ray approach, GF of the waveguide is developed as a sum of quasi-plane wave fields arriving along ray paths:

$$g(\mathbf{r},\mathbf{r}';\tau) = \sum_{\mu=1}^{M(\mathbf{r},\mathbf{r}')} A_\mu(\mathbf{r},\mathbf{r}') \cdot \delta(\tau - t_\mu(\mathbf{r},\mathbf{r}')), \tag{2.4}$$

$$G(\mathbf{r},\mathbf{r}';\omega) = \sum_{\mu=1}^{M(\mathbf{r},\mathbf{r}')} A_\mu(\mathbf{r},\mathbf{r}';\omega) e^{i\omega t_\mu(\mathbf{r},\mathbf{r}')} = \tag{2.4'}$$

$$= \oint \sum_{\mu=1}^{M(\mathbf{r},\mathbf{r}')} A_\mu(\mathbf{r},\mathbf{r}';\omega) e^{i\omega t_\mu(\mathbf{r},\mathbf{r}')} \delta(\mathbf{e} - \mathbf{e}_\mu(\mathbf{r},\mathbf{r}')) d\Omega(\mathbf{e}),$$

where $M(\mathbf{r},\mathbf{r}')$ is the total number of rays connecting the observation point $\mathbf{r}$ and the point $\mathbf{r}'$ where the incident source is located, $A_\mu(\mathbf{r},\mathbf{r}';\omega) = = (f_\mu(\mathbf{r},\mathbf{r}')V_\mu(\mathbf{r},\mathbf{r}';\omega))^{1/2}/|\mathbf{x}-\mathbf{x}'|$ is amplitude of the μ-th ray path, $f_\mu(\mathbf{r},\mathbf{r}')$ is its focusing factor, the factor $V_\mu(\mathbf{r},\mathbf{r}';\omega) = |V_{\text{Surf}}(\omega)|^{2n_{\mu\text{Surf}}} |V_{\text{Bot}}(\omega)|^{2n_{\mu\text{Bot}}} 10^{-0,1\beta_{\text{Wat}} c\, t_\mu(\mathbf{r},\mathbf{r}')}$ is field weakening due to propagation along the μ-th ray path with n_μSurf and n_μBot - numbers of reflections on ocean boundaries with reflection indexes $V_{\text{Surf}}(\omega)$, $V_{\text{Bot}}(\omega)$, β_{Wat} is *dB/km* absorption of acoustical energy in the sea water, $t_\mu(\mathbf{r},\mathbf{r}')$ is the ray's travel time.

Taking into account all advantages of using high frequency range in the FS-ABS acoustic systems to increase the object strength and decrease ambient noises, following theoretical developments and numerical simulations will be based on the above described ray model of the sea waveguide's GF.

2.1.2. GF model for stochastic sea environments with slow large-scale volume roughness

In the presence of large-scale volume roughness in the waveguide being SS fluctuations $\mu(\mathbf{r},t)=c(\mathbf{r},t)/c_0(\mathbf{r})$ on the background of mean SS field $c_0(\mathbf{r})$, the mean GF under the ray approximation is

$$\overline{G}(\mathbf{r},\mathbf{r}';\omega) = E[G(\mathbf{r},\mathbf{r}';\omega)] = E\left[\sum_{\nu=1}^{N(\mathbf{r},\mathbf{r}')} A_\nu(\mathbf{r},\mathbf{r}';\omega) \exp\{i\omega t_\nu(\mathbf{r},\mathbf{r}')\}\right], \tag{2.5}$$

where E[.] is the averaging on the ensemble of SS fluctuations, G(.) is GF of perturbed waveguide, $N(\mathbf{r},\mathbf{r}')$ is the total number of ray paths connecting the points $\mathbf{r}$ and $\mathbf{r}'$, $A_\nu(\mathbf{r},\mathbf{r}';\omega)$ is the amplitude of the ν-th ray path, $t_\nu = t_\nu(\mathbf{r},\mathbf{r}')$ is the travel time for the ν-th ray path.

If SS fluctuations are relatively "slow", current GF realization under the ray approximation is computed [5] as:

$$G(\mathbf{r},\mathbf{r}';\omega) = \sum_{\nu=1}^{N(\mathbf{r},\mathbf{r}')} A_\nu(\mathbf{r},\mathbf{r}';\omega)\exp\left\{i\omega\left(\bar{t}_\nu(\mathbf{r},\mathbf{r}') + \delta t_\nu(\mathbf{r},\mathbf{r}')\right)\right\}, \qquad (2.6)$$

where $\bar{t}_\nu$ is the mean travel time of the ν-th ray path, it is equal to the travel time in the reference waveguide where $c = c_0(\mathbf{r})$, $\delta t_\nu = t_\nu - \bar{t}_\nu$ is the travel time fluctuation of the ν-th ray path.

Thus, SS fluctuations effect only ray travel times and resume as phase perturbations to be computed by integrating the field $\mu(\mathbf{r})$ along reference ray paths:

$$\delta t_\nu = -\int_{\mathfrak{L}_\nu} \frac{\mu(\mathbf{r})}{c_0(\mathbf{r})} ds \,. \qquad (2.7)$$

Ray amplitudes and the number of ray paths remain the same as for the reference waveguide. After averaging the exponent, the well-known equation for the coherent field derives:

$$\bar{G}(\mathbf{r},\mathbf{r}';\omega) = \sum_{\nu=1}^{N(\mathbf{r},\mathbf{r}')} A_\nu(\mathbf{r},\mathbf{r}';\omega)\exp\left\{i\omega\,\bar{t}_\nu(\mathbf{r},\mathbf{r}') - \frac{1}{2}\omega^2 D_{t_\nu}(\mathbf{r},\mathbf{r}')\right\}, \qquad (2.8)$$

where $D_{t_\nu} = \mathrm{E}\left[(\delta t_\nu)^2\right]$ is the travel time variance for the ν-th ray path. It is computed from the covariance function $K_\mu(\mathbf{r}_1,\mathbf{r}_2) = \mathrm{E}[\mu(\mathbf{r}_1)\mu(\mathbf{r}_2)]$ of the field $\mu(\mathbf{r})$ by integrating along the reference ν-th ray path connecting the points $\mathbf{r}'$ and $\mathbf{r}$:

$$D_{t_\nu}(\mathbf{r},\mathbf{r}') = \int_{\mathfrak{L}_\nu}\int_{\mathfrak{L}_\nu} \frac{K_\mu(\mathbf{r}(s'),\mathbf{r}(s''))}{c_0(\mathbf{r}(s'))c_0(\mathbf{r}(s''))} ds'ds'' \approx \int_{\mathfrak{L}_\nu} \frac{Z_\mu(\mathbf{r}(s))}{c_0^2(\mathbf{r}(s))} ds,$$

$$Z_\mu(\mathbf{r}) = \int_{\mathfrak{L}_\nu} B_\mu(\mathbf{r}, s\boldsymbol{\tau}) ds, \quad \boldsymbol{\tau} = \left.\frac{d\mathbf{r}(s)}{ds}\right|_{\mathfrak{L}_\nu}, \qquad (2.9)$$

$$B_\mu(\mathbf{r},\boldsymbol{\rho}) = K_\mu(\mathbf{r}+\boldsymbol{\rho}/2, \mathbf{r}-\boldsymbol{\rho}/2).$$

The meaning of Z_ν is the integral correlation interval of the field $\mu(\mathbf{r})$ along the ν-th ray path. Thus, the effect of the scattering from large-scale volume inhomogeneities is manifested as additional attenuation of the coherent field in comparison with the case of propagation in the reference waveguide. For some field of fluctuations $\mu(\mathbf{r})$, this additional attenuation is determined by corresponding travel time variances along ray paths and by the frequency. Numerical evaluations show that in the case of scattering from inhomogeneities due to Harret-Munk's internal waves, RMS of ray travel times may reach units of ms (millisecond) for ranges of tens of kilometers. So, in this case at frequency 1 kHz the factor of the additional weakening of the coherent

field due to the scattering may be $\sim \exp\{-(2\pi)^2/2\} \sim \exp\{-20\} < 10^{-8}$.

For the coherence function (the second order moment), the following equation derives after averaging:

$$\Gamma(\mathbf{r}_1,\mathbf{r}_2,\mathbf{r}_0;\omega_1,\omega_2) = \\ = \sum_{\kappa=1}^{K(\mathbf{r}_1,\mathbf{r}_0)} \sum_{\nu=1}^{N(\mathbf{r}_2,\mathbf{r}_0)} A_\kappa(\mathbf{r}_1,\mathbf{r}_0;\omega_1) A_\nu^*(\mathbf{r}_2,\mathbf{r}_0;\omega_2) \exp\{i\omega_1 t_\kappa(\mathbf{r}_1,\mathbf{r}_0) - \omega_2 t_\nu(\mathbf{r}_2,\mathbf{r}_0)\} \times \\ \times \exp\left\{-\frac{\omega_1^2}{2} D_{t_\kappa}(\mathbf{r}_1,\mathbf{r}_0) - \frac{\omega_2^2}{2} D_{t_\nu}(\mathbf{r}_2,\mathbf{r}_0) + \omega_1\omega_2 R_{\kappa\nu}(\mathbf{r}_1,\mathbf{r}_2;\mathbf{r}_0)\right\}, \tag{2.10}$$

where

$$R_{\kappa\nu}(\mathbf{r}_1,\mathbf{r}_2;\mathbf{r}_0) = \int_{S_\kappa}\int_{S_\nu} \frac{K_\mu(\mathbf{r}(s'),\mathbf{r}(s''))}{c_0(\mathbf{r}(s'))c_0(\mathbf{r}(s''))} ds'ds'', \; R_{\nu\nu}(\mathbf{r},\mathbf{r};\mathbf{r}_0) = D_{t_\nu}(\mathbf{r},\mathbf{r}_0) \tag{2.11}$$

is the cross-correlation of travel times along the κ-th and ν-th ray paths. Thus, the cross covariance function $R_{\kappa\nu}(\mathbf{r}_1,\mathbf{r}_2;\mathbf{r}_0)$ defines, as one can see, the two first moments under the geometric (ray) approximation.

If the distance between the points $\mathbf{r}_1$ and $\mathbf{r}_2$ is much larger than the correlation interval of inhomogeneities, then the correlation of travel time fluctuations is defined, firstly, by the source vicinity whose contribution is

$$\int_0^\infty\int K_\mu(\mathbf{e}_\kappa(\mathbf{r}_0)s',\mathbf{e}_\nu(\mathbf{r}_0)s'')c_0^{-2}(\mathbf{r}_0)ds'ds'' \;,$$

where $\mathbf{e}_\kappa(\mathbf{r}_0)$, $\mathbf{e}_\nu(\mathbf{r}_0)$ are the unit vectors tangent to the κ-th and ν-th ray paths at the source point. This fact is evident if the observation points $\mathbf{r}_1$ and $\mathbf{r}_2$ lie in some horizontal plane because the reference ray paths have a constant divergence in the horizontal plane, so that if they pass through volumes of medium with not correlated fluctuations after the first cycle, they do the same further more. If the observation points lie in some vertical plane, the vicinities of reference rays' intersection points $\mathbf{r}_q$ give also contributions into the travel times' correlation:

$$\sum_q \int_{-\infty}^{\infty}\int K_\mu(\mathbf{e}_\kappa(\mathbf{r}_q)s',\mathbf{e}_\nu(\mathbf{r}_q)s'')c_0^{-2}(\mathbf{r}_q)ds'ds'' \;.$$

However, for the Harret-Munk's spectrum, as for any other one vanishing to zero when the wave number tends to zero, this integral is equal to zero.

Let it be $\mathbf{r}_1+\mathbf{r}_2 = 2\mathbf{r}$, $\rho = \mathbf{r}_1-\mathbf{r}_2$ for small separations of observation points. Let the

point $\mathbf{r}$ is connected to the source point $\mathbf{r}_1$ by N ray paths in the reference medium. Let also consider such separations of observation points that are not larger than the characteristic width of reference ray beams. That means that if a reference ray connecting the points $\mathbf{r}_1$ and $\mathbf{r}$ is described by a function $r_\nu(s)$, then the corresponding reference ray connecting the points $\mathbf{r}_0$ and $\mathbf{r}\pm\rho/2$ is described by the function $\mathbf{r}_\nu(s)\pm(\rho/2)\Lambda_\nu(s,L)$, where $\Lambda_\nu(s,L)$ is the matrix solution of the problem

$$\mathbf{F}(s)\Lambda_\nu(s,L)=0,\ \Lambda_\nu(0,L)=0,\ \Lambda_\nu(L,L)=\mathbf{P}_\nu,\ [\mathbf{P}_\nu]^{\alpha\beta}=\delta^{\alpha\beta}-e_\nu^\alpha e_\nu^\beta,$$
$$\mathbf{F}(s)=\mathrm{diag}\left\{n^{-1}\frac{d}{ds}\left(n\frac{d}{ds}\right)+\left(\kappa^2-\frac{\partial^2\ln n}{\partial\nu^2}\right),n^{-1}\frac{d}{ds}\left(n\frac{d}{ds}\right)\right\}. \tag{2.12}$$

The operator $\mathbf{P}_\nu$ does projection onto the subspace that is orthogonal to the tangent vector $\mathbf{e}_\nu=\{e^\alpha_\nu\}$ of the ν-th ray path. Under the above conditions, the correlation of travel time fluctuations along a single reference ray path is computed as follows

$$R_{\nu\nu}(\mathbf{r},\rho;\mathbf{r}_0)=$$
$$=D_{t_\nu}(\mathbf{r},\mathbf{r}_0)-\frac{1}{2}\frac{B_\mu(\mathbf{r},0)(\mathbf{e},\rho)^2}{c_0^2(\mathbf{r})}-\frac{1}{2}\int_0^\infty\rho_\alpha\Lambda_\nu^{\alpha\gamma}(s,L)\frac{\mu_{\gamma\delta}(s,l(s))}{c_0^2(\mathbf{r})}\Lambda_\nu^{\delta\beta}(s,L)\rho_\beta\,ds,$$
$$\mu_{\gamma\delta}(s,l(s))=\int_{-\infty}^{\infty}\partial^2_{\rho_\gamma\rho_\delta}B_\mu(u,\boldsymbol{\rho}_1)\Big|_{\rho_\alpha=0}du \tag{2.13}$$

and the correlation for any two different reference rays can be written as follows

$$R_{\kappa\nu}(\mathbf{r},\rho;\mathbf{r}_0)=\int_0^\infty\!\!\int\frac{K_\mu(\mathbf{e}_\kappa(\mathbf{r}_0)s',\mathbf{e}_\nu(\mathbf{r}_0)s'')}{c_0^2(\mathbf{r}_0)}ds'ds''+\int_0^\infty\!\!\int\frac{K_\mu(\mathbf{e}_\kappa(\mathbf{r})s',\mathbf{e}_\nu(\mathbf{r})s'')}{c_0^2(\mathbf{r})}ds'ds''-$$
$$-\frac{B_\mu(\mathbf{r},0)}{4c_0^2(\mathbf{r})}\left\{(\mathbf{e}_\kappa(\mathbf{r}),\rho)(\mathbf{e}_\nu(\mathbf{r}),\rho)-(\mathbf{e}_\kappa(\mathbf{r}),\mathbf{e}_\nu(\mathbf{r}))\left[(\mathbf{e}_\kappa(\mathbf{r}),\rho)^2+(\mathbf{e}_\nu(\mathbf{r}),\rho)^2\right]\right\}+ \tag{2.14}$$
$$+\frac{1}{4c_0^2(\mathbf{r})}\left(\int_{-\infty}^0\!\!\int K_\mu(\mathbf{e}_\kappa(\mathbf{r})s',\mathbf{e}_\nu(\mathbf{r})s'')ds'ds''(\rho_1^\kappa+\rho_1^\nu),(\rho_1^\kappa+\rho_1^\nu)\right).$$

It follows from the equation (10) that the matrix

$$\Lambda_\nu^{\alpha\beta}(\mathbf{r},\mathbf{r}_0)=c_0^2(\mathbf{r})\int_0^\infty\Lambda_\nu^{\alpha\gamma}(s,L)\frac{\mu_{\gamma\delta}(s,l(s))}{c_0^2(\mathbf{r})}\Lambda_\nu^{\delta\beta}(s,L)ds \tag{2.15}$$

may be understood as the covariance matrix of ray paths' arrival angle fluctuations. In force of the space symmetry of the internal wave spectrum and thanks to the layered model for the deterministic part of the SVF, this matrix is diagonal: arrival angle

fluctuations in the horizontal plane are not correlated with those in the vertical plane. The travel time fluctuations and arrival angle ones are also not correlated.

In the equation (2.15), the two first terms describe the correlation of travel time along the κ-th and ν-th ray paths, and the last term does the same for the correlation of ray arrival angles. Correlation of arrival angles of different rays is only determined by the vicinity of the receiver, and the correlation of travel time fluctuations is determined by the vicinities of the source and the receiver (the vicinities of the intersection points of any two different reference ray paths do not contribute to the correlation). As the variances of ray travel time and arrival angle fluctuations should grow with the distance from the source but theirs correlation for different ray paths should not globally grow, hence they may vary from one cycle to another, the correlation coefficient decreases when the number of ray cycles grows, though the correlation coefficient for one cycle can be considerable.

One can transform the equation for statistical characteristics of arrival time and angle fluctuations to express them via the spectrum of inhomogeneities. Then using the Harret-Munk's internal waves' spectrum, equations derive that are not present here because of their volume [6]. Those equations allow computing of variances of travel time fluctuations and modeling of correlation functions of arrival angle fluctuations in the vertical and horizontal plane by means of simple integrating along ray paths. It follows from the equation that the main contribution to the correlation functions in the deep ocean case is given by ray turning points. Expressions for time correlation intervals of ray travel times and of grazing arrival angles were also obtained in [6].

The equation (2.9) for the variance of ray travel times can be simplified under the supposition that the covariance function of sound velocity fluctuations can be approximated by a gaussian function

$$K_\mu(\mathbf{r},\mathbf{r}') = D_\mu(z)\exp\left\{-\frac{1}{2}(\mathbf{r}-\mathbf{r}')\mathbf{R}_\mu^{-1}(\mathbf{r}-\mathbf{r}')\right\}, \qquad (2.16)$$

where $\mathbf{R}_\mu^{-1} = diag\left(\rho_H^{-2}(z), \rho_H^{-2}(z), \rho_V^{-2}(z)\right)$, $\rho_H(z)$ and $\rho_V(z)$ are horizontal and vertical correlation intervals for the field μ. One integration in (2.9) can be done by the Laplace method and the following equation derives:

$$D_{t_\nu}(\mathbf{r},\mathbf{r}_0) = \frac{\sqrt{2\pi}}{c_\nu^2}\int_{S_\nu}\frac{D_\mu(z)\rho_V(z)}{\cos^2\chi\sqrt{\sin^2\chi+\varepsilon^2(z)\cos^2\chi}}ds, \qquad (2.17)$$

$\varepsilon(z) = \rho_V(z)/\rho_H(z)$, $c_\nu = c_0/\cos\chi_0$ (c_ν is sound velocity at the returning point of the ν-th ray path). By the same way similar equations derive for variances of fluctuations of ray arrival angles:

$$D_{\varphi_v}(\mathbf{r},\mathbf{r}_0)=\frac{\sqrt{2\pi}}{R^2(\mathbf{r},\mathbf{r}_0)}\int_{\Lambda_v}\frac{D_\mu(z)\varepsilon(z)R^2(\mathbf{r}(s),\mathbf{r}_0)}{\rho_H(z)\cos^2\chi\sqrt{\sin^2\chi+\varepsilon^2(z)\cos^2\chi}}ds\,, \tag{2.18}$$

$$D_{\chi_v}(\mathbf{r},\mathbf{r}_0)=\frac{\sqrt{2\pi}}{\Delta^2(\mathbf{r},\mathbf{r}_0)}\int_{\Lambda_v}\frac{D_\mu(z)\varepsilon(z)\Delta^2(\mathbf{r}(s),\mathbf{r}_0)}{\rho_H(z)\cos^2\chi\left(\sin^2\chi+\varepsilon^2(z)\cos^2\chi\right)^{2/3}}ds\,. \tag{2.19}$$

where $\Delta=\left(\partial R/\partial\chi_0\right)\sin\chi$. Time correlation interval of fluctuations is

$$\tau_v(\mathbf{r},\mathbf{r}_0)=\sqrt{\int_{\Lambda_v}\frac{\cos^{-2}\chi K_\tau(z)\rho_V(z)}{\sqrt{\sin^2\chi+\varepsilon^2(z)\cos^2\chi}}ds\Bigg/\int_{\Lambda_v}\frac{\cos^{-2}\chi D_\mu(z)\rho_V(z)}{\sqrt{\sin^2\chi+\varepsilon^2(z)\cos^2\chi}}ds}\,. \tag{2.20}$$

In the case where sound velocity fluctuations are effect of free internal waves they are related by a simple equation:

$$\mu(\mathbf{r},t)=DN^2(z)\xi(\mathbf{r},t)\,, \tag{2.21}$$

with $\xi(\mathbf{r},t)$ the function describing the field of internal waves, $N(z)$ the frequency profile of free gravitational waves: $N^2(z)=d\ln\rho_{Wat}(z)/dz$, with $\rho_{Wat}(z)$ water density at depth z. The value D depends slightly on ocean regions and on depth and is equal to ~10 sec^2/m. For the case of ocean internal waves the parameter $\rho_H \sim 7$ km and the anisotropy factor $\varepsilon(z)$ depends on depth and varies usually in the range from 1/70 to 1/100.

Computer modeling results of statistical characteristics of ray paths for shallow water conditions (for the Pekeris waveguide) are presented with the figure 2.1. General conclusions for the deep ocean case are as follows. As it has been shown that the main contribution to ray travel time fluctuations is done by ray turning points, then, taking into account that in the deep ocean 1) the frequency $N(z)$ decreases quickly when the depth increases and 2) the variance of $\mu(z)$ is proportional to the third power of $N(z)$, one concludes that the maximal contribution in the ray parameters' fluctuations in these conditions is done by the upper turning point. Really, simulations demonstrate clearly the difference between water-born, surface-water-born and bottom-born ray paths. It follows also from the simulations that the level of ray travel time fluctuations is maximal in a shallow water channel and minimal in a deep-water channel. It agrees well with the above conclusions about contributions of ray turning points. Our simulations show also that ray travel time fluctuations vary from several fractions of ms for steep ray paths to several units of ms for gentle ray paths. The RMS of grazing arrival angle varies from fractions of degree for steep ray paths to 1°...2° for gentle ray paths if one pays no attention to jets in the graphics occurring when a ray passes focal points. Horizontal arrival angle fluctuations are so small that

one may neglect them for distances about first hundreds kilometers from the source. Modeling for correlation intervals of ray travel time and arrival angle fluctuations shows them varying from tens minutes for steep ray paths to 1...2 hours for gentle ray paths.

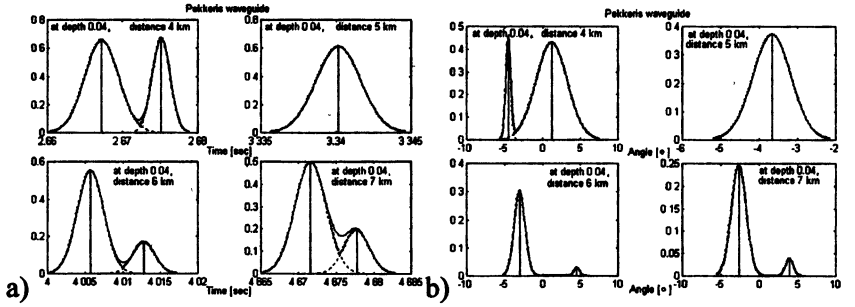

Figure 2.1. Modeling of fluctuations of travel time (a) and arrival grazing angle (b) of source field's rays in the Pekeris waveguide.

Errors due to the use of the geometrical (ray) approximation can be evaluated. Thereby frequency and distance ranges of its validity can be estimated. To do it, let use the Rytov's method of smooth perturbations [7].

2.1.3. GF model for sea environments with large-scale bottom roughness

High-frequency banded signals in sea environments with reflection on a bottom having roughness, whose scale is larger than the field's Fresnel radius, should have a multi speck-patch structure. Such signals consist of many neighboring ray arrivals in the time domain. This effect, whose nature is the same as of the "moon light band" effect, was studied in [8] on experimental and simulated data. Figure 2.2 shows two correlation functions for two consecutive signal pulses obtained on experimental and simulated raw signal data where the simulation was done for a flat smooth bottom. Figure 2.3 shows the time evolution of correlation peaks when the source moved to the receiver. The experimental and simulated situation were for the Barents sea summer propagation conditions (sub-bottom channel) with mean bottom depth about 240 m. The source of LFM signals (central frequency 3240 Hz, band 600 Hz, duration 0.01 sec, depth 7.5 m, speed 6 m/sec) moved from 15 km to 6 km range directly to the receiver (vertical linear array at depth 150 m) and radiated LFM pulses each 10 sec. Although the correlation function structures on the figures 2.2 and 2.3 are rather different, one can find the same general behavior of experimental and simulated correlation functions when observing their time evolution. The difference is that for the simulated data the evolution of maximums has rather regular and deter-

ministic character: peaks form curved lines in the (Delay, Time) plane. It's as each simulated peak corresponds to a group of experimental peaks. Peak amplitudes in each group are fluctuating very quickly although their time coordinates are rather stable and change slowly by the same manner as solitaire peaks in the simulated data.

This effect is due to large-scale bottom roughness whose correlation scale is larger then the Fresnel radius of rays reflected on the bottom. When a sufficiently high frequency sound field is reflected (scattered) on the bottom, there is always such roughness (since the spectrum of the bottom roughness is continuous) on which the scattering resumes as specula reflection. Quantity of such roughness is determined by the ratio of the efficiently sounded area to the projection of the area of the Fresnel zone of a ray path. The efficiently sounded area may be determined as bottom area from which specula reflected ray paths can arrive to the receiver. For some propagation conditions this area is mainly depending on the RMS of roughness slope.

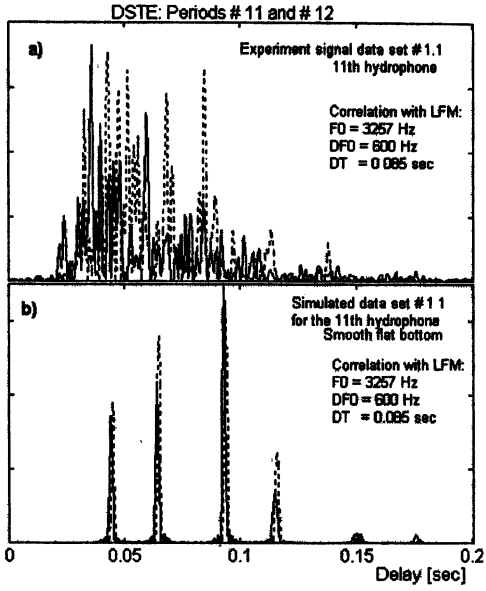

Figure 2.2. Two correlation functions of two consecutive periods for one hydrophone: a) experiment data (Barents sea), b) simulated data (flat smooth bottom).

The quick amplitude fluctuations of peaks of experimental correlation functions are effect of the source motion. It follows from the simulation that each correlation peak corresponds not to a solitary ray arrival but to a couple of ray arrivals very close in time domain. When the source moves phase difference between rays in each couple changes, and the interference between fields arriving along close ray paths creates the amplitude fluctuations. Some correlation peaks be corresponding not to couples but to couples of ray couples since the time resolution of the signal may be not sufficient to segregate maximums of these ray couples. In this case, those maximums should be some more rapidly fluctuating in amplitude.

To simulate this effect, numerical modeling of the source sound field was done for the experimental situation. In this simulation the real bottom was modeled as a) flat smooth or b) rough surface. This simulation was conducted by using a 3D ray-tracing

program. Roughness correlation radius for this modeling had to be equal or greater than the Fresnel radius. Figure 2.4 shows time-angular structures from these simulations. RMS of roughness was 50 m and correlation length was 2 km for the axis source-receiver, and RMS was 20 m and correlation length was 0.2 km for the perpendicular direction. One can really observe the same effect of appearing of groups of arrivals as in the experiment.

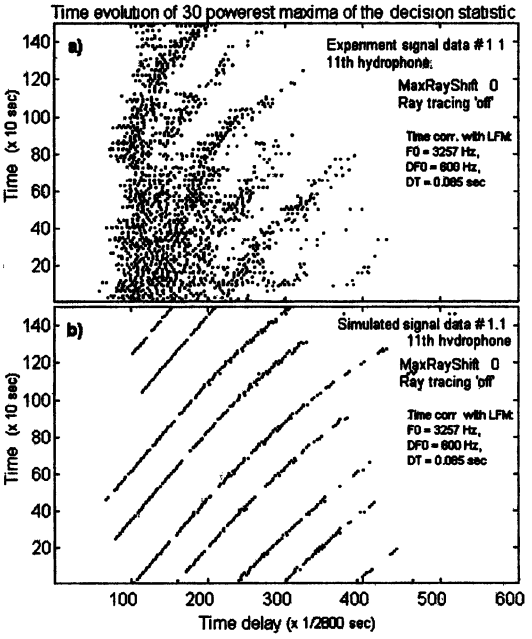

Figure 2.3. Time evolution of correlation maximums for one hydrophone: a) experiment data (Barents sea), b) simulated data (flat smooth bottom).

Bottom reflected sound fields having such structure need a statistical description and may be considered as coherent reverberation. Really, even if the sound speed field is "frozen" and perfectly known, the waveguide should be considered as random one since the bottom is rough, so when a sound source moves, bottom realizations are different for consecutive periods of signal radiation. It makes moving points of specula reflection on the bottom and makes corresponding correlation maximums fluctuating in delay and amplitude.

When doing the statistical description, all parameters of one-time reflected field (number of rays n, their travel times t and arrival angles χ, φ forming a vector $\xi=(t,\chi,\varphi)$) should be considered as random and described by some probability density function (PDF). The simplest model for the parameter n, which must have value 1 or higher, may be the Rayleigh model, where the PDF is:

$$\Phi(n) = n\exp\left\{-n^2/2N^2\right\}/N^2, \quad n \geq 1$$
$$\left(\bar{n} = \mathrm{E}[n] = \sqrt{\pi/2}N, \sigma_n^2 = D[n] = (4-\pi)N^2/2\right) \qquad (2.22)$$

(the maximum of this PDF is for the argument $n = N$). The simplest model which

could be proposed for ξ is the gaussian one, where fluctuations of field parameters (arrival times and angles) are fully described by theirs two first moments (mean values, variances and cross-correlation). If propagation conditions are such that fluctuations of field parameters are not able to change radically the ray path then the mean values $\bar{\xi} = (\bar{t}, \bar{\chi}, \bar{\varphi})$ are those calculated (following the model described in 2.1.1) by a ray program for corresponding environment with a flat smooth bottom. The PDF under the gaussian model is

$$\Phi(\xi) = \frac{\exp\left\{-\left\langle \Xi^{-1}(\xi - \bar{\xi})(\xi - \bar{\xi})\right\rangle\right\}}{\det 2\pi\Xi}, \qquad (2.23)$$

where Ξ is the cross-covariance matrix of parameters ξ. In the case where statistical relationships of time and arrival angle fluctuations can be neglected, the matrix Ξ is diagonal:

$\Xi = \mathrm{diag}\{\sigma_t^2, \sigma_\chi^2, \sigma_\varphi^2\}$.

When using this simplest model only the parameters N, σ_t, σ_χ, σ_φ are needed for modeling. To estimate them one could proceed as follows. Firstly let estimate the parameter σ_φ. If one ray of grazing angle χ is reflected from a plane having a slope angle α then the angle ψ of horizontal refraction due to this reflection satisfies the equation

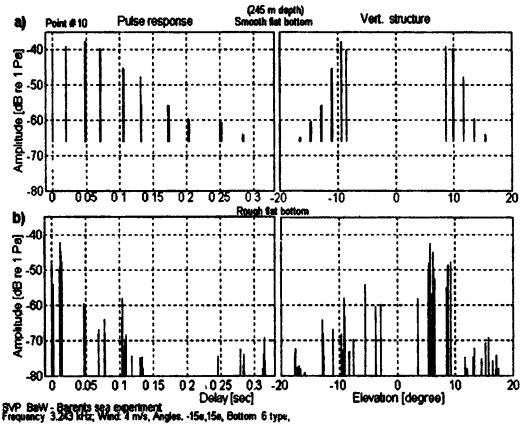

Figure 2.4. Field time-angle structure simulated for a flat (a) and a rough (b) bottom (RMS of dual-scale roughness height 50 m and 20 m, correlation length 2 km and 0.2 km).

$$\sin\psi = \sin 2\alpha \sin\chi. \qquad (2.24)$$

For small angle values χ which are usually realized for sound propagation in sea environments this gives the estimate $\psi \sim 2\alpha\chi$. So, as $\psi \sim 2\varphi$, then the parameter σ_φ may be estimated as $\sigma_\varphi \sim \sigma_\alpha \chi_m$, where χ_m is some characteristic grazing angle value for bottom reflections. The parameter σ_χ may be simply estimated as $\sigma_\chi \sim \sigma_\alpha$. As travel time fluctuations are due to the horizontal refraction effect then the travel time increasing is about

$$[L_1/\cos\varphi+(L-L_1)/\cos(\psi-\varphi)-L]/c \sim [\varphi^2 L_1 + (\psi-\varphi)^2(L-L_1)]/c, \quad (2.25)$$

where L is the range form the source to the receiver, L_1 is the range form the reflection point to the receiver and c is the sound speed. So, an estimate for the parameter σ_t is

$$\sigma_t \sim \sqrt{3}\,\sigma_\varphi^2 L/c \sim \sqrt{3}\,\sigma_\alpha^2 \chi_m^2 L/c. \quad (2.26)$$

For the experimental data presented with the figure 2.3 the parameter σ_t may be estimated as 0.004 sec for the range $L \sim 10$ km, so the RMS of slope of bottom large-scale roughness can be evaluated as $\sigma_\alpha \sim 1/6 \sim 9°$, which may be a rather realistic value.

Finally, an estimate of the parameter N may be the done by estimating the bottom area S from which ray paths having such angle fluctuations are able to reach the receiver. When considering the Pekeris waveguide case this bottom area may be estimated as

$$S \sim (2L\sigma_\chi/\sin 2\chi)(L\,\mathrm{tg}\varphi)\,. \quad (2.27)$$

If the roughness correlation interval is l and σ_H is the RMS of bottom depth ($l \sim \sigma_H \mathrm{ctg}\alpha$) then the parameter N is evaluated as.

$$N \sim L^2\sigma_\alpha^2 / \pi l^2 \sim L^2\sigma_\alpha^4 / \pi\sigma_H^2. \quad (2.28)$$

For the experiment the parameter N may be estimated as 10 for the range $L \sim 10$ km, so the RMS of bottom depth can be evaluated: $\sigma_H \sim 50$ m.

2.2. Echo-signal model

In the general case, when there are surface, bottom and water ray paths connecting the source array (S), an object (T) and the receiving array (R), an echo-signal created by the object is a sum of coherent and diffused components. Under the both DSE or SSE models, the coherent echo-signal component is a quasi deterministic vector process. The diffused component that is due to single scattering from rough object body, from rough bottom and sea surfaces may be supposed normally distributed. As to the field component being two-time scattered from boundary and body rough surfaces, it is randomly modulated random fields (under supposition that surface roughness is normally distributed). Neglecting the two-time scattering component of the echo-signal, one shell consider the incoherent component as homogeneous and stationary gaussian field on the receiving array.

Reflection capability of some object is described by equivalent radius $R_T(\mathbf{e},\mathbf{e}';\omega)$, where $\mathbf{e}$, $\mathbf{e}'$ are normalized vectors determining directions of the reflected and inci-

dent waves. By definition, it is equal to the radius of a perfectly reflecting sphere creating in its Fraunhofer ("far field") zone a reflected signal of the same level that the object.

Using the ray notations, the time-space structure of coherent echo-signal component of an underwater object is

$$\bar{P}_T(\mathbf{r}_R,\mathbf{r}_T,\mathbf{r}_S;\omega)=\sqrt{\frac{W\rho c\gamma}{4\pi}}\cdot\sum_{\nu=1}^{N(\mathbf{r}_R,\mathbf{r}_T)}\sum_{\mu=1}^{M(\mathbf{r}_T,\mathbf{r}_S)}A_\nu(\mathbf{r}_R,\mathbf{r}_T;\omega)A_\mu(\mathbf{r}_T,\mathbf{r}_S;\omega)\times$$
$$\times e^{i\omega(t_\mu(\mathbf{r}_T,\mathbf{r}_S)+t_\nu(\mathbf{r}_R,\mathbf{r}_T))}\frac{1}{2}R_T(\mathbf{e}_\nu,\mathbf{e}_\mu;\omega)\cdot B_S(\mathbf{e}_\mu-\mathbf{e}_S^0;\omega), \tag{2.29}$$

where W, γ, ρc are the radiated acoustic power, the concentration coefficient of the source array (pattern factor) and the wave resistance of medium. All other values were described above.

Usually one makes following assumptions on statistic properties of echo-signals:

1. Their phases are random and uniformly distributed in the interval $(0;2\pi)$.
2. Depending on propagation conditions, the echo-signal amplitude is considered as determinist or randomly distributed under the Raleigh low.
3. So far the echo-signal in waveguide environments is a multi-path signal, it is assumed for such propagation conditions that amplitude fluctuations and initial phases of signals arriving along different paths are statistically independent.

2.3. Object model

The term "object model" means hereafter some method to calculate the object strength or equivalent radius.

2.3.1. Object model for ABS

Under the classic ABS approach an object is described by its capability to sound reflection that is characterized by equivalent radius (ER) R_T equal to radius of a sphere creating an echo-signal of the same level than the object. Under the FS-ABS approach it is common to call the useful signals "scattered", or "diffracted" instead of "reflected". Nevertheless this type of signal shall be also considered as a special kind of echo-signal and one may use the ER term to characterize such signals.

For the frequency range above several hundreds of Hz and for any ABS scheme other then the FS one the ER of common underwater objects usually slightly depends on incident and reflection angles. When the object is sounded from the bow or in a wide angle sector around this direction, the ER depends on object sizes and on qual-

ity of special anechoic covering, if there is one. In this case, it depends smoothly on frequency (as the square root). To do numerical modeling one may use the estimate $R_T = 5 \div 10$ m for common ER increases sharply when the object is illuminated in the board direction. Nevertheless, this effect appears only for narrow angle sector. For conventional active pulse system modeling one should neglect this effect having small probability.

At lower frequencies (about tens of *Hz*), resonance of object body structure will appear and the equivalent radius increases sharply. In this case, the object reflection capability has a well-pronounced angular pattern in both vertical and horizontal planes.

2.3.2. Object model for FS-ABS

It's already mentioned above that for the FS-ABS case when an object is placed in the vicinity of the vertical plane containing the emitter and the receiver, the ER increases sharply up to the ratio $\sim 2S/\lambda$, where S is the area of object projection onto the incident wave front, λ is the wave length. Previous estimate of the useful effect (modulation coefficient) under the FS-ABS approach was made in the section 1.2 and it was shown how one could obtain an estimate of the ER for FS-ABS by using a heuristic approach. Let us found this estimate of ER by using more rigorous formalism of wave diffraction on a perfectly rigid body.

Let $P_S(\mathbf{r})$ and $G_0(\mathbf{r}-\mathbf{r}')$ are the incident field and GF of free space without body, $P_T(\mathbf{r})$ is the field scattered by a body, Σ_T is the surface of the body. Each point on the surface Σ_T may be considered as source of waves forming the field P_T. Using the Green theorem (otherwise called sometimes [1] the Huygens principle), it's possible to represent it as a surface integral

$$P_T(\mathbf{r}) = \oint_{\Sigma_T} \left\{ \left(P_S(\mathbf{r}') + P_T(\mathbf{r}')\right) \frac{\partial}{\partial n'} - \frac{\partial \left(P_S(\mathbf{r}') + P_T(\mathbf{r}')\right)}{\partial n'} \right\} G_0(\mathbf{r}-\mathbf{r}')\, d\sigma \ , \quad (2.30)$$

where n is the external normal to Σ_T. So far as the body is perfectly rigid, then

$$\left. \frac{\partial \left(P_S(\mathbf{r}') + P_T(\mathbf{r}')\right)}{\partial n'} \right|_{\mathbf{r}' \in \Sigma_T} = 0, \text{ therefore,}$$

$$P_T(\mathbf{r}) = \oint_{\Sigma_T} \left(P_S(\mathbf{r}') + P_T(\mathbf{r}')\right) \frac{\partial G_0(\mathbf{r}-\mathbf{r}')}{\partial n'}\, d\sigma \ . \quad (2.31)$$

Let the observation point $\mathbf{r}$ tends to the body's surface. Taking into account that GF has a pole when $\mathbf{r} = \mathbf{r}'$, the following equation deduces

$$P_T(\mathbf{r}) = P_S(\mathbf{r}') + 2\oint_{\Sigma_1}\left(P_S(\mathbf{r}') + P_T(\mathbf{r}')\right)\frac{\partial G_0(\mathbf{r}-\mathbf{r}')}{\partial n'}\,d\sigma\,, \quad \mathbf{r}\in\Sigma_T\,, \tag{2.32}$$

where the surface integral must be calculated as the Cauchy main value.

Let us use now the Kirchhoff approach with shadowing. It means that one must use the first iteration $P_T = P_S$ of the equation (2.31) as the first order approximation of the scattered field on the sounded surface Σ_T^+, and zero field on the black side of the body. This approach corresponds really to the well-known fact that the total field near some perfectly reflecting plane is equal to the incident field multiplied by 2. Thus, the following derives:

$$P_T(\mathbf{r}) = 2\oint_{\Sigma_T^+} P_S(\mathbf{r}')\frac{\partial G_0(\mathbf{r}-\mathbf{r}')}{\partial n'}\,d\sigma\,. \tag{2.33}$$

It's known [1] the Kirchhoff approximation is well working in the Fraunhofer zone if the wave length is much smaller than the body's maximal dimension ($\lambda << L$).

To simplify the calculation of this integral, let us consider a free homogeneous space where $G_0(\mathbf{r}-\mathbf{r}') = \dfrac{1}{4\pi}\dfrac{e^{ik|\mathbf{r}-\mathbf{r}'|}}{|\mathbf{r}-\mathbf{r}'|}$ and approach the object using a perfectly thin and rigid rectangular screen with dimensions L and D such that $S = LD$, and let us consider finally the plane wave incidence. Having placed the coordinate center in the center of the screen and having oriented axes x and y along its sides, one has $P_S = e^{ikz}$ and $\dfrac{\partial}{\partial n'} = -\dfrac{\partial}{\partial z'}$. Therefore,

$$P_T(\mathbf{r}) = -\frac{1}{2\pi}\int_{-L/2}^{L/2}dx'\int_{-D/2}^{D/2}dy'\frac{\partial}{\partial z'}\frac{e^{ik|\mathbf{r}-\mathbf{r}'|}}{|\mathbf{r}-\mathbf{r}'|}, \quad |\mathbf{r}-\mathbf{r}'| = \sqrt{(x-x')^2+(y-y')^2+z^2}\,.$$

Having calculated the derivative, one has

$$P_T(\mathbf{r}) = \frac{1}{2\pi}\int_{-L/2}^{L/2}dx'\int_{-D/2}^{D/2}dy'\left(ik-\frac{1}{|\mathbf{r}-\mathbf{r}'|}\right)\frac{z}{|\mathbf{r}-\mathbf{r}'|}\frac{e^{ik|\mathbf{r}-\mathbf{r}'|}}{|\mathbf{r}-\mathbf{r}'|}\,,$$

from which it follows for $|\mathbf{r}-\mathbf{r}'| >> 1/k$:

$$P_T(\mathbf{r}) = \frac{ik}{2\pi}\int_{-L/2}^{L/2}dx'\int_{-D/2}^{D/2}dy'\,\frac{z}{|\mathbf{r}-\mathbf{r}'|}\frac{e^{ik|\mathbf{r}-\mathbf{r}'|}}{|\mathbf{r}-\mathbf{r}'|}\,.$$

Since $|\mathbf{r}-\mathbf{r}'| = \sqrt{r^2 - 2(\mathbf{r},\mathbf{r}') + r'^2}$, for $r >> r'$ one has $|\mathbf{r}-\mathbf{r}'| = r - (\mathbf{e},\mathbf{r}') + \bar{o}(r'/r)$, with $\mathbf{e} = \mathbf{r}/r$. By applying the common procedure for this type of calculations, values of the order $O(r'/r)$ into the amplitude factor of the integrand should be neglected but conserved in the phase of the fast oscillating exponent, then the following derives

$$P_T(\mathbf{r}) = \frac{ik}{2\pi}\frac{z}{r}\frac{e^{ikr}}{r}\int_{-L/2}^{L/2} dx' \int_{-D/2}^{D/2} dy'\, e^{-ik(e_x x' + e_y y')} = -i\frac{LD}{\lambda} e_z \frac{\sin\frac{ke_x L}{2}}{\frac{ke_x L}{2}} \frac{\sin\frac{ke_y D}{2}}{\frac{ke_y D}{2}} \cdot \frac{e^{ikr}}{r},$$

therefore,

$$f_T(\mathbf{e}) = -i\frac{S}{\lambda} e_z \frac{\sin\frac{ke_x L}{2}}{\frac{ke_x L}{2}} \frac{\sin\frac{ke_y D}{2}}{\frac{ke_y D}{2}}. \qquad (2.34)$$

Thus, the estimate $R_T = 2S/\lambda$ for the case where the scattering direction is equal to the incident wave direction ($\mathbf{e} = (0,0,1)$) is proved.

More rigorous validation of the increasing of object ER for FS-ABS schema can be the accurate asymptotic solutions of the sound wave diffraction problem for a rigid sphere [1] or for ideal rigid spheroids [9]. These asymptotic solutions should be used for numerical modeling of echo-signals when doing computer simulations of FS-ABS systems.

2.4. Interference models

It will be assumed hereafter that interference fields for an ABS system are statistically independent from the probing and echo-signal fields. Total interference for an ABS system consists of

1. system interference (electronic noises of the receiving system, and so on),
2. sea ambient noise (dynamic noise of wind perturbed surface, far ship traffic noise and so on),
3. noises coming from point noisy sources (from surface ships, oil installations, etc., located in the vicinity of the receiving array),
4. sea reverberation.

It will be assumed on all these interference fields that they are normally time-space distributed (taking into account some limitations) and have zero mean values. Thus, they are fully statistically described by the time-space covariance function $K_N(\mathbf{r}_s,\mathbf{r}_q,t_1,t_2)$.

2.4.1. System noise

Regarding the system noise, one assumes that it is gaussian, mean-zero, stationary in time, homogeneous and non-correlated on sensors, so it is fully described by such time covariance function:

$$\mathrm{K}_{\mathrm{N}_{\mathrm{Sys}}}(\mathbf{r}_s,\mathbf{r}_q,t_1,t_2)=\mathrm{K}_{\mathrm{N}_{\mathrm{Sys}}}(t_1-t_2)\delta(\mathbf{r}_s-\mathbf{r}_q)\ . \tag{2.35}$$

2.4.2. Ambient sea noise

Ambient sea noise sources are the dynamics of ocean waters and of the free sea surface, seismic activity, distributed far ship traffic, biological and temperature noises. In the case where sonar operating frequency is hundreds Hz up to several kHz, the dominating source of ambient noise is the wind near the sea surface and the wind agitation (so-called dynamic sea noises).

It is common to model the ambient sea noise as a field generated by uniformly randomly distributed sound sources in a thin subsurface layer. In mean-layered horizontally regular sea environments the vertical angle spectrum of the dynamic noise at the free surface $N^{\mathrm{Surf}}(\chi;\omega)$ doesn't depend on azimuth angle φ and on horizontal coordinates. To calculate it with taking into account the impact of multiple scattering from the free surface one needs to solve an integral Fredholm 2nd kind equation [10]

$$\begin{aligned} N^{\mathrm{Surf}}(\chi;\omega) &= S_{\mathrm{Surf}}(\chi;\omega)+N^{\mathrm{Surf}}(\chi;\omega)\left|V_{\mathrm{Surf}}(\chi;\omega)V_{\mathrm{Bot}}(\chi_{\mathrm{Bot}}(\chi,0);\omega)e^{-\beta R(\chi)}\right|^2+ \\ &+\int_0^{\pi/2} N^{\mathrm{Surf}}(\chi';\omega)\left|V_{\mathrm{Bot}}(\chi_{\mathrm{Bot}}(\chi',0);\omega)e^{-\beta R(\chi')}\right|^2 M_{\mathrm{Surf}}(\chi,\chi';\omega)\frac{\cos\chi'}{\sin\chi}d\chi', \\ M_{\mathrm{Surf}}(\chi,\chi';\omega) &= \frac{1}{2\pi}\int_0^{2\pi} m_{\mathrm{Surf}}(\chi,\chi',\varphi-\varphi';\omega)d\varphi', \end{aligned} \tag{2.36}$$

where $S_{\mathrm{Surf}}(\chi;\omega)=\kappa_{\mathrm{Surf}}(\omega)\sin^{2u_S-1}\chi$ is the angle-frequency spectrum of subsurface noise sources, with $\kappa_{\mathrm{Surf}}(\omega)$ their power spectral density, u_S the power parameter for the pattern lobe of these sources, $R(\chi)$ is the horizontal length of the ray path having the grazing angle χ (so-called cyclic distance), $m_{\mathrm{Surf}}(\ldots)$ is the energetic surface scattering index, $\chi_{\mathrm{Bot}}(\chi,z)$ is the grazing angle of the ray whose grazing angle is χ at the depth z, $\beta = 0{,}1(\ln 10)\beta_{\mathrm{Wat}}(\omega)$ is the weakening-in-the-water coefficient.

Neglecting the surface scattering, the well-known classic equation [4] for $N^{\mathrm{Surf}}(\chi;\omega)$ derives:

$$N_0^{\mathrm{Surf}}(\chi;\omega)=S_{\mathrm{Surf}}(\chi;\omega)\left(1-\left|V_{\mathrm{Surf}}(\chi;\omega)V_{\mathrm{Bot}}(\chi_{\mathrm{Bot}}(\chi,0);\omega)e^{-\beta R(\chi)}\right|^2\right)^{-1}. \tag{2.37}$$

Calculation of the ambient sea noise angular spectrum at some depth z is done as follows:

$$N^{\text{Surf}}(\chi,z;\omega)=N^{\text{Surf}}(\chi_{\text{Surf}}(\chi,z);\omega)\frac{c^2(0)}{c^2(z)}e^{-2\beta R_{\text{Surf}}(\chi,z)}\left|V_{\text{Bot}}(\chi_{\text{Bot}}(\chi,z);\omega)\right|^2 , \quad (2.38)$$

where $R_{\text{Surf}}(\chi,z)$ is the length of ray arc, which has the grazing angle χ at the array's phase center at depth z and goes to the free surface, $\chi_{\text{Surf}}=\chi_{\text{Surf}}(\chi,z)$ is the grazing angle that this ray has near the free surface.

Instead of the above presented model a more simple model may be used where the impact of the multiple scattering is simulated by the presence of phantom bottom noise sources with frequency-angle spectrum $S_{\text{Bot}}(\chi,\omega)$:

$$N^{\text{Surf}}(\chi,z;\omega)=$$
$$=\frac{S_{\text{Fst}}(\chi_{\text{Fst}}(\chi,z);\omega)c_{\text{Fst}}^2+S_{\text{Snd}}(\chi_{\text{Snd}}(\chi,z);\omega)e^{-\beta R(\chi)}V_{\text{Fst}}^2c_{\text{Snd}}^2}{c^2(z)(1-V_{\text{Surf}}^2V_{\text{Bot}}^2e^{-2\beta R(\chi)})}e^{-2\beta R_{\text{Fst}}(\chi)} , \quad (2.39)$$

where the subscript Fst takes the value "Surf" or "Bot" depending on what boundary is encountered first by the ray, and accordingly to it the subscript Snd takes the other value; c_{Fst} and c_{Snd} are sound speed near corresponding boundaries.

As the result of modeling of ambient sea noise angular spectrum under equations (2.36)-(2.38) or (2.39) the function $N^{\text{Surf}}(\chi;\omega)$ slightly varying on grazing angle χ is obtained. In not-regular environments (for example having 3D bottom surface) the integration on φ in (2.36) should not be done. In this case the ambient noise angle spectrum is a function of two angles and frequency.

In the frame of the above-presented models the ambient sea noise is a gaussian zero-mean field being homogeneous in the array's receiver space. Its variability time interval is determined by the sea and atmosphere variability. Taking into account that the most powerful are large-scale processes, one may consider the ambient sea noise as stationary process on time intervals not exceeding this scale:

$$\mathrm{K}_{\mathrm{N}_{\text{Amb}}}(\mathbf{r}_s,\mathbf{r}_q,t_1,t_2)=\mathrm{K}_{\mathrm{N}_{\text{Amb}}}(\mathbf{r}_s,\mathbf{r}_q,t_1-t_2) . \quad (2.40)$$

Furthermore, for receiving arrays whose vertical size does not exceed the interval of vertical variability of sea noise this one can be considered as homogeneous on the array and is described by its angle spectrum $N^{\text{Surf}}(\chi;\omega)$.

2.4.3. Interference from local sources

This interference component is due to the presence of close ship traffic or industrial installations or some other power localized noisy sources. As to the ship traffic one

has to distinguish two types: "near" and "far" traffic. The "far" traffic increases the variance of signal processing output and its effect can not be suppressed by time accumulation. This particularity distinguishes the "far" local noises from the ambient sea noise. As to the "near" traffic, one must consider each ship as a powerful local noise source that should be suppressed by using an appropriate algorithm with adaptive beam forming.

Supposing that movements of local noise sources are small during the primary processing time interval, one may consider the noise of local sources to be stationary, with covariance matrix

$$\mathbf{K}_{\mathrm{N_{Loc}}}(\mathbf{r}_s,\mathbf{r}_q,t_1,t_2)=\mathbf{K}_{\mathrm{N_{Loc}}}(\mathbf{r}_s,\mathbf{r}_q,t_1-t_2)\ . \tag{2.41}$$

Spectral density matrix of this noise component is

$$\left[\mathbf{K}_{\mathrm{N_{Loc}}}(\omega)\right]_{sq}=\sum_l \kappa_l(\omega)\left|G(\mathbf{r}_s,\mathbf{r}_l;\omega)\right\rangle\left\langle G(\mathbf{r}_q,\mathbf{r}_l;\omega)\right|\ , \tag{2.42}$$

where $\kappa_l(\omega)$, $\mathbf{r}_l$ are the spectral power density and coordinates of the l-th local noise source.

2.4.4. Sea reverberation

Sea reverberation is an interference field created by sound scattering from inhomogeneities of sea environment. The main sources of sea reverberation are rough boundaries of the waveguide (bottom and surface) and volume scatterers. So, the total reverberation may be devised on surface, bottom and volume reverberations regarding its generating mechanism.

In the general case, the reverberation noise is not a stationary process. Its variability interval is the same or greater then the incident signal duration if this one doesn't exceed several seconds. Nevertheless it may be often considered as random process similar to quasi-stationary one whose correlation coefficient depends on time difference and the variance depends on current time moment. If this dependence is sufficiently "slow", then one may consider the reverberation process as stationary on time intervals several seconds or less which are equal to the echo-signal duration for classic ABS systems. For FS-ABS systems when prolonged or continuous signals are radiated this approach is still more right. The correlation coefficient of reverberation is known for the observer and is equal to that of the probing signal. If the vertical size of a receiving array is not more than the vertical variability interval of the reverberation, one may consider it as homogeneous random field and describe it by an angle spectrum.

Models for all types of reverberation - boundary reverberation (BR) including the surface and the bottom ones and the volume reverberation (VR) - for classic pulse

ABS systems as well as for FS-ABS systems are formulated below. Also, models for energetic scattering coefficients $m_{\mathrm{I}}(\mathbf{e},\mathbf{e}';\omega,\mathbf{r})$, (M = "Surf", "Bot" or "Vol") describing the sound scattering from boundary or volume perturbations are presented.

Reverberation model is formulated hereafter for some receiving array being compensated in the direction $\mathbf{e}_{\mathrm{R}}^{0}$ and having a pattern lobe in pressure described by the function $\mathrm{B_R}(\mathbf{e})$. It's supposed as usually that the reverberation process at the array exit is gaussian with some non-zero mean value and covariance function $\mathrm{K}_{\mathrm{I}}^{\mathrm{Rev}}(t_1,t_2)$ (M = "Surf", "Bot" or "Vol"). The intensity of reverberation is defined as follows: $\mathrm{I}_{\mathrm{I}}^{\mathrm{Rev}}(t)=\mathrm{K}_{\mathrm{I}}^{\mathrm{Rev}}(t,t)$. If there is a fan beam forming, one may consider the covariance matrix $\left[\mathbf{K}_{\mathrm{I}}^{\mathrm{Rev}}(t_1,t_2)\right]_{ij}$ in the beam space. Its elements are covariance functions of beam exits. In force of these definitions, the intensity and the covariance matrix are related:

$$\mathrm{I}_{\mathrm{I}}^{\mathrm{Rev}}(t)=\left[\mathbf{K}_{\mathrm{I}}^{\mathrm{Rev}}(t,t)\right]_{ii}\Big|_{\mathbf{e}_{\mathrm{R}}^{0}=\mathbf{e}_i}. \tag{2.43}$$

By its definition, the instant angular spectrum of reverberation $N_{\mathrm{I}}^{\mathrm{Rev}}(\mathbf{e},t)$ is related to the covariance matrix:

$$\left[\mathbf{K}_{\mathrm{I}}^{\mathrm{Rev}}(t,t)\right]_{ij}=\oint N_{\mathrm{I}}^{\mathrm{Rev}}(\mathbf{e},t)\,\mathrm{B_R}(\mathbf{e}-\mathbf{e}_i)\,\mathrm{B_R}(\mathbf{e}-\mathbf{e}_j)\,d\Omega(\mathbf{e}), \tag{2.44}$$

and to the intensity:

$$\mathrm{I}_{\mathrm{I}}^{\mathrm{Rev}}(t)=\oint N_{\mathrm{I}}^{\mathrm{Rev}}(\mathbf{e},t)\mathrm{B}_{\mathrm{R}}^{2}(\mathbf{e}-\mathbf{e}_{\mathrm{R}}^{0})\,d\Omega(\mathbf{e}). \tag{2.45}$$

If the reverberation can be considered as a quasi-stationary process, then

$$\mathrm{K}_{\mathrm{I}}^{\mathrm{Rev}}=\mathrm{K}_{\mathrm{I}}^{\mathrm{Rev}}(t_2-t_1),\ \left[\mathbf{K}_{\mathrm{I}}^{\mathrm{Rev}}(t_1,t_2)\right]_{ij}=\left[\mathbf{K}_{\mathrm{I}}^{\mathrm{Rev}}(t_2-t_1)\right]_{ij}, \tag{2.46}$$

$$\mathrm{I}_{\mathrm{I}}^{\mathrm{Rev}}(t)=\mathrm{K}_{\mathrm{I}}^{\mathrm{Rev}}(0)=const,\ \left[\mathbf{K}_{\mathrm{I}}^{\mathrm{Rev}}(t,t)\right]_{ij}=const_{ij},\ N_{\mathrm{I}}^{\mathrm{Rev}}=N_{\mathrm{I}}^{\mathrm{Rev}}(\mathbf{e}). \tag{2.47}$$

Hereafter following notations other than above ones are used: $S(t)$ is the normalized signal envelope of radiated narrow band pulse signals, $\mathbf{r}$ is the point of scattering, $\mathbf{e}(\mathbf{r},\mathbf{r}',\mathbf{e}')$ is the normalized tangent vector of a ray path connecting points $\mathbf{r}'$ and $\mathbf{r}$ when it is considered at the point $\mathbf{r}$ and is equal to $\mathbf{e}'$ at the point $\mathbf{r}'$, $\mathbf{e}_{\mathrm{R}}$ is the normalized vector of the observing direction, $M(\mathbf{r},\mathbf{r}')$ is the number of ray paths connecting points $\mathbf{r}'$ and $\mathbf{r}$, $\mathrm{t}(\mathbf{e},\mathbf{r},\mathbf{r}')$ is the time of propagation along the ray path connecting points $\mathbf{r}$ and $\mathbf{r}'$ if it has $\mathbf{e}$ as tangent vector at the point $\mathbf{r}$, $\chi(\mathbf{e})$ is the grazing angle of the vector $\mathbf{e}$, W, γ are the radiated acoustical power and the array pattern factor (the concentration coefficient), $dV(\mathbf{r})$, $d\Sigma(\mathbf{r})$ are volume and surface elements containing the point $\mathbf{r}$.

2.4.4.1. Volume reverberation

Using above introduced notations and supposing the space correlation interval of volume scatterers to be less than the space interval of sound field interference variability in the ocean, the instant intensity of volume reverberation created by sound scattering from one elementary volume element dV can be written as

$$\begin{aligned} dI_{\text{Vol}}^{\text{Rev}}(t) = \frac{W\rho c\gamma}{4\pi} dV(\mathbf{r}) \sum_{\mu=1}^{M(\mathbf{r}_R,\mathbf{r})} \sum_{\nu=1}^{N(\mathbf{r},\mathbf{r}_S)} m_{\text{Vol}}(-\mathbf{e}_\mu(\mathbf{r},\mathbf{r}_R),\mathbf{e}_\nu(\mathbf{r},\mathbf{r}_S);\omega,\mathbf{r}) \times \\ \times f_\nu(\mathbf{r},\mathbf{r}_S)\cdot V_\nu(\mathbf{r},\mathbf{r}_S;\omega) R^{-2}(\mathbf{r},\mathbf{r}_S) B_S^2(\mathbf{e}_\nu(\mathbf{r}_S,\mathbf{r}) - \mathbf{e}_S^0) \times \\ \times f_\mu(\mathbf{r}_R,\mathbf{r})\cdot V_\mu(\mathbf{r}_R,\mathbf{r};\omega) R^{-2}(\mathbf{r}_R,\mathbf{r}) B_R^2(\mathbf{e}_\mu(\mathbf{r}_R,\mathbf{r}) - \mathbf{e}_R^0) \times \\ \times S^2(t - t_\mu(\mathbf{r}_R,\mathbf{r}) - t_\nu(\mathbf{r},\mathbf{r}_S)). \end{aligned} \tag{2.48}$$

Full amount of intensity of VR is the integral all over the waveguide's volume:

$$I_{\text{Vol}}^{\text{Rev}} = \int_V dI_{\text{Vol}}^{\text{Rev}} \cdot \tag{2.49}$$

When calculating the intensity of reverberation by integrating all over the waveguide's volume, the signal envelope $S(t)$ works as "window function" determining in the waveguide a volume in form of pseudo-ellipsoidal layer encircling the source and the receiving arrays.

Using the equation (2.4') for ray presentation of GF as a surface integral and the equation (2.45), the following expression for the angular spectrum derives

$$\begin{aligned} N_{\text{Vol}}^{\text{Rev}}(\mathbf{e}_R,t) = \frac{W\rho c\gamma}{4\pi} \int dV(\mathbf{r}) \sum_{\mu=1}^{M(\mathbf{r}_R,\mathbf{r})} \sum_{\nu=1}^{N(\mathbf{r},\mathbf{r}_S)} m_{\text{Vol}}(-\mathbf{e}_\mu(\mathbf{r},\mathbf{r}_R),\mathbf{e}_\nu(\mathbf{r},\mathbf{r}_S);\omega,\mathbf{r}) \times \\ \times \delta(\mathbf{e}_R - \mathbf{e}_\mu(\mathbf{r}_R,\mathbf{r})) f_\nu(\mathbf{r},\mathbf{r}_S)\cdot V_\nu(\mathbf{r},\mathbf{r}_S;\omega) R^{-2}(\mathbf{r},\mathbf{r}_S) B_S^2(\mathbf{e}_\nu(\mathbf{r}_S,\mathbf{r}) - \mathbf{e}_S^0) \times \\ \times f_\mu(\mathbf{r}_R,\mathbf{r})\cdot V_\mu(\mathbf{r}_R,\mathbf{r};\omega) R^{-2}(\mathbf{r}_R,\mathbf{r}) \times S^2(t - t_\mu(\mathbf{r}_R,\mathbf{r}) - t_\nu(\mathbf{r},\mathbf{r}_S)). \end{aligned} \tag{2.50}$$

The volume element dV may be represented as $dV = ds d\sigma$, where ds is the elementary length element of the ray path, σ is the area of small elementary surface that is transversal to the ray. Introducing the ray coordinates (s,η,ζ) so that $d\sigma = R^2 d\eta d\zeta$, where R is the distance between the source and the receiver, one may pass from volume integrating in Descartes coordinates to integrating in the ray coordinate space. This means to replace $\mathbf{r} = \mathbf{r}(s;\eta,\zeta)$ in (2.50) and to omit the index μ and the sum on μ-th rays connecting the receiver and the scatterer since they will be all taken into account because of the integrating on the "transversal" ray coordinates (η,ζ). As result of this substitution the single meaning functions $\mathbf{e}(\mathbf{r}',s,\eta,\zeta) = \mathbf{e}_\mu(\mathbf{r}',\mathbf{r}(s;\eta,\zeta)$

and $\mathbf{e}(s,\eta,\zeta,\mathbf{r}') = \mathbf{e}_\mu(\mathbf{r}(s;\eta,\zeta,\mathbf{r}')$ will arise which determine tangent vectors of ray paths connecting two points ($\mathbf{r}'$ and $\mathbf{r}(s;\eta,\zeta)$) when these vectors are considered at points $\mathbf{r}'$ and $\mathbf{r}(s;\eta,\zeta)$ respectively under the condition that the ray coordinates are (s,η,ζ) at the point $\mathbf{r}(s;\eta,\zeta)$.

Moreover, using the definition of focusing factor the following derives:

$$dV(\mathbf{r}) = ds R^2(\mathbf{r}_R, \mathbf{r}(s;\eta,\zeta)) d\eta d\zeta = ds \frac{R^2(\mathbf{r}_R, \mathbf{r}(s;\eta_0,\zeta_0))}{f(\mathbf{r}_R, \mathbf{r}(s;\eta_0,\zeta_0))} d\eta_0 d\zeta_0 , \quad (2.51)$$

and it's possible to pass to integration on "transversal" ray coordinates (η_0,ζ_0) at the observing point.

$$\begin{aligned} N_{Vol}^{Rev}(\mathbf{e}_R) = \frac{W\rho c\gamma}{4\pi} \iint d\eta_0 d\zeta_0 \int ds \sum_{v=1}^{N(\mathbf{r}(s),\mathbf{r}_S)} m_{Vol}(-\mathbf{e}_\mu(\mathbf{r}(s),\mathbf{r}_R), \mathbf{e}_v(\mathbf{r}(s),\mathbf{r}_S);\omega,\mathbf{r}(s)) \times \\ \times \delta(\mathbf{e}_R - \mathbf{e}(\mathbf{r}_R,\mathbf{r}(s))) V(\mathbf{r}_R,\mathbf{r}(s);\omega) f_v(\mathbf{r}(s),\mathbf{r}_S) \times \\ \times V_v(\mathbf{r}(s),\mathbf{r}_S;\omega) R^{-2}(\mathbf{r}(s),\mathbf{r}_S) B_S^2(\mathbf{e}_v(\mathbf{r}_S,\mathbf{r}(s)) - \mathbf{e}_S^0), \end{aligned} \quad (2.52)$$

with $\mathbf{r}(s) = \mathbf{r}(s;\eta_0,\zeta_0)$. Let use as (η_0,ζ_0) the spherical coordinates (θ,φ) on the unit sphere surface. Notice that the unit vector $\mathbf{e}(\mathbf{r}_R,\mathbf{r}(s;\theta_0,\varphi_0))$ has (θ_0,φ_0) as its spherical coordinates because of its definition. Therefore the result of integrating on (θ_0,φ_0) in the presence of the δ-function in the integrand is the following result equation for modeling of the instant angle spectrum of volume reverberation:

$$\begin{aligned} N_{Vol}^{Rev}(\mathbf{e}_R,t) = \frac{W\rho c\gamma}{4\pi} \int ds \sum_{v=1}^{N(\mathbf{r}(s),\mathbf{r}_S)} m_{Vol}(-\mathbf{e}(\mathbf{r}(s),\mathbf{r}_R), \mathbf{e}_v(\mathbf{r}(s),\mathbf{r}_S);\omega,\mathbf{r}(s)) \times \\ \times f_v(\mathbf{r}(s),\mathbf{r}_S) V_v(\mathbf{r}(s),\mathbf{r}_S;\omega) B_S^2(\mathbf{e}_v(\mathbf{r}_S,\mathbf{r}(s)) - \mathbf{e}_S^0) R^{-2}(\mathbf{r}(s),\mathbf{r}_S) \times \\ \times V(\mathbf{r}_R,\mathbf{r}(s);\omega) S^2(t - t_\mu(\mathbf{r}_R,\mathbf{r}(s)) - t_v(\mathbf{r}(s),\mathbf{r}_S)), \end{aligned} \quad (2.53)$$

where the integration is made along the ray path $\mathbf{r} = \mathbf{r}(s;\theta_R,\varphi_R)$ with the tangent vector $\mathbf{e}_R = (\cos\varphi_R\sin\theta_R, \sin\varphi_R\sin\theta_R, \cos\theta_R)$ at the receiver point.

One may model the intensity and the angle spectrum of reverberation by using 1) the equations (2.48), (2.49) or (2.45), (2.50), but also by using 2) the equations (2.45), (2.50). The calculation algorithm for the first case (when integrating on all the waveguide's volume) is radically different from that for the second case (when integrating on ray paths). When integrating on all the waveguide's volume one needs to choose the scattering element dimensions (the element of integration) so that it would be smaller than the interval of the field space variability due to the interference of reflected and refracted waves. If it is done and if one finds all main ray paths

connecting three points (the receiver, the scattering element and the source), one may be sure the reverberation is "completely" modelled (taking into account limitations of the model). By the same manner, to ensure the "complete" modeling when integrating along ray paths one needs the steps of integration on ray length and on angles at the receiver to be so small that the field varies a little on these steps.

2.4.4.2. Boundary reverberation

Using the above notations and the same supposition about space correlation interval of scatterers, the intensity of single time scattered narrow-band boundary reverberation (BR) from an element $d\Sigma$ of the boundary Σ (of the sea surface, for example) can be expressed as

$$\begin{aligned} d\,\mathrm{I}_{\mathrm{Surf}}^{\mathrm{Rev}}(t) = \frac{W\rho c\gamma}{4\pi} d\Sigma(\mathbf{r}) \sum_{\mu=1}^{M(\mathbf{r}_R,\mathbf{r})} \sum_{\nu=1}^{N(\mathbf{r},\mathbf{r}_S)} m_{\mathrm{Surf}}(-\mathbf{e}_\mu(\mathbf{r},\mathbf{r}_R),\mathbf{e}_\nu(\mathbf{r},\mathbf{r}_S);\omega,\mathbf{r}) \times \\ \times f_\nu(\mathbf{r},\mathbf{r}_S)\cdot V_\nu(\mathbf{r},\mathbf{r}_S;\omega) R^{-2}(\mathbf{r},\mathbf{r}_S)\,\mathrm{B}_S^2(\mathbf{e}_\nu(\mathbf{r}_S,\mathbf{r})-\mathbf{e}_S^0)\times \\ \times f_\mu(\mathbf{r}_R,\mathbf{r})\cdot V_\mu(\mathbf{r}_R,\mathbf{r};\omega) R^{-2}(\mathbf{r}_R,\mathbf{r})\,\mathrm{B}_R^2(\mathbf{e}_\mu(\mathbf{r}_R,\mathbf{r})-\mathbf{e}_R^0)\times \\ \times S^2(t-\mathrm{t}_\mu(\mathbf{r}_R,\mathbf{r})-\mathrm{t}_\nu(\mathbf{r},\mathbf{r}_S)). \end{aligned} \tag{2.54}$$

The total amount of BR is calculated as integral of (2.54) all over the boundary. If the boundary is horizontal and homogeneous (as it may be usually admitted for problems considered in this paper) then the scattering coefficient doesn't depend on horizontal coordinates. To calculate the angle spectrum of BR, one may consider the BR as a particular case of VR in which the volume scattering coefficient is equal to product of boundary scattering coefficient and of Dirac function of depth $\delta(z\text{-}z_{\mathrm{Surf}})$. Thus, using (2.53) and taking into account that

$$\mathrm{cosang}\big(\mathbf{e}(\mathbf{r},\mathbf{r}_R,\mathbf{e}_R),\mathbf{e}_\perp\big)ds = dz\ ,$$

where $\mathbf{e}_\perp$ is a unit vector transversal to the boundary, one can calculate the integral on ds and obtain the following equations:

$$\begin{aligned} N_{\mathrm{Surf}}^{\mathrm{Rev}}(\mathbf{e}_R,t) = \frac{W\rho c\gamma}{4\pi} \sum_{\nu=1}^{N(\mathbf{r}(\mathbf{e}_R),\mathbf{r}_S)} \frac{m_{\mathrm{Surf}}(-\mathbf{e}(z_{\mathrm{Surf}},z_R,\mathbf{e}_R),\mathbf{e}_\nu(z_{\mathrm{Surf}},z_S);\omega)}{\big(\mathbf{e}(z_{\mathrm{Surf}},z_R,\mathbf{e}_R),\mathbf{e}_\perp\big)} \times \\ \times V(\mathbf{r}_R,\mathbf{r}(\mathbf{e}_R);\omega) f_\nu(\mathbf{r}(\mathbf{e}_R),\mathbf{r}_S) V_\nu(\mathbf{r}(\mathbf{e}_R),\mathbf{r}_S;\omega)\,\mathrm{B}_S^2(\mathbf{e}_\nu(z_S,z_{\mathrm{Surf}})-\mathbf{e}_S^0) \\ \times R^{-2}(\mathbf{r}(\mathbf{e}_R),\mathbf{r}_S) S^2(t-\mathrm{t}_\mu(\mathbf{r}_R,\mathbf{r}(\mathbf{e}_R))-\mathrm{t}_\nu(\mathbf{r}(\mathbf{e}_R),\mathbf{r}_S)), \end{aligned} \tag{2.55}$$

with $\mathbf{r}(\mathbf{e}_R) = (\mathbf{x}(\mathbf{e}_R), z_{\mathrm{Surf}})$ the point where the ray having the direction $\mathbf{e}_R$ at the reception point arrives onto the boundary.

As for the VR case, the intensity of BR is calculated by integrating elementary parts all over the waveguide's boundary under consideration. The signal envelope is acting as "window function", which determines on the boundary a band area of pseudo-ellipse form, which encircles the projections of the receiving and source arrays' positions on the boundary.

2.4.4.3. About scattering index modeling

Other than the reverberation model structure such as is described by equations (2.53) and (2.55), the main factor determining the reverberation interference in sea environments is the model of scattering coefficient entering in the reverberation model. As to the volume reverberation, the scattering from small-scale scatterers creates it. The main scatterers are air bobbles in the sub-surface layer or gas bobbles owned/created by sea biological organisms or the organisms themselves. Those scatterers are sufficiently well described by a frequency-depending scattering index, which does not depend on both incident and scattering directions. It may be depending on space coordinates since the scattering properties (e.g. density of scatterers) are usually changing with depth and sometimes with range. Results of boundary reverberation modeling will be determined by used scattering index model for the boundary. This model can not be a frequency-depending scattering index as it is for the volume reverberation. The sea surface is an interface between two different media (water and air) which can be considered as homogeneous for the sound scattering problem. So, the scattering properties of this boundary are determined by the physical parameters of the media and by the boundary's shape. This one is very complex: there is roughness of various scales relatively the wave's length. As to the sea bottom, its scattering properties are determined not only by the shape of the interface between the water and bottom media but also by internal structure of the bottom media, which can not be considered as homogeneous. There are inhomogeneities of various scales in the bottom and internal interfaces between layers having different physical properties. So, the bottom scattering is summarized effect of the scattering from rough interfaces and from volume inhomogeneities in the bottom media. Nevertheless, higher is the sound frequency, smaller is the effect of the volume inhomogeneities and internal interfaces since the sound can not penetrate far into the bottom medium.

Simulations show that the behavior of available models for the scattering index is rather similar for high incident angles (10° and more), but it is very different for slow incident grazing angles. As the slow angle case is realized for the sound propagation in shallow water sea environments (SWSE), the forward scattering reverberation and its model for SWSE shall be studied and validated by conducting sea experiments.

3. PARAMETERS OF FS-ABS SYSTEMS

3.1. Thickness of the FS detection zone and life time of echo-signals

Horizontal thickness of the FS-ABS detection zone is determined by the half-width $\Delta\varphi$ of the main lobe of the scattering amplitude of an object. Using its model deduced under the Kirchhoff approximation with shadowing

$$f_T(\mathbf{e}) = -i\frac{S}{\lambda}e_z \frac{\sin ke_x L/2}{ke_x L/2}\cdot\frac{\sin ke_y D/2}{ke_y D/2}, \tag{3.1}$$

one can estimate

$$\Delta\varphi \sim \lambda/(L_T \sin(\alpha-\alpha_1)), \tag{3.2}$$

where α is the course angle between the acoustical path source-receiver and the object's speed vector, α_1 is the angle between the direction "SR" (from the source to the receiver) and the direction "ST" (from the source to the object, see the figure 1). For the FS scheme $\alpha \sim \pi/2$, $\alpha_1 << 1$ and $\sin(\alpha-\alpha_1) \sim 1$. Quantitative estimates of the width $2\Delta\varphi$ of the main lobe are given in the table 3.1.

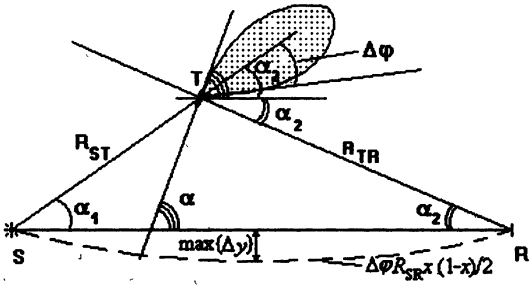

Figure 3.1. Scattering geometry.

The receiver begins to "sense" the echo-signal due to the main lobe if is satisfied the condition

$$\Delta\varphi > \alpha_1 + \alpha_2, \tag{3.3}$$

where α_2 is the angle between the direction "RS" (from the receiver to the source) and the direction "RT" (from the receiver to the object). Since it can be estimated: $\alpha_1 \sim \Delta y/R_{ST}$, $\alpha_2 \sim \Delta y/R_{TR}$, where Δy is the distance between the object and the vertical plane including the source and the receiver, one can deduce following estimate for the half-thickness of the FS-ABS detection zone:

$$\max\{\Delta y\} \sim [\lambda/L_T]R_{ST}R_{TR}/R_{SR} = \Delta\varphi R_{SR}x(1-x), \; x = R_{ST}/R_{SR}. \tag{3.4}$$

Table 3.1.
Quantitative estimates of FS-ABS systems' parameters.

Parameters of object and ABS system	f_0 **= 1 kHz,** Δf **= 100 Hz**	F_0 **= 6 kHz,** Δf **= 600 Hz**
object. v_T = 5 m/s (10 knots) system's base length: R_{SR} = 50 km	$2\Delta\varphi \sim 0.03$ ($\approx 1.7°$) $2\max\{\Delta y\} \sim 0.36$ km $\max\{T\} \sim 72$ sec $2\Delta\chi \sim 0.3$ ($\approx 17°$) $\max\{\delta t^{(1)}\} \sim 5\cdot10^{-3}$ $\max\{\delta t^{(2)}\} \sim 1\cdot10^{-3}$	$2\Delta\varphi \sim 0.005$ ($\approx 0.3°$) $2\max\{\Delta y\} \sim 0.06$ km $\max\{T\} \sim 12$ sec $\Delta\chi \sim 0.05$ ($\approx 3°$) $\max\{\delta t^{(1)}\} \sim 2.5\cdot10^{-5}$ $\max\{\delta t^{(2)}\} \sim 2.5\cdot10^{-5}$
object: v_T = 5 m/s (10 knots) system's base length: R_{SR} = 15 km	$2\Delta\varphi \sim 0.15$ ($\sim 8.5°$) $2\max\{\Delta y\} \sim 0.6$ km $\max\{T\} \sim 120$ sec $2\Delta\chi \sim 0.85$ ($\approx 50°$) $\max\{\delta t^{(1)}\} \sim 7.2\cdot10^{-2}$ $\max\{\delta t^{(2)}\} \sim 1\cdot10^{-2}$	$2\Delta\varphi \sim 0.025$ ($\approx 1.5°$) $2\max\{\Delta y\} \sim 0.1$ km $\max\{T\} \sim 20$ sec $2\Delta\chi \sim 0.14$ ($\approx 8°$) $\max\{\delta t^{(1)}\} \sim 1.5\cdot10^{-4}$ $\max\{\delta t^{(2)}\} \sim 3\cdot10^{-4}$

Therefore, the detection zone of an FS-ABS system has the maximal thickness $2\max\{\Delta y\} \sim [\lambda/L_T]R_{SR}/2$ at its middle point where $x = 1/2$. The detection zone has the parabolic shape $x(1-x)$ in the horizontal plane (see the figure 3.1). The thickness of the detection zone is proportional to the wavelength, to the length R_{SR} of the FS-ABS system's base and is inverse proportional to the object's length. Maximal relative half-thickness of the detection zone is $2\max\{\Delta y\}/R_{SR} \sim [\lambda/L_T]/2 = \Delta\varphi/2$. Quantitative estimates of the detection zone's maximal thickness are given in the table 3.1.

Total duration of the forward-scattered signal created by the main lobe of the scattering amplitude may be estimated as:

$$T \sim 2\Delta y / (v_T \sin\alpha) \sim [2\lambda / (v_T \sin\alpha) L_T] R_{SR} x(1-x)\,, \qquad (3.5)$$

where v_T is the horizontal speed of the object. Thus, the duration of the FS signal is proportional to the wave length, to the system's base length and inverse proportional to the object's speed and to the object's length. It depends on the point where the object crosses the vertical plane, by the same way as the detection zone's thickness depends on it. Quantitative estimates of the maximal duration $\max\{T\}$ of the FS signal are given in the table 3.1.

3.2. Amplitude, angle and time structure of FS-ABS signals

It follows from the approximation (3.1) and from the FS signal model that echo-signal ray amplitudes depend on geometrical parameters of an FS-ABS system as follows:

$$P_T \sim \frac{D_T L_T \sin(\alpha-\alpha_1)}{\lambda} \frac{\sin\dfrac{\pi \sin(\alpha_1+\alpha_2) L_T \sin(\alpha-\alpha_1)}{\lambda}}{\dfrac{\pi \sin(\alpha_1+\alpha_2) L_T \sin(\alpha-\alpha_1)}{\lambda}} \cos(\alpha_1+\alpha_2) \cdot \quad (3.6)$$

If the object moves in the waveguide the angles α_1 and α_2 change. Let's note t_0 the moment of the object's crossing the system's vertical plane. One can deduce from the sine theorem a system of equations (see the figure 3.1):

$$\frac{v_T(t-t_0)}{\sin\alpha_1} = \frac{R_{ST}(t_0)}{\sin(\alpha-\alpha_1)} = \frac{R_{TR}(t_0)}{\sin(\alpha-\alpha_2)},$$

from which it follows:

$$\alpha_1 = \operatorname{arcctg}\left(\operatorname{ctg}\alpha + \frac{x(t_0)R_{SR}}{v_T \sin\alpha (t-t_0)}\right), \quad \alpha_2 = \operatorname{arcctg}\left(\operatorname{ctg}\alpha + \frac{[1-x(t_0)]R_{SR}}{v_T \sin\alpha (t-t_0)}\right).$$

Thus, echo-signal rays' amplitudes are "copying" the shape of the horizontal cross-section of the object's scattering amplitude's main lobe:

$$P_T \sim P_T(t_0)\sin(\alpha-\alpha_1) \frac{\sin\dfrac{\pi \sin(\alpha_1+\alpha_2) L_T \sin(\alpha-\alpha_1)}{\lambda}}{\dfrac{\pi \sin(\alpha_1+\alpha_2) L_T \sin(\alpha-\alpha_1)}{\lambda}} \cos(\alpha_1+\alpha_2) \cdot \quad (3.7)$$

In the case where $\alpha \approx \pi/2$ and the system's detection zone is very narrow, one has approximately

$$\alpha_1 \approx \frac{v_T(t-t_0)}{x(t_0)R_{SR}}\sin\alpha << 1, \alpha_2 = \frac{v_T(t-t_0)}{[1-x(t_0)]R_{SR}}\sin\alpha << 1, \quad (3.8)$$

therefore,

$$P_T \approx P_T(t_0)\sin\frac{\pi L_T \sin\alpha}{\lambda}(\alpha_1+\alpha_2) \Big/ \frac{\pi L_T \sin\alpha}{\lambda}(\alpha_1+\alpha_2) \cdot \quad (3.9)$$

It's possible to approximate well the main lobe of the function $\sin x/x$ by a gaussian function (see the figure 3.2)

$$\frac{\sin x}{x} \approx \exp\left\{-\frac{1}{2}\frac{x^2}{(\pi/2)^2}\right\}, |x| \le \pi \ . \tag{3.10}$$

Thus, the following time dependence of the echo-signal rays' amplitudes derives

$$P_T(t-t_0) \approx P_T(t_0) b(t-t_0, x(t_0)), b(t,x) = \exp\left\{-\frac{1}{2}\left(\frac{L_T \sin^2\alpha}{\lambda/2}\frac{v_T t}{x[1-x]R_{SR}}\right)^2\right\} . \tag{3.11}$$

Vertical space ray structure of echo-signal fields is determined by the half-width $\Delta\chi$ of the object's scattering amplitude's main lobe. Based on the approximation (3.1), one can estimate

$$\Delta\chi \sim \lambda / D_T .$$

This value and the distance from the object to the receiver R_{TR} are determining the number of echo-signal rays on the receiving array. Quantitative estimates of the angle width $2\Delta\chi$ are given in the table 3.1.

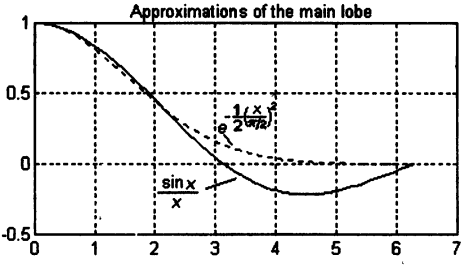

Figure 3.2. Approximations for the main lobe of the object's scattering amplitude.

While the object is moving, geometrical parameters of the triangle source–object–receiver are changing and therefore, echo-signal ray delays are also changing. Let us write as follows the delay of the ν-th echo-signal ray path given birth by the scattering of the μ-th ray of the source field

$$t_{\mu\nu}(t) = t_{\mu\nu}(t_0) + \delta t_{\mu\nu}(t) \ . \tag{3.13}$$

The variation part δt of this delay can be represented under the form

$$\delta t_{\mu\nu}(t) = \delta t^{(1)}_{\mu\nu}(t) + \delta t^{(2)}_{\mu\nu}(t),$$

$$\delta t^{(1)}_{\mu\nu} = \frac{\partial\left(t_\mu(\mathbf{x}_T, \mathbf{x}_S) + t_\nu(\mathbf{x}_R, \mathbf{x}_T)\right)}{\partial x_T^\alpha} v_T^\alpha (t-t_0), \tag{3.14}$$

$$\delta t^{(2)}_{\mu\nu} = \frac{1}{2}\frac{\partial^2\left(t_\mu(\mathbf{x}_T, \mathbf{x}_S) + t_\nu(\mathbf{x}_R, \mathbf{x}_T)\right)}{\partial x_T^\alpha \partial x_T^\beta} v_T^\alpha v_T^\beta (t-t_0)^2,$$

where $\mathbf{v}_T = \{v_T^1, v_T^2\} = v_T\{\cos\alpha, \sin\alpha\}$ is the vector of object's horizontal speed,

t_0 is the moment of object's crossing the system's vertical plane. Calculating the linear-on-time term, one has

$$\delta t_{\mu\nu}^{(1)}(t) = \frac{\cos\chi_{\mu T} - \cos\chi_{\nu T}}{c_T} v_T \cos\alpha (t - t_0), \tag{3.15}$$

where $\chi_{\mu T}$, $\chi_{\nu T}$ are grazing angles of the rays at the object's location at the moment t_0, c_T is the sound velocity at the object's depth. The squared-on-time term is

$$\delta t_{\mu\nu}^{(2)}(t) = \left(\frac{\cos\chi_{\mu T}}{R_{ST}} + \frac{\cos\chi_{\nu T}}{R_{TR}} \right) \frac{(v_T \sin\alpha)^2}{2c_T} (t - t_0)^2 + \frac{(v_T \cos\alpha)^2}{2c_T} (t - t_0)^2 \times \tag{3.16}$$
$$\times \left[\cos\chi_{\mu T} \operatorname{tg}\chi_{\mu R} \left(\partial R_{TR} / \partial \chi_{\mu R} \right)^{-1} + \cos\chi_{\nu T} \operatorname{tg}\chi_{\nu S} \left(\partial R_{ST} / \partial \chi_{\nu S} \right)^{-1} \right],$$

where $\chi_{\mu S}$, $\chi_{\nu S}$ and $\chi_{\mu R}$, $\chi_{\nu R}$ are grazing angles of the rays at the source and receiver locations, respectively. It follows from (3.13) - (3.16) that if the object is crossing some ray path of the source field, then $\chi_{\mu T} = \chi_{\nu T}$ and there is no linear term in the expression (3.14), that agrees with the Fermat principle. Quantitative estimates of the squared term is given in the table 3.1. If $\chi_{\mu T} \neq \chi_{\nu T}$ that means that the ν-th echo-signal ray path is a "new" path being given birth by the diffraction on the object, then the difference $\chi_{\mu T} - \chi_{\nu T}$ is smaller than the angle half-width $2\Delta\chi$ of the object's scattering amplitude's main lobe having been estimated above. Quantitative estimates of the linear-on-time term in the equation (3.14) are also given in the table 3.1.

Let us show that signals coming along echo-signal rays that one can not resolve in the time-space domain from some rays of the source field give birth to a time modulation of corresponding correlation maximums. The modulation is the result of the summation of the source and diffracted fields. One can write the result as follows:

$$\left[P_S + P_T(t - t_0) \exp\left\{ -i\omega \delta t^{(2)}(t - t_0) \right\} \right] S_0(t) \exp\{-i\omega t\},$$

where $S_0(t)$ is the envelope of the amplitude of the radiated narrow-band signal with the central frequency ω, P_S is the amplitude of the source field's ray, $P_T(t)$ is given by the equation (3.11) and $\delta t^{(2)}(t)$ by the equation (3.16). After correlating with the radiated signal $S_0(t)\exp\{-i\omega t\}$ taking into account that its correlation interval is much smaller than variability scales of $b(t)$ and $\delta t^{(2)}(t)$, and after making normalization with respect to the amplitude of the source field's ray, one obtains a correlation function

$$\left[1 + \varepsilon b(t - t_0) \exp\left\{ -i\omega \delta t^{(2)}(t - t_0) \right\} \right] K_S(\tau) \exp\{-i\omega\tau\},$$

where $K_S(\tau)$ is the correlation function of the radiated signal's envelope and ε is determined by the object's equivalent radius. The square of its amplitude maximum varies in time as follows

$$1+\varepsilon^2 b^2(t-t_0)+2\varepsilon b(t-t_0)\cos\left\{\omega\delta\, t^{(2)}(t-t_0)\right\}.$$

Having removed the constant part and taking into account that $\varepsilon << 1$, one has a normalized signal

$$b(t-t_0)\cos\left\{\omega\delta\, t^{(2)}(t-t_0)\right\}, \qquad (3.17)$$

that is a linear frequency modulated (LFM) on amplitude signal with the gaussian envelope (3.11). This signal has a frequency deviation $\omega^* = \omega\delta t^{(2)}(t)/(t-t_0)$ linearly changing in time. Such signals are shown with the figure 3.3.

Echo-signal rays whose correlation maximums can be separated from those of rays of the source field, bring signals whose complex envelopes are the shape

$$P_T(t-t_0)\exp\left\{-i\omega\delta\, t^{(1)}(t-t_0)-i\omega\delta\, t^{(2)}(t-t_0)\right\}S_0(t)\ , \qquad (3.18)$$

where $P_T(t)$ is also given by the equation (3.11), and $\delta t^{(1)}(t)$, $\delta t^{(2)}(t)$ are given by the equations (3.15) - (3.16). The signal (3.18) is also a complex linear frequency modulated (LFM) signal, nevertheless the squared module of the corresponding correlation maximum is not LFM and changes only following the gaussian low (3.11).

One can see on the figure 3.3 that when the parameter $a\Delta t^2$ is small, then the squared amplitudes of correlation maximums of both types (segregated and not) echo-signal rays are changing in time as the gaussian signal. If the parameter $a\Delta t^2$ is big, then the squared amplitudes of correlation maximums corresponding to the non-separated rays are LFM signals with gaussian envelopes. Therefore, to feel the structure of the LFM signals due to non-separated echo-signal rays and to use it to improve the SNR when making detecting, one needs the condition

$$\omega\delta\, t^{(2)}\left(\frac{v_T x(t_0)[1-x(t_0)]R_{SR}\lambda/2}{L_T\sin^2\alpha}\right) >> 1\ .$$

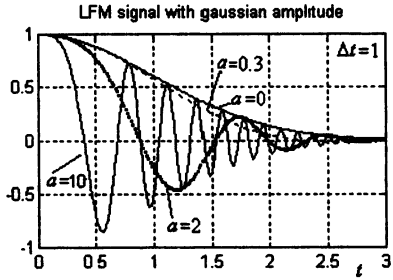

Figure 3.3. LFM signals $\exp\left\{-\frac{1}{2}\frac{t^2}{\Delta t^2}\right\}\cos at^2$ *for different parameters a.*

to be satisfied. The time shift $\delta t^{(1)}(t)$ of segregated echo-signal correlation maximums corresponds to the constant shift $\omega\delta t^{(1)}(t)/(t-t_0)$ of the central frequency of the echo-signal. It can shown that this shift is due to the Doppler effect. Really, it arises thanks to the difference of speeds of changing the acoustical lengths of two ray paths that have different grazing angles at the object's location, when the changing is due to the movement of the object along the axis "source-receiver". The Doppler effect works so that the frequency of a harmonic wave of initial frequency ω_0 after scattering from a body moving at speed v_T becomes $\omega = \omega_0\left(1+\dfrac{(\mathbf{v}_T,\mathbf{e})+(\mathbf{v}_T,\mathbf{e}_0)}{c_T}\right) = \omega_0(1+\beta)$, where $\mathbf{e}$ and $\mathbf{e}_0$ are unit vector of the directions from the scatterer to the receiver and from the scatterer to the source. Therefore, in the case where the body is in a free homogeneous medium, the scattered signal being created by the scattering of the incident signal with the spectrum $S_0(\omega_0-\omega_1)$, where ω_1 is its central frequency, is

$$S(t) = \int S_0(\omega_0-\omega_1)\,f_T(\mathbf{e},\mathbf{e}_0;\omega)\exp\{-i\omega(t-r/c)\}\frac{d\omega}{2\pi} = \tag{3.20}$$
$$= (1+\beta)S_0((1+\beta)(t-r/c))\,f_T(\mathbf{e},\mathbf{e}_0;\omega_1)\exp\{-i\omega_1(1+\beta)(t-r/c)\}.$$

Thus, the Doppler effect gives a shift of the signal's central frequency, a compression of the signal envelope and corresponding increasing of its amplitude.

Let us study the effect that it causes for the correlation processing of signals. As result of correlation between the signal (3.20) and the radiated signal $S_0(t)\exp\{-i\omega_1 t\}$ the correlation function is obtained

$$K(\tau) = (1+\beta)f_T(\mathbf{e},\mathbf{e}_0;\omega_1)e^{-i\omega_1(\tau-r/c)}\int S_0((1+\beta)\left[t-\frac{r}{c}\right])S_0^*(t-\tau)e^{-i\omega_1\beta(t-r/c)}dt = \tag{3.21}$$
$$= \frac{(1+\beta)}{2\pi}f_T(\mathbf{e},\mathbf{e}_0;\omega_1)e^{-i\omega_1(1+\beta)(\tau-r/c)}\int S_0(\omega)S_0^*(\omega(1+\beta)+\omega_1\beta)e^{-i\omega(1+\beta)(t-r/c)}d\omega.$$

For narrow-band signals with a band $\Delta\omega$: $\Delta\omega/\omega_1 \geq 0.01$, one has $\omega_1 >> \omega$ under the integral, so it's possible to neglect $\beta\omega$ with respect to $\beta\omega_1$ when calculating the integral on frequency in (3.21). On the other hand, since $\beta \sim v_T/c$ then one can also neglect $\beta\omega_1$ with respect to ω for common underwater objects. In this case, it derives from (3.21)

$$K(\tau) \approx (1+\beta) f_T(\mathbf{e}, \mathbf{e}_0; \omega_1) K_0((1+\beta)(\tau - r/c)),$$
$$K_0(\tau) = e^{-i\omega_1 \tau} \frac{1}{2\pi} \int |S_0(\omega)|^2 e^{-i\omega\tau} d\omega, \tag{3.22}$$

where $K_0(\tau)$ is the correlation function of the probing signal. Thus, the Doppler effect gives for such narrow-band signals a shift of the central frequency and a compression of the correlation function with corresponding increasing of its maximum amplitude.

In the waveguide case the echo-signal has a multi-ray structure. Signal $S_{\mu\nu}(t)$ coming by the μ-th ray path and being the result of the scattering from the object of the field of the ν-th ray path of the source field, is strained with the coefficient

$$1+\beta, \beta = \frac{v_T}{c_T}\left(\cos(\alpha+\alpha_2)\cos\chi_{\mu T} - \cos(\alpha-\alpha_1)\cos\chi_{\nu T}\right). \tag{3.23}$$

Since the angles α_1 and α_2 are small for the FS-ABS, so β is

$$\beta = \left(\cos\chi_{\mu T} - \cos\chi_{\nu T}\right)\frac{v_T}{c_T}\cos\alpha \ . \tag{3.24}$$

Rays' grazing angles χ are small for common sea environments: $\chi \sim 0.1$, so one can estimate

$$\beta \sim \chi^2 \frac{v_T}{c_T}\cos\alpha \approx 3\cdot 10^{-5}\cos\alpha \ . \tag{2.25}$$

When making correlative processing, the Doppler signal decompressing will give, accordingly to the equation (3.22), some decreasing of the correlation of received signals with the model where it is not taken into account. This Doppler decorrelation is of the order $\sim \beta$, so one can neglect it practically always for the FS-ABS systems.

3.3. Validity conditions of used mathematical models for FS-ABS systems

The echo-signal's model used in this study and estimating is working truly when are satisfied following conditions:

1) Receiving system is placed in the "far field" (Fraunhofer) zone of the scatterer (object):

$$R_{TR} > (L_T)^2/\lambda, \tag{3.26}$$

where one can use the directed spherical model for the scattered fields.

2) The distance from the object to the source is big enough to consider incident wave fronts as planar one on the object's length. This condition is also equivalent to this one that the source of the probing field is placed at the "far field" (Fraunhofer) zone of the scatterer

$$R_{SR} > (L_T)^2 / \lambda . \tag{3.27}$$

Thus, one can formulate the two conditions as

$$\min\{R_{ST}, R_{TR}\} > (L_T)^2 / \lambda . \tag{3.28}$$

Another equivalent formulation of the condition (3.28) is that the object length is smaller than the Fresnel zone radius calculated for the distances from the object to the source and to the receiver.

For 1 kHz: $\min\{R_{ST}, R_{TR}\} > 6.8$ km for a object of 100 m length and is increasing as the frequency and the squared object's length, so that at 6 kHz: $\min\{R_{ST}, R_{TR}\} >$ 40 km for the same object, and $\min\{R_{ST}, R_{TR}\} > 1.7$ km in the case where the object's length is 20 m.

3) The object is placed in the "far field" (Fraunhofer) zone of the emitting and receiving arrays. If L_S and L_R are their lengths, this condition is formulated as follows

$$\min\{R_{ST}, R_{TR}\} > (L_{S,R})^2 / \lambda . \tag{3.29}$$

Another equivalent formulation of the condition (3.29) is that the arrays' lengths are smaller than the Fresnel zone radius calculated for the distances from the object to the arrays.

The condition (3.29) is automatically satisfied if the condition (3.28) is satisfied and if maximal sizes of the arrays don't exceed the object's maximal size.

The above presented estimates allow to conclude that the validity conditions of the main approximations will be satisfied practically for all situations for a object of 20 m × 3.5 m size and a FS-ABS system of ~ 15 km base length working at central frequency ~ 6 kHz. Hence, they may not be satisfied for a object of 100 m × 10 m size for some situations, especially in the high frequency case where the wave fronts' curvature and the Fresnel diffraction should be taken into account.

3.4. Tactics of use of FS-ABS systems

By force of its characteristic properties, FS-ABS systems may be used to protect and survey straits, to create acoustic barrier, if only a sufficient efficiency when applying

adequate signal processing algorithms is proved for them. When they are used to create acoustic "barriers", emitter and receiving arrays need to be placed on two sides of a strait or along the barrier line. The system will operate not in pulse as a common ABS system, but in quasi-continuous emitting mode, where emitting arrays continuously radiate probing signals and receiving subsystems continuously receive and process those signals.

When using an FS-ABS one will have the following situation. The sonar's source array will emit continuously probing signals. When an object crosses an acoustic ray path from source to receiver or is near the vertical plane containing this path, distortions of the source signal arise at the receiving array. Such distortion may be generated not only by the sound scattering from the object's body but also by the sound scattering from hydrodynamic inhomogeneities accompanying the object. Those sound field distortions may be classified in two types:

1) modulation of quasi plane fields arriving along the ray paths of the source field; this modulation is due to the interference between the scattered and source fields, which follow the same ray path,

2) arising of new ray paths belonging to the scattered field; their arrival times and angles are different from those of source field's ray paths.

When the FS-ABS scheme is used, TS is much greater then that for the monostatic or common bi-static sonar scheme, therefore distortions of those two types are more appearing at reception.

If propagation conditions are those where sufficiently multi-ray signal structure can develop, then one should solve the UDL problem by using the ray paths of scattered field that are different from the source field's ray paths. In this case optimal frequencies will be higher as it is for the classic ABS. Nevertheless the reverberation will be much greater in this case than for the classic ABS because the angle lobe of the scattering index is very narrow when high frequencies are used.

If propagation conditions are those where sufficiently multi-ray signals can not develop, then one needs to solve the UDL problem using the first type modulation of quasi plane fields arriving along the ray paths of the source field. In this case one should increase the time of signal accumulation to improve the probability of good detection. Therefore optimal frequencies should be lower because the time interval where an object crosses the narrow FS-ABS detection zone is proportional to the width of the main lobe of the scattering coefficient, and this width is inverse proportional to the carrier frequency of probing signals. When using this signal detection mode, the signal modulation of the source field due to the scattering from the object body and accompanying inhomogeneities will be mixed with signal distortions due to the scattering from natural inhomogeneities such as small-scale internal waves or turbulence.

Notice also that the general physical principle used by FS-ABS systems (detection of distortions of probing signals) is very common and used anywhere, in sciences applications.

4. SIGNAL PROCESSING FOR FS-ABS

The underwater object survey (UOS) problem consists of solving three main problems: *detection* of an object, *localization* (determining object's coordinates) and *classification* (determining of class to which the object belongs; it means to make choice between a submarine, surface ship, torpedo, imitator, and so on). Hereafter the only detection and localization problems are considered. They may be solved separately or simultaneously. The last approach is more effective.

Signal fields in common sea environments have some complex space-time structure (multi-ray or multi-mode composition). It gives unique opportunities to localize objects when using only small (with respect to the waveguide's depth and object range) receiving arrays.

In this chapter the methodology of designing MFP algorithms for solving the underwater detection and localization (UDL) problem by using an ABS are presented. The methodology is developed for the determinist sea environment (DSE) model (section 4.2.1) as well as for the stochastic sea environment (SSE) model (sections 4.2.2 and 4.3). All the signal and interference models being needed for this methodology are described above in the 2.

4.1. Model of signal measurement

Signals at exits of N_R receivers of the receiving array are proportional to sound pressure at points $\mathbf{r}_s$ where the receivers are placed. Under the supposition that the hypothesis H_ε is true ($\varepsilon = 1$ if there is an object and $\varepsilon = 0$ if there no object) the signal measurement is (see the section 2):

$$p(\mathbf{r}_s,t) = p_S(\mathbf{r}_s,t) + \varepsilon\, p_T(\mathbf{r}_s,t) + p_N(\mathbf{r}_s,t), \quad s = 1,\ldots,N_R, \quad t \in (0,T). \quad (4.1)$$

Let consider the interference $p_N(\mathbf{r}_q,t)$ in the equation (4.1) as normally distributed stationary field having zero mean value and a covariance matrix $[\mathbf{K}_N(\tau)]_{ql} = K_N(\mathbf{r}_q,\mathbf{r}_l,\tau)$ which is not know *a priori*. For common sea environments and periods of signal processing T_0 not larger than several seconds the supposition about interference's stability may be assumed. This supposition is well founded for the system noise, interference of local noisy sources and sea ambient noise since theirs time intervals of stability are about tens of seconds or more. It's also valid for

the forward-scattered reverberation (FSR) in the case where complex probing signals of quasi constant module (like the linear frequency modulated pulses) are radiated within a period equal to the signal's duration. The probing signal's and echo-signal's fields are multi-path signals whose structures are determined by GF of the waveguide and are described by models being presented above in the section 2.

Since the signal and noise fields are supposed to be stationary, it is convenient to use theirs spectral representations. To obtain a spectral representation of a measurement, signals at exits of all array's sensors are Fourier transformed on the time interval T_0 being equal to the probing signal's period:

$$P(\mathbf{r}_q,\omega) = \int_0^{T_0} p(\mathbf{r}_q,t)\exp\{i\omega t\}dt \tag{4.2}$$

When a digital signal processing is realized, the sensors' time exits are firstly sampled on the period T_0 at N+1 moments t_n and measured signal amplitudes compose a vector of measurement. Then, its complex spectrum is obtained by using the discrete Fourier transform:

$$\begin{aligned} P(\mathbf{r}_q,\omega_m) &= \frac{T_0}{N}\sum_{n=1}^{N} p(\mathbf{r}_q,t_n)\exp\{i\omega_m t_n\} \\ t_n &= \frac{T_0}{N}n, \omega_n = \frac{2\pi}{T_0}m, n,m = 0,1,\ldots,N. \end{aligned} \tag{4.3}$$

So, under the digital spectral representation the model of measurement is

$$\begin{aligned} &P(\mathbf{r}_q,\omega_n) = P_S(\mathbf{r}_q,\omega_n) + \varepsilon P_T(\mathbf{r}_q,\omega_n) + P_N(\mathbf{r}_q,\omega_n), \\ &\omega_n = \frac{2\pi}{T_0}n, n = 0,1,\ldots,N. \end{aligned} \tag{4.4}$$

Under the approximation where a receiving array having its center located at point $\mathbf{r}_R$ has a smaller dimension than those of ray beams, and where the array is not placed in the vicinity of some caustic surface those spectral models can be written as follows:

- model for the source field (probing signal):

$$\begin{aligned} P_S(\mathbf{r}_q;\omega) &= S(\omega)\sum_{\mu=1}^{M(\mathbf{r}_q,\mathbf{r}_S)} A_\mu(\mathbf{r}_q,\mathbf{r}_S;\omega)\cdot e^{i\omega t_\mu(\mathbf{r}_q,\mathbf{r}_S)}\sqrt{\frac{Wpc\gamma}{4\pi}}\,\mathbf{B}_S(-\mathbf{e}_\mu(\mathbf{r}_S,\mathbf{r}_q)-\mathbf{e}_S^0;\omega) \approx \\ &\approx S(\omega)\sum_{\mu=1}^{M(\mathbf{r}_R,\mathbf{r}_S)} A_\mu(\mathbf{r}_R,\mathbf{r}_S;\omega)\cdot e^{i\omega t_\mu(\mathbf{r}_R,\mathbf{r}_S)+i\frac{\omega}{c}\left(\mathbf{e}_\mu(\mathbf{r}_R,\mathbf{r}_S),\mathbf{r}_q-\mathbf{r}_R\right)}\sqrt{\frac{Wpc\gamma}{4\pi}}\,\mathbf{B}_S(-\mathbf{e}_\mu(\mathbf{r}_S,\mathbf{r}_R)-\mathbf{e}_S^0;\omega), \end{aligned} \tag{4.5}$$

where: W, γ, ρc are the radiated acoustical power, the array pattern factor (the concentration coefficient) and the wave resistance of the medium, $S(\omega)$ is the spectrum of the probing signal, $B_S(.)$, $\mathbf{e}_S^0$ are the emitter's lobe and its compensation vector, $M(\mathbf{r},\mathbf{r}')$ is the number of ray paths connecting two points $\mathbf{r}$ and $\mathbf{r}'$, $A_\mu = A_\mu(\mathbf{r},\mathbf{r}';\omega)$ is the amplitude of the μ-th ray path connecting the points $\mathbf{r}$ and $\mathbf{r}'$, $t_\mu = t_\mu(\mathbf{r},\mathbf{r}')$ is the travel time of the μ-th ray path connecting the points $\mathbf{r}$ and $\mathbf{r}'$, $\mathbf{e}_\mu = \mathbf{e}_\mu(\mathbf{r},\mathbf{r}')$ is the unit vector tangent at the point $\mathbf{r}$ to the μ-th ray path connecting the points $\mathbf{r}$ and $\mathbf{r}'$;

- model for echo-signals:

$$P_T(\mathbf{r}_q;\omega) = S(\omega)\sum_{\nu=1}^{N(\mathbf{r}_q,\mathbf{r}_T)} A_\nu(\mathbf{r}_q,\mathbf{r}_T;\omega)e^{i\omega t_\nu(\mathbf{r}_q,\mathbf{r}_T)}\sum_{\mu=1}^{M(\mathbf{r}_T,\mathbf{r}_S)} A_\mu(\mathbf{r}_T,\mathbf{r}_S;\omega)e^{i\omega t_\mu(\mathbf{r}_T,\mathbf{r}_S)}\times$$

$$\times\frac{1}{2}R_T(-\mathbf{e}_\nu(\mathbf{r}_T,\mathbf{r}_R),\mathbf{e}_\mu(\mathbf{r}_T,\mathbf{r}_S);\omega)\sqrt{\frac{W\rho c\gamma}{4\pi}}B_S(-\mathbf{e}_\mu(\mathbf{r}_S,\mathbf{r}_T)-\mathbf{e}_S^0;\omega)\approx$$

$$\approx S(\omega)\sum_{\nu=1}^{N(\mathbf{r}_R,\mathbf{r}_T)} A'_\nu(\mathbf{r}_R,\mathbf{r}_T;\omega)e^{i\omega t_\mu(\mathbf{r}_R,\mathbf{r}_T)+i\frac{\omega}{c}(\mathbf{e}_\mu(\mathbf{r}_R,\mathbf{r}_T),\mathbf{r}_q-\mathbf{r}_R)},$$

$$A'_\nu(\mathbf{r}_R,\mathbf{r}_T;\omega) = A_\nu(\mathbf{r}_R,\mathbf{r}_T;\omega)\sum_{\mu=1}^{M(\mathbf{r}_T,\mathbf{r}_S)} A_\mu(\mathbf{r}_T,\mathbf{r}_S;\omega)e^{i\omega t_\mu(\mathbf{r}_T,\mathbf{r}_S)}\times \tag{4.6}$$

$$\times\frac{1}{2}R_T(-\mathbf{e}_\nu(\mathbf{r}_T,\mathbf{r}_R),\mathbf{e}_\mu(\mathbf{r}_T,\mathbf{r}_S);\omega)\sqrt{\frac{W\rho c\gamma}{4\pi}}B_S(-\mathbf{e}_\mu(\mathbf{r}_S,\mathbf{r}_T)-\mathbf{e}_S^0;\omega),$$

where $R_T(.)$ is the object's equivalent radius (ER);

- model for interference:

The interference is a gaussian stationary field with zero mean value and a cross-spectrum matrix (CSM) $[\mathbf{K}_N(\omega)]_{ql} = K_N(\mathbf{r}_q,\mathbf{r}_l,\omega)$ related to the local angular spectrum $N_N(\mathbf{e},\mathbf{r};\omega)$:

$$K_N(\mathbf{r}_q,\mathbf{r}_l;\omega) = \oint N_N(\mathbf{e},\mathbf{r};\omega)e^{i\frac{\omega}{c}(\mathbf{e},\boldsymbol{\rho})}d\Omega(\mathbf{e}),\quad \mathbf{r} = \frac{\mathbf{r}_q+\mathbf{r}_l}{2},\ \boldsymbol{\rho} = \mathbf{r}_q-\mathbf{r}_l\ . \tag{4.7}$$

For the multi-component interference in sea environments the CSM is

$$K_N(\mathbf{r}_s,\mathbf{r}_q,\omega) = K_{N_{Sys}}(\omega)\delta(\mathbf{r}_s-\mathbf{r}_q)+K_{N_{Amb}}(\mathbf{r}_R,\mathbf{r}_s-\mathbf{r}_q,\omega)+$$
$$+\sum_l \kappa_l(\omega)\left|G(\mathbf{r}_s,\mathbf{r}_l;\omega)\right\rangle\left\langle G(\mathbf{r}_q,\mathbf{r}_l;\omega)\right| + K_{N_{Rev}}(\mathbf{r}_R,\mathbf{r}_s-\mathbf{r}_q,\omega), \tag{4.8}$$

so, the interference is locally homogeneous field. In the case of relatively small arrays the covariance matrix becomes of the Toeplitz type: $[\mathbf{K}_N(\omega)]_{qs} = K_N(\mathbf{r}_q - \mathbf{r}_s, \omega)$ and the angular spectrum is constant on the array's aperture: $N_N = N_N(\mathbf{e}, \omega)$.

4.2. MFP algorithms for detection and localization

4.2.1. MFP for determinist sea environments

Let begin with the case of deterministic sea environments (DSE). In despite that this model is rather unrealistic it's a good start point to present the methodology of signal processing design. This methodology remains the same in its main moments for stochastic sea environments (SSE), which needs only some modifications to account various random factors.

4.2.1.1. Signals with predictable phase and amplitude

When using the DSE model one must consider the probing signal and the echo-signal to be determinist with fully known phase and amplitude. In this case, under above admitted suppositions about statistical properties of signal and interference fields the probability density of an array measurement $\mathbf{P}(\omega_n) = \left| P(\mathbf{r}_s, \omega_n) \right\rangle$ is:

$$\Phi_\varepsilon(\mathbf{P}) = \prod_{\omega_n > 0} \frac{\exp\left\{ \left\langle \mathbf{K}_N^{-1}(\omega_n)\left(\mathbf{P}(\omega_n) - \mathbf{P}_S(\omega_n) - \varepsilon \mathbf{P}_T(\omega_n)\right), \left(\mathbf{P}(\omega_n) - \mathbf{P}_S(\omega_n) - \varepsilon \mathbf{P}_T(\omega_n)\right) \right\rangle \right\}}{\det 2\pi \mathbf{K}_N(\omega_n)}, \quad (4.9)$$

where $\mathbf{K}_N(\omega_n)$ is the noise spectral density matrix (NSDM), the angle brackets means the time-space scalar product of $\mathbf{U}(\omega_n)$ and $\mathbf{V}(\omega_n)$: $\langle \mathbf{U}, \mathbf{V} \rangle = \sum_s U_s(\omega_n) V_s^*(\omega_n)$.

Under the Bayessian statistical approach to making decision [11], the optimal decision statistics (ODS) is the likelihood log-ratio:

$$L\{\mathbf{P}\} = \ln \frac{\Phi_1(\mathbf{P})}{\Phi_0(\mathbf{P})} = 2\,\mathrm{Re} \sum_{\omega_n > 0} \left\langle \mathbf{K}_N^{-1}(\omega_n)\left(\mathbf{P}(\omega_n) - \mathbf{P}_S(\omega_n)\right), \mathbf{P}_T(\omega_n) \right\rangle - \\ - \sum_{\omega_n > 0} \left\langle \mathbf{K}_N^{-1}(\omega_n)\mathbf{P}_T(\omega_n), \mathbf{P}_T(\omega_n) \right\rangle. \quad (4.10)$$

So the signal processing algorithm for solving the UDL problem based on this ODS is following. All the waveguide area to be observed is covered by a grid in depth and range. For each grid point considered as possible object location the vector $\mathbf{P}_T(\omega_n)$ of complex spectra of the echo-signal and the vector $\mathbf{P}_S(\omega_n)$ of complex spectra of the

probing signal on receiving array's receivers are modeled. After the measurement having been done and its complex spectrum $\mathbf{P}(\omega_n)$ being obtained, one calculates the ODS (3) on the grid. The ODS (3) means that the model of known source field has to be subtracted from the measurement and the result has to be correlated with the model of echo-signal. The correlation to be calculated is the scalar product in the space having the metric tensor $\mathbf{K}_N^{-1}(\omega_n)$. The correlation will be maximal for the more likelihood position of echo-signal source. As result the ODS (4.3) as function of probable object coordinates is built. After that one searches for its global maximum (main lobe) which is compared to some threshold having been calculated from some given probability of false alert. If the maximum value is higher than the threshold then the detection problem is considered as solved and the coordinates of this maximum are considered as estimate of object's coordinates. If the main lobe is lower than the threshold, the detection problem is considered as unsolved and there is no built estimate of object's coordinates.

To increase the power of this signal processing algorithm one may do incoherent accumulation of decision statistics over processing periods with taking into account a possible object motion. By making parameterization of the motion and accumulating decision statistics with taking into account different values of motion parameters one can determine by the way estimates of these parameters and solve the problem of following the object.

4.2.1.2. Signals with unpredictable phase

In the cases where it's not possible to control positions of the source and receiving arrays within the wave-length precision one must use for the probing and echo signals the model of unknown phase. On the other hand, the object strength is never know *a priori*, therefore the echo-signal amplitude is not known. In this case the unknown phase signal model for probing signals and the unknown complex amplitude signal model for echo-signals shall be applied.

To get ODS for this case one may apply the maximum likelihood principle that means the maximization of the spectral power densities of hypothesis H_0 and H_1 versus the unknown parameters to get their maximum likelihood estimates (MLE). Further, MLE are substituted into the spectral power density equations and the log-ratio is calculated. Having done all these procedures, the ODS for the UOS problem deduces under the form

$$L\{\mathbf{P}\}=\frac{\left[\left|\sum_{\omega_n>0}\left\langle \mathbf{K}_N^{-1}(\omega_n)\mathbf{P}(\omega_n),\mathbf{P}_T(\omega_n)\right\rangle\right|-\left|\sum_{\omega_n>0}\left\langle \mathbf{K}_N^{-1}(\omega_n)\mathbf{P}_S(\omega_n),\mathbf{P}_T(\omega_n)\right\rangle\right|\right]^2}{\sum_{\omega_n>0}\left\langle \mathbf{K}_N^{-1}(\omega_n)\mathbf{P}_T(\omega_n),\mathbf{P}_T(\omega_n)\right\rangle} \quad .(4.11)$$

The signal processing algorithm for solving the UDL problem based on the ODS (4.11) rests the same as for the previous case. The meaning of this ODS is calculation of difference between the amplitude envelopes of correlation i) between the measurement and echo-signal model and ii) between the source and echo-signal model. If there is no echo-signal in the received field the difference will be minimal and it will be maximal for the more likelihood position of echo-signal source.

4.2.1.3. Signals with unpredictable phase and amplitude

If the absolute amplitude of probing signal is also unknown as well as characteristics of the receiving and emitting systems, then the signal model of unknown complex amplitude must be used for both the probing and echo-signals. Having applied in this case the maximum likelihood principle, one gets the ODS under the form

$$L\{\mathbf{P}\} = \frac{\left|\sum_{\omega_n>0}\left\langle \mathbf{K}_N^{-1}(\omega_n)\mathbf{P}(\omega_n),\mathbf{P}_T^{\perp}(\omega_n)\right\rangle\right|}{\sqrt{\sum_{\omega_n>0}\left\langle \mathbf{K}_N^{-1}(\omega_n)\mathbf{P}_T^{\perp}(\omega_n),\mathbf{P}_T^{\perp}(\omega_n)\right\rangle}}, \tag{4.12}$$

where $$\mathbf{P}_T^{\perp}(\omega_n) = \mathbf{P}_T(\omega_n) - \mathbf{P}_S(\omega_n)\frac{\sum_{\omega_n>0}\left\langle \mathbf{K}_N^{-1}(\omega_n)\mathbf{P}_S(\omega_n),\mathbf{P}_T(\omega_n)\right\rangle}{\sum_{\omega_n>0}\left\langle \mathbf{K}_N^{-1}(\omega_n)\mathbf{P}_S(\omega_n),\mathbf{P}_S(\omega_n)\right\rangle}. \tag{4.13}$$

In the classic ABS case the probing and echo-signals are separated in the time domain, then $\left\langle \mathbf{K}_N^{-1}(\omega_n)\mathbf{P}_S(\omega_n),\mathbf{P}_T(\omega_n)\right\rangle = 0$, and ODS becomes simpler

$$L\{\mathbf{P}\} = \frac{\left|\sum_{\omega_n>0}\left\langle \mathbf{K}_N^{-1}(\omega_n)\mathbf{P}(\omega_n),\mathbf{P}_T(\omega_n)\right\rangle\right|^2}{\sum_{\omega_n>0}\left\langle \mathbf{K}_N^{-1}(\omega_n)\mathbf{P}_T(\omega_n),\mathbf{P}_T(\omega_n)\right\rangle}. \tag{4.14}$$

The signal processing algorithm for solving the UDL problem based on the ODS (4.12) or (4.14) rests the same as for the previous cases. The meaning of this ODS is calculation of scalar product (within the metric $\mathbf{K}_N^{-1}(\omega_n)$) of the measurement and orthogonal supplement to the echo-signal model.

4.2.1.4. Quality estimation of DSE-matched algorithms

Probability of false alert per one signal processing period per one grid point for the ODS (4.11) is

$$P_F(\tau) = \int_0^\infty H\left[(r - r_0)^2 - \tau\right] e^{-r^2 - r_0^2} I_0(2rr_0) r dr,$$

$$r_0 = \frac{\left| \sum_{\omega_n > 0} \left\langle \mathbf{K}_N^{-1}(\omega_n) \mathbf{P}_S(\omega_n), \mathbf{P}_T(\omega_n) \right\rangle \right|}{\sqrt{\sum_{\omega_n > 0} \left\langle \mathbf{K}_N^{-1}(\omega_n) \mathbf{P}_T(\omega_n), \mathbf{P}_T(\omega_n) \right\rangle}}, \tag{4.15}$$

where H(.) is the Heaviside function, M_0 is the zero-order Bessel function of imaginary argument. For the ODS (4.12) the distribution low under the hypothesis H_0 is exponential with unit mean value, so the false alert probability is

$$P_F(\tau) = e^{-\tau}. \tag{4.16}$$

Under the hypothesis H_1 the ODS (4.12) has the Rice distribution. Probability of good detection for ODS (4.11) and (4.12) is

$$P_D(\tau) = \int_0^\infty H\left[(r - r_0)^2 - \tau\right] e^{-r^2 - r_1^2} I_0(2rr_1) r dr,$$

$$r_1 = \frac{\left| \sum_{\omega_n > 0} \left\langle \mathbf{K}_N^{-1}(\omega_n) \left(\mathbf{P}_S(\omega_n) + \mathbf{P}_T(\omega_n)\right), \mathbf{P}_T(\omega_n) \right\rangle \right|}{\sqrt{\sum_{\omega_n > 0} \left\langle \mathbf{K}_N^{-1}(\omega_n) \mathbf{P}_T(\omega_n), \mathbf{P}_T(\omega_n) \right\rangle}}, \quad \text{(statistics (4.11))}, \tag{4.17}$$

$$P_D(\tau) = \int_0^\infty e^{-r^2 - \rho^2} I_0(2r\rho) r dr,$$

$$\rho = \frac{\left| \sum_{\omega_n > 0} \left\langle \mathbf{K}_N^{-1}(\omega_n) \mathbf{P}_T(\omega_n), \mathbf{P}_T^{\perp}(\omega_n) \right\rangle \right|}{\sqrt{\sum_{\omega_n > 0} \left\langle \mathbf{K}_N^{-1}(\omega_n) \mathbf{P}_T^{\perp}(\omega_n), \mathbf{P}_T^{\perp}(\omega_n) \right\rangle}} \quad \text{(statistics (4.12))}. \tag{4.18}$$

Grid steps on depth and range are determined by corresponding widths of the ambiguity function (AF) main lobe. AF is calculated using following expression

$$N(\mathbf{r}_1, \mathbf{r}_0) = \frac{\left| \sum_{\omega_n > 0} \left\langle \mathbf{K}_N^{-1}(\omega_n) \mathbf{P}_T(\omega_n; \mathbf{r}_0), \mathbf{P}_T^{\perp}(\omega_n; \mathbf{r}_1) \right\rangle \right|}{\sqrt{\sum_{\omega_n > 0} \left\langle \mathbf{K}_N^{-1}(\omega_n) \mathbf{P}_T^{\perp}(\omega_n; \mathbf{r}_1), \mathbf{P}_T^{\perp}(\omega_n; \mathbf{r}_1) \right\rangle}}. \tag{4.19}$$

The widths of the main lobe determine also the precision of object localization. It follows from theorems of mathematical statistics that the mean value of the second order derivative matrix of the AF in the global maximum point is asymptotically equal to the minus Fisher information matrix (FIM) for estimates of object coordinates:

$$\mathrm{I}(\mathbf{r}) = 2\,\mathrm{Re}\sum_{\omega_n>0}\left\langle \mathbf{K}_{\mathrm{N}}^{-1}(\omega_n)\mathbf{Q}(\omega_n)\partial \mathbf{P}_{\mathrm{T}}(\omega_n;\mathbf{r}_0), \partial \mathbf{P}_{\mathrm{T}}(\omega_n;\mathbf{r}_0)\right\rangle, \qquad \mathbf{Q}(\omega_n) = \mathbf{E} - \boldsymbol{P}(\omega_n), \tag{4.20}$$

where $\boldsymbol{P}$ is the operator of projecting onto hyper-space of vectors $\mathbf{P}_{\mathrm{S}}(\omega_n)$ and $\mathbf{P}_{\mathrm{T}}(\omega_n;\mathbf{r}_0)$:

$$\boldsymbol{P}(\omega_n) = \sum_{\alpha,\beta=\mathrm{S},\mathrm{T}} \left|\mathbf{P}_\alpha(\omega_n)\right\rangle \left\langle \mathbf{K}_{\mathrm{N}}^{-1}(\omega_n)\mathbf{P}_\alpha(\omega_n;\mathbf{r}_0), \mathbf{P}_\beta(\omega_n)\right\rangle^{-1} \left\langle \mathbf{P}_\beta(\omega_n)\right| \mathbf{K}_{\mathrm{N}}^{-1}(\omega_n) \cdot \tag{4.21}$$

Signal-to-noise ratio (SNR) is

$$\rho = \sum_{\omega_n>0}\left\langle \mathbf{K}_{\mathrm{N}}^{-1}(\omega_n)\mathbf{P}_{\mathrm{T}}(\omega_n), \mathbf{P}_{\mathrm{T}}(\omega_n)\right\rangle - \frac{\left|\sum_{\omega_n>0}\left\langle \mathbf{K}_{\mathrm{N}}^{-1}(\omega_n)\mathbf{P}_{\mathrm{S}}(\omega_n), \mathbf{P}_{\mathrm{T}}(\omega_n)\right\rangle\right|^2}{\sum_{\omega_n>0}\left\langle \mathbf{K}_{\mathrm{N}}^{-1}(\omega_n)\mathbf{P}_{\mathrm{S}}(\omega_n), \mathbf{P}_{\mathrm{S}}(\omega_n)\right\rangle} \cdot \tag{4.22}$$

For the convenient active pulse sonar the SNR is determined by the first term in (22). For the FS sonar the SNR is cut down because of the effect of the second term in (22). Equations for ODS and SNR clarify the main difference between the conventional mono or bi-static ABS and the FS-ABS. For the conventional sonar the ODS is proportional to the time-space correlation of the measurement and the echo-signal model. For the FS sonar the ODS is proportional to the time-space correlation of the measurement and the orthogonal addendum (13) of the echo-signal field to the source field. It means that a new kind of interference appears for FS-ABS systems - the source field. Its effect has to be suppressed like that of the ambient noise and reverberation. The effect of the source field is as smaller as small is the second term in (22) which is proportional to the scalar product of the source and echo fields. To have this term as small as possible the FS-ABS system's parameters and configuration should be chosen to ensure the separation of source and echo-signal ray arrivals in the time-angle space. Horizontal arrival angles of the source and echo-signal rays differ very slightly but their grazing angles may be rather different. It follows from this consideration that the receiving sub-system of FS sonar should have a rather big vertical wave dimension to ensure the ray separation on grazing angle. It follows also

that the FS sonar should use pulse signals with high time resolution, which is determined by the signal band width. So, the radiated probing signal should have some large band to ensure needed time resolution. Finally, the central frequency of probing signals has to be chosen to have the living time of echo-signal much smaller than the variability time scale of the source field.

Characteristics of an UOS system as used for modeling may have some mismatches from real values. Those characteristics may be:

1) parameters of the waveguide (total depth or bottom profile, bottom type and parameters, sound velocity field, wind speed, etc.);

2) parameters of emitter or receiving arrays (their depths, space orientation, etc.).

Mismatches in these parameters between real situations and used models make so that real fields of probing and echo signals will be different from model ones. Marking the real fields by the upper script (0), the following expression for the ambiguity function (AF) characterizing mismatches derives:

$$N(\mathbf{r}_1,\mathbf{r}_0)=\frac{\left|\sum_{\omega_n>0}\left\langle \mathbf{K}_N^{-1}(\omega_n)\left(\mathbf{P}_S^{(0)}(\omega_n)+\mathbf{P}_T^{(0)}(\omega_n;\mathbf{r}_0)\right)\mathbf{P}_T^{\perp}(\omega_n;\mathbf{r}_1)\right\rangle\right|}{\sqrt{\sum_{\omega_n>0}\left\langle \mathbf{K}_N^{-1}(\omega_n)\mathbf{P}_T^{\perp}(\omega_n;\mathbf{r}_1),\mathbf{P}_T^{\perp}(\omega_n;\mathbf{r}_1)\right\rangle}}. \qquad (4.23)$$

4.2.1.5. Algorithm for estimation of unknown interference and field parameters

In the above presented algorithm of making decision it is considered that the noise spectral density matrix (NSDM) $\mathbf{K}_N(\omega)$ is known *a priory*. In fact, one has no such *a priori* information. Moreover, the noise field may vary during the survey, for example, because of variations of the wind speed or movements of surface ships (local noisy sources). Nevertheless, as a rule one has *a priory* information about time intervals of variability of different types of interference. Usually they exceed correlation intervals for all types of interference. On the other hand, some *a priori* information about space variability of this interference is available. It may be formulated as smoothness characteristics of angular spectrum or as spectral characteristics of interference. This *a priori* information allows to design adaptive algorithms with NSDM estimating.

Let first suppose that the NSDM $\mathbf{K}_N$ doesn't depend on frequency for the frequency range of probing signals. While probing signals are narrow-band, this supposition is unconditionally valid regarding the system and the sea ambient noises. The reverberation interference has a spectral density that is proportional to the squared module

of the probing signal's spectrum. One uses usually complex signals where only the spectrum's phase depends on frequency but not the spectral amplitude. In this case one may consider that the spectral density of reverberation isn't also depending on frequency. If some frequency dependence is still present, our previous numerical modeling shows that the optimization of processing algorithms for active systems by means of making interference whitening gives rather small amelioration of the result, which is not important.

To get estimation of the NSDM one may as well use the maximum likelihood approach. In this case it's necessary to calculate derivatives of the logarithms of the probability density functions (log-PDF) of measurements

$$\ln \Phi_\varepsilon(\mathbf{P}) = -\sum_{n=1}^{N_\omega} \left\langle \mathbf{K}_N^{-1} \left(\mathbf{P}^n - \mathbf{P}_S^n - \varepsilon \mathbf{P}_T^n\right) \right\rangle \left(\mathbf{P}^n - \mathbf{P}_S^n - \varepsilon \mathbf{P}_T^n\right) - N_\omega \ln \det \mathbf{K}_N , \quad (4.24)$$

where $\mathbf{P}^n = \mathbf{P}(\omega_n)$, $\mathbf{P}_S^n = \mathbf{P}_S(\omega_n)$, $\mathbf{P}_T^n = \mathbf{P}_T(\omega_n)$, with respect to elements of the matrix $\mathbf{K}_N$ and to equal them to zero. Solution of such obtained equations is

$$\hat{\mathbf{K}}_N^{(\varepsilon)} = \frac{1}{N_\omega} \sum_{n=1}^{N_\omega} \left| P^n - P_S^n - \varepsilon P_T^n \right\rangle \left\langle P^n - P_S^n - \varepsilon P_T^n \right| . \quad (4.25)$$

Substituting (4.25) in (4.24) one derives:

$$\ln \hat{\Phi}_\varepsilon(\mathbf{P}) = -N_\omega \left\{ N_R + \ln \det \hat{\mathbf{K}}_N^{(\varepsilon)} \right\}, \quad (4.26)$$

where N_R is the number of receivers in the array.

The NSDM estimate for the hypothesis with H_ε may be presented as

$$\hat{\mathbf{K}}_N^{(\varepsilon)} = \hat{\mathfrak{R}} + \frac{1}{N_\omega} \sum_{\mu,\nu=1}^{M_S+\varepsilon M_T} R_S(t_\mu - t_\nu) \left| A_\mu \mathrm{E}_\mu - \tilde{q}(t_\mu) \right\rangle \left\langle A_\nu \mathrm{E}_\nu - \tilde{q}(t_\nu) \right|, \quad (4.27)$$

$$\begin{gathered}
\hat{\mathfrak{R}} = \mathfrak{R} - \frac{1}{N_\omega} \sum_{\mu,\nu=1}^{M_S+\varepsilon M_T} \left[R_S(t_\mu - t_\nu)\right]^{-1} \left| q(t_\mu) \right\rangle \left\langle q(t_\nu) \right|, \quad \mathfrak{R} = \frac{1}{N_\omega} \sum_n \left| P(\omega_n) \right\rangle \left\langle P(\omega_n) \right|, \\
\left| \mathrm{E}_\mu \right\rangle = \left| \exp\left\{ i \frac{\omega_0}{c} \left(\mathbf{e}_\mu, \mathbf{r}_q - \mathbf{r}_R\right) \right\} \right\rangle, \quad R_S(\tau) = \sum_n e^{i\omega_n \tau} \left|S(\omega_n)\right|^2 \Big/ \sum_n \left|S(\omega_n)\right|^2 , \\
\tilde{q}(t_\mu) = \sum_{\nu=1}^{M_S} \left[R_S(t_\mu - t_\nu)\right]^{-1} q(t_\nu), \quad \left| q(t) \right\rangle = \frac{1}{N_\omega} \sum_n \left| P(\omega_n) \right\rangle e^{-i\omega_n t} S^*(\omega_n).
\end{gathered} \quad (4.28)$$

There $R_S(\tau)$ is the probing signal's correlation function normalized so that $R_S(0) = 1$,

$|R_S(\tau)| \le R_S(0)$, matrix $[R_S(t_\mu - t_\nu)]^{-1}$ is inverse of the matrix $R_S(t_\mu - t_\nu)$, $q(t)$ is the cross-covariance functions of measurement and probing signal. Using these notations the term $\ln\det\hat{\mathbf{K}}_N^{(\varepsilon)}$ may be presented as

$$\ln\det\hat{\mathbf{K}}_N^{(\varepsilon)} = \ln\det\Re + \\ + \ln\det\left[\mathrm{E} + \frac{1}{N_\omega}\Re^{-1}\sum_{\mu,\nu=1}^{M_S+\varepsilon M_T} R_S(t_\mu - t_\nu)\left|A_\mu \mathrm{E}_\mu - \bar{q}(t_\mu)\right\rangle\left\langle A_\nu \mathrm{E}_\nu - \bar{q}(t_\nu)\right|\right]. \tag{4.29}$$

The last term in (4.29) may be approximated by

$$\frac{1}{N_\omega}\sum_{\mu,\nu=1}^{M_S+\varepsilon M_T} R_S(t_\mu - t_\nu)\left\langle \Re^{-1}\left(A_\mu \mathrm{E}_\mu - \bar{q}(t_\mu)\right)\left(A_\nu \mathrm{E}_\nu - \bar{q}(t_\nu)\right)\right\rangle . \tag{4.30}$$

This approximation gives a quasi-optimal processing algorithm where the mismatch vector $A_\mu \mathrm{E}_\mu - \bar{q}(t_\mu)$ should have smallest length.

Therefore, the log-PDF for the hypothesis H_ε is

$$\ln\hat{\Phi}_\varepsilon(\mathbf{P}) = -N_\omega\left\{N_R + \ln\det\Re\right\} - \\ -\sum_{\mu,\nu=1}^{M_S+\varepsilon M_T} R_S(t_\mu - t_\nu)\left\langle \Re^{-1}\left(A_\mu \mathrm{E}_\mu - \bar{q}(t_\mu)\right)\left(A_\nu \mathrm{E}_\nu - \bar{q}(t_\nu)\right)\right\rangle. \tag{4.31}$$

Making maximization of this PDF on unknown complex ray amplitudes one obtains estimates

$$\hat{A}_\mu = \sum_{\nu=1}^{M_S+\varepsilon M_T}\left[R_S(t_\mu - t_\nu)\left\langle \Re^{-1}\mathrm{E}_\nu, \mathrm{E}_\mu\right\rangle\right]^{-1}\left\langle \Re^{-1}\mathrm{E}_\nu, q(t_\nu)\right\rangle , \tag{4.32}$$

which have to be substituted into (4.30) to derive the log-PDF for ray phase parameters estimating:

$$\ln\hat{\Phi}_\varepsilon(\mathbf{P}) = -N_\omega\left\{N_R + \ln\det\Re\right\} - \\ -\sum_{\mu,\nu=1}^{M_S+\varepsilon M_T}\left\langle \Re^{-1}\mathrm{E}_\mu, q(t_\mu)\right\rangle\left[R_S(t_\mu - t_\nu)\left\langle \Re^{-1}\mathrm{E}_\nu, \mathrm{E}_\mu\right\rangle\right]^{-1}\left\langle \Re^{-1}\mathrm{E}_\nu, q(t_\nu)\right\rangle. \tag{4.33}$$

By searching for maximums of (4.30) in the space of ray arrival angles and delays one obtains estimates of these parameters.

In the case where ray arrivals are different from each other by time delays which are larger than the probing signal's correlation interval then the PDF is simplified:

$$\ln \hat{\Phi}_\varepsilon(\mathbf{P}) = -N_\omega \left\{ N_R + \ln \det \Re \right\} - \sum_{\nu=1}^{M_S+\varepsilon M_T} \frac{\left| \left\langle \Re^{-1} \mathrm{E}_\nu, q(t_\nu) \right\rangle \right|^2}{\left\langle \Re^{-1} \mathrm{E}_\nu, \mathrm{E}_\mu \right\rangle}. \tag{4.34}$$

In the case where signal processing for ray parameters estimating is made on some time interval equal to several source signal periods the time accumulation may be applied to calculate PDF:

$$\ln \Phi_\varepsilon(\mathbf{P}) = \\ = -\sum_t \left\{ \sum_{n=1}^{N_\omega} \left\langle \mathbf{K}_\mathrm{N}^{-1} \left(\mathbf{P}''(t) - \mathbf{P}_\mathrm{S}'' - \varepsilon \mathbf{P}_\mathrm{T}''(t) \right) \left(\mathbf{P}''(t) - \mathbf{P}_\mathrm{S}'' - \varepsilon \mathbf{P}_\mathrm{T}''(t) \right) \right\rangle - N_\omega \ln \det \mathbf{K}_\mathrm{N}(t) \right\}. \tag{4.35}$$

After making the same developments as above one obtains the PDF

$$\ln \hat{\Phi}_\varepsilon(\mathbf{P}) = -N_\omega \sum_t \left\{ N_R + \ln \det \Re(t) \right\} - \\ - \sum_{\mu,\nu=1}^{M_S+\varepsilon M_T} \sum_t \left\langle \Re^{-1}(t) \mathrm{E}_\mu, q(t_\mu) \right\rangle \left[R_\mathrm{S}(t_\mu - t_\nu) \sum_t \left\langle \Re^{-1}(t) \mathrm{E}_\nu, \mathrm{E}_\mu \right\rangle \right]^{-1} \times \tag{4.36}$$
$$\times \sum_t \left\langle \Re^{-1}(t) \mathrm{E}_\nu, q(t_\nu) \right\rangle.$$

4.2.2. MFP for stochastic sea environments

Space-time variability of sea environments and the impossibility to know precisely their parameters influence on the efficiency of functioning of UOS systems especially on those based on the use of MFP. The MFP algorithms use the fine space-time structure of sound fields in the ocean to solve the UOS problem and just this structure is the most sensible to variability of medium parameters. Certainly, to avoid this problem one can use very low frequency range (units or tens of Hz) where the sea surface agitation and volume inhomogeneities don't affect considerably the sound field structure. Nevertheless, the use of this frequency range decreases sharply the noise resistance of the system (since it is not optimal for ranges tens of km in shallow water conditions) and decreases also the resolution of the algorithms. It needs also to develop and use powerful low-frequency sources and long receiving arrays. Thus the reasonable way to solve the mismatch problem is to design MFP algorithms being matched to stochastic structure of signals. Evidently such processing algorithms will have the maximal resolution and noise resistance when they are used in environments being adequate to the algorithm's structure.

MFP algorithms for solving the UOS problem in deterministic sea environments (DSE) are presented above. For the stochastic sea environments (SSE) model the principle scheme is the same in all its points other then the optimal decision statistics (ODS). Since fluctuations of waveguide parameters make GF random then to obtain the ODS it's necessary to average the expressions (4.9) over fluctuations. In the most general case there are on this way mathematical difficulties that are not resolved yet. Nevertheless it's possible to do the averaging for two cases that are very important for applications.

Let suppose the full statistical description of all waveguide parameters is known. In this case it would be reasonable to apply the Bayes approach to obtain the ODS for optimal solving the UOS problem. Denote $\Phi(\Omega)$ the probability density function of waveguide parameters describing some sea environment, where

$$\Omega = \left\{\zeta_{\text{Surf}}(\mathbf{x},t),\zeta_{\text{Bot}}(\mathbf{x},t),\mu(\mathbf{x},z,t),\mu_{\text{L}}(\mathbf{x},z),\mu_{\text{T}}(\mathbf{x},z)\right\}, \tag{4.37}$$

with μ of different indexes describes fluctuations of phase velocity of longitudinal (L) and transversal (T) waves in the bottom. One supposes usually that $\Phi(\Omega)$ is the normal (gaussian) distribution with some mean values and space-time covariance functions of the above mentioned parameters and hydrophysic fields. When there are fluctuations, the probability density functions (4.9) should be considered as conditional:

$$\Phi_{\varepsilon} = \Phi_{\varepsilon}(\mathbf{P}|\Omega) \ . \tag{4.38}$$

Corresponding to the Bayessian approach these conditional probabilities have to be averaged over the medium fluctuations:

$$\overline{\Phi}_{\varepsilon}(\mathbf{P}) = \int \Phi_{\varepsilon}(\mathbf{P}|\Omega)\Phi(\Omega)d\Omega \ , \tag{4.39}$$

The log-ratio

$$\mathrm{L}(\mathbf{P}) = \ln\frac{\overline{\Phi}_1(\mathbf{P})}{\overline{\Phi}_0(\mathbf{P})} = \ln\overline{\Phi}_1(\mathbf{P}) - \ln\overline{\Phi}_0(\mathbf{P}) \tag{4.40}$$

is the Bayessian ODS. Nevertheless, as it was already mentioned above, there is no possibility to calculate rigorously the integrals (4.39) in the general case. Firstly, they prove to be continual (functional) integrals (taken in the functional space), that is not a great problem, but secondly there is the ocean waveguide's GF entering in the conditional probability to be averaged that depends on medium parameters μ by rather non-linear way. Moreover, it's not at all possible to express in the most cases this dependence as analytical one. That's why there is a need to apply some corresponding approximation, as it happens generally in physics, to solve the problem of optimal Bayes algorithm design for UOS systems.

To make optimal and well-founded approximation, the essential difference between the signal processing time interval and the time of sound field variability in SSE due to fluctuating waveguide parameters should be used.

The characteristic time correlation interval of a sound field having been one time scattered from the wind perturbed free sea surface is about several sec for the frequency range from hundreds of Hz up to several kHz. When subsurface channel propagation conditions in shallow waters are realizing, the greatest ray cycle length is about several km. Thus, the touching bottom ray has about ten reflections on the surface for ranges about tens of km. Since the correlation interval of scattered field is decreasing as $\sqrt{N}$, where N is number of reflections, then the time correlation interval of a sound field multi-time scattered from the free sea surface is usually much smaller than one second.

Evidently, the time correlation interval of sound field fluctuations due to the scattering from volume random hydrodynamic inhomogeneities in sea environments is determined by the time correlation interval of these inhomogeneities. In the open ocean, these ones have a large spectrum of correlation intervals: from several minutes up to ten or more hours. It's known nevertheless that the long period inhomogeneities are the most powerful and the fast inhomogeneities are weak and faintly influencing sound fields. That's why common time correlation intervals of phase parameters of sound fields in the ocean (ray arrival time and angle) are about tens of minutes or more for the range tens of km and more.

Such are characteristic time intervals of sound speed variability due to fluctuations in sea environments. On the other hand, the common duration of probing signals is about several seconds or tens of seconds and it is equal to the time interval of the primary processing. The total processing time with account of the trajectory filtering is about several minutes or maybe tens of minutes. Thus, the signal processing time interval is, on one hand, much greater then the time interval of sound field variability due to the scattering from the wind perturbed surface. On the other hand it is much smaller then the time interval of the variability due to the scattering from volume inhomogeneities. During the signal processing time interval a surface scattered field changes many times and one may consider that there is a well-established statistical ensemble. So, these fluctuations may be named "fast". In the same time, the field having been scattered from volume fluctuations practically doesn't change during the signal processing period and one may consider that there is no established statistical ensemble for this time interval. So, fluctuations of this type may be named "slow".

The facts presented above regarding the ratio between characteristic time correlation intervals of sound fields in the ocean and the time intervals of signal processing procedures offer the possibility to calculate approximately the integrals (4.39).

4.2.2.1. "Fast" fluctuations

Averaging of the conditional probability densities over "fast" sound field fluctuations due to the scattering from the wind surface agitation is resumed as the necessity to average the exponent arguments over the fluctuations:

$$\overline{\Phi}_{\varepsilon}^{\mathrm{Surf}}(\mathbf{P}) = \int \Phi_{\varepsilon}(\mathbf{P}|\zeta_{\mathrm{Surf}})\Phi(\zeta_{\mathrm{Surf}})d\zeta_{\mathrm{Surf}} =$$

$$= \prod_{\omega_n>0} \frac{\exp\left\{-\frac{1}{2}\left\langle \mathbf{K}_{\mathrm{N}}^{-1}(\mathbf{P}-\mathbf{P}_{\mathrm{S}}-\varepsilon\,\mathbf{P}_{\mathrm{T}})(\mathbf{P}-\mathbf{P}_{\mathrm{S}}-\varepsilon\,\mathbf{P}_{\mathrm{T}})\right\rangle\right\}}{\sqrt{\det 2\pi\mathbf{K}_{\mathrm{N}}}}. \tag{4.41}$$

Since scalar products are averaged, ODS depends only on the two first moments of fields $\mathbf{P}_{\mathrm{S}}$ and $\mathbf{P}_{\mathrm{T}}$. The second order moment may be expressed through the product of the mean values and through the second order moment of the incoherent sound field component. Primary evaluations and experiments show that in shallow waters where the channel angle of a subsurface sound channel is about 3°-5° for wind agitation with index about 3 or 4, the scattering coefficient main lobe width is greater then the channel angle. Then the scattered field in such conditions is radiated from the surface to the bottom and it is not accumulated or conserved in the channel but is rapidly eliminated because of the bottom absorption. There is only a coherent field existing in such waveguide environments, and one may neglect the scattered one. Thus, the conditional probability density function after having been averaged over surface scattered field fluctuations obtains the form

$$\overline{\Phi}_{\mathrm{I}}^{\mathrm{Surf}}(\mathbf{P}) = \prod_{\omega_n>0} \exp\left\{-\frac{1}{2}\left\langle \mathbf{K}_{\mathrm{N}}^{-1}(\mathbf{P}-\overline{\mathbf{P}}_{\mathrm{S}}-\overline{\mathbf{P}}_{\mathrm{T}})(\mathbf{P}-\overline{\mathbf{P}}_{\mathrm{S}}-\overline{\mathbf{P}}_{\mathrm{T}})\right\rangle\right\}(\det 2\pi\mathbf{K}_{\mathrm{N}})^{-1/2}, \tag{4.42}$$

Thus, in the case of "fast" sound field fluctuations such as those due to the scattering from the waving sea surface, and when one can neglect the scattered field because it is absorbed in the bottom, ODS is of the same form that for the DSE case. The difference consists of using mean probing signal's and echo-signal's fields having been averaged on "fast" fluctuations as model fields in the processing algorithm.

4.2.2.2. "Slow" fluctuations

One must proceed by different way to average the conditional probability densities over "slow" sound field fluctuations due to the scattering from water volume inhomogeneities. The most informative in MFP algorithms are phase parameters of sound fields: arrival times and angles of ray paths on the receiving array. That's these parameters that determine the resolution of localization. Let denote $\xi_{\mathrm{S}} = \left\{t_1^{\mathrm{S}},\ldots,t_M^{\mathrm{S}},\chi_1^{\mathrm{S}},\ldots,\chi_M^{\mathrm{S}}\right\}$ the vector of phase parameters of the source field.

When there are random volume inhomogeneities the phase parameter vector ξ_S is also random. Let it is possible to recalculate the *a priori* probability density $\Phi(\mu)$ of volume inhomogeneities as the probability density $\Phi(\xi_S)$ by using some mathematical or numerical model of sound fields developed for the random sea environments. Let also $\Phi(\xi_S)$ is not depending on time because the random field $\mu(\mathbf{r},t)$ is stationary and the primary processing time is rather small in comparison with the time correlation interval of the vector ξ_S.

When considering the optimal Bayes algorithm with taking into account fluctuations of the interference structure of sound fields one needs to calculate the integral

$$\Phi_0^{\text{Wat}}(\mathbf{P}) = \int \Phi_0(\mathbf{P}|\xi_S)\Phi(\xi_S)d\xi_S \ . \tag{4.43}$$

By the above definition of "slow" fluctuations of GF, the time correlation interval of phase parameters of sound fields is much greater then the time interval T of one period of primary processing. Therefore the processing system can get a rather likelihood estimate $\hat{\xi}_S$ of the vector ξ_S during the time where the ocean waveguide should be considered as "invariable". Typical "slow" fluctuations of this type are those due to the scattering from natural internal waves in the ocean (time correlation intervals of arrival angle and time fluctuations prove to be tens of minutes or maybe hours). The possibility to get this rather likelihood estimate of ξ_S means that the distribution low $\Phi(\xi_S)$ is rather narrow. This fact allows to calculate the integral (4.43) by using the Laplace method:

$$\begin{aligned}
&\Phi_0^{\text{Wat}}(\mathbf{P}) = \int \exp\left\{\ln \Phi_0(\mathbf{P}|\xi_S)\right\}\Phi(\xi_S)d\xi_S = \\
&= \Phi_0(\mathbf{P}|\hat{\xi}_S)\Phi(\hat{\xi}_S)\int \exp\left\{-\frac{1}{2}\left\langle \partial^{\ 2}_{\xi_S} \ln \Phi_0(\mathbf{P}|\hat{\xi}_S)(\xi_S,\hat{\xi}_S),(\xi_S,\hat{\xi}_S)\right\rangle\right\}d\xi_S = \\
&= \Phi_0(\mathbf{P}|\hat{\xi}_S)\Phi(\hat{\xi}_S)\left[\det\left(-\frac{1}{2\pi}\partial^{\ 2}_{\xi_S} \ln \Phi_0(\mathbf{P}|\hat{\xi}_S)\right)\right]^{-1/2},
\end{aligned} \tag{4.44}$$

where $\hat{\xi}_S$ is the maximum likelihood estimate (MLE) of the vector ξ_S. It satisfies to equation

$$\frac{\partial \ln \Phi_0(\mathbf{P}|\xi_S)}{\partial \xi_S} = 0 , \tag{4.45}$$

with $\partial^{\ 2}_{\xi_S} \ln \Phi_0(\mathbf{P}|\hat{\xi}_S)$ the second order derivative matrix of the logarithm of the conditional probability density with respect to components of the vector ξ_S being

calculated at the MLE point. It's well known [11] that the mean value of this matrix is equal to the minus Fisher information matrix (FIM). Therefore it characterizes the precision of the estimate of the vector ξ_S. The applicability condition for the obtained equation follows from this consideration: the error of estimate of the vector ξ_S needs to be much smaller than its fluctuations due to the medium instability.

Proceed by the same way when averaging the conditional probability density of measurement when the hypothesis H_1 is true and introducing the phase parameter vector of echo-signal $\xi_T = \left\{ t_1^T, \ldots, t_N^T, \chi_1^T, \ldots, \chi_N^T \right\}$ let suppose that it is possible to recalculate the distribution low of medium volume fluctuations as the joint probability density $\Phi(\xi_S, \xi_T)$. Then the integral in (4.39) for $\varepsilon = 1$ can be calculated by the Laplace method:

$$\overline{\Phi}_1^{Wat}(\mathbf{P}) = \Phi_1(\mathbf{P}|\hat{\xi}_S, \hat{\xi}_T)\Phi(\hat{\xi}_S, \hat{\xi}_T)\left[\det\left(-\frac{1}{2\pi}\partial^2_{\xi_S\xi_T} \ln \Phi(\mathbf{P}|\hat{\xi}_S, \hat{\xi}_T)\right)\right]^{-1/2}, \quad (4.46)$$

where $\hat{\xi}_S, \hat{\xi}_T$ are simultaneous estimates of the vectors ξ_S and ξ_T satisfying equations

$$\frac{\partial \ln \Phi_1(\mathbf{P}|\xi_S, \xi_T)}{\partial(\xi_S, \xi_T)} = 0, \quad (4.47)$$

The log-ratio of densities (44) and (45) is the Bayessian optimal decision statistics (ODS).

$$L_{Wat}(\mathbf{P}) = \ln\left\{\frac{\Phi_1(\mathbf{P}|\hat{\xi}_S, \hat{\xi}_T)}{\Phi_0(\mathbf{P}|\hat{\xi}_S)}\frac{\Phi(\hat{\xi}_S, \hat{\xi}_T)}{\Phi(\hat{\xi}_S)}\sqrt{\frac{\det \partial^2_{\xi_s} \ln \Phi_0(\mathbf{P}|\hat{\xi}_S)}{\det \partial^2_{\xi_s\xi_T} \ln \Phi_1(\mathbf{P}|\hat{\xi}_S, \hat{\xi}_T)}}\right\}. \quad (4.48)$$

In the case where the object is far from the vertical plane containing acoustical ray paths, those of the source field and those of the echo-signal are independent. In this case the joint probability density is factored: $\Phi(\xi_S, \xi_T) = \Phi(\xi_S)\Phi(\xi_T)$, so that the ODS (4.48) is simplified

$$\begin{aligned} L_{Wat}(\mathbf{P}) &= \frac{1}{2}\sum_{\omega_n>0}\left\langle \mathbf{K}_N^{-1}\left(\mathbf{P} - \mathbf{P}_S(\hat{\xi}_S)\right)\left(\mathbf{P} - \mathbf{P}_S(\hat{\xi}_S)\right)\right\rangle - \\ &- \frac{1}{2}\sum_{\omega_n>0}\left\langle \mathbf{K}_N^{-1}\left(\mathbf{P} - \mathbf{P}_S(\hat{\xi}_S) - \mathbf{P}_T(\hat{\xi}_T)\right)\left(\mathbf{P} - \mathbf{P}_S(\hat{\xi}_S) - \mathbf{P}_T(\hat{\xi}_T)\right)\right\rangle + \\ &+ \ln\Phi(\hat{\xi}_T) - \sum_{\omega_n>0}\ln\det\left(-\partial^2_{\xi_S\xi_T}\ln\Phi_1(\mathbf{P}|\hat{\xi}_S, \hat{\xi}_T)\right). \end{aligned} \quad (4.49)$$

The equation (4.48) has been obtained under supposition that not only the measurement error of parameters ξ_S is much smaller then their fluctuations due to those of the medium, but also the measurement error of parameters ξ_T satisfies to this limitation. Nevertheless, while the echo-signal energy is usually much smaller then the energy of the source field, the latest condition may not be satisfied in some cases, for example for estimating of ray arrival angles in the vertical plane if the receiving array has no sufficient vertical length. In this case, the use of the Laplace method gives no the MLE of the vector ξ_T but its estimate of maximum of *a posteriori* probability. By taking into account that fluctuations of phase parameters are usually gaussian, the expression for the probability density $\overline{\Phi}_1^{\text{Wat}}(\mathbf{P})$ having been averaged over medium volume fluctuations should be the following

$$\overline{\Phi}_1^{\text{Wat}}(\mathbf{P}) = \frac{\Phi_1(\mathbf{P}|\hat{\xi}_S,\tilde{\xi}_T)\Phi(\hat{\xi}_S,\tilde{\xi}_T)}{\sqrt{\det\left(\mathbf{E}-\partial^2_{\xi_S\xi_T}\ln\Phi_1(\mathbf{P}|\hat{\xi}_S,\tilde{\xi}_T)\Xi_T\right)}}\sqrt{\det(2\pi\Xi_T)}, \tag{4.50}$$

where Ξ_T is the covariance matrix of ξ_T, and $\tilde{\xi}_T$ is its estimate of maximum of *a posteriori* probability that satisfies to equation

$$\frac{\partial \ln\Phi_1(\mathbf{P}|\hat{\xi}_S,\tilde{\xi}_T)}{\partial\xi_T} - \Xi_T^{-1}(\tilde{\xi}_T-\bar{\xi}_T) = 0\,, \tag{4.51}$$

with $\bar{\xi}_T$ the mean value of ξ_T. Under this approximation, the ODS is

$$\mathrm{L}_{\text{Wat}}(\mathbf{P}) = \ln\left\{\frac{\Phi_1(\mathbf{P}|\hat{\xi}_S,\tilde{\xi}_T)}{\Phi_0(\mathbf{P}|\hat{\xi}_S)}\frac{\Phi(\hat{\xi}_S,\tilde{\xi}_T)}{\Phi(\hat{\xi}_S)}\sqrt{\frac{\det\left(-\partial^2_{\xi_s}\ln\Phi_0(\mathbf{P}|\hat{\xi}_S)\right)\det 2\pi\Xi_T}{\det\left(\mathbf{E}-\partial^2_{\xi_S\xi_T}\ln\Phi_1(\mathbf{P}|\hat{\xi}_S,\tilde{\xi}_T)\right)}}\right\}. \tag{4.52}$$

Usually the signal-to-noise ratio (SNR) is high so that one may replace the second order derivative matrices $\partial^2_{\xi_s}\ln\Phi_0$ and $\partial^2_{\xi_S\xi_T}\ln\Phi_1$ by their mean values that are equal to minus Fisher information matrices (FIM) for estimates of corresponding parameters:

$$\overline{\partial^2_{\xi_s}\ln\Phi_0(\mathbf{P}|\tilde{\xi}_S)} = -\mathbf{I}(\xi_S)\,,\quad \overline{\partial^2_{\xi_S\xi_T}\ln\Phi_1(\mathbf{P}|\tilde{\xi}_S,\tilde{\xi}_T)} = -\mathbf{I}(\xi_S,\xi_T)\,. \tag{4.53}$$

These MFP algorithms for the SSE model having been designed on the base of the Bayes approach are less precise than the algorithms for the DSE model, but they are more robust regarding possible mismatching of the model and a real ocean medium. In this case the precision is "exchanged" against the robustness and, if fluctuations of

waveguide parameters are rather small, a little loss of precision allows us to design a robust algorithm. Nevertheless if the *a priori* uncertainty of ocean waveguide parameters is considerable, then, using the above approach a robust but very lowly precise algorithm or an uncertain algorithm giving in some situations a good precision of object localization will be designed.

4.2.2.3. Quality estimating for SSE-matched algorithms

Under usual situations when solving the UOS problem, the echo-signal energy on receiving array is much smaller than the source field's or noise's energy. To solve the detection and localization problem in this case one may use the so-called local-optimal algorithm. It consists of building an estimate of the echo-signal field amplitude, and this estimate is used as the optimal decision statistics (ODS). In this case the signal-to-noise ratio (SNR) is defined as

$$\rho = \frac{\left(\mathrm{M}\left[\mathrm{L}_{\mathrm{Wat}} \middle| H_1\right] - \mathrm{M}\left[\mathrm{L}_{\mathrm{Wat}} \middle| H_0\right]\right)^2}{\mathrm{D}\left[\mathrm{L}_{\mathrm{Wat}} \middle| H_0\right]}, \tag{4.54}$$

proves to be equal to the Fisher information (FI) for the echo-signal amplitude estimate. When introducing the notation ε for the echo-signal amplitude so that $\varepsilon^{-1}\mathbf{P}_{\mathrm{T}} = O(\mathbf{P}_{\mathrm{S}})$, the Fisher information matrix (FIM) has the following structure

$$\mathbf{I} = \begin{bmatrix} I_{\varepsilon\varepsilon} & \mathbf{I}_{\varepsilon\xi_{\mathrm{S}}} & \mathbf{I}_{\varepsilon\xi_{\mathrm{T}}} \\ \mathbf{I}_{\xi_{\mathrm{S}}\varepsilon} & \mathbf{I}_{\xi_{\mathrm{S}}\xi_{\mathrm{S}}} & \mathbf{I}_{\xi_{\mathrm{S}}\xi_{\mathrm{T}}} \\ \mathbf{I}_{\xi_{\mathrm{T}}\varepsilon} & \mathbf{I}_{\xi_{\mathrm{T}}\xi_{\mathrm{S}}} & \mathbf{I}_{\xi_{\mathrm{T}}\xi_{\mathrm{T}}} \end{bmatrix}, \tag{4.55}$$

where

$M_{\varepsilon\varepsilon}$ is the Fisher information (FI) for echo-signal amplitude estimate,
$\mathbf{I}_{\xi_{\mathrm{S}}\xi_{\mathrm{S}}}$ is FIM for estimates of source field parameters,
$\mathbf{I}_{\xi_{\mathrm{T}}\xi_{\mathrm{T}}}$ is the FIM for estimates of echo-signal parameters,

$\mathbf{I}_{\varepsilon\xi_{\mathrm{S}}}, \mathbf{I}_{\varepsilon\xi_{\mathrm{T}}}, \mathbf{I}_{\xi_{\mathrm{S}}\xi_{\mathrm{T}}}$ are mutual FI for estimates of source and echo-signal fields' parameters.

The SNR is given by the following expression

$$\rho = I_{\varepsilon\varepsilon} - \mathbf{I}_{\varepsilon\xi_{\mathrm{S}}}\mathbf{D}_{\xi_{\mathrm{S}}\xi_{\mathrm{S}}}\mathbf{I}_{\xi_{\mathrm{S}}\varepsilon} - 2\mathbf{I}_{\varepsilon\xi_{\mathrm{S}}}\mathbf{D}_{\xi_{\mathrm{S}}\xi_{\mathrm{T}}}\mathbf{I}_{\xi_{\mathrm{T}}\varepsilon} - \mathbf{I}_{\varepsilon\xi_{\mathrm{T}}}\mathbf{D}_{\xi_{\mathrm{T}}\xi_{\mathrm{T}}}\mathbf{I}_{\xi_{\mathrm{T}}\varepsilon}, \tag{4.56}$$

where $\mathbf{D}_{\xi_{\mathrm{S}}\xi_{\mathrm{S}}}, \mathbf{D}_{\xi_{\mathrm{S}}\xi_{\mathrm{T}}}, \mathbf{D}_{\xi_{\mathrm{T}}\xi_{\mathrm{T}}}$ are covariance matrices of estimates of parameters of

source and echo-signal fields. They are corresponding blocks of the matrix that is the inverse of the FIM (4.55):

$$\mathbf{D} = \mathbf{I}^{-1} = \begin{bmatrix} D_{\varepsilon\varepsilon} & \mathbf{D}_{\varepsilon\xi_S} & \mathbf{D}_{\varepsilon\xi_T} \\ \mathbf{D}_{\xi_S\varepsilon} & \mathbf{D}_{\xi_S\xi_S} & \mathbf{D}_{\xi_S\xi_T} \\ \mathbf{D}_{\xi_T\varepsilon} & \mathbf{D}_{\xi_T\xi_S} & \mathbf{D}_{\xi_T\xi_T} \end{bmatrix}. \tag{4.55'}$$

Precision of estimating of object's coordinates are given by their FIM. So far the information about object's coordinates that is given by the phase parameters of the echo-signal field is much greater than the information given by amplitude parameters, then the FIM for object coordinate estimates may be expressed through the FIM of echo-signal field phase parameter estimates and the covariance matrix of fluctuations of these parameters due to volume fluctuations into the sound propagation medium is:

$$\mathbf{I}_{\mathbf{r}_T\mathbf{r}_T} = \left\langle \left(\mathbf{D}_{\xi_T\xi_T} + \Xi_T\right)^{-1} \frac{\partial \xi_T}{\partial \mathbf{r}_T}, \frac{\partial \xi_T}{\partial \mathbf{r}_T} \right\rangle, \tag{4.57}$$

where $\frac{\partial \xi_T}{\partial \mathbf{r}_T}$ is the partial derivative of the echo-signal field phase parameters with respect to object coordinates.

The precision of estimating of source field parameters is rather high because of high SNR of probing signals and while the time variability interval of the medium is also rather big. If one neglect the impact of errors of estimating the source field parameters then the covariance matrix of echo-signal parameter estimates may be expressed as following

$$\mathbf{D}_{\xi_T\xi_T} = \mathbf{I}^{-1}_{\xi_T\xi_T} + \frac{\mathbf{I}^{-1}_{\xi_T\xi_T}\mathbf{I}_{\xi_T\varepsilon}\mathbf{I}_{\varepsilon\xi_T}\mathbf{I}^{-1}_{\xi_T\xi_T}}{I_{\varepsilon\varepsilon} - \mathbf{I}^{-1}_{\xi_T\xi_T}\mathbf{I}_{\xi_T\varepsilon}\mathbf{I}_{\varepsilon\xi_T}}. \tag{4.58}$$

When taking into account errors of source field parameter estimates, this matrix is obtained as the corresponding block of the inverse-to-FIM (4.55) matrix.

In the determinist medium case, the FIM of object coordinate estimates is

$$\mathbf{I}_{\mathbf{r}_T\mathbf{r}_T} = \left\langle \mathbf{D}_{\xi_T\xi_T}^{-1} \frac{\partial \xi_T}{\partial \mathbf{r}_T}, \frac{\partial \xi_T}{\partial \mathbf{r}_T} \right\rangle, \tag{4.59}$$

and it is different from the FIM (4.57) by absence of the Ξ_T matrix. The presence of the matrix Ξ_T makes worse the precision characteristics of the object localization solution in the SSE case when comparing with the DSE case but it makes the coordi-

nate estimating more stable to mismatches of real propagation conditions to those of the model being used by the MFP algorithm.

As to probability densities Φ_0 and Φ_1 given by the equations (4.9), the expressions for SNR ρ, ambiguity function $N(\mathbf{r}_1,\mathbf{r}_0)$ and FIM of object coordinate estimates are

$$\rho(\mathbf{r}_0) = \sum_{\omega_n>0} \left| \left\langle \mathbf{K}_N^{-1}\mathbf{P}_T(\mathbf{r}_0), \mathbf{n}_T(\mathbf{r}_0) \right\rangle \right|^2 , \tag{4.60}$$

$$N(\mathbf{r},\mathbf{r}_0) = \frac{\sum_{\omega_n>0} \left| \left\langle \mathbf{K}_N^{-1}\mathbf{P}_T(\mathbf{r}_0), \mathbf{n}_T(\mathbf{r}) \right\rangle \right|^2}{\sum_{\omega_n>0} \left\langle \mathbf{K}_N^{-1}\mathbf{P}_T(\mathbf{r}_0), \mathbf{P}_T(\mathbf{r}_0) \right\rangle} , \tag{4.61}$$

$$\mathbf{I}_{\mathbf{r}_T\mathbf{r}_T} = \left\langle \left(\mathbf{E} + \mathbf{J}_{\xi_T\xi_T}\Xi_T \right)^{-1} \mathbf{J}_{\xi_T\xi_T} \frac{\partial \xi_T}{\partial \mathbf{r}_T}, \frac{\partial \xi_T}{\partial \mathbf{r}_T} \right\rangle , \quad \mathbf{J}_{\xi_T\xi_T} = \left(\mathbf{D}_{\xi_T\xi_T} \right)^{-1} , \tag{4.62}$$

$$\text{where } \mathbf{n}_T(\mathbf{r}) = \frac{\sum_{\omega_n>0} \mathbf{Q}_S\mathbf{P}_T(\mathbf{r})}{\sqrt{\sum_{\omega_n>0} \left\langle \mathbf{K}_N^{-1}\mathbf{Q}_S\mathbf{P}_T(\mathbf{r}), \mathbf{Q}_S\mathbf{P}_T(\mathbf{r}) \right\rangle}} , \tag{4.63}$$

the operator $\mathbf{Q}_S$ is the projector onto the hyper space determined by the source field and its parameters' estimates:

$$\mathbf{Q}_S = \mathbf{E} - \boldsymbol{P}_S , \quad \boldsymbol{P}_S = \frac{\partial \mathbf{P}_S}{\partial \xi_S} \left[\left\langle \mathbf{K}_N^{-1} \frac{\partial \mathbf{P}_S}{\partial \xi_S}, \frac{\partial \mathbf{P}_S}{\partial \xi_S} \right\rangle \right]^{-1} \frac{\partial \mathbf{P}_S}{\partial \xi_S} \mathbf{K}_N^{-1} , \tag{4.64}$$

and the matrix $\mathbf{J}_{\xi_T\xi_T}$ is

$$\mathbf{J}_{\xi_T\xi_T} = \sum_{\omega_n>0} \left\langle \mathbf{K}_N^{-1}\mathbf{Q}_S \frac{\partial \mathbf{P}_T}{\partial \xi_T}, \frac{\partial \mathbf{P}_T}{\partial \xi_T} \right\rangle . \tag{4.65}$$

The Bayes approach being described above allows to design MFP less precise then that for the DSE model but much more stable regarding possible mismatches between the real OWG and its model used in the processing. When using this approach one exchanges, in fact, the precision *vis-à-vis* the stability. If the waveguide fluctuations are rather small, one will have a stable algorithm with lose of some small precision of localization. Nevertheless if the *a priori* uncertainty of the waveguide is considerable then by using the above described approach one will design a stable but very rough algorithm or maybe an unstable algorithm giving sometimes in some particular situations a very high precision of object localization.

4.3. Union of the underwater object survey and of the acoustic tomography of the ocean

The way to solve the above presented dilemma is to join the UOS problem and the acoustic tomography of the ocean (ATO) to solve them together by applying the MFP approach.

The FS-ABS observation mode seems to be the most perspective for such a "great" union. In this mode one has a continuously radiating source of probing signals, then the source field energy at reception may considerably exceed noise fields; it allows us to estimate very well ocean waveguide parameters. Wile the source radiates continuously one can also continuously solve the ATO problem and to survey the evolution of waveguide parameters. On this way it is possible to know them at any time with rather smaller variations then when using some *a priori* SSE model. Another advantage of FS-ABS systems is following. While having one emitter and one receiver array it's possible to reconstruct the sound velocity field in some vicinity of the vertical plane containing the emitter and the receiver. The width of this volume is determined by the space correlation interval of inhomogeneities that is about several km for the case of free internal waves. Therefore if a object is out of this volume, the joint solving of UOS problem by using the classic ABS schema and of ATO problem by using the source field doesn't permit us to improve the localization procedure. Otherwise, when using the FS-ABS schema, the volume where the object is detected and localized by the system is just the vicinity of the source-receiver vertical plane (while that's where the object strength grows sharply), where the solving of the ATO problem is possible by using the source field. Thus, the FS-ABS mode is that where one can effectively join the UOS and ATO solutions. Let us note that it's always possible (in principle) to solve the tomography problem when using the classic mono- or bistatic active sonar or a passive sonar by using the echo-signal field or the object noise field. Nevertheless the SNR on reception is rather little in these cases and it may well not be possible to obtain a good solution of the ATO problem. The presence of the strong source field when using the FS-ABS schema is a good factor allowing to solve well the ATO problem and then to use the solution to improve characteristics of the UOS solution and get it practically the same as in the determinist waveguide case. Notice that when solving the ATO problem the best reconstruction is done for the large-scale ocean variability. That's just this type of fluctuations that is the most powerful in the ocean and has the most of impact onto sound fields. The small-scale variability will be reconstructed with less of precision but their intensity in the ocean is rather little and, therefore, its impact on sound fields is less important.

4.3.1. FS-MFP algorithms adaptive to stochastic sea environments

Let us present the formalism of the procedure of joint solving of UOS and ATO problems. One shell name corresponding algorithms "Adaptive MFP" (AMFP) for FS-ABS systems.

While the hypothesis H_ε is true, the probability density of measurement is (4.9), where $\mathbf{P}_S = \mathbf{P}_S(\mu)$ is the source field that depends on fluctuations $\mu = \mu(\mathbf{r},t)$ of sound velocity, and $\mathbf{P}_T = \mathbf{P}_T(\mathbf{r}_T,\mu)$ that means that the echo-signal field depends on object coordinates $\mathbf{r}_T$ and also on sound velocity fluctuation. Let the *a priori* distribution of $\mu(\mathbf{r},t)$ is normal zero-mean with some given time-space correlation function $K_\mu(\mathbf{r},\mathbf{r}',t,t')$ and with the *a priori* given probability distribution

$$\Phi(\mu) = \frac{\exp\left\{-\frac{1}{2}\left\langle \mathbf{K}_\mu \mu,\mu\right\rangle\right\}}{\sqrt{\det 2\pi\mathbf{K}_\mu}}. \tag{4.66}$$

Joint probability densities of the measurement $\mathbf{P}$ and fluctuations μ for hypothesis H_0 and H_1 are

$$\Phi_0(\mathbf{P},\mu) = \Phi_0(\mathbf{P}|\mu)\Phi(\mu) \tag{4.67}$$

$$\Phi_1(\mathbf{P},\mu|\mathbf{r}_T) = \Phi_1(\mathbf{P}|\mathbf{r}_T,\mu)\Phi(\mu) \tag{4.68}$$

Let us calculate the estimate of maximum of *a posteriori* probability of μ and $\mathbf{r}_T$. To do it one needs to resolve a system of equations with partial and functional derivatives:

$$\begin{cases} \dfrac{\delta}{\delta\mu(\mathbf{r})}\left\{\ln\Phi_0(\mathbf{P}|\mu)+\ln\Phi(\mu)\right\}=0 \quad (eq.\,1) \\ \dfrac{\delta}{\delta\mu(\mathbf{r})}\left\{\ln\Phi_1(\mathbf{P}|\mathbf{r}_T,\mu)+\ln\Phi(\mu)\right\}=0 \quad (eq.\,2) \\ \dfrac{\partial}{\partial\,\mathbf{r}_T}\ln\Phi_1(\mathbf{P}|\mathbf{r}_T,\mu)=0 \qquad\qquad (eq.\,3) \end{cases} \tag{4.69}$$

Let us note $\mu_0(\mathbf{P})$ the solution of equation (4.69-1), $\mu_1(\mathbf{P})$ and $\mathbf{r}_T(\mathbf{P})$. solutions of equations (4.69-2,3) which are related since the corresponding equations need to be solved simultaneously. After substitution of these solutions into (4.67)-(4.68) one obtains the optimal decision statistics (ODS) under the form

$$L = \ln\left\{\Phi_1(\mathbf{P}|\mathbf{r}_T(\mathbf{P}),\mu_1(\mathbf{P}))\Phi(\mu_1(\mathbf{P}))\right\} - \ln\left\{\Phi_0(\mathbf{P}|\mu_0(\mathbf{P}))\Phi(\mu_0(\mathbf{P}))\right\}. \quad (4.70)$$

The detection problem is solved by comparing the main lobe level of this statistics with a threshold. If there is a detection fact then $\mu_1(\mathbf{P})$ is the sound velocity field estimate and the corresponding $\mathbf{r}_T(\mathbf{P})$ is the object coordinate estimate. If there is no detection then $\mu_0(\mathbf{P})$ is adopted as sound velocity field estimate but one doesn't build a object coordinate estimate.

Let us consider more in detail the equations (4.69). The equation (4.69-1) when the probability density $\Phi_0(\mathbf{P}|\mu)$ is given by (4.9) with $\varepsilon = 0$ is

$$\sum_{\omega_n>0}\left\langle \mathbf{K}_N^{-1}(\mathbf{P}-\mathbf{P}_S), \frac{\delta \mathbf{P}_S}{\delta\mu(\mathbf{r})}\right\rangle + \mathbf{K}_\mu^{-1}[\mu] = 0. \quad (4.71)$$

If may be rewritten under the form convenient for solving by an iteration process

$$\mu(\mathbf{r}) = \int K_\mu(\mathbf{r},\mathbf{r}')\sum_{\omega_n>0}\left\langle \mathbf{K}_N^{-1}\frac{\delta \mathbf{P}_S}{\delta\mu(\mathbf{r}')}, \mathbf{P}_S(\mu) - \mathbf{P}\right\rangle d\mathbf{r}'. \quad (4.72)$$

The functional derivative of the source field with respect to $\mu(\mathbf{r})$ presents in this equation. The source field $\mathbf{P}_S$ is expressed through the ocean waveguide's GF $\mathbf{G}(\mathbf{r}_S;\omega) = |G(\mathbf{r}_m,\mathbf{r}_S;\omega)>$ and through the spectrum of the probing signal $S(\omega)$: $\mathbf{P}_S = S(\omega)\mathbf{G}`(\mathbf{r}_S;\omega)$. That's why the calculation of the functional derivative of the source field reduces to calculation of the functional derivative of GF. It's made by the following way:

$$\frac{\delta G(\mathbf{r}_m,\mathbf{r}_S;\omega)}{\delta\mu(\mathbf{r})} = G(\mathbf{r}_m,\mathbf{r};\omega)\frac{2\omega^2}{c^2(\mathbf{r})}G(\mathbf{r},\mathbf{r}_S;\omega). \quad (4.73)$$

After using (4.73), the equation (4.72) obtains the form

$$\mu(\mathbf{r}) = \int K_\mu(\mathbf{r},\mathbf{r}')\sum_{\omega_n>0}\left(\mathbf{K}_N^{-1}(\omega_n)\mathbf{G}(\mathbf{r}';\omega_n), \mathbf{P}_S(\mu;\omega_n) - \mathbf{P}(\omega_n)\right)\times \times \frac{2\omega_n^2}{c^2(\mathbf{r}')}G^*(\mathbf{r}',\mathbf{r}_S;\omega_n)S^*(\omega_n)d\mathbf{r}'. \quad (4.74)$$

One can solve the equation (4.74) by an iteration process. For example, the field $\mu^{(0)}(\mathbf{r}) = 0$ may be used as initial approximation. After that GF for the *a priori* mean sound velocity field is calculated and substituted into the right part of the equation (4.74). By having done the integration the first order approximation $\mu^{(1)}(\mathbf{r})$ is ob-

tained. Furthermore GF is computed for $\mu(\mathbf{r}) = \mu^{(1)}(\mathbf{r})$, substituted it into the right part of (4.74) and the second order approximation $\mu^{(2)}(\mathbf{r})$ is calculated, and so on until the iteration process converge to the solution $\mu_0(\mathbf{P})$. At very low frequency range where one should use some grid finite differences' method to model GF of 3D waveguides it is necessary to calculate the integral (4.74) by some numerical method. At sufficiently high frequency range where one may use the ray or adiabatic normal mode approximations of GF its interference structure will be very important for the integrating. In this case one may calculate the 3D integrals by using methods of integrating of strongly oscillating functions. In this case the main contribution in the integral will be done by the vicinity of the vertical plane containing the source and the receiver since the points of constant phase of the integrand are lied in this plane. By the same reason, $\mu_0(\mathbf{P})$ is zero outside this vicinity that has the width equal to the horizontal space correlation interval of the field $\mu(\mathbf{r})$ being equal to the dimension of the support of the correlation function $K_\mu(\mathbf{r},\mathbf{r}')$.

One builds by exactly the same way the solution of the equation (4.69-2) with functional derivatives. It just needs to be taken into account that not only the source field is depending on the field μ_1 to be found, but also the echo-signal field. Since the echo-signal energy is always small regarding the source field energy one may use the field $\mu_0(\mathbf{P})$ as initial approximation to the solution. In some cases one may do only one iteration or do no iterations at all and use the initial approximation as the solution. The estimate of the field $\mu_1(\mathbf{P})$ depends on possible object coordinates $\mathbf{r}_T$. Thus, by varying possible object coordinates on some grid one will obtain each time a new estimate $\mu_1(\mathbf{P})$, then will calculate the decision statistics (4.70), will compare it to values having been obtained for other possible object locations and finally to search for its maximum on possible object coordinate space. This procedure may be simpler but we don't want to consider it in all details in this paper and only the general view on it is presented here.

4.3.2. Quality estimation of adaptive MFP algorithms

Let study the quality of the UOS+ATO solution. It will be done under the approximation of "weak" signal ($\varepsilon << 1$, where ε is the introduced above parameter characterizing the echo signal's level). Let denote hereafter the true sound velocity field (SVF) on the time interval of the measurement as $\mu^{(0)}$, the true object coordinates as $\mathbf{r}_T^{(0)}$, and the maximum *a posteriori* probability (MAP) estimates as $\mu_0(\mathbf{P})$, $\mu_1(\mathbf{P})$, $\mathbf{r}_T(\mathbf{P})$ (as above). *A priori* probability density function (PDF) depends also on the parameter ε: $\Phi_1 = (\mathbf{P}|\mathbf{r}_T,\varepsilon,\mu)$. As the true value of this parameter isn't known, the maximum likelihood estimate (MLE) is used, which satisfies the equation

$$\frac{\partial}{\partial \varepsilon} \ln \Phi_1(\mathbf{P}|\mathbf{r}_T, \varepsilon, \mu) = 0\,, \tag{4.75}$$

One must solve this equation together with the equations (4.69-2) and (4.69-3). The MLE $\varepsilon_1(\mathbf{P})$ being obtaining by this way is then substituted into the equation (4.39) for the decision statistic. Thus, the functional derives

$$\begin{aligned} &L(\mathbf{P}) = L_1(\mathbf{P}\,|\,\varepsilon_1, \mu_1) - L_0(\mathbf{P}\,|\,\mu_0)\,, \\ &L_1 = \ln\left\{\Phi_1(\mathbf{P}|\mathbf{r}_T(\mathbf{P}), \varepsilon_1(\mathbf{P}), \mu_1(\mathbf{P}))\Phi(\mu_1(\mathbf{P}))\right\}, \\ &L_0 = \ln\left\{\Phi_0(\mathbf{P}|\mu_0(\mathbf{P}))\Phi(\mu_0(\mathbf{P}))\right\}. \end{aligned} \tag{4.76}$$

Let's expand the functions L_1 and L_0 as Taylor series in ε and μ_1, μ_0 in the vicinity of the point $\varepsilon = 0$, $\mu = \mu^{(0)}$. Taking into account that these functions have a maximum in the points $\varepsilon_1(\mathbf{P})$, $\mu_0(\mathbf{P})$ and $\mu_1(\mathbf{P})$, the expansion is restricted by conserving only the zero-order and second-order terms:

$$\begin{aligned} &L_1(\mathbf{P}\,|\,\varepsilon_1(\mathbf{P}), \mu_1(\mathbf{P})) = L_1(\mathbf{P}\,|\,0, \mu^{(0)}) - \\ &-\frac{1}{2}\begin{bmatrix} \partial_\varepsilon L_1(\mathbf{P}\,|\,0,\mu^{(0)}) \\ \delta_\mu L_1(\mathbf{P}\,|\,0,\mu^{(0)}) \end{bmatrix}^T \begin{bmatrix} \partial^2_{\varepsilon\varepsilon} L_1(\mathbf{P}\,|\,0,\mu^{(0)}) & \partial_\varepsilon \delta_\mu L_1(\mathbf{P}\,|\,0,\mu^{(0)}) \\ \delta_\mu \partial_\varepsilon L_1(\mathbf{P}\,|\,0,\mu^{(0)}) & \delta^2_{\mu\mu} L_1(\mathbf{P}\,|\,0,\mu^{(0)}) \end{bmatrix}^{-1} \begin{bmatrix} \partial_\varepsilon L_1(\mathbf{P}\,|\,0,\mu^{(0)}) \\ \delta_\mu L_1(\mathbf{P}\,|\,0,\mu^{(0)}) \end{bmatrix}, \\ &L_0(\mathbf{P}\,|\,\mu_0(\mathbf{P})) = L_0(\mathbf{P}\,|\,\mu^{(0)}) - \frac{1}{2}\delta_\mu L_0(\mathbf{P}\,|\,\mu^{(0)})\left[\delta^2_{\mu\mu} L_0(\mathbf{P}\,|\,\mu^{(0)})\right]^{-1}\delta_\mu L_0(\mathbf{P}\,|\,\mu^{(0)})\,. \end{aligned}$$

Having made subtraction of the second equation from the first one with regard to $L_1(\mathbf{P}|0,\mu^{(0)}) = L_0(\mathbf{P}|\mu^{(0)})$, one obtain the following expression for the decision statistic

$$L(\mathbf{P}) = -\frac{1}{2}\frac{\left[\partial_\varepsilon L_0 - \delta_\mu \partial_\varepsilon L_0 \left(\delta^2_{\mu\mu} L_0\right)^{-1} \delta_\mu L_0\right]^2}{\partial^2_{\varepsilon\varepsilon} L_0 - \delta_\mu \partial_\varepsilon L_0 \left(\delta^2_{\mu\mu} L_0\right)^{-1} \partial_\varepsilon \delta_\mu L_0}, \quad L_0 = L_0(\mathbf{P}|\mu^{(0)})\,. \tag{4.77}$$

Furthermore, the second-order derivatives in (4.77) can be replaced by theirs mean values. These ones are the same (with the accuracy ε) for hypotheses H_0 and H_1 and equal to

$$\partial^2_{\varepsilon\varepsilon} L_0 = -I_{\varepsilon\varepsilon}\,, \quad \delta_\mu \partial_\varepsilon L_0 = -\mathbf{I}_{\varepsilon\mu}\,, \quad \delta^2_{\mu\mu} L_0 = -\mathbf{I}_{\mu\mu} - \mathbf{K}^{-1}_{\mu}\,, \tag{4.78}$$

where $I_{\varepsilon\varepsilon}$ is the Fisher information quantity (FIQ) for the estimate of ε, $\mathbf{I}_{\varepsilon\mu}$ is the mutual Fisher information for the estimates of ε and μ and $\mathbf{I}_{\mu\mu}$ is the Fisher information operator for the estimates of the field μ. Dropping the denominator and power

two in (4.77) that don't affect the efficiency of this decision statistic, one derives for it a final expression

$$\mathbf{L}(\mathbf{P}) = \partial_{\varepsilon}\, \mathbf{L}_0(\mathbf{P}|\mu^{(0)}) - \mathbf{I}_{\varepsilon\mu}(\mu^{(0)})\left(\mathbf{I}_{\mu\mu}(\mu^{(0)}) + \mathbf{K}_{\mu}^{-1}\right)^{-1}\delta_{\mu}\, \mathbf{L}_0(\mathbf{P}|\mu^{(0)}) \,. \quad (4.79)$$

Under the weak signal approximation, the signal-to-noise ratio (SNR) is defined as the ratio of the squared difference of mean values of the decision statistic under hypotheses H_0 and H_1 to the variance of the decision statistic under the hypothesis H_0:

$$\rho = \frac{\left(\mathrm{M}[L|H_1] - \mathrm{M}[L|H_0]\right)^2}{\mathrm{D}[L|H_0]} \,. \quad (4.80)$$

Using this equation one derives the SNR of the decision statistic (4.79) as follows

$$\rho = \frac{\varepsilon^2 J_{\varepsilon\varepsilon}^2}{J_{\varepsilon\varepsilon} - \mathbf{J}_{\varepsilon\mu}\mathbf{K}_{\mu}^{-1}\mathbf{J}_{\mu\varepsilon}}, \quad (4.81)$$

$$J_{\varepsilon\varepsilon} = I_{\varepsilon\varepsilon} - \mathbf{I}_{\varepsilon\mu}\left(\mathbf{I}_{\mu\mu} + \mathbf{K}_{\mu}^{-1}\right)^{-1}\mathbf{I}_{\mu\varepsilon}, \mathbf{J}_{\varepsilon\mu} = \mathbf{I}_{\varepsilon\mu}\left(\mathbf{I}_{\mu\mu} + \mathbf{K}_{\mu}^{-1}\right)^{-1}.$$

The quantities $J_{\varepsilon\varepsilon}$ have the meaning of the Fisher information quantity (FIQ) for the estimate of ε under the condition that the field μ is also estimated. The quantities $J_{\varepsilon\mu}$ have the meaning of the mutual information of the estimate of ε and of the field μ under the same condition, and ε is the true echo signal level. The expression (4.81) is the SNR provided that the coordinates of the grid node $\mathbf{r}_T$ where the decision statistic is computed: $\rho = \rho(\mathbf{r}_T)$, coincide with the true object's coordinates $\mathbf{r}_T^{(0)}$. If this is not the case, the SNR can be calculated as follows

$$\rho(\mathbf{r}_T, \mathbf{r}_T^{(0)}) = \frac{\varepsilon^2 J_{\varepsilon\varepsilon}^2(\mathbf{r}_T, \mathbf{r}_T^{(0)})}{J_{\varepsilon\varepsilon}(\mathbf{r}_T, \mathbf{r}_T) - \mathbf{J}_{\varepsilon\mu}(\mathbf{r}_T, \mathbf{r}_T)\mathbf{K}_{\mu}^{-1}\mathbf{J}_{\mu\varepsilon}(\mathbf{r}_T, \mathbf{r}_T)}, \quad (4.82)$$

where the mutual information $J_{\varepsilon\varepsilon}(\mathbf{r}_T, \mathbf{r}_T^{(0)})$ is

$$\begin{aligned} J_{\varepsilon\varepsilon}(\mathbf{r}_T, \mathbf{r}_T^{(0)}) &= I_{\varepsilon\varepsilon}(\mathbf{r}_T, \mathbf{r}_T^{(0)}) - \mathbf{I}_{\varepsilon\mu}(\mathbf{r}_T, \mathbf{r}_T)\left(\mathbf{I}_{\mu\mu} + \mathbf{K}_{\mu}^{-1}\right)^{-1}\mathbf{I}_{\mu\varepsilon}(\mathbf{r}_T, \mathbf{r}_T^{(0)}), \\ I_{\varepsilon\varepsilon}(\mathbf{r}_T, \mathbf{r}_T^{(0)}) &= \int \frac{\partial}{\partial\varepsilon}\ln\Phi_1(\mathbf{P}|\varepsilon, \mathbf{r}_T, \mu^{(0)})\Big|_{\varepsilon=0} \frac{\partial}{\partial\varepsilon}\ln\Phi_1(\mathbf{P}|\varepsilon, \mathbf{r}_T^{(0)}, \mu^{(0)})\Big|_{\varepsilon=0} \Phi(\mathbf{P})\, D\mathbf{P}, \\ \mathbf{I}_{\mu\varepsilon}(\mathbf{r}_T, \mathbf{r}_T^{(0)}) &= \int \frac{\delta}{\delta\mu}\ln\Phi_1(\mathbf{P}|0, \mathbf{r}_T, \mu^{(0)})\Big|_{\mu=\mu^{(0)}} \frac{\partial}{\partial\varepsilon}\ln\Phi_1(\mathbf{P}|\varepsilon, \mathbf{r}_T^{(0)}, \mu^{(0)})\Big|_{\varepsilon=0} \Phi(\mathbf{P})\, D\mathbf{P}. \end{aligned} \quad (4.83)$$

Also, one may consider the ambiguity function (AF)

$$N(\mathbf{r}_T, \mathbf{r}_T^{(0)}) = \frac{\rho(\mathbf{r}_T, \mathbf{r}_T^{(0)})}{\rho(\mathbf{r}_T)\rho(\mathbf{r}_T^{(0)})}. \tag{4.84}$$

The ambiguity function (AF) (4.84) is equal to one when the points $\mathbf{r}_T$ and $\mathbf{r}_T^{(0)}$ coincide. Spatial widths of its main lobe in the vicinity of the point $\mathbf{r}_T^{(0)}$ determine precision characteristics of the obtained estimate of object coordinates. Presence of other maximums and theirs levels determine the probability of abnormal errors. The precision characteristics of the object coordinates' estimate can be calculated directly from the Fisher information matrix (FIM) of this estimate under the condition of estimating the level of echo signal field ε and the field μ. This Fisher information matrix (FIM) is

$$\mathbf{J}_{\mathbf{r}_T\mathbf{r}_T} = \mathbf{I}_{\mathbf{r}_T\mathbf{r}_T} - \frac{\left[\mathbf{I}_{\mathbf{r}_T\varepsilon} - \mathbf{I}_{\mathbf{r}_T\mu}\mathbf{J}_{\mu\varepsilon}\right]\left[\mathbf{I}_{\varepsilon\mathbf{r}_T} - \mathbf{J}_{\varepsilon\mu}\mathbf{I}_{\mu\mathbf{r}_T}\right]}{J_{\varepsilon\varepsilon}} - \mathbf{I}_{\mathbf{r}_T\mu}\left(\mathbf{I}_{\mu\mu} + \mathbf{K}_{\mu}^{-1}\right)^{-1}\mathbf{I}_{\mu\mathbf{r}_T}, \tag{4.85}$$

where matrices $\mathbf{I}$ with different subscripts are FIM of corresponding estimates in the deterministic oceanic waveguide (DSE).

For probability densities Φ_ε defined by (4.9), the SNR, the ambiguity function (AF) and the FIM are

$$\rho(\mathbf{r}_T) = \frac{\sum\limits_{\omega_n>0}\left\langle \mathbf{K}_N^{-1}\mathbf{Q}(\mathbf{r}_T)\mathbf{P}_T(\mathbf{r}_T), \mathbf{P}_T(\mathbf{r}_T)\right\rangle^2}{\sum\limits_{\omega_n>0}\left\langle \mathbf{K}_N^{-1}\mathbf{Q}(\mathbf{r}_T)\mathbf{P}_T(\mathbf{r}_T), \mathbf{Q}(\mathbf{r}_T)\mathbf{P}_T(\mathbf{r}_T)\right\rangle}, \tag{4.86}$$

$$N(\mathbf{r}_T, \mathbf{r}_T^{(0)}) = \frac{\sum\limits_{\omega_n>0}\left\langle \mathbf{K}_N^{-1}\mathbf{Q}(\mathbf{r}_T)\mathbf{P}_T(\mathbf{r}_T), \mathbf{P}_T(\mathbf{r}_T^{(0)})\right\rangle^2}{\sum\limits_{\omega_n>0}\left\langle \mathbf{K}_N^{-1}\mathbf{Q}(\mathbf{r}_T)\mathbf{P}_T(\mathbf{r}_T), \mathbf{P}_T(\mathbf{r}_T)\right\rangle \sum\limits_{\omega_n>0}\left\langle \mathbf{K}_N^{-1}\mathbf{Q}(\mathbf{r}_T^{(0)})\mathbf{P}_T(\mathbf{r}_T^{(0)}), \mathbf{P}_T(\mathbf{r}_T^{(0)})\right\rangle} \times \tag{4.87}$$

$$\times \sqrt{\frac{\sum\limits_{\omega_n>0}\left\langle \mathbf{K}_N^{-1}\mathbf{Q}(\mathbf{r}_T^{(0)})\mathbf{P}_T(\mathbf{r}_T^{(0)}), \mathbf{Q}(\mathbf{r}_T^{(0)})\mathbf{P}_T(\mathbf{r}_T^{(0)})\right\rangle}{\sum\limits_{\omega_n>0}\left\langle \mathbf{K}_N^{-1}\mathbf{Q}(\mathbf{r}_T)\mathbf{P}_T(\mathbf{r}_T), \mathbf{Q}(\mathbf{r}_T)\mathbf{P}_T(\mathbf{r}_T)\right\rangle}},$$

$$\mathbf{J}_{\mathbf{r}_T\mathbf{r}_T} = \sum_{\omega_n>0}\left\langle \mathbf{K}_N^{-1}\mathbf{Q}(\mathbf{r}_T)\mathbf{P}_T(\mathbf{r}_T), \mathbf{P}_T(\mathbf{r}_T)\right\rangle - \tag{4.88}$$

$$- \frac{\sum\limits_{\omega_n>0}\left\langle \mathbf{K}_N^{-1}\mathbf{P}_T(\mathbf{r}_T), \mathbf{Q}(\mathbf{r}_T)\mathbf{P}_T(\mathbf{r}_T)\right\rangle \sum\limits_{\omega_n>0}\left\langle \mathbf{K}_N^{-1}\mathbf{Q}(\mathbf{r}_T)\mathbf{P}_T(\mathbf{r}_T), \mathbf{P}_T(\mathbf{r}_T)\right\rangle}{\sum\limits_{\omega_n>0}\left\langle \mathbf{K}_N^{-1}\mathbf{Q}(\mathbf{r}_T)\mathbf{P}_T(\mathbf{r}_T), \mathbf{Q}(\mathbf{r}_T)\mathbf{P}_T(\mathbf{r}_T)\right\rangle},$$

where

$$\mathbf{Q} = \mathbf{E} - \boldsymbol{P}, \quad \boldsymbol{P} = \frac{\delta \mathbf{P}_S}{\delta \mu}\left(\mathbf{E} + \mathbf{K}_\mu \mathbf{I}_{\mu\mu}\right)^{-1} \mathbf{K}_\mu \frac{\delta \mathbf{P}_S}{\delta \mu} \mathbf{K}_N^{-1}. \tag{4.89}$$

The above defined operator $\boldsymbol{P}$ determines in the measurement space the subspace of source field's fluctuations that are due to the SVF fluctuations. If the norm of the operator $\boldsymbol{P}$ is large and, respectively, the norm of the operator $\mathbf{Q}$ is small then the SNR and the FIM of the object coordinates decrease. That causes a decreasing of efficiency of the object detection and localization solution.

Such are equations for accuracy characteristics of the joint UOS+ATO solution. We don't describe details on the procedure of its computation in this paper. We only note that the main new and difficult moment in it will be the calculation of Fisher information kernels for the SVF estimate. Methods of computing these kernels and some results are presented in detail in [12]-[13], where corresponding equations are derived in the cases of deterministic, quasi deterministic and random probing signals. Also, the informativeness of field parameters for all essential sound field representations in the ocean (ray, mode, etc.) is evaluated for the ATO problem in the cases of inhomogeneities of various scales: for small-scale ones (whose scales are smaller than the Fresnel radius), large-scale ones (whose scales are larger than the Fresnel radius but smaller than cycle lengths of main strongest rays) and global ones (whose scales are larger than cycle lengths of main strongest rays).

4.4. Features of proposed MFP algorithms for SSE

Other known algorithms are:

(1) either heuristic ones [14]-[20], using
   - the decision statistics of the high resolution methods (Capon's method with different constraints) [14]-[17], whose optimality can be proved only for signal-noise scenarios of the deterministic ocean,
   - or the decision statistics (AHD, NOLOSS) [18]-[20] close to those that should derive from the rigorous statistical approach,

(2) either based on the rigorous statistical approach with maximization of the *a posteriori* probability density of measurements [21]-[23], but in this case the computation of decision statistic is made by a computer.

In the first case, it is not clear what criterion the algorithms correspond to. So, one needs to reinvestigate their efficiency for each particular case. In the second case, CPU restrictions don't allow to take into account such moments as, for example, the variability of hydrophysical conditions along a sound acoustical path.

The proposed algorithms are derived from the rigorous statistical statement of the underwater survey problem by using rigorous methods of mathematical statistics based on the Bayesian approach. The classification of fluctuations of GF on "fast" (due to the scattering from the sea surface) and "slow" (due to the scattering from large-scale volume inhomogeneities), allow us to compute analytically the decision statistic. In the case of the surface scattering the decision statistic is close to the NOLOSS algorithm. In the other case (volume scattering) it is close to the AHD algorithm. Nevertheless, in our algorithms, in opposition to the AHD, the *a priori* spread of GF parameters is not arbitrary assigned but results from the distribution low of fluctuations of these parameters that is defined by the statistics of volume inhomogeneities. Moreover, it should be noted that the use of the Bayes' criterion leads to another form of decision statistic than that of the AHD algorithm.

Our algorithm of joint solving the tomography and underwater survey problems described above is conceptually closed to the algorithm considered in [21]-[23]. However, we note as difference that in that work the computation of the *a posteriori* PDF is realized by a computer. In our approach, the integral of joint PDF in the functional space of sound velocity fields (SVF) is developed by applying the Laplace method, that allows to reduce the volume of needed calculations and to examine a real variability of the oceanic medium (in particular, along an acoustical path). So derived algorithms are able to perform not only for the low frequency range that is optimal for distances about hundreds kilometers, but also for the high frequency range that is optimal for smaller distances and more informative because of a wide signal bandwidth that is available for use.

4.5. FS-MFP algorithms

Detection and localization MFP algorithms for only one probing signal period have been considered in sections 4.2 – 4.4. Let design now detection and localization MFP algorithms, which will use the time-space structure of echo-signal field being considered in its main details in the 3. Let consider some time interval T on which the source field is invariable. For common sea environments this interval is much larger than the probing signal's period T_0: $T = N_T T_0$, $N_T >> 1$.

Logarithms of probability density functions of measurement for hypothesises H_ε for the time interval T are

$$\ln \Phi_\varepsilon(\mathbf{P}) = \\ = -\sum_{k=1}^{N_T}\sum_{n=1}^{N_\omega}\left\{\mathbf{K}_N^{nk-1}\left(\mathbf{P}^{nk} - \mathbf{P}_S^n - \varepsilon\,\mathbf{P}_T^{nk}\right)\left(\mathbf{P}^{nk} - \mathbf{P}_S^n - \varepsilon\,\mathbf{P}_T^{nk}\right) + N_\omega \ln\det \mathbf{K}_N^{nk-1}\right\}, \tag{4.90}$$

where $\mathbf{K}_{\mathrm{N}}^{nk} = \mathbf{K}_{\mathrm{N}}(\omega_n, t_k)$, $\mathbf{P}^{nk} = \mathbf{P}(\omega_n, t_k)$, $\mathbf{P}_{\mathrm{S}}^{n} = \mathbf{P}_{\mathrm{S}}(\omega_n)$, $\mathbf{P}_{\mathrm{T}}^{nk} = \mathbf{P}_{\mathrm{T}}(\omega_n, t_k)$.

It's supposed that the NCSM may be changing during the time T. The source and echo-signal models are described by the equations (5) and (6). Parameters of the echo-signal A_v, t_v, $\mathbf{e}_v$, N are changing while the parameters A_μ, t_μ, $\mathbf{e}_\mu$, M of the source field are invariant. Time dependence of the echo-field parameters is considered in the section 3. It will be admitted below that ray parameters of the source and echo fields are not known *a priori* but it is known that the source field is invariant during the time T and the time evolution of the echo field follow some known low with unknown parameters.

Accordingly to the Bassian approach to making decision the ODS is

$$\mathrm{L}\{\mathbf{P}\} = \ln\Phi_1(\mathbf{P}) - \ln\Phi_0(\mathbf{P}) = \frac{\left|\sum_{\omega_n>0}\left\langle \mathbf{K}_{\mathrm{N}}^{-1}(\omega_n)\mathbf{P}(\omega_n), \mathbf{P}_{\mathrm{T}}^{\perp}(\omega_n)\right\rangle\right|}{\sqrt{\sum_{\omega_n>0}\left\langle \mathbf{K}_{\mathrm{N}}^{-1}(\omega_n)\mathbf{P}_{\mathrm{T}}^{\perp}(\omega_n), \mathbf{P}_{\mathrm{T}}^{\perp}(\omega_n)\right\rangle}}, \quad (4.91)$$

where $\mathbf{P}_{\mathrm{T}}^{\perp}(\omega_n) = \mathbf{P}_{\mathrm{T}}(\omega_n) - \mathbf{P}_{\mathrm{S}}(\omega_n)\dfrac{\sum_{\omega_n>0}\left\langle \mathbf{K}_{\mathrm{N}}^{-1}(\omega_n)\mathbf{P}_{\mathrm{S}}(\omega_n), \mathbf{P}_{\mathrm{T}}(\omega_n)\right\rangle}{\sum_{\omega_n>0}\left\langle \mathbf{K}_{\mathrm{N}}^{-1}(\omega_n)\mathbf{P}_{\mathrm{S}}(\omega_n), \mathbf{P}_{\mathrm{S}}(\omega_n)\right\rangle}$. (4.92)

4.6. Implementation of FS-MFP algorithms

The signal processing algorithm (SPA) presented above consists of three processing stages. The first stage is to estimate ray parameters A_μ, t_μ, $\mathbf{e}_\mu$ of the received field on the time interval equal to the probing signal's period. The second stage is to select echo-signal parameters from the set of all estimated ray parameters. It's done by some kind of spectral processing of those parameters, which is made on time intervals not exceeding the time of stability of the environment. Finally, on the third stage the inverse problem of object localization is solved using the SSE-matched MFP approach.

4.6.1. 1st stage: Estimating of ray parameters of received fields

So, the first problem to be solved during the time interval equal to the probing signal's period is estimating of ray parameters A_μ, t_μ, $\mathbf{e}_\mu$ of the received field which include the source and echo-signal fields and interference of various kinds. We present below a processing procedure allowing to get these estimates when there is no full *a priori* information about the interference field.

4.6.1.1. Adaptation to the interference

In the above presented algorithm of making decision it is considered that the noise spectral density matrix (NSDM) $\mathbf{K}_N(\omega)$ is known *a priory*. In fact, there is no such *a priori* information. Moreover, the noise field may vary during the survey. Nevertheless, as a rule we have *a priory* information about time intervals of variability for the interference. Usually they exceed by several orders its correlation interval. On the other hand, we have also some *a priori* information about space variability of the interference that may be formulated as smoothness characteristics of angular spectra or as spectral characteristics of noises. This *a priori* information allows to design adaptive algorithms with estimating of NSDM.

Let us firstly suppose that the NSDM $\mathbf{K}_N$ doesn't depend on frequency for the frequency range of the probing signal. While probing signals are narrow band, this supposition is unconditionally valid regarding the system and the sea ambient noises. The reverberation interference has a spectral density that is proportional to the squared module of the probing signal's spectrum. One uses usually complex signals where only the spectrum's phase depends on frequency but not the spectral amplitude. In this case one may consider that the spectral density of reverberation isn't also depending on frequency. If some frequency dependence is still present, our previous numerical modeling shows that the optimization of processing algorithms for active systems by means of making "white" the interference gives rather small amelioration of the result that we can neglect.

To get estimation of the NSDM we use the maximum likelihood approach. We need to calculate derivatives of the logarithm of the the probability density function (4.9) (log-PDF) of measurements with respect to elements of the matrix $\mathbf{K}_N$ and to equal them to zero. Solution of such obtained equations is

$$\hat{\mathbf{K}}_N = \frac{1}{N_\omega}\sum_n \left| P(\omega_n) - P_S(\omega_n) - P_T(\omega_n)\right\rangle\left\langle P(\omega_n) - P_S(\omega_n) - P_T(\omega_n)\right| . \quad (4.93)$$

It follows from this formula that we need to know ray parameters of probing and echo-signals to produce the maximum likelihood estimate (MLE) of the NSDM. If we neglect the direct and the echo-signal fields in (4.93), we obtain following estimate for the matrix $\mathbf{K}_N$

$$\hat{\mathbf{K}}_N \approx \Re = \frac{1}{N_\omega}\sum_n \left| P(\omega_n)\right\rangle\left\langle P(\omega_n)\right| . \quad (4.94)$$

Mathematical expectation (mean value) of this approximate MLE is:

$$\overline{\Re} = \mathbf{K}_N + \frac{1}{N_\omega}\sum_{\mu,\nu} A_\mu A_\nu^* \left|\mathrm{E}_\mu\right\rangle\left\langle\mathrm{E}_\nu\right| \cdot R_S(t_\mu - t_\nu)\,, \tag{4.95}$$

where $\left|\mathrm{E}_\mu\right\rangle = \left|\exp\left\{i\frac{\omega_0}{c}\left(\mathbf{e}_\mu, \mathbf{r}_q - \mathbf{r}_R\right)\right\}\right\rangle$, $R_S(\tau) = \sum_n e^{i\omega_n\tau}\left|S(\omega_n)\right|^2 \Big/ \sum_n \left|S(\omega_n)\right|^2$ is the probing signal's correlation function normalized so that $R_S(0) = 1$, $|R_S(\tau)| \le R_S(0)$. If ray delays exceed the signal's correlation interval, then $|R_S(t_\mu - t_\nu)| \cong 0$ and the equation (4.94) becomes.

If ray delays exceed the signal's correlation interval, then $|R_S(t_\mu - t_\nu)| \cong 0$ and we have

$$\overline{\Re} = \mathbf{K}_N + \frac{1}{N_\omega}\sum_{\mu} \left|A_\mu\right|^2 \left|\mathrm{E}_\mu\right\rangle\left\langle\mathrm{E}_\nu\right| \cdot \tag{4.96}$$

Thus, the mean value of this estimate is equal to the sum of the NSDM and of the energy matrix of the probing signal with the echo-signal calculated per one frequency at the spectrum. To have the good detection probability $P_D = 0.9$ the signal-to-noise ratio (SNR) needs to be about 50...100. Therefore, if $N_\omega \sim 10^3$ then the SNR per one frequency should be about 0.05...0.1. Thus, the expression (4.95) may be used as estimate of the NSDM with a precision about 5...10%.

After substituting (4.94) into (4.9), it follows

(4.97)

$$\ln\Phi_1(\mathbf{P}) = -N_\omega \times$$

$$\times\left[\mathrm{Sp}\mathbf{E} - \sum_\mu \left(A_\mu\,\mathrm{Sp}(\Re^{-1}\Re_\mu^+) + A_\mu^*\,\mathrm{Sp}(\Re^{-1}\Re_\mu)\right) + \sum_{\mu,\nu} A_\mu A_\nu^*\,\mathrm{Sp}(\Re^{-1}\Re_{\mu\nu}) + \ln\det\Re\right],$$

$$\Re_\mu = \frac{1}{N_\omega}\sum_n \left|P(\omega_n)\right\rangle\left\langle\mathrm{E}_\mu\right| e^{-i\omega_n t_\mu} S^*(\omega_n)\,,\quad \Re_{\mu\nu} = \frac{1}{N_\omega}\sum_{\omega_n>0}\left|\mathrm{E}_\mu\right\rangle\left\langle\mathrm{E}_\nu\right| \cdot R_S(\mathrm{t}_\mu - \mathrm{t}_\nu)\,.$$

4.6.1.2. Decision statistic for ray parameters estimating

To estimate unknown ray complex amplitude the maximum likelihood principle is applied once more. Deriving the log-PDF (4.97) with respect to estimated amplitude and equaling the result to zero one obtains equations to be solved. Thus, the estimations are obtained

$$\hat{A}_\mu = \left[\mathrm{Sp}(\Re^{-1}\Re_{\mu\nu})\right]^{-1}\mathrm{Sp}(\Re^{-1}\Re_\nu)\,. \tag{4.98}$$

Using (4.98) in (4.97) one derives

$$\ln \Phi_1(\mathbf{P}) =$$

$$= -N_\omega \left[\mathrm{Sp}\,\mathbf{E} - \sum_{\mu,\nu} \mathrm{Sp}(\mathfrak{R}^{-1}\mathfrak{R}_\mu^+) \left[\mathrm{Sp}(\mathfrak{R}^{-1}\mathfrak{R}_{\mu\nu})\right]^{-1} \mathrm{Sp}(\mathfrak{R}^{-1}\mathfrak{R}_\nu) + \ln \det \mathfrak{R} \right]. \quad (4.99)$$

It follows from the equations (4.97) for matrices $\mathfrak{R}_{\mu\nu}$ that if ray delays t_μ–t_ν are larger than the probing signal's correlation interval then $\mathfrak{R}_{\mu\nu} \cong 0$, $\mu \neq \nu$. In this case the equation (4.99) is simplified

$$\ln \Phi_1(\mathbf{P}) = -N_\omega \left[\mathrm{Sp}\,\mathbf{E} - \sum_{\mu} \left[\mathrm{Sp}(\mathfrak{R}^{-1}\mathfrak{R}_{\mu\mu})\right]^{-1} \left|\mathrm{Sp}(\mathfrak{R}^{-1}\mathfrak{R}_\mu)\right|^2 + \ln \det \mathfrak{R} \right]. \quad (4.100)$$

It follows from (4.100) that one may use the following function as decision statistic to estimate signal's ray arrival angles and travel times:

$$\mathrm{T}(\mathbf{e},t) = N_\omega \frac{\left|\mathrm{Sp}(\mathfrak{R}^{-1}\mathfrak{R}_\mu(\mathbf{e},t))\right|^2}{\mathrm{Sp}(\mathfrak{R}^{-1}\mathfrak{R}_{\mu\mu}(\mathbf{e}))}. \quad (4.101)$$

Let's write more detailed the numerator and denominator of the statistics (4.101):

$$\begin{aligned} \mathrm{Sp}(\mathfrak{R}^{-1}\mathfrak{R}_\mu(\mathbf{e},t)) &= \frac{1}{N_\omega}\left\langle \mathfrak{R}^{-1}\mathbf{E}(\mathbf{e}), \mathbf{q}(t)\right\rangle, \\ \mathrm{Sp}(\mathfrak{R}^{-1}\mathfrak{R}_{\mu\mu}(\mathbf{e})) &= \frac{1}{N_\omega}\left\langle \mathfrak{R}^{-1}\mathbf{E}(\mathbf{e}), \mathbf{E}(\mathbf{e})\right\rangle, \\ \mathbf{q}(t) &= \left|q(t)\right\rangle = \sum_n \left|P(\omega_n)\right\rangle e^{-i\omega_n t} S^*(\omega_n). \end{aligned} \quad (4.102)$$

Thus, the final equation for the decision statistic derives

$$\mathrm{T}(\mathbf{e},t) = \frac{\left|\left\langle \mathfrak{R}^{-1}\mathrm{E}(\mathbf{e}), \mathbf{q}(t)\right\rangle\right|^2}{\left\langle \mathfrak{R}^{-1}\mathrm{E}(\mathbf{e}), \mathrm{E}(\mathbf{e})\right\rangle}. \quad (4.103)$$

4.6.1.3. Time-space processing for ray parameters estimating

Processing procedure realizing the above described algorithm of primary processing may be structured as follows.

(0) Making FFT (on the probing signal period) of signals received by array's sensors and obtains the vector of complex spectra.

(1) Producing the NSDM estimate as it's described by (2), then the matrix is inverted.

(2) Setting a grid of space directions (for a linear vertical array it is a set of angles in the vertical plane) and forms the optimal weight vector (WV) $\mathbf{W(e)} = |W(\mathbf{e})\rangle = \Re^{-1}|\mathrm{E(e)}\rangle$ and the SNR $\rho(\mathbf{e}) = \langle \mathbf{W(e)}, \mathrm{E(e)} \rangle$ for each direction $\mathbf{e}$ of the grid.

(3) Realization of the correlation processing of the measurement by forming the vectors $\mathbf{q}(t) = |q(t)\rangle = \sum_n |P(\omega_n)\rangle e^{-i\omega_n t} S^*(\omega_n)$ for all time moments with using the FFT procedure.

(4) Computation of the decision statistic $\mathrm{T}(\mathbf{e},t) = \dfrac{|\langle \mathbf{W(e)}, \mathbf{q}(t) \rangle|^2}{\rho(\mathbf{e})}$ versus $(\mathbf{e},t)$ coordinates.

(5) Calculation of a threshold τ_0 determined by the false alert probability P_F. If only an interference comes to the system's input, then the decision statistic $T(\mathbf{e},t)$ at each point $(\mathbf{e},t)$ is distributed following the Rayleigh's low with the mean value $\overline{T}(\mathbf{e},t) = 1$. So that when the false alert probability and numbers of angels N_e and of arrival times N_t are set up, the threshold is $\tau_0 = -\ln \dfrac{P_F}{N_e N_t}$.

(6) Comparison of the decision statistic to the threshold τ_0 for each point of the space $(\mathbf{e},t)$ where the decision statistic has a local maximum. If one of maximums exceeds the threshold, one makes decision that there is a signal ray, and accepts the maximum's coordinates as estimates of ray arrival angles and travel time. Then one estimates the ray's complex amplitude following the equation $\hat{A}(\mathbf{e},t) = \dfrac{\langle \mathbf{W(e)}, \mathbf{q}(t) \rangle}{\rho(\mathbf{e})}$.

Thus, one has the decision statistic's field $T(\mathbf{e},t)$ formed at the output of this part of the processing algorithm for estimating source signal's and echo-signal's parameters. During one period of the above-described primary processing, one isn't still able to decide which correlation maximums belong to the source field or to the echo-signal.

One of advantages of the above-described primary processing algorithm in comparison with the convenient space-time correlation is that there is a real-time produced estimate of NSDM. It allows to follow efficiently an interference's variability thanks to the use of probing signals of high complexity. Also, one makes the space

"whitening" of the interference thanks to the optimal weight vector forming. It allows to improve considerably the SNR in the presence of an anisotropy interference such as the sea ambient noise or reverberation.

Another advantage of the above described primary processing is the fact that the decision statistic $T(\mathbf{e},t)$ is insensible to movements of receiving and emitting arrays' phase centers such as those due to a ship tossing.

4.6.2. 2nd stage: Selection of echo-signal rays

Processing algorithm to select echo-signal's correlation maximums amongst those of the source field is based of the difference of theirs dynamics. Correlation maximums of the source field change slowly theirs coordinates in the space $(\mathbf{e},t)$: the time correlation intervals of arrival angles and travel times of source field's rays are about hundreds of thousands of seconds (for free internal waves in the ocean). These time correlation intervals for each whether season should be previously studied (measured) for some given sea area where a FS-ABS system will work. On the other hand, the echo-signal's ray parameters change much more quickly because the object moves. When the object is far from the system's vertical plane containing the acoustical path, the object's equivalent radius (ER) is small and one can't "see" the echo-signal on the noise background. When the object comes in the vicinity of the system's vertical plane, the ER grows sharply thanks to what levels of echo-signal's correlation maximums also grow sharply and the echo-signal in the statistic's field becomes visible. After the object has crossed the system's vertical plane the correlation maximums' levels decrease and finally they vanish in the interference background.

To design an algorithm for echo-signal's correlation maximums selecting one uses the estimates of the FS-ABS detection zone's thickness, of the living time of echo-signals and of the envelope's shape of echo-signal's amplitudes, which have been derived previously in the 3. Let us resume once more main conclusions following from these estimates:

- the FS-ABS detection zone is narrow in the horizontal plane, its thickness is $\sim \lambda/2L_T$ relatively to the length of the system's base R_{SR};
- the living time of echo-signal's correlation maximums is $\sim [\lambda/2L_T][R_{SR}/v_T]$;
- amplitude of the complex envelope of each correlation maximum corresponding to an echo-signal ray being segregated in the angle-time space from those of the source field practically follows the shape of the object scattering amplitude's main lobe in the horizontal plane. When neglecting its side lobes, one may approximate the main lobe by a gaussian function as it is done above in the 3 (equation (3.11)):

$$A_v(t) \approx A_v(t_0)\exp\left\{-\frac{1}{2}\left(\frac{L_T \sin^2\alpha}{\lambda/2}\frac{v_T(t-t_0)}{x(t_0)[1-x(t_0)]R_{SR}}\right)^2\right\}. \qquad (4.104)$$

- amplitude of the complex envelope of each correlation maximum corresponding to an echo-signal ray being not segregated in the angle-time space from a source field's ray is a linear frequency modulated (LFM) signal with the envelope (4.104) and an LFM structure

$$\cos\{\omega\delta t_v^{(2)}\}, \qquad (4.105)$$

where $\delta t_v^{(2)}$ is the second-order-in-time phase term, being described in the chapter 1.

Basing on these particularities of echo-signal's correlation maximums, the following processing algorithm of the decision statistic $T_t(\mathbf{e},\tau)$ being built on each primary processing period derives.

1) Making of time averaging of the decision statistic's field $T_t(\mathbf{e},\tau)$ at all points $(\mathbf{e},\tau)$ within some time interval T' that is much larger than the echo-signal's living time but smaller than the time of instability of source field's ray parameters:

$$\hat{T}_t(\mathbf{e},\tau) = \frac{1}{T'}\int_{t-T'/2}^{t+T'/2} T_{t'}(\mathbf{e},\tau)dt'. \qquad (4.106)$$

Then one subtracts the averaged statistic from the initial one:

$$\tilde{T}_t(\mathbf{e},\tau) = T_t(\mathbf{e},\tau) - \hat{T}_t(\mathbf{e},\tau). \qquad (4.107)$$

2) Comparison of the above result with a threshold determined by the false alert probability P_F and find $\tilde{\tilde{T}}_t(\mathbf{e},\tau)$ exceeding the threshold to process them further.

3) Computation of the time correlation of $\tilde{\tilde{T}}_t(\mathbf{e},\tau)$ regarding to t with a model signal that is the LFM signal (4.105) with the gaussian amplitude envelope (4.104). Nevertheless our estimations of the time first-order term $\delta t^{(1)}$ show that one may neglect the corresponding time shift of echo-signal correlation maximums because it is not larger than the correlation interval of the probing signal ($\sim 2\cdot10^{-3}$ sec if its band is 600 Hz). Our estimations of the time second-order term $\delta t^{(2)}$ show that one may also neglect the corresponding time shift of correlation maximums as well as their linear frequency modulation while the

corresponding frequency deviation $\omega\delta t^{(2)}/(t-t_0)$ is rather smaller than the inverted echo-signal's living time that is determined by the gaussian envelope (4.104). Thus, the optimal processing in our case resumes as computation of the correlation

$$K(\mathbf{e},\tau;t_0,\Delta t) \triangleq \frac{1}{T'}\int_{t-T'/2}^{t+T'/2} \tilde{\tilde{\mathrm{T}}}_{t'}(\mathbf{e},\tau)\exp\left\{-\frac{1}{2}\left(\frac{t'-t_0}{\Delta t}\right)^2\right\}dt' \qquad (4.108)$$

and following estimation of the model signal's parameters $\hat{t}_0$, $\Delta\hat{t}$ that give the maximal correlation:

$$(\hat{t}_0,\Delta\hat{t}) = \arg\max_{t_0,\Delta t}\left\{K(\mathbf{e},\tau;t_0,\Delta t)\right\}, \qquad (4.109)$$

5) Comparison of the maximums of correlation functions $K(\mathbf{e},\tau;\hat{t}_0,\Delta\hat{t})$ to some threshold. If some maximum exceeds the threshold the decision is made that it belongs to some echo-signal ray path. Maximum's coordinates and the maximum likelihood estimates $\hat{t}_0$, $\Delta\hat{t}$ of the model signal's parameters are accepted as parameters of this echo-signal ray path and of its time dynamics.

4.6.3. 3rd stage: MFP processing

If the tasks of the two previous processing stages (building of the decision statistic T and estimation of echo-signal ray parameters: number of ray paths $\hat{M}_\mu$, theirs complex amplitudes $\hat{A}_\mu$, travel times $\hat{\mathrm{t}}_\mu$ and arrival angles $\hat{\mathbf{e}}_\mu$) are solved then all data needed to solve the object localization problem by using the MFP approach are collected. To solve the problem the system's vertical plane is covered by a range-depth grid (r_i,z_j) with certain steps in range and depth

$$r_i = i\Delta r, i = 0,1,\ldots I, I = \mathrm{int}(\frac{R_{SR}}{\Delta r}), z_j = j\Delta z, j = 0,1,\ldots J, J = \mathrm{int}(\frac{H}{\Delta z}) \quad (4.110)$$

and echo-signal fields coming to the receiving array have to be modeled for each point of the grid considered as possible object location. In fact, echo-signal's ray parameters should be predicted: number of ray paths N_{ij}, theirs amplitudes A_{ijv}, travel times t_{ijv} and arrival grazing angles χ_{ijv} in the phase center of the receiving array. All these parameters are calculated at advance and stored in a file.

So, while the system works, signal measurements on sensors of the receiving array are made. Then, estimates of echo-signal's ray parameters are obtained by applying the above described algorithms and for each grid point the statistic is computed

$$T_{ij} = \left(\sum_{\mu=1}^{\hat{M}} \hat{A}_{\mu}^2 \sum_{v=1}^{N_{ij}} A_{ijv}^2 \right)^{-1/2} \sum_{\mu=1}^{\hat{M}} \sum_{v=1}^{N_{ij}} \hat{A}_{\mu}^2 A_{ijv}^2 \Re(\hat{e}_{\mu} - e_{ijv}) R(\hat{t}_{\mu} - t_{ijv}) \cdot \qquad (4.111)$$

Further, one has to search for a global maximum $T_m = \max\{T_{ij}\}$, $(i^*, j^*) = \arg\max\{T_{ij}\}$ of this decision statistics and to compare its level with some threshold calculated previously for some given false alert probability. If the maximum's level exceeds the threshold then the detection problem is considered as solved and coordinates of the maximum (r_{i^*}, z_{j^*}) are accepted as estimate of object coordinates when it crosses the system's vertical plane.

Having estimated living times of echo-signal's correlation maximums it becomes possible also to estimate the orthogonal component of the object's speed

$$v_T = \frac{2\lambda}{L_T} \frac{R_{ST}(R_{SR} - R_{ST})}{TR_{SR}}, \; R_{ST} = r_{i^*} \cdot \qquad (4.112)$$

5. NUMERICAL AND EXPERIMENTAL STUDY OF SIGNAL PROCESSING ALGORITHMS FOR FS-ABS

5.1. Choice of hydrophysical models for numerical studying

Let consider four types of shallow water sea environments (SWSE) for numerical investigations of the above considered signal processing algorithms for FS-ABS:

(1) *Pekeris SWSE* with following parameters:

- sound velocity in the water: 1.5 km/s,
- sound velocity in the bottom: 1,7 km/s,
- waveguide's total depth 0.2 km,
- surface waving: median (5 points), wind 10 m/s,
- length of the system's base 50 km.

(2) *Summer SWSE.* As example the Barents sea summer environment is chosen. It differs from the Pekeris ones by following parameters:

- sound velocity in the water: sub-bottom duct (figure 5.1a),
- bottom is defined by a table of reflection coefficients.

(3) *Winter SWSE.* As example the Barents sea winter environment is chosen. It differs from the summer SWSE by following parameters:

- sound velocity in the water: surface duct (figure 5.1b),
- length of the system's base 15 km.

(4) *Test SWSE.* As example the tropical sea summer environment of the strait between the islands Maui and Lanai (Hawaii) is chosen. Such an environment may be common for possible sea trials of FS-ABS system prototype or for operational use of such systems. It differs from the summer SWSE by following parameters:

- sound velocity in the water: sub-bottom duct (figure 5.1c),
- total depth: 50 m.

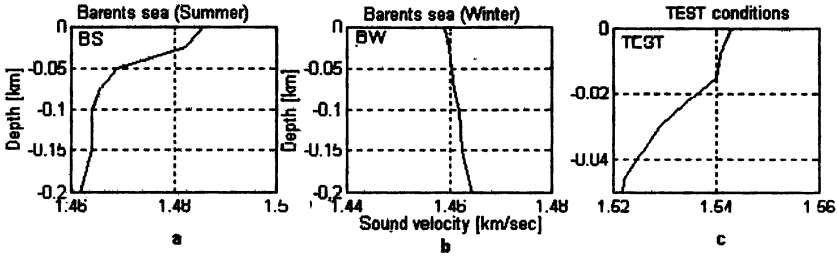

Figure 5.1. Characteristic SSP chosen for computer modeling: a) summer SWSE (sub-bottom channel), b) winter SWSE (subsurface channel), c) Test SWSE (sub-bottom channel).

For all cases the Harret-Munk's spectrum of free internal waves in the ocean for volume random inhomogeneities modeling in all types of SWSE is used, with calculating frequency profiles from $c(z)$ profiles for those SWSE.

Coefficients of weakening in the water, of reflection and scattering indexes of the waveguide's boundaries, the object strength and other parameters are calculated following the models being described in the section 2. The model of stationary reverberation is used for forward scattering reverberation modeling.

In all cases a linear vertical array of 10 m length of 80 sensors with $\lambda/2$ spacing is considered as receiving subsystem. As probing

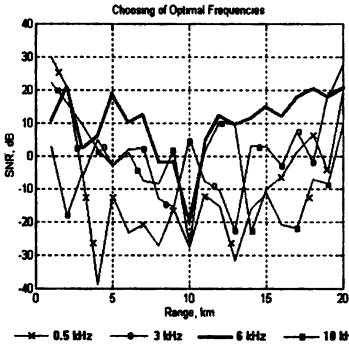

Figure 5.2. SNR as function of object range calculated for DSE-matched FS-MFP algorithms (SWSE TEST) for different frequencies.

signal the LFM pulse signal with central frequency 6 kHz is used, which is optimal for those environments (under the limitation to have 10% band signals). Such a signal has a correlation interval ~ $1.5 \cdot 10^{-3}$ s.

To study the quality and robustness of solutions of the underwater object survey (UOS) problem based on the studied MFP-FS algorithms various positions of an object in the waveguide are considered. Hereafter several examples of building the ambiguity surfaces (AS) for these algorithms are presented for following object's positions (z_T,x_T) and types:

Table 5.1.
Object positions and geometry of surveyed zones for modeling

Waveguide	Surveyed zone	(z_T,x_T)
Summer SWSE BS	0.2 km × 50 km	100 m, 20 km
Winter SWSE BW	0.2 km × 15 km	60 m, 7 km
SWSE TEST	0.05 km × 15 km	30 m, 7 km

5.2. Studying the MFP-FS algorithms for DSE

5.2.1. Frequency optimization

Figure 5.2 shows SNR versus object distance and probing signal's central frequency modeled for studied deterministic FS-MFP algorithms for all typical SWSE. Based on these results, optimal frequencies for FS-ABS systems using these algorithms could be chosen. The optimal frequencies are given with the table 5.2.

Table 5.2.

Waveguide	Optimal frequencies for DSE	Optimal frequencies for SSE
Pekeris SWSE (0.2 km × 50 km)	6 - 8 kHz	6 - 8 kHz
Winter SWSE (0.2 km × 50 km)	6 - 8 kHz	6 - 8 kHz
Summer SWSE (0.2 km × 15 km)	6 - 8 kHz	6 - 8 kHz
SWSE TEST (0.05 km × 15 km)	12 - 14 kHz	11 - 12 kHz

5.2.2. Calculation of detection zones

Figures 5.3 - 5.4 show detection zones calculated for the two DSE-matched FS-MFP algorithms (equations (8) for statistics 1 and (9) for statistics 2). Different intensities

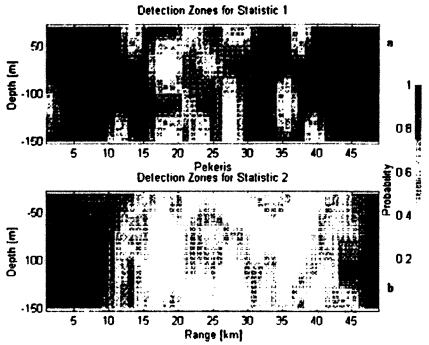

Figure 5.3. Detection zones of DSE-matched FS-MFP algorithms (Pekeris SWSE).

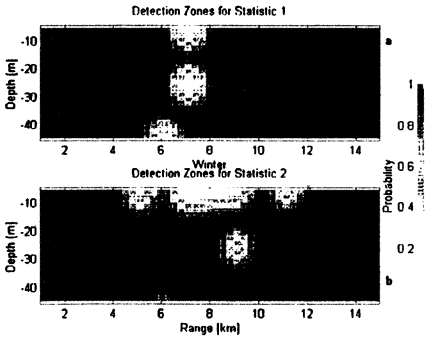

Figure 5.4. Detection zones of DSE-matched FS-MFP algorithms (Test SWSE).

of black and gray colors correspond to different probabilities of good detection. Figures 5.5 - 5.6 show axes of dispersion ellipses that characterize the width of the main lobe of ODS in the points of detection zones of the FS-MFP. These results prove the general low that the DSE-matched MFP algorithms (and not only of FS-type) provide very high precision of object localization.

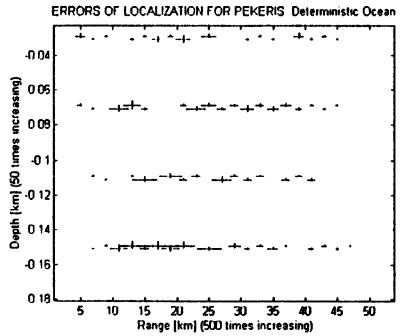

Figure 5.5. Axes of dispersion ellipses of DSE-matched FS-MFP algorithms (Pekeris SWSE).

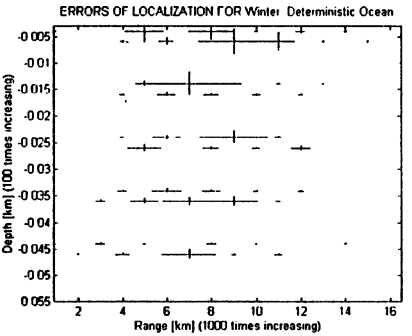

Figure 5.6. Axes of dispersion ellipses of DSE-matched FS-MFP algorithms (Test SWSE).

5.2.3. Study of the effect of local noisy sources

To study the effect of local noisy sources at the efficiency of an UOS solution in the DSE we make modeling of detection zones for all model situations when a local noisy source is present. We considered a surface ship with 2 Pa level per 1 Hz band at 1 kHz (depth 5 m) and with 6 dB per octave decreasing. The distance between the ship and the receiving subsystem varies from 1 km to 50 km.

Analyzing these modeling results we conclude that the use of the correlation processing and of algorithms with adaptation to vertically anisotropy noises allows to eliminate practically a negative effect of a surface ship's noise even if it is located very close to the receiving subsystem. It is possible, firstly, thanks to the correlation processing with a signal model having high complexity and also thanks to the receiving array's vertical dimension and to the fact that the ray structure of a surface ship's sound field is relatively poor (low number of strongest rays with rather distinct arrival grazing angles). We make the modeling only for one local noisy source presented in the surveyed zone but it should be possible to suppress an interference generated by 4 or 5 incoherent local noise sources in this zone thanks to a large number of sensors at reception (20-25 groups) we have with a vertical array.

We don't present in this paper corresponding modeling results for MFP algorithms for DSE since theirs detection zones in the presence of local noisy sources are practically the same that theirs detection zones having being calculated without such sources.

5.3. Efficiency of DSE-matched MFP-FS algorithms in SSE

As it was already noted for several times, the most informative parameters of sound fields in the ocean for solving the UOS problem are phase parameters ξ being in use for building a decision statistic, such as ray travel times and arrival angles. Under the DSE model statistical properties of estimates ξ_1 of these parameters are determined by statistical properties of interferences and are characterized by conditional probability density function (PDF) (that is the distribution under condition that "true" values of measured parameters are ξ). The corresponding variance $D[\xi_1|\xi]$ is determined by the Fisher information quantity $\mathbf{I}$ of the measurement: $D[\xi_1|\xi] = \mathbf{I}^{-1}$. Under the SSE model, the parameters ξ fluctuate because of the time variability of the waveguide. These fluctuations are described by *a priori* PDF. By applying corresponding signal and noise models being described in 2, statistical characteristics of random medium fluctuations in the waveguide can be recalculated as *a priori* statistical characteristics of fluctuations of the parameters ξ. The main characteristic is their *a priori* variance $D[\xi]$.

Let ξ_1 is a measured estimate of parameters ξ in the SSE. As in the DSE case, its statistical properties are described, firstly, by a conditional PDF when the true value

is ξ. Corresponding variance is determined by the FIQ of the measurement: $D[\xi_1|\xi] = I^{-1}$. The unconditional PDF of the estimate ξ_1 is determined by integrating the product of its conditional PDF and *a priori* PDF of fluctuations of the parameters ξ due to the medium random fluctuations. The variance of this PDF is equal to the sum of the *a priori* variance and of the conditional variance of the estimate: $D[\xi_1] = D[\xi]+D[\xi_1|\xi]$. *A posteriori* PDF of parameters ξ under the condition that theirs measured values are ξ_1, is described by the variance $D[\xi|\xi_1]$, and the corresponding precision is a sum of the precision of the *a priori* PDF of fluctuations and of the conditional PDF of the estimate: $1/D[\xi|\xi_1] = 1/D[\xi]+1/D[\xi_1|\xi]$. Therefore, if the Fisher's information of the measurement $1/D[\xi_1|\xi]$ grows then one is able to measure better the "true" values of ray parameters.

We have studied these modeling results to evaluate the efficiency of the MFP algorithms for DSE model used in the SSE conditions. To do it we model building decision statistics of the algorithms by the following way: the echo-signal field is modeled for the "true" object location and we add random simulated fluctuations to its phase parameters with *a posteriori* variances calculated for the considered stochastic propagation conditions and for the simulated signal-to-noise ratio (SNR). After that the decision statistics is computed following the studied algorithm. Examples of building of decision statistics for the both MFP-FS algorithms matched to the DSE model when applied in the SSE demonstrate that there is a degradation of the DS (sometimes rather significant) resuming as stretching and movement of its maximums and as appearing of side lobes that may in some cases exceed the initial main lobe and produce abnormal errors of localization. Note that the algorithm #1 matched to the random phase signal model is usually more robust than the algorithm #2 matched to the random complex amplitude signal model.

As we have already many times noted, the most informative from the point of view of solving the UOS problem in the ocean are the phase sound field parameters (such as ray arrival times and angles). They are varying (fluctuating) in SSE conditions because of time variability of the waveguide. One may calculate statistical characteristics of field phase parameters by using corresponding theoretical and numerical models of sound fields in the ocean waveguide (OWG) and statistical characteristics of medium fluctuations in the SSE. If the processing time interval is much smaller then the time correlation interval of medium fluctuations, one has no exact knowledge on waveguide's parameters and, firstly, on the sound velocity field (SVF), because of this time variability. If may be interpreted as a random component in the SVF whose statistic characteristics are determined by those of fluctuations that may be recalculated by the same way into those of field phase parameters' fluctuations.

Results of this modeling were used to estimate the efficiency of FS-MFP algorithms matched to DSE when applied in SSE. To do it, optimal decision statistics (ODS) of

these algorithms were built by the following way: echo-signal was modeled when object is placed in the above given point and then random fluctuations with RMS having been calculated for this point and propagation conditions were added to phase parameters of the signal. Then the ODS were built by the common way. Examples of such building of ODS for two FS-MFP algorithms matched to DSE are presented shows that the ODS is degraded (sometimes to a rather marked degree). This fact is expressed as a more large main lobe, movement and dividing of the main lobe, appearance of new lobes and abnormal errors (false solutions).

5.4. Studying the MFP-FS algorithms for SSE

Since the signal-to-noise ratio (SNR) of SSE-matched FS-MFP algorithms is not very different from that of DSE-matched one, then their detection zones are also very close. Examples of ambiguity functions (AF) built for the both two algorithms for above given object location and axes of dispersion ellipses calculated in points of detection zones are shown with figures 5.7 – 5.8. Precision of localization for SSE-matched FS-MFP algorithms are greater then those for DSE-matched ones, but these precision is rather satisfying and exceed considerably limitations which may be imposed on parameters of underwater survey systems for shallow waters.

To demonstrate the stability of solution being obtained in SSE conditions by using SSE-matched FS-MFP algorithms, we have done modeling of optimal decision statistics (ODS) forming by the same way as above. Examples of ODS being built by this way for two SSE-matched FS-MFP algorithms applied in SSE conditions demonstrate that the ODS is much less degraded than in the above case.

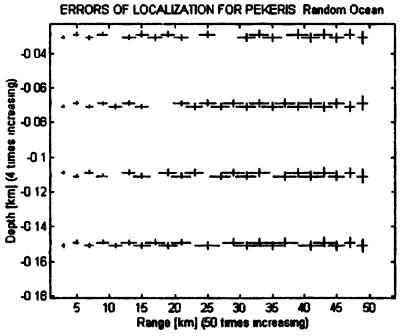

Figure 5.7. Axes of dispersion ellipses of SSE-matched FS-MFP (Pekeris SWSE).

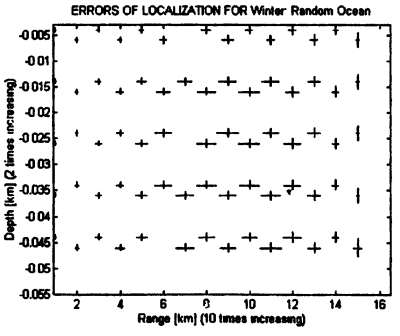

Figure 5.8. Axes of dispersion ellipses of SSE-matched FS-MFP (Test SWSE).

To study the robustness of the SSE-matched MFP algorithms, modeling of theirs decision statistics following the approach of the section 4.3 was conducted. Examples of so simulated decision statistics for the both MFP-FS algorithms matched to the SSE model when applied in SSE conditions show the robustness of solutions of these algorithms in SSE situations to be usually qualitatively compatible to that of the deterministic MFP algorithms. The reason is that even in the idealized case without adding fluctuations to the field's parameters the decision statistics of DSE and SSE-matched MFP algorithms in our situations are often rather similar from the point of view of its space distribution and side lobes' level. In this case the use of a probing signal having some correlation interval that isn't very different from the RMS of ray travel times implemented in the SSE model robustness of the both deterministic or random algorithms to fluctuations of field's parameters in the scope of the RMS is qualitatively the same. To show the robustness of stochastic MFP algorithms against fluctuations of ray parameters in comparison with that of the deterministic MFP algorithms, probing signals with some correlation interval being smaller than the RMS of fluctuations of ray travel times should be used.

5.5. Impact of mismatches on the efficiency of DSE and SSE-matched FS-MFP algorithms

When some UOS system is operating in real ocean waveguide (OWG) conditions, the real parameters of the OWG and of the system may differ from those being implemented in the MFP algorithms on the use of which the system is based. Such mismatch between the algorithms and the real parameters may be the reason of various errors when solving the UOS problem. Errors of measurements (of actual SVP, depth, etc.), various hydrophysical processes, as well as the random time variability of the OWG may be the source of these mismatches. Parameters on which a mismatch may be important, especially for solving the localization problem, are listed below:

- mean sound velocity profile (SVP),
- mean bottom depth,
- statistical characteristics of fluctuations in the frame of used SSE model,
- length of the system base,
- parameters of the emitting array (power, pattern factor, array pattern, space position and orientation, etc.),
- parameters of the receiving array (sensitivity, pattern factor, array pattern, space position and orientation, etc.),
- noise parameters,

and so on.

Errors of localization arising as effect of some mismatch may be of two kinds:

- *displacement* errors when there is only one solution but in some different position than the "true" one, and
- *abnormal* errors (false solutions) when there are several solutions; in this case one maximum may be rather close to the "true" object location but it may be only a local maximum of the decision statistics and not the global one.

To estimate possible errors due to different types of mismatches, on the stage 2 of this study we have conducted numerical simulations for all mismatch types. To simplify the review and understanding of results of this modeling, we present quantitative characteristics of mismatches' effect and mismatches' parameters in the table 4.2 (for SVP and bottom depth mismatches) and in the table 4.3 (for mismatches in receiving and emitting systems' parameters). The quantitative characteristics are RMS of errors of localization in depth and range. There are also false solutions (abnormal errors) noted as AE. The sign (~;~) means that there is no solution (the decision statistic doesn't exceed the threshold).

Table 5.3.
Mismatch effect for SVP and bottom depth mismatches

Waveguide	**RMS of SVP**	**RMS of displacement of object localization solution** (z,x) [km] D – DSE, S – SSE, AE statistic 1 / 2	**RMS of bottom depth**	**RMS of displacement of object localization solution** (z,x) [km] D – DSE, S – SSE, AE statistic 1 / 2
	1		2	
Summer SWSE	1 m/s	D: (0.025;15)/(0.035;3) S: (0.005;15)/(0.005;1)	0.5 m	D: (0.02;20)/(0.03;20) AE S: (0.03;10)/(0.02;5) AE
0.2 km × 50 km	3 m/s	D: (0.005;13)/(0.005;4) AE S: (0.005;13)/(0.005;4) AE	1 m	D: (0.02;13)/(0.03;5) AE S: (0.02;13)/(0.03;10) AE
Winter SWSE	1 m/s	D: (~ ; ~)/(0.03;1) S: (0.1;5)/(0.05;1)	0.5 m	D: (0.02;0.2)/(0.030;0.15) S: (0.03;0.3)/(0.025;0.20)
0.2 km × 15 km	3 m/s	D: (~ ; ~)/(0.1;3) AE S: (~ ; ~)/(0.1;3) AE	1 m	D: (0.03;0.3)/(0.04;0.3) S: (0.02;0.3)/(0.03;0.3)
Test SWSE	0.5 m/s	S: (0.002;0.5)/(0.003;0.8) AE	0.5 m	S: (0.002;6)/(0.002;6) AE
0.05 km × 15 km	1 m/s	S: (0.012;1.2)/(0.005;1.2) AE	1 m	S: (0.003;4)/(0.003;3) AE

5.5.1. SVP mismatch

To study numerically the SVP mismatch effect, we have considered profiles that differ from the reference ones being chosen in the section 4.1 so that theirs RMS are equal to values in the colon 1 of the table 4.2. Based on simulation results we evalu-

ate RMS of displacements of the solution and present them in the table 4.2. It proves the general conclusion that when a mismatch of this type is present, there is firstly a range displacement of the solution and then side lobes grow and give false solutions. Nevertheless, if we use a narrower band to solve the localization problem, the robustness of the solution to different mismatches increases.

5.5.2. Bottom depth mismatch

Second type of environmental mismatch we have investigated is the mismatch in bottom's total depth. To study its effect on solutions of the both deterministic and stochastic MFP-FS algorithms, we have simulated ambiguity surfaces (AS) when mismatches shown in the colon 2 of the table 4.1 were introduced. Based on these simulation results we evaluate RMS of displacements of the solution and present them in the table 5.3.

Table 5.4.
Effects of mismatches in receiving array depth on object localization solutions by FS-MFP.

Waveguide	Displacement of receiving array	RMS of displacement of object localization solution (z,x) [km] D - DSE, S – SSE statistic 1 / 2
BS	1 m	D: (0.02;20)/(0.02;20) AE S: (0.03;20)/(0.03;20) AE
0.2 km × 50 km	5 m	D: (0.02;20)/(0.03;20) AE S: (0.02;20)/(0.03;20) AE
BW	1 m	D: (0.020;0.5)/(0.020;0.3) S: (0.015;0.4)/(0.015;0.3)
0.2 km × 15 km	5 m	D: (0.030;0.8)/(0.025;0.8) S: (0.025;0.8)/(0.020;0.8)
WC	1 m	D: (0.03;7)/(0.02;1.5) S: (0.02;5)/(0.02;1.0) AE
0.2 km × 50 km	5 m	D: (0.03;8)/(0.05;5) AE S: (0.03;12)/(0.05;10)
TEST	0.5°	S: (0.001;0.1)/(0.001;0.1) AE
0.05 km × 14 km	1.0°	S: (0.100;5.0)/(0.100;6.0) AE

5.5.3. Mismatch in source or receiver position

The third type of environmental mismatch we have studied is that of receiving or emitting arrays' parameters such as theirs positions (range, depth) and space orientations (for vertical linear arrays it is the angle from the vertical direction).

It follows from the structure of considered MFP algorithms that such mismatches will effect the decision statistics if variations of field's parameters due to them differ from the model ones more than the signal's model (signal's correlation interval) or the waveguide's model (a priori RMS) allows. Therefore, to avoid it, displacements of sensors must be smaller than the space interval of field variability due to the mode or ray summation in the waveguides.

To study numerically effects of such mismatches on localization solutions obtained by the both types (deterministic or stochastic) of our MFP-FS algorithms, we have built ambiguity surfaces (AS) when mismatches in position of array's centers as given in the colon 2 of the table 4.3 were introduced. It is clear that mismatches in source depth will effect localization solutions by the same manner. Based on these simulation results we evaluate RMS of displacements of the solution and present them in the table 5.4.

5.5.4. Signal mismatch

Spectrum of signals being really radiated by a source of probing signals may differ from the model implemented in the processing algorithm because the source may be technically unperfected or changing its transfer function. Nevertheless, one is able to take easily in account such a mismatch by realizing a previous or, if necessary, a periodic calibration of the source (measuring its transfer function) and by using the measured one to produce a matched signal model. One may also correct the source's transfer function by modifying the source input to compensate this type of mismatch.

A theoretical evaluation of the effect of a signal model mismatch was done in the section 1.1.2 when we considered the impact of the Doppler effect on the correlation's output. Such a mismatch will manifest itself for all ray paths and will resume firstly as decreasing of correlation maximums. As result, the SNR of our MFP algorithms will also decrease and it will effect the detection zones. We evaluate to be insignificant the effect of this type of mismatch on ambiguity functions.

5.5.5. Conclusion on the numerical modeling of mismatches

Main conclusion to be done basing on results of this numerical modeling of mismatching effects is that when a mismatch on some parameter grows, displacement errors occur firstly (the solution is displaced from the "true" object location). In the same time we observe side lobes of decision statistics increasing. Then the side lobes' level becomes high enough to create false solutions, one of which is the main by its level (the initial solution being already displaced far from the "true" one, may decrease at all below the detection threshold). Sometimes, we have situations (in the winter SWSE) where one of strong new side lobes of the decision statistic arises close to the "true" object location. It is clear that it is related to the high periodicity of

sound fields in such waveguides. We must note a higher probability to have false solutions for the algorithms #2 both for the DSE and SSE models but smaller displacement errors.

Effect of mismatches on MFP algorithms is not significant till they don't change main echo-signal's parameters outside the limits allowed by the used model of sound fields in the waveguide or by the used model of the probing signal. When the parameters' variability due to some mismatch becomes larger than these limits, solutions of MFP algorithms become non-robust. For example the solution of SSE-matched MFP algorithms rests robust till the variations of ray travel times or ray arrival angles due to some mismatch rest into the limits of RMS used by the SSE model to which the algorithm is matched. Similarly, the DSE-matched MFP algorithms rest robust till a mismatch produces ray delay mismatches that are smaller than the correlation interval of probing signals.

5.6. FS-ABS system working as convenient ABS

As the results of detection zone modeling for convenient pulse ABS (PABS) systems show, its efficiency is worse than that of an FS-ASB system when all systems' parameters are closes to each other. To estimate qualitatively the efficiency lose one may consider that it is proportional to the decreasing of the signal-to-noise ratio (SNR) SNR_{PABS}/SNR_{FS-ABS}, that must be proportional to the squared ratio of object's equivalent radiuses for PABS and FS-ABS scheme $(ER_{PABS}/ER_{FS-ABS})^2$ and inverse proportional to the ratio of energies of reverberation noises (RN) for these two types of systems:

$$SNR_{PABS}/SNR_{FS-ABS} \sim (ER_{PABS}/ER_{FS-ABS})^2 (RN_{PABS}/RN_{FS-ABS})^{-1} .$$

Using our estimates of ER being presented in the section 3 the following derives:

$$(ER_{PABS}/ER_{FS-ABS})^2 \sim (D_T(2D_T L_T/\lambda)^{-1})^2 \sim (\lambda/2L_T)^2 .$$

At 6 kHz frequency one has: $(ER_{PABS}/ER_{FS-ABS})^2 \sim (0.25\ m/2{\cdot}100\ m)^2 \sim 2{\cdot}10^{-6}$. Further, using the reverberation model, one can evaluate:

$$RN_{PABS}/RN_{FS-ABS} \sim \left(\int d\chi \int m_1(\chi,\varphi;\chi_0)|_{|\varphi|>2\sigma_\gamma^2} d\varphi \right) \left(\int d\chi \int m_1(\chi,\varphi;\chi_0) d\varphi \right)^{-1} ,$$

where χ is the characteristic grazing angle's value of the strongest ray, φ is the azimuth scattering angle. In the case of surface reverberation from a developed sea waving at 6 kHz frequency $|V_S(\chi)| << 1$, then $RN_{PABS}/RN_{FS-ABS} \sim 4\pi m_S(\chi_1,\varphi_1;\chi_1)$. For test SWSE $\chi_1 \sim 0.1$, $\varphi_1 \sim 0.5$ and therefore, $m_S(\chi_1,\varphi_1;\chi_1) \sim 10^{-5}$ at the frequency

6 kHz, therefore the estimate $RN_{PABS}/RN_{FS-ABS} \sim 10^{-4}$ derives. Thus, the ratio is $SNR_{PABS}/SNR_{FS-ABS} \sim 2 \cdot 10^{-2}$. Therefore, one needs to increase the "power" of signal processing algorithms by corresponding number of times to ensure (under condition to have the same other parameters) a SNR for PABS of the same level that for FS-ABS.

In the case where the object has left the always narrow (in the horizontal plane) detection zone of a FS-ABS system, this one becomes an ABS system working under the convenient bistatic schema but using continuously radiated probing signals. If even one supposes that the echo-signal can be efficiently segregated from the source field as it is realized for pulse systems, nevertheless one will have a higher reverberation level at the signal processing algorithm's input because of the continuous radiation. It means that when using the continuous radiation the SNR decreases by $(ER_{PABS}/ER_{FS-ABS})^{-2}$ times for the convenient ABS schema but not by $(RN_{PABS}/RN_{FS-ABS})(ER_{PABS}/ER_{FS-ABS})^{-2}$ times as it is for the pulse radiation.

Let's note as conclusion to this section that in propagation conditions where the reverberation is the most important interference, one is not able to increase the SNR by increasing the radiated power when using active systems because the reverberation interference will also increase in parallel to the echo-signal's level. There is only one way to combat the reverberation that is to use more complex probing signals of a larger band or bigger receiving arrays. All this will need to use a higher computer power when making the signal processing.

5.7. Conclusions

5.7.1. Detection

1. Signal processing algorithms for ABS systems that are proposed above have the highest possible noise robustness thanks to the use of a complex probing signal and of the correlation processing and also thanks to the adaptation to space distributions of interference in the vertical plane. For example, detection zones of these algorithms calculated for situations where there are local noisy sources or not are practically identical. Big vertical dimension of a receiving array allows to eliminate efficiently the anisotropy reverberation interference that's the most important for the FS-ABS schema of observation. If a horizontal array is used, we'll have no gain in the signal-to-reverberation ratio since the arrival directions in the horizontal plane of the maximum of the reverberation's angular spectrum and of the echo-signal's field are practically the same. Also, the use of a complex signal gives a big contribution in eliminating the reverberation interference. The use of a tone signal doesn't allow to do it because the Doppler effect is

much smaller for the FS schema then for the convenient monostatic one. As additional to these positive moments we note the use of the squared module of the correlation function's complex amplitude as decision statistic in our signal algorithms but not the use of the amplitude itself, since this decision statistic is more robust to possible factors of instability such as a "jolting" of emitting of receiving arrays.

2. Comparison of detection zones of a FS-ABS system with those of UOS systems based on the convenient active or passive sonar shows that the detection range of the FS systems is much bigger than that of convenient systems (when all other system parameters are equal). Nevertheless, the FS detection zone is very narrow in the horizontal plane - it may be hundreds of meters when the system's base length between the source and the receiver is tens of kilometers - against the detection zones of convenient systems. It means that FS-ABS systems belong to the "barrier type" of UOS systems.

5.7.2. Localization

1. When using the MFP-FS algorithms for both the deterministic and stochastic ocean waveguide's models one has a very high precision of object coordinates estimating, in particular of the object depth. Thanks to this fact one has also a rather good estimate of the object's speed in the direction being orthogonal to the system's vertical plane.

2. The main problem when solving the localization problem by MFP-FS algorithms is the robustness of the solution being characterized by the probability of false solution appearing. It follows from presented results of numerical simulations that in some situations even in the ideal case (without mismatching or fluctuations of field's ray parameters) under the DSE model the ambiguity functions of MFP-FS algorithms have several maximums whose levels are compatible, and therefore false solutions are appearing. In these cases the use of the SSE-matched MFP-FS algorithms doesn't eliminate these false solutions. In the cases where the solution of the DSE-matched MFP-FS algorithms is rather "good", having one well-expressed maximum of the ambiguity function, the SSE-matched MFP-FS algorithms should , in principle, produce a more robust solution. Nevertheless it isn't seen in some situations since the correlation interval of the used probing signal being determined by it's frequency band doesn't differ considerably from the *a priori* RMS of ray of parameters of echo-signals being determined by the used SSE model. In this case fluctuations of measured ray parameters with such RMS manifest themselves in corresponding fluctuations of the decision statistic by the same manner for the DSE-matched MFP-FS algorithms as well as for the SSE-matched ones. Robustness of SSE-matched MFP-FS algorithms against fluctuations of ray parameters when compared to

that of the DSE-matched MFP-FS algorithms will manifest itself if the correlation interval of probing signals is much smaller than the variance of fluctuations of ray travel times.

3. The main conclusion of the numerical study on the effect of different environmental or system mismatches when solving the localization problem is that when a mismatch grows, there are firstly displacement errors (the solution moves from the "true" location of a object. Also there is in parallel an increasing of side lobes of the decision statistic. Then this increasing becomes significant enough to create false solutions one of which becomes the global maximum (during this evolution the initial solution being already displaced from the "true" object position may at all decrease below the threshold of detection). It often happens that one of new strong maximums arises close to the "true" object position. Probability of this event grows when the sound field's periodicity in the waveguide is higher.

4. Different mismatches don't effect the SSE-matched MFP-FS algorithms till they disturb the echo-signal field into the limits allowed by the model of the field in the SSE. When the disturbances exceed these limits, the MFP-FS algorithms matched to the SSE model become non-robust. The same is true for the DSE-matched MFP-FS algorithms, but in this case the limits of allowed mismatches in field's parameters, one of which - the ray travel time - is the most informative, are determined by the time correlation interval of probing signals.

   In connection to this, there are two ways to improve the robustness of SSE-matched MFP algorithms:

- to make more "rude" the localization algorithms (for example, by decreasing the effective signal's band used by the algorithm),
- to solve together the UOS and ATO problems, with determining the bottom depth and with solving the positioning problem for emitting and receiving arrays.

AKNOWLEGMENT

This study was conducted during 1995-96 with a support from Sanders, a Lockheed Martin Company, USA. Our special thanks come to Robert Saffer, Kennet Rolt and Geoffrey Edelson for cooperation and useful discussions.

References

[1] *Hönl H., Maue A.W., Westpfahl K.* Theorie der Beugung. Springer-Verlag, Berlin – Göttingen – Heidelberg, 1961.

[2] *Flatté S.M.* (Ed.). Sound transmission Trough A Fluctuating Ocean. Cambridge University Press, Cambridge – London – New York – Melbourne, 1982.

[3] *Borodin V.V., Galaktionov M.Yu.* New mathematical model of sound field fluctuations in shallow water environments with boundary and volume roughness // The formation of acoustical fields in Oceanic waveguides. Coherence phenomena. Nizhny Novgorod: Applied Phisics Institute of RAS. 1997. P. 161-185.

[4] *Brekhovskikh L.M.* (Ed.). Ocean Acoustics. Moscow: Nauka, 1954.

[5] *Kravtsov Yu.A., Orlov Yu.M.* Geometrical Optics of Inhomogeneous Media. Moscow: Nauka, 1980.

[6] *Borodin V.V.* D.Sc. Thesis. Andreyev Acoustics Institute, Moscow, 1989.

[7] Full version of this article in the Internet at URL http:\\www.geocities.com\SiliconValley\Pines\4745\lipps\lib\fundamentals.htm

[8] *Galaktionov M.Yu., Borodin V.V., Mamayev A.V.* Numerical and Experimental Study of Sound Field Forming in Shallow Water Environments // The Formation of Acoustical Fields in Shallow Water Waveguides. Coherence Phenomena. Nizhniy Novgorod: Applied Phisics Institute of RAS, 1997. P. 134-161.

[9] *Kleshev A.A.* High frequency sound scattering by idealised spheroid // Sov. Acoust. Phys. 1973. V. 19, № 5.

[10] *Galaktionov M.Yu.* Modelling of sea noise angular spectra with taking into account the multiple scattering from the sea surface // Proc. of the 1st French Congress on Acoustics, 1992.

[11] *Van Trees G.* Theory of Detection, Estimation and Modulation. V. 3. Signal Processing for Radar and Sonar.

[12] *Borodin V.V.* // Proc. of the SACLANT Conference, 1994.

[13] *Borodin V.V.* // Phys. Acoust., 1995. № 1.

[14] *Baggeroer A.B., Kuperman W.A., H. Schmidt, E.K. Sheer.* Environmentally tolerant beamforming for high-resolution matched field processing: Deterministic mismatch // J. Acoust. Soc. Am., 1990. V. 88(4). P. 1851-1862.

[15] *Feuillade C., C.L. Byrne, G.M. Frichter.* Sector-focused stability methods for robust source localization in matched field processing // J. Acoust. Soc. Am. 1990. V. 88(6). P. 2843-2851.

[16] *Feuillade C., H.A. Chandler, G.B. Smith.* Sector-focused processing for stabilized resolution of multiple acoustic sources // J. Acoust. Soc. Am. 1995. V. 97(4). P. 2159-2172.

[17] *Krolik J.L.* Matched-field minimum variance beamforming in a random ocean channel // J. Acoust. Soc. Am. 1992. V. 92(3). P. 1408-1419.

[18] *Lourtie M.M.G., Carter G.C.* Acoustic signal detection in uncertain ocean environments // Proc. of the NATO ASM "Acoustic signal processing for ocean exploration". 1992. P. 293-310.

[19] *Lourtie M.M.G., Carter G.C.* Signal detection in a multiple time delay environment // MEEE Trans. on Signal Processing. 1992. V. 40(6). P. 1587-1590.

[20] *Lourtie M.M.G., Carter G.C.* Signal detectors for random ocean // J. Acoust. Soc. Am. 1992. V. 92(3). P. 1420-1427.

[21] *Richardson A.M., Nolte L.W.* A posteriori probability source localization in an uncertain sound speed, deep ocean environment // J. Acoust. Soc. Am. 1991. V. 89(5). P. 2280-2284.

[22] *Richardson A.M., Nolte L.W.* A posteriori probability source localization with array tilt uncertainty // J. Acoust. Soc. Am. 1992. V. 92(3). P. 1578-1582.

[23] *Richardson A.M., Nolte L.W., Haralabus G., Premus V., Alexandrou D.* Source localization in an uncertain acoustic scattering environment // J. Acoust. Soc. Am. 1993. V. 94(6). P. 3379-3386.